Adeno-Associated Virus Gene Therapy for Maple Syrup Urine Disease

Kathryn Louise Mullany

A thesis submitted in fulfilment of the requirements for admission to the degree of Doctor of Philosophy

Children's Medical Research Institute

Faculty of Medicine, The University of Sydney

2025

This project was supported through stipend funding generously provided by the Johnston Foundation and James Fairfax Institute of Nutrition

Declaration

I declare that the work described in this thesis is entirely my own, unless otherwise specifically stated in the document. All animal experiments and procedures were approved by Children's Medical Research Institute Animal Care and Ethics Committee. The studies described in this thesis have not been previously submitted for any degree at any institution. No content produced by generative AI tools has been used in the preparation of this thesis. No content in this thesis has previously been published.

Kathryn Louise Mullany
Candidate

As the primary supervisor for this PhD student, I attest to the above statement.

Prof Ian Alexander
Supervisor

Acknowledgment of country

This PhD project follows in the scientific tradition of the First Nations people of Australia. Indigenous Australians were the first astronomers, engineers and healers of this Country. I acknowledge and honour the Gadigal, Burramattagal and Darug peoples on whose ancestral lands this research was undertaken.

Always was, always will be.

An Ode of Gratitude

Those who follow are but some of the inspirational humans, supportive friends, outstanding people and scientific family that have made this thesis possible, and I warmly thank them.

Firstly, to my supervisors, Ian Alexander and Susan Siew. Without your belief, support and continual guidance I would never have started this epic journey into gene therapy, nor surely finished it. Ian, you have built an incredible foundation which is expanding exponentially, and it has been an honour to learn from you and be a small part of the legacy you have created. Susan, I looked up to you from the moment I heard about you, thank you for your mentorship, your humanity and lending your impressively brilliant brain to help me in this project.

Thanks also to Sharon Cunningham, my adoptive in-house supervisor, who did much to get me going in the early days of this PhD. No problem was ever too big and you always made time for me, even when you were so busy with your own projects.

To the Gastroenterology department at Westmead Children's hospital, Michael Stormon, Shoma Dutt, Ted O'Loughlin, Kunal Thacker, Annabel Magoffin, Juliana Puppi, Janine Sawyer, Brooke Andersen, Merran Spargo, Jocelyn Vosu and Katie Marks, you have all taught me so much, thank you for mentoring me from the start of my Gastroenterology journey and allowing me to continue to moonlight as a fellow during these past few years. Thank you also for the financial support through the Johnston Foundation and James Fairfax Institute of Nutrition, without which this project would not have been possible.

To the children and families I have been privileged to care for, I will never stop striving to try to find better ways to help you. Thank you for the trust you place in me and my colleagues, you continue to inspire me.

A hearty thank you to Beena Devanapalli and Ayper Tolun at The Children's Hospital at Westmead for running the BCAA assays and always meeting me with a big smile, no matter the number of samples I dropped down nor the time frame I asked you to turn them around in. Thank you for your commitment to research and for supporting this project.

Thank you also to the CMRI bioresources team, Shelley, Ness, Bella and Mehtap, as well as past members Irma Villaflor and Megan Reddel. You are a tireless, compassionate and always helpful team and I am so grateful to each of you, and especially the irreplaceable Ness, for all your assistance, encouragement and animal house companionship.

The Gene Therapy Research Unit is a unique and special group of people and it has been a pleasure to learn from all past and present members. Thank you Margot Latham, Sam Ginn and Grant Logan for your help guiding this project. Thank you, Cindy Erhua Zhu, for being my lab mum, plying me with snacks and tea, handmaking me clothes, making sure I ate, always knowing what to do when I was getting muddled and always making me feel like I could do this. Neeta Kandekar, thank you for being my early morning friend, getting me out of untold lab dilemmas and always making sure I was doing okay, especially transitioning back from maternity leave. Fatemeh Doroudian you are the coolest person I know, and also the kindest, thank you for being such a stellar friend and lab mate. To the GTRU old guard, Claus, Natsuki, Sharon, Sophia, Fiona, Elena, Maya, Daniel and Anais, thank you for building the foundation on which we all have the privilege of standing, it really is an honour. To the GTRU Next Gen, Ann, Lakshmy, Otillia, Bradley, Imogen and Vasilia: the future of gene therapy is in good hands, I am sure. I can't wait to see the heights to which you take it.

To my fellow PhD students who were there from the first day, comrades in arms, pickles in a jar, eggs in a frying pan, how in the world would this have been possible without you? Caitlin Lucas, Lara Graves, Eva Van Djik, Sharntie Christina, and Mawj Mwande: your collective science wizardry is matched only by your personal generosity. I don't really have words to thank each of you enough. Thank you for sharing laughs, tears, teas, tips and tricks, snacks, bottles of FBS, pipettes, playlists, braving a pandemic and Sydney Trains together, weathering the protocol failures and most importantly, celebrating all the successes.

To my loves: Andrew, you gave me time, space, and all of the second chances to explore this part of my career. I started this project for me, but I am finishing it for you and our daughter. At the end of the day, nothing really matters except you two and that I get to love you both every day. Maeve, my little love, you have turned my life technicolour and in realising a dream of mine, know I will always be there to help you realise yours, whatever they may be.

Mum and Dad, thank you for your unassailable love and support. You sacrificed so much to prioritise education for your children and in doing so gave us all every opportunity to succeed, thank you, I love you both so very much. Steenie, Phill, Bee and Tashi, thanks for being my original and unsurpassed cheer squad; whilst I am proud of this project, it will never come close to how proud I am of you four and to have you as my siblings, I love you each forever. Deb and Stephen, thank you for your endless kindness, love and support in helping to keep our little family afloat, and for always being genuinely interested in my research. Nettie, you and Oumpa supported CMRI before I even was born, it is wonderful and curious to know you both made this project possible before it was even conceived, your passion for research and giving back to the community inspires all your grandchildren and we are so lucky to have you. Granny B and Papa, I wish I could have told you about this project, we love and miss you very much. Newt, you helped in your own way, you loveable scallywag.

To Sally, Siem, Min (maker of truly the best care packages and my personal PhD motivation coach), Lach, Ella, Tim, Talia, Will, Harrison, Ben, Dan, Zoe, Erin, Grace, Joce, Katie, Jess, Rach, Dave, Inca, Lauren and Sam, you always fill my heart when I see you, thank you for your enduring friendship and forgiveness in my abandoning you all so completely during the past year or so.

Finally, this PhD has taught me the art of science, the art of persistence, the art of rolling on despite seemingly insurmountable reasons to stand still, and the art - by way of receiving - of how to support the soul attempting "the PhD". I will forever be grateful, again and again, for the lessons accompanying and arising from this scientific journey, and will never forget the people, or support, I encountered along the way.

Generally speaking, 'there is no truth on earth'
– although that is itself untrue,
for truth does exist on earth,
but only in science and art.

Nikolai Rimsky-Korsakov

Let everything happen to you,
Beauty and terror.
Just keep going
no feeling is final.

Rainer Maria Rilke, *circa*. 1905

Abstract

Advancements in genetic therapies, including recombinant adeno-associated virus (AAV) technologies, have now reached a point where potential curative treatments are within reach for incurable genetic diseases such as Maple Syrup Urine Disease (MSUD). MSUD is caused by a deficiency in the enzyme BCKDH and occurs secondary to biallelic mutations in one of five autosomal genes. Genetically MSUD is highly heterogenous, and current treatment options are not curative. Existing pre-clinical MSUD research has explored the potential of recombinant AAV-mediated gene transfer and mRNA technologies across murine models corresponding to the three most common MSUD genotypes, *BCKDHA*, *BCKDHB* and *DBT*. Tissues targeted in these studies included a combination of liver, muscle or central nervous system with some encouraging results, however key research questions remain unanswered. The exact hepatic threshold of BCKDH activity required for phenotypic correction in mice and humans, has yet to be established and whilst success of liver transplantation for MSUD patients offers some insights it is not known if this can be replicated with AAV-mediated gene transfer. Furthermore, whilst gene transfer to the liver with current AAV technologies is highly efficient, AAV persists predominantly as episomes in transduced cells. This represents an inherent challenge in maintaining a durable therapeutic effect of AAV-mediated vectors in tissue with dividing cells, like the paediatric liver. In humans and mice, skeletal muscle is the largest single tissue contributor to total body BCKDH activity and has yet to be successfully explored as a single organ strategy with AAV mediated gene transfer. Myocytes are post-mitotic and a more stable cell population compared to juvenile hepatocytes and represent a target tissue for MSUD gene therapy with enormous potential for clinical translation in both paediatric and adult patient populations.

This thesis explored the potential of recombinant AAV technology to treat MSUD through both liver directed and muscle restricted approaches. The first component of the project formally

characterised a neonatal lethal *DBT*-deficient transgenic mouse model of MSUD which faithfully recapitulated the physical and biochemical phenotype of classical MSUD. The second component of this thesis explored the feasibility of a liver directed recombinant gene addition using AAV8 pseudoserotyped vector carrying a human *DBT* transgene under the transcriptional regulation of a putatively liver specific APOe/hAAT enhancer/promoter. These experiments used conventional and hybrid AAV/*piggyBac* transposase vectors and found that both integrating and non-integrating AAV vectors significantly improved the physical and biochemical phenotype of DBT-deficient mice. Whilst the non-integrating liver targeted vectors only provided transient phenotypic rescue, integrating strategies using hybrid AAV/*piggyBac* vectors improved the durability of vector and conferred phenotypic correction in DBT-deficient mice, independent of hepatic transgene integration. These experiments highlighted significant contributions from extrahepatic transgene expression to phenotypic rescue, which was conferred by inclusion of the Woodchuck-hepatitis virus Post-transcriptional Regulatory Element (WPRE) in the expression cassette. In order to explore muscle-restricted expression, a muscle optimised recombinant expression cassette including a muscle restricted CK8e promoter/enhancer and the human *DBT* transgene was generated and packaged in the muscle trophic AAVMYO capsid. MicroRNA targeting site sequences were also included in this vector to de-target expression in liver and brain. This muscle optimised vector successfully rescued DBT-deficient mice to adulthood with growth and leucine levels statistically equivalent to those observed in wildtype mice during periods of metabolic stability. Molecular analysis demonstrated a highly muscle restricted profile of transgene expression with enduring phenotypic correction to adulthood in a post mitotic tissue. Whilst further, rigorous pre-clinical testing is required before an equivalent muscle optimised vector would be safe for human clinical application, this thesis has demonstrated the viability of AAV-mediated gene transfer to striated myocytes in a neonatal lethal MSUD murine model and is an encouraging step in the search for a cure for MSUD patients and their families.

Presentations arising from this thesis

Kathryn Mullany, Susan Siew, Ian Alexander (Poster). Liver directed *in utero* AAV gene therapy for Maple Syrup Urine Disease in a neonatal lethal murine model. *International Liver Congress 2022,* European Association for the Study of the Liver (EASL), London, United Kingdom.

Kathryn Mullany, Susan Siew, Ian Alexander (Poster). Humanised Disease Model for Maple Syrup Urine Disease. *Westmead Precision Medicine Conference,* 2021, Westmead Institute of Medical Research, Westmead, NSW, Australia.

Kathryn Mullany, Susan Siew, Ian Alexander (Oral presentation). Gene Therapy for genetic metabolic liver disease: correcting Maple Syrup Urine Disease in a pre-clinical neonatal lethal disease model. *Australian Gastroenterology Week Conference,* September 2022, Sydney, NSW, Australia.

Kathryn Mullany, Susan Siew, Sharon Cunningham, Ian Alexander (Oral presentation). AAV gene delivery rescues a neonatal lethal MSUD murine model. *Australian Gene and Cell Therapy Society Conference,* 13th Biennial Meeting, November 2024, Sydney, NSW, Australia.
AGCTS talk

Awards arising from this thesis

Winner - Gastroenterology Society of Australia, June Halliday Basic Science Young Investigator Award, 2022, awarded at Australian Gastroenterology Week Conference, Sydney, Australia.

Winner - Panos Ioannou Young Investigator Award, Australian Gene and Cell Therapy Society, 2024, awarded at Australian Gene and Cell Therapy Society 13th Biennial Meeting, Sydney Australia.

Scholarships supporting this thesis

The Johnston Foundation Research Scholarship, administered through the James Fairfax Institute of Nutrition and Research, Gastroenterology Department, The Children's Hospital at Westmead.

AI Statement

No content produced by generative AI tools has been used in the preparation of this thesis.

List of Abbreviations

AAV	Adeno-associated virus
BCAA	Branched chain amino acid
BCAT	Branched chain aminotransferase
BCKDH	Branched chain ketoacid dehydrogenase
BGHpA	Bovine growth hormone poly-adenylation sequence
cDNA	Coding DNA
CNS	Central nervous system
CRISPR	Clustered regularly interspaced short palindromic repeats
DAPI	4',6-Diamidino-2-phenylindole dihydrochloride
DBT	Dihydrolipoamide branched chain transacylase
ddPCR	Digital droplet Polymerase chain reaction
DLD	Dihydrolipoamide dehydrogenase
DMEM	Dulbecco's modified eagle medium
DNA	Deoxyribonucleic acid
dsDNA	Double stranded deoxyribonucleic acid
EDTA	Ethylenediaminetetraacetic acid
FRG	$Fah^{-/-}/Rag2^{-/-}/Ilrg2^{-/-}$
HDR	Homology directed repair
HITI	Homology-independent targeted integration
IEM	Inborn error of metabolism
IMDM	Iscove's modified dulbecco's medium
ITR	Inverted terminal repeats
KIC	α-Ketoisocaproate
LB	Lysogeny Broth

LNP	Lipid nanoparticle
MMA	Methylmalonic aciduria
mRNA	Messenger RNA
MSDS	Material safety data sheet
MSUD	Maple Syrup Urine Disease
NAb	Neutralising antibodies
NHEJ	Non-homologous end joining
OTC	Ornithine Transcarbamylase
PA	Propionic aciduria
pB	*piggyBac*
PCR	Polymerase chain reaction
PEG	Polyethylene glycol
PPE	Personal protective equipment
rAAV	Recombinant adeno-associated virus
SB	Sleeping beauty
ssDNA	Single strand deoxyribonucleic acid
TALEN	Transcription activator-like effector nucleases
TCA	Tricarboxylic acid cycle
TIR	Transposon inverted repeats
WPRE	Woodchuck hepatitis posttranscriptional regulatory element
ZFN	Zinc finger nucleases

Table of Contents

DECLARATION…… ii

ACKNOWLEDGMENT OF COUNTRY……iii

AN ODE OF GRATITUDE……...iv

ABSTRACT……vii

PRESENTATIONS ARISING FROM THIS THESIS……ix

AWARDS ARISING FROM THIS THESIS……ix

SCHOLARSHIPS SUPPORTING THIS THESIS……..ix

AI STATEMENT……ix

LIST OF ABBREVIATIONS…….……x

TABLE OF CONTENTS……..……xii

LIST OF FIGURES……..……xxii

LIST OF TABLES…….…....xxvii

CHAPTER 1 - MAPLE SYRUP URINE DISEASE AND GENE THERAPY

1.1 Introduction.....1

1.2 Maple Syrup Urine Disease is a candidate disease for Gene Therapy..... 3

1.2.1 Maple Syrup Urine Disease is a rare condition 3

1.2.2 Historical context of Maple Syrup Urine Disease 4

1.2.3 Pathophysiology of Maple Syrup Urine Disease.....5

1.2.3.1 Altered BCAA metabolism in MSUD is secondary to BCKDH enzyme deficiency 5
1.2.3.2 Normal metabolism of BCAA is reliant on BCAT and BCKDH 6
1.2.3.3 Branched chain Amino Transferase initiates BCAA catabolism 6
1.2.3.4 Branched chain ketoacid dehydrogenase commits BCAA to the degradation pathway 7
1.2.3.5 Branched chain ketoacid dehydrogenase enzyme is tightly regulated 10
1.2.3.6 Alterative Leucine Degradation Pathway 12
1.2.3.7 Accumulated leucine drives metabolic intoxication and neuronal damage in MSUD 12
1.2.4 MSUD clinical phenotypes, classification and presentation 14
1.2.4.1 Classical MSUD is the most severe and commonest MSUD phenotype 15
1.2.4.2 Intermediate and intermittent MSUD 15
1.2.4.3 Rarer forms of MSUD 16
1.2.4.4 Sotolone causes the characteristic urinary aroma in maple syrup urine disease 16
1.2.5 Newborn screening allows for early diagnosis and improved prognosis in MSUD 17
1.2.6 Characterising the genetic basis of MSUD has implications for developing a genetic therapy 18
1.2.6.1 MSUD is genetically heterogenous 18
1.2.6.2 Genetic subtypes of MSUD 18
1.2.6.3 MSUD Genotype prevalence 20
1.2.6.4 Genetic polymorphism in BCKDH subunits 20
1.2.7 Tissue expression of Branched chain Ketoacid Dehydrogenase 21
1.3 Contemporary Maple Syrup Urine Disease treatments are not curative 24
1.3.1 Dietary Therapy for Maple Syrup Urine Disease 24
1.3.2 Metabolic decompensations are a major source of morbidity for Maple Syrup Urine Disease patients on dietary therapy 25
1.3.3 Liver Transplantation in Maple Syrup Urine Disease 26
1.3.4 Disease prognosis in individuals affected by MSUD 28
1.3.5 Experimental therapies for MSUD have yet to prove clinically successful 30
1.4 Gene Therapy 32
1.4.1 Origins of Gene Therapy 33
1.4.2 Vector Systems 34

1.4.2.1 Viral Vectors 35
1.4.2.2 Non-viral vectors 36
1.4.3 Adeno-associated Virus Vectors 37
1.4.3.1 Adeno-associated viral vector Structure 37
1.4.3.2 Adeno-associated virus as a gene therapy vector 38
1.4.3.3 Adeno-associated virus capsid biology and considerations for gene therapy strategies 39
1.4.3.4 Tissue Tropism of recombinant AAV vectors 41
1.4.3.5 Designing recombinant AAV vector expression cassettes for therapeutic gene transfer 42
1.4.3.6 AAV vector genomes remain predominantly episomal 44
1.4.4 Improving the durability of recombinant AAV Vectors 44
1.4.4.1 Genomic Editing 45
1.4.4.2 Hybrid Gene Addition with Transposases 49
1.4.5 Challenges and barriers in AAV gene therapy 52
1.4.5.1 Intracellular barriers to AAV gene therapy 54
1.4.5.2 Extracellular barriers to AAV gene therapy 54
1.4.5.3 Host immune responses to AAV vectors 55
1.4.5.4 Maintaining off-target genomic integrity and AAV associated genotoxicity 55
1.4.5.5 Immune Activation and Systemic Inflammatory Responses 56
1.4.5.6 AAV pathogenicity and immunogenicity 57
1.4.5.7 Considerations in the clinical translation of gene therapies 57
1.4.5.8 Commercial viability of Gene Therapies 58

1.5 Gene therapy for Maple Syrup Urine Disease 60

1.5.1 *In vitro* maple syrup urine disease models and early gene therapy attempts 60
1.5.2 Mammalian experimental models of maple syrup urine disease 60
1.5.3 *In vivo* AAV Gene Therapy in pre-clinical animal models 62
1.5.4 *In vivo* non-viral gene therapy for MSUD 65
1.5.5 The Liver as a target for Gene Therapy in MSUD 67
1.5.5.1 Liver anatomy 68
1.5.5.2 Liver specific considerations for MSUD AAV gene therapy 69
1.5.5.3 Liver targeted AAV therapy in the clinic 72
1.5.6 The Muscle as a Target for AAV Gene Therapy 73
1.5.6.1 Structure and Function of Mammalian Myocytes 73

1.5.6.2 Considerations in developing a muscle targeted AAV gene therapy for maple syrup urine disease 75

1.6 Rationale for Gene therapy in Maple Syrup Urine Disease 78

CHAPTER 2 - MATERIALS AND METHODS

2.1 Materials 81

2.1.1 Chemicals and general reagents 81
2.1.2 Kits and Antibodies 85
2.1.3 Bacterial Strains 86
2.1.4 Primers 86
2.1.5 Plasmids 88
2.1.6 AAV Vectors 89
2.1.7 Mouse strains 90

2.2 Methods 90

2.2.1 Molecular Biology 90
2.2.1.1 Small-scale plasmid purification 90
2.2.1.2 Large-scale plasmid purification 90
2.2.1.3 Restriction endonucleases 91
2.2.1.4 Gel electrophoresis 91
2.2.1.5 Purification of PCR amplicons and DNA products 91
2.2.1.6 A-tailing of PCR DNA fragments 92
2.2.1.7 DNA ligation 92
2.2.1.8 Ligating clones with T4 DNA ligase 92
2.2.1.9 Transformation of competent cells 93
2.2.1.10 Glycerol bacterial stocks 93
2.2.2 Sequencing 93
2.2.3 Nucleic Acid quantification 94
2.2.4 Tissue Culture 94
2.2.4.1 Cell passaging 94
2.2.4.2 Cell counting 95
2.2.5 Recombinant Adeno-Associated Virus Production 95
2.2.5.1 Viral packaging in HEK293 cells 95

2.2.5.2 Caesium Chloride Gradient Purification of AAV Virions 96
2.2.5.3 Quantitative PCR analysis of AAV vector preparations with qPCR 98
2.2.6 Animal Work 98
2.2.6.1 Genotyping DBT mice 99
2.2.6.2 Blood sampling 99
2.2.6.3 Dried blood spots 100
2.2.6.4 Intraperitoneal injections 100
2.2.6.5 Intrauterine surgery 100
2.2.6.6 High protein diet challenge protocol 101
2.2.6.7 Mouse weighing 101
2.2.6.8 Humane euthanasia and terminal sample collection 102
2.2.6.9 BCAA Quantitation 102
2.2.7 Molecular Analysis 103
2.2.7.1 Viral titre determination with digital droplet PCR 103
2.2.7.2 Using digital droplet PCR to analyse tissue vector copy number 103
2.2.7.2 DNA Extraction 104
2.2.7.3 RNA extraction 104
2.2.7.4 cDNA Synthesis 105
2.2.7.5 Protein Extraction 106
2.2.7.6 Protein Quantitation 106
2.2.7.7 Western Blot 107
2.2.8 Histology 108
2.2.8.1 Tissue Fixation 108
2.2.8.2 Tissue sectioning 108
2.2.8.3 Immunofluorescence staining 108
2.2.9 Statistical analysis 109
2.2.10 Figures 109

CHAPTER 3 - CHARACTERISING THE NEONATAL LETHAL DBT$^{-/-}$ MURINE MODEL OF MAPLE SYRUP URINE DISEASE

3.1 Introduction 110

3.1.2 Homology between human and murine DBT genes 111
3.1.3 Dietary rescue of the DBT$^{-/-}$ Model is impractical 112
3.1.4 Gender and developmental age-related changes to BCKDH activity 112

3.2 Chapter Specific Methods 113

3.2.1 Sequencing the Mutant and WT DBT Locus 113

3.2.2 Genotyping 113

3.2.3 Obtaining controls for relevant genotypes and retrospective genotyping 114

3.2.4 Timed mating to enhance birth detection and determine gestation duration 116

3.3 Results 118

3.3.1 Sequencing the mutant allele 118

3.3.2 Genotyping 118

3.3.3 Survival of *DBT*-deficient mice characterised as neonatal lethal 119

3.3.4 Growth failure in *DBT*-deficient mice 120

..... 121

3.3.5 The *DBT* protein E2 is undetectable in *DBT*-deficient mice 122

3.3.6 Biochemical phenotype in *DBT*-Deficient mice recapitulates Classical MSUD 125

3.3.7 Gestational length and congenital abnormalities 131

3.4 Discussion and Conclusions 132

3.4.1 $DBT^{-/-}$ is a neonatal lethal murine model 132

3.4.2 Autosomal recessive inheritance pattern and genotype incidence 134

3.4.3 Gestation length for $DBT^{-/-}$ mouse similar to that of background strain C57Bl/6J 135

3.4.4 Congenital and developmental abnormalities 136

3.4.5 Model Limitations 136

CHAPTER 4 - LIVER DIRECTED AAV-MEDIATED GENE ADDITION FOR MAPLE SYRUP URINE DISEASE IN A NEONATAL LETHAL $DBT^{-/-}$ MURINE MODEL

4.1 Introduction 137

4.2 Chapter specific methods 140

4.2.1 Construction of a rAAV vector plasmid containing human *DBT* 140

4.2.2 *In vitro* validation of pAAV2.APOe/hAAT.hDBT expression cassette 142

4.2.3 Neonatal injections and experimental design 142

4.2.4 In utero AAV Gene Addition 143

4.2.5 Vector biodistribution 143

4.3 Results 144

4.3.1 Functional validation of rAAV2/DJ.APOe/hAAT.hDBT *in vitro* 144

4.3.2 Liver directed gene addition provides transient biophysical phenotypic rescue with rAAV2/8.APOe-hAAT.*DBT* viral vector 147

4.3.3 rAAV2/8.APOe-hAAT.DBT vector biodistribution following neonatal intra-peritoneal vector administration 150

4.3.4 rAAV2/8.APOe-hAAT.DBT viral vector drives supraphysiological expression of human E2 protein across whole murine livers 151

4.3.5 Human E2 expression provides transient biochemical phenotype correction 156

4.3.6 *In utero* gene therapy with gene addition did not confer survival advantage in $DBT^{-/-}$ model 159

4.4 Discussion 165

4.4.1 rAAV2/8.APOe/hAAT.hDBT provides transient rescue of DBT-deficient pups 165

4.4.2 Insights into the hepatic phenotype correction threshold in the $DBT^{-/-}$ MSUD Model 166

4.4.3 Timing of metabolic intoxication may offer insight into dynamic metabolic pressures in developing $DBT^{-/-}$ neonates 167

4.4.4 Limited extra-hepatic contribution of rAAV2/8.APOe/hAAT.hDBT in phenotype rescue 168

4.4.5 Bi-modal survival pattern reflects limitations of AAV vector onset of action in neonatal lethal model 169

4.4.6 Overcoming AAV Episome Loss in tissues with high rates of mitosis 170

CHAPTER 5 - GENE ADDITION WITH A HYBRID AAV/PIGGYBAC TRANSPOSASE SYSTEM IN A NEONATAL LETHAL $DBT^{-/-}$ MSUD MODEL

5.1 Introduction 171

5.2 Chapter 5 materials and methods 173

5.2.1 Construction of *piggyBac* transposon expression plasmid encoding the human DBT cDNA 173

5.2.2 Generation of vectors to explore the effects of the WPRE and pBTIR elements on tissue expression 175

5.2.3 *In vitro* validation of transposon vectors in Huh7 cells 177

5.2.4 Neonatal Hybrid AAV/*piggyBac* gene addition experiments 177

5.2.5 Inducing a metabolic stress with a high protein chow 178
5.2.6 Assessing reproductive status in two vector-rescued male DBT$^{-/-}$ mice 179
5.2.7 Statistical analysis 179

5.3 Results 180

5.3.1 *In vitro* validation of the hybrid AAV/*piggyBac* Transposon vectors in Huh7 cells 180
5.3.2 Survival to adulthood following neonatal administration of *piggyBac* transposon encoding vector independent of transposase encoding vector co-administration 183
5.3.3 Growth improvements in vector treated DBT$^{-/-}$ mice are independent of co-administration of *piggyBac* transposase vector 186
5.3.4 Hybrid AAV/PiggyBac transposon conferred no advantage to vector retention in DBT$^{-/-}$ murine model 189
5.3.5 Improved hepatic transgene expression in DBT$^{-/-}$ mice treated with high dose hybrid AAV/*piggyBac* transposon system 191
..... 194
5.3.6 Correction of biochemical phenotype in DBT$^{-/-}$ mice treated with high dose hybrid AAV/*piggyBac* system was independent of hepatic transgene expression 196
5.3.7 Quantitating extra-hepatic expression in DBT$^{-/-}$ mice treated with the high dose hybrid AAV/piggyBac transposon expression cassette 199
5.3.8 DBT$^{-/-}$ mice treated with low dose hybrid AAV/*piggyBac* transposon system cohorts died early despite high levels of hepatic expression 199
5.3.10 Metabolic stress unmasks persistent deficiency in total body BCKDH activity in hybrid AAV/*piggyBac* vector rescued DBT$^{-/-}$ mice 202
5.3.11 Cis-regulatory elements in the transposon encoding expression cassette postulated to influence expression profile of transposon encoding vector 205
5.3.12 Evaluating the effects of cis-regulatory elements on DBT-/- mouse survival and growth 206
5.3.13 Interpreting biodistribution in vectors with different *cis*-regulatory elements 209
5.3.14 Effect of cis-regulatory elements on the tissue expression of AAV transgene cassette in DBT$^{-/-}$ mice. 211
5.3.15 Biochemical phenotype of DBT$^{-/-}$ treated with hDBT transgene cassette improved with inclusion of WPRE in expression cassette 215
5.3.16 Reproductive success in two male DBT$^{-/-}$ rescued with AAV *piggyBac* transposon system 216

5.4 Discussion 217

5.4.1 First report of AAV-mediated rescue of neonatal lethal DBT$^{-/-}$ MSUD model to adulthood 217

5.4.2 Hybrid AAV/*piggyBac* System underperformed compared to other published studies 218

5.4.3 Implications for extra-hepatic transgene expression under the putatively liver specific enhancer promoter APOe/hAAT 219

5.3.4 WPRE improves expression of APOe/hAAT.hDBT AAV cassette in extra-hepatic tissues in the DBT$^{-/-}$ mouse model 220

5.4.5 Dose of AAV/*piggyBac* transposon encoding vector influences tissue biodistribution in organs relevant to BCKDH expression 222

5.4.6 Translational lessons from hybrid AAV/*piggyBac* gene addition 223

CHAPTER 6 - MUSCLE TARGETED AAV GENE THERAPY RESCUES MSUD MODEL TO ADULTHOOD

6.1 Introduction 224

6.1.1 Muscle Trophic Capsids 224

6.1.2 Engineering *cis*-regulatory elements of the rAAV cassette to improve muscle transgene expression 225

6.1.2.1 Selecting promoters for enhanced AAV vector transgene expression in muscle 226

6.1.2.2 MicroRNAs can be used to direct tissue specificity of transgene expression 227

6.2 Chapter 6 specific methods 228

6.2.1 Identifying miRNA-TS sequences for liver and brain 229

6.2.2 Synthesis of muscle optimised AAV hDBT expression vector 230

6.2.3 Animal Experiments 232

6.2.4 Statistical Analyses 232

6.3 Results 233

6.3.1 Muscle optimised AAV vector provides enduring rescue of neonatally treated DBT$^{-/-}$ to adulthood 233

6.3.2 Neonatally administered rAAV2/AAVMyo.Ck8e.hDBT.miRNA broadly transduces striated muscle groups 235

6.3.3 CK8e promoter drives supraphysiological expression of hDBT transgene across whole skeletal muscles in DBT$^{-/-}$ mice 236

6.3.4 Biochemical phenotype of DBT$^{-/-}$ rescued with muscle optimised AAV vector equivalent to wildtype 241
6.3.5 Physiological and induced metabolic challenges in DBT$^{-/-}$ rescued with rAAV2/AAVMYO.CK8e.hDBT.WPRE.miRNA-TS viral vector 244
6.4 Discussion.....247
6.4.1 CK8e transcriptional regulation of hDBT main driver in phenotypic correction provided by rAAV2/AAVMYO.CK8e.hDBT.WPRE.miRNA-TS viral vector 247
6.4.2 Insights into disease correction threshold in DBT$^{-/-}$ mice treated with muscle optimised AAV vector 248
6.4.3 Future directions in pre-clinical muscle directed AAV gene therapy for MSUD..... 251
6.4.4 Clinical translation considerations of muscle directed AAV therapy for MSUD..... 252
CHAPTER 7 – GENERAL DISCUSSION & FINAL CONCLUSIONS…….254
APPEXDIX……268
REFERENCES……272

List of Figures

CHAPTER 1

Figure 1-1 Chemical structure of the Branched Chain Amino Acids: leucine, isoleucine and valine……... 5

Figure 1-2 Cellular Metabolism of Branched Chain Amino Acids by cytosolic BCAT and the mitochondrial enzyme BCKDH..…….…….…….…...7

Figure 1-3 Protein structure of branched chain ketoacid dehydrogenase..……...9

Figure 1-4 Leucine influx through the SLC7A5 transporter is implicated in the cerebral pathogeneiss of MSUD……...14

Figure 1-5 Interspecies differences in organ contributions to total body branched chain ketoacid dehydrogenase enzyme oxidation..……..…….……...21

Figure 1-6 Genome of wildtype AAV..……..…….……37

Figure 1-7 DNA repair mechanisms after double stranded DNA breakages..…….47

Figure 1-8 Biological barriers to successful gene therapy…….53

Figure 1-9 Liver microarchitecture and the hepatic acinus oxygen gradient and associated metabolic zonation..……..…….70

Figure 1-10 Structural anatomy of skeletal muscles……..……75

CHAPTER 3

Figure 3-1 Described DBT Alleles in MSUD Murine Model……..113

Figure 3-2 Murine identification system……..……..117

Figure 3-3 Mutant Allele Sequence……..……..118

Figure 3-4 Genotyping Gel ……..119

Figure 3-5 Survival in DBT MSUD Mouse Model. Figure 3-6 Growth of DBT MSUD Mouse Model……...120

Figure 3-7 Growth failure in $DBT^{-/-}$ Mice……..121

Figure 3-8 Hepatic E2 expression in MSUD DBT model…….……..122

Figure 3-9 E2 protein expression across cellular compartments…….……123

Figure 3-10 Tissue expression of E2 protein across brain, heart and skeletal muscle in $DBT^{+/+}$ neonates and adults and $DBT^{-/-}$ neonates……..124

Figure 3-11 Hepatic E2 protein immunofluorescence in DBT Mouse Model…….……125

Figure 3-12 Branched Chain Amino Acid levels in DBT MSUD Model……..…127

Figure 3-13 Branched Chain Amino Acids in WT and heterozygous adults……..128
Figure 3-14 Neonatal L-alloisoleucine levels in DBT MSUD Mouse model. ……..…128
Figure 3-15 Adult L-alloisoleucine levels in DBT Murine Model……129
Figure 3-16 Biochemical Phenotype of DBT$^{-/-}$ progressively worsens over time…….……130

CHAPTER 4

Figure 4-1 Molecular sub-cloning history of pAAV2.APOe/hAAT.hDBT……141
Figure 4-2 Functional Transduction of hDBT expression cassette……145
Figure 4-3 Functional transduction of hDBT expression cassette in Huh7 over increased range of MOIs..……..……146
Figure 4-4 Survival of DBT$^{-/-}$ rAAV8.APOe/hAAT.hDBT vector treated mice.……148
Figure 4-5 Growth in DBT$^{-/-}$ Mice treated with rAAV2/8.APOe/hAAT.hDBT vector……...…149
Figure 4-6 Vector Biodistribution following neonatal administration of rAAV2/8.APOE/hAAT.hDBT……...…150
Figure 4-7 Transgene RNA transcripts quantified with qPCR……...… 152
Figure 4-8 Hepatic E2 protein expression in vector treated in short- and long-term cohorts of DBT$^{-/-}$…… 153
Figure 4-9 E2 protein expression in long-term cohort of vector treated DBT$^{-/-}$ mice……...154
Figure 4-10 Representative Hepatic E2 protein immunofluorescence in vector treated DBT$^{-/-}$ ……155
Figure 4-11 Branched Chain Amino Acid levels in rAAV8.APOe/hAAT.hDBT vector treated DBT$^{-/-}$.……..…155
Figure 4-12 Hepatic vector copy number positively correlates with Hepatic E2 protein expression……...……...…… 158
Figure 4-13 Serum leucine inversely proportional to hepatic vector copy number..……...….158
Figure 4-14 Serum leucine inversely proportional to hepatic E2 protein expression……..159
Figure 4-15 Survival in DBT$^{-/-}$ mice treated with *in utero* rAAV8.APOe/hAAT.hDBT……..161
Figure 4-16 Post-natal growth in DBT$^{-/-}$ mice treated with *in utero* AAV Gene Addition vector……..……...……...…….. 162
Figure 4-17 Hepatic vector copy number in DBT$^{-/-}$ mouse treated with *in utero* AAV Gene Addition vector……...162
Figure 4-18 Serum branched chain amino acids in DBT$^{-/-}$ treated with *in utero* AAV Gene Addition vector. ……...……...……..163

Figure 4-19 E2 protein expression in DBT$^{-/-}$ treated with *in utero* AAV Gene Addition vector….164
Figure 4-20 Hepatic E2 Immunofluorescence of DBT$^{-/-}$ treated with *in utero* AAV Gene Addition vector..……..……..…….164

CHAPTER 5

Figure 5-1 Cloning history of pAAV2.APOe/hAAT.hDBT.WPRE.pBTIR……..174
Figure 5-2 Cloning history of pAAV2.APOe/hAAT.hDBT.pBTIR and pAAV2.APOe/hAAT.hDBT.WPRE.……..……....176
Figure 5-3 Evidence of functional transduction with eGFP transposon vector in Huh7 cells……..……..……..……. 180
Figure 5-4 RNA transcripts from *in vitro* vector validation of hDBT AAV/*piggyBac* transposon vector in Huh7 cells..……..……...181
Figure 5-5 Protein expression from hDBT AAV/*piggyBac* transposon vector in Huh7 cells across cellular compartments.……..……....182
Figure 5-6 Survival in DBT$^{-/-}$ mice treated with hybrid AAV/piggyBac vectors in the newborn period..……..……..…….185
Figure 5-7 Growth of DBT$^{-/-}$ mice treated with hybrid AAV/piggyBac vectors..…….187
Figure 5-8 Average weight of DBT$^{-/-}$ mice treated with high dose piggyBac transposase AAV hybrid gene addition vectors at 8 weeks post injection. ……..……..188
Figure 5-9 Vector biodistribution in DBT$^{-/-}$ mice treated with high and low dose hybrid AAV/piggyBac vectors……..…….…..190
Figure 5-10 RNA transcripts of hDBT transgene for neonatal DBT$^{-/-}$ mice treated with neonatal piggyBac AAV Hybrid Gene Addition vectors……..192
Figure 5-11 E2 protein expression as detected on western blots in DBT$^{-/-}$ mice treated with high or low dose neonatal piggyBac AAV Hybrid Gene Addition vectors…..……193
Figure 5-12 (PREVIOUS PAGE) Immunofluorescence of Hepatic E2 expression in neonatal DBT$^{-/-}$ mice treated with high and low dose Hybrid AVV/*piggyBac* vectors……194
Figure 5-13 Biochemical phenotype in DBT$^{-/-}$ treated with high dose hybrid AAV/piggyBac vectors……..……..……..197
Figure 5-14 Leucine:Valine serum concentration ratio in neonatal DBT$^{-/-}$ mice treated with high dose neonatal piggyBac AAV Hybrid Gene Addition vectors……198
Figure 5-15 Biochemical phenotype in DBT$^{-/-}$ treated with low dose hybrid AAV/piggyBac vectors. ……..……..……201

Figure 5-16 Transduction efficiency in DBT$^{-/-}$ mice treated with high dose hybrid AAV/PiggyBac vectors.……...……...……203
Figure 5-17 Weight loss during a simulated metabolic stress in neonatal DBT$^{-/-}$ mice treated with high dose neonatal piggyBac AAV Hybrid Gene Addition vectors……204
Figure 5-18 Survival data from DBT$^{-/-}$ treated with AAV hDBT transgene vectors containing WPRE and/or pBTIR..……207
Figure 5-19 Growth data from DBT$^{-/-}$ treated with AAV hDBT transgene vectors containing WPRE and/or pBTIR……..208
Figure 5-20 Vector biodistribution of vectors with differing *cis*-regulatory elements in DBT$^{-/-}$ mice…….210
Figure 5-21 Transgene RNA expressed across tissues in DBT$^{-/-}$ treated with rAAV vectors with different *cis*-regulatory elements……212
Figure 5-22 E2 protein expression as determined by western blot for DBT$^{-/-}$ treated with AAV with different cis-regulatory elements…...…… 213
Figure 5-23 Biochemical phenotype in DBT-/- mic treated with AAV vectors with different cis-regulatory elements……...215
Figure 5-24 Example genogram from pairing a DBT$^{+/-}$ female with DBT$^{-/-}$ male rescued with neonatal administration of piggyBac transposase hybrid gene addition vectors…….216

CHAPTER 6

Figure 6-1 Candidate human miRNAs and their relative expression in muscle, liver, heart and brain tissue……229
Figure 6-2 Flow diagram of molecular sub-cloning steps taken to generate pAAV2.CK8e.hDBT.WPRE.miRNA-TS from pAPOe/hAAT.eGFP.WPRE. ……231
Figure 6-3 Survival of DBT$^{-/-}$ following neonatal delivery of muscle optimised AAV gene delivery vector. ……..…232
Figure 6-4 Growth of DBT$^{-/-}$ following neonatal delivery of muscle optimised AAV gene delivery vector. …….234
Figure 6-5 Comparison of weights at 8 weeks of age for wildtype and select vector treated DBT$^{-/-}$.……....235
Figure 6-6 Vector biodistribution at in DBT$^{-/-}$ 8 weeks after neonatal IP injection with with rAAV2/AAVMYO. CK8e.hDBT.WPRE.miRNA-TS. ……235
Figure 6-7 Relative transgene RNA transcripts detected in DBT$^{-/-}$ mice 8 weeks after treatment with rAAV2/AAVMYO.CKe.hDBT.WPRE.miRNA-TS. ……...237

Figure 6-8 E2 protein detected in DBT$^{-/-}$ treated with muscle optimised AAV vector……..238
Figure 6-9 Representative liver immunofluorescence images from 8 week old DBT$^{-/-}$ mice treated with rAAV2/AAVMYO.CK8e.hDBT.WPRE.miRNA-TS..…….239
Figure 6-10 Transduction efficiency of muscle optimised vector……..240
Figure 6-11 Branched chain amino acid levels and L-alloisoleucine levels in muscle optimised vector treated DBT$^{-/-}$……...242
Figure 6-12 Leucine:Valine ratio of vector treated DBT$^{-/-}$……243
Figure 6-13 Branched chain amino acids and L-alloisoleucine trend downwards over first two months of life.……..244
Figure 6-14 Weight loss during 48-hour high protein dietary challenge in all mice exposed to metabolic stress.……... 245
Figure 6-15 Leucine and L-Alloisoleucine levels increase during 48-hour high protein dietary challenge in vector treated DBT$^{-/-}$……246

APPENDIX

Figure A-1 Development of DBT Murine Mouse Model of Maple Syrup Urine Disease……..268
Figure A-2 Sequence of DBT gene knockout allele in the DBT$^{-/-}$ mouse model of MSUD…….269

List of Tables

Chapter 1

Table 1-1 Maple Syrup Urine Disease Genotypes……..……...…..19

Table 1-2 Commonly used viral vectors in pre-clinical and clinical research …….36

Table 1-3 Commercially available gene-based therapies available in Australia……...58

Chapter 2

Table 2-1 Chemicals and reagents ……..……81

Table 2-2 Solutions and Buffers…….…….83

Table 2-3 Commercial Kits……85

Table 2-4 Antibodies……..85

Table 2-5 Bacterial Host Strains……..…86

Table 2-6 Primers ……..……86

Table 2-7 Parental Plasmids……..88

Table 2-8 Plasmids synthesised by candidate…….88

Table 2-9 AAV Vectors……..89

Chapter 3

Table 3-1 Oligonucleotides use for sequencing wildtype and mutant DBT allele in MSUD mouse model…….……...…115

Table 3-2 Mouse activity levels……116

Table 3-3 Age based Leucine:Valine ratios across genotypes in DBT MSUD murine model ……127

Chapter 4

Table 4-1 End point assays performed on *In utero* vector treated DBT$^{-/-}$……...……...….160

Chapter 5

Table 5-1 Cohorts of DBT$^{-/-}$ mice treated with Hybrid *piggyBac*/AAV Vectors……..184

Appendix

Table A-1 Components of each vector used to explore the effect of cis regulatory elements…....271

Chapter 1

Maple Syrup Urine Disease and Gene Therapy

1.1 Introduction

Advancements in genetic therapies have reached a point where potential curative treatments are within reach for previously incurable, rare, genetic diseases. Rare genetic diseases are those which affect less than 1 in 2000 people [1]. Individually rare genetic diseases are by definition uncommon but collectively affect 1 in 17 people worldwide [2]. Maple syrup urine disease (MSUD) is one such rare disease, globally affecting 1 in 150,000 live births [3]. MSUD is an inborn error of protein metabolism, and affected individuals are unable to metabolise branched chain amino acids due to a deficiency in the branched chain ketoacid dehydrogenase (BCKDH) enzyme complex [4]. This deficiency arises from biallelic mutations in one of five autosomal genes [5]. The most severe and common type of MSUD presents in the newborn period with muscle weakness, poor feeding, seizures and encephalopathy. Untreated, MSUD can lead to devastating consequences of permanent brain damage and death. Currently, available treatment options are not curative and limited to dietary therapy and/or liver transplantation. Clearly, there is a need for a superior therapy for MSUD patients.

Recent therapeutic advances in genomic technologies offer a potentially viable alternative for MSUD patients. The genetic basis of MSUD is heterogenous. Diagnosis previously relied upon clinical presentation and pathognomonic biochemistry, however contemporary genetic diagnostics have made a genetic phenotyping in MSUD highly accessible [6-9]. Accompanying the improvements in understanding the genetic basis of MSUD, have been advancements in understanding BCKDH activity and branched chain amino acid (BCAA) metabolism. In humans,

skeletal muscle supplies between 50-60% of BCKDH activity, and the liver around 8-10% [10-12]. Coupled with the knowledge that a liver transplant can normalise serum BCAA's and allow dietary protein liberalisation, there is now a greater understanding of potential target organs for a MSUD gene therapy.

The human liver has been successfully targeted by multiple gene transfer therapies. Liver targeted pre-clinical gene therapy trials are plentiful and there are now several commercially available liver targeted gene therapies including some using Adeno-associated virus (AAV) vectors [13]. Skeletal muscle has also been the subject of multiple pre-clinical trials and the first muscle targeted commercially available gene therapy was approved by the U.S Food and Drug Administration in June 2023 [14]. Though liver and muscle both have tissue-specific barriers to consider and overcome, they hold promise as target tissues to explore an AAV-mediated gene therapy for MSUD as novel, potentially curative therapy for this devastating disease.

1.2 Maple Syrup Urine Disease is a candidate disease for Gene Therapy

MSUD is a rare, inherited inborn error of amino acid metabolism with an unmet clinical need of a definitive cure. The underlying basis of the disease is secondary to biallelic genetic mutations in one of five autosomal genes required for the synthesis of BCKDH. BCKDH is critical in the metabolism of BCAAs and a deficiency causes their toxic accumulation and potentially irreversible central nervous system tissue damage and if untreated, death. MSUD is classified both clinically and genetically, based on the clinical phenotype and underlying genetic mutation respectively. Currently available treatments are limited to dietary protein restriction and/or liver transplantation. Without transplant, affected individuals remain at risk of episodic serious metabolic decompensations throughout their lives, especially during periods of metabolic stress, such as intercurrent illness, fasting, exercise or poor dietary compliance. Clearly, there is a clinical need to develop superior therapies for MSUD and gene therapy represents an advanced therapeutic strategy with enormous potential for this. Research efforts must be founded on a comprehensive understanding of pathophysiology, genetics and patient outcomes in MSUD and how these uniquely relate to currently available gene therapy platforms.

1.2.1 Maple Syrup Urine Disease is a rare condition

The incidence of MSUD is approximately 1 in 150,000 – 185,000 births worldwide and occurs across all ethnic groups [3, 15, 16]. In Australia, incidence is reported as 1 in 150,000 live births, equating to 1 to 2 new cases per year in the country [17]. Certain populations have higher disease incidence with associated founder mutations. In the North American Old Order Mennonite Christian community, a founder mutation in one of the causative genes for MSUD, *BCKDHA* (c.1312T > A, p.Tyr438Asn) is associated with the highest incidence of MSUD in the world,

affecting ~1 in 360 births with a carrier frequency of ~10% in some of these Mennonite communities [18-20]. A higher incidence of MSUD is also reported in some populations with higher rates of consanguinity for example in Kuwait, MSUD affects 1 in 60,000 births [21]. There have also been founder mutations documented in other culturally consanguineous populations including the *BCKDHB* gene in Ashkenazi Jewish communities in New York [22], and in the *BCKDHA* gene in Portuguese cigano (Roma) communities [23]. Although MSUD is a rare disease, researching findings in the pursuit of a novel advanced therapeutic strategy for MSUD may be more broadly applicable across other metabolic genetic conditions and thus important overall in the field of gene therapy.

1.2.2 Historical context of Maple Syrup Urine Disease

Maple syrup urine disease was described relatively recently in medical history, with the first described cases in the English literature attributed to the Austrian-American physician Dr John Menke, 70 years ago [24]. An established neurologist and budding playwright, Menke encountered a family in Boston, U.S.A and observed over a period of 8 years that all 6 infants born to these parents were well, however one girl and three boys were then became affected by a "*progressive familial neurological dysfunction with an unusual urinary substance*" and succumbed by 2 weeks of life after deterioration in their '*mentation, feeding and muscle tone progressing to opisthotonos, irritability and death"* [24]. Most peculiarly, their urine smelt like maple syrup. Menke and his team published their findings in *Pediatrics* in November 1954 titled: "A new syndrome: progressive familial infantile cerebral dysfunction associated with an unusual urinary substance". With the benefit of genetic diagnostics and functional enzyme studies, we now know that Menke had cared for a family of children with classical MSUD, the most severe form of the disease and he elegantly described the typical tragic rapid, fatal neurodegenerative natural history that befalls affected children without contemporary medical interventions.

1.2.3 Pathophysiology of Maple Syrup Urine Disease

1.2.3.1 Altered BCAA metabolism in MSUD is secondary to BCKDH enzyme deficiency

Disturbance in BCAA homeostasis underpins the pathophysiology and disease phenotype in MSUD. The BCAAs, isoleucine, leucine and valine are a group of three, essential amino acids characterised by an alpha amino group, an alpha carboxylic acid group and an aliphatic carbon chain with a branch, (Figure 1-1). These hydrophobic amino acids fulfil important biological roles in proteinogenesis, protein structure, glucose metabolism and cell signalling. They can either be metabolised through oxidation by BCKDH or shuttled though anabolic pathways to build proteins.

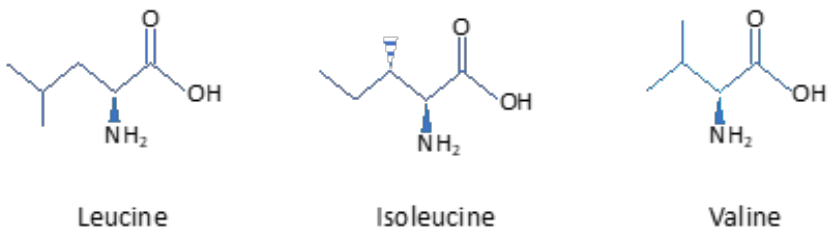

Figure 1-1 Chemical structure of the Branched Chain Amino Acids: leucine, isoleucine and valine. Blue lines represent carbon-carbon bonds, O (oxygen), H (hydrogen) and N nitrogen atoms bound covalently. A dashed wedge represents a bonded methyl group going into the plane, a solid wedge represents a bonded amine group coming out of the plane.

BCAA are essential amino acids in humans. They are found in protein-rich foods and make up approximately 20-25% of most dietary proteins [4]. Leucine is the most abundant branched chain amino acid and comprises 8% of human tissue protein. Upon ingestion, BCAA are absorbed from the intestine via the portal circulation into the systemic circulation where they can be utilised for cellular functions. When there is protein breakdown or excess BCAA, a two-step process degrades BCAA and then shuttles the metabolites into the tricarboxylic acid cycle (TCA) for cellular energy

generation (Figure 1-2). The three BCAA have distinct roles in protein catabolism and anabolism. Leucine is ketogenic, valine is glucogenic, and isoleucine is both glucogenic and ketogenic.

1.2.3.2 Normal metabolism of BCAA is reliant on BCAT and BCKDH

Metabolism of the three BCAA occurs in parallel and is dependent upon two enzymes: branched chain aminotransferase (BCAT) and BCKDH (Figure 1-2). BCKDH maintains tight stoichiometric relationships between the three BCAA, with plasma concentrations (μmol/L) of valine:leucine and leucine:isoleucine conserved at 2.0 across diverse biological states including overnight fasting, protein loading and catabolism during illness. In MSUD where BCAA homeostasis is disturbed, these ratios are not maintained and vary by several orders of magnitude [20, 25]. Interestingly, BCAA largely escape first-pass hepatic catabolism, likely due to the relative reduced expression of BCAT in hepatocytes [26, 27]).

1.2.3.3 Branched chain Amino Transferase initiates BCAA catabolism

The first step in BCAA catabolism is the readily reversible transamination of BCAA catalysed by the pyridoxal phosphate-dependant enzyme BCAT [28]. BCAT exists in two forms, cytosolic BCAT-1 and the more ubiquitous mitochondrial BCAT-2. These isoforms have 53% homology but differ in cellular location and tissue expression. Tissue expression of BCAT is primarily extra-hepatic and predominantly in skeletal muscle with some expression in fat, renal, intestinal, cardiac and neural tissues [26, 29]. Utilising α-ketoglutarate, BCAT converts leucine, isoleucine and valine to their respective branched-chain α-ketoacids: α-ketoisocaproate (KIC), α-keto-beta-methylvalerate (KMV) and α-ketoisovalerate (KIV).

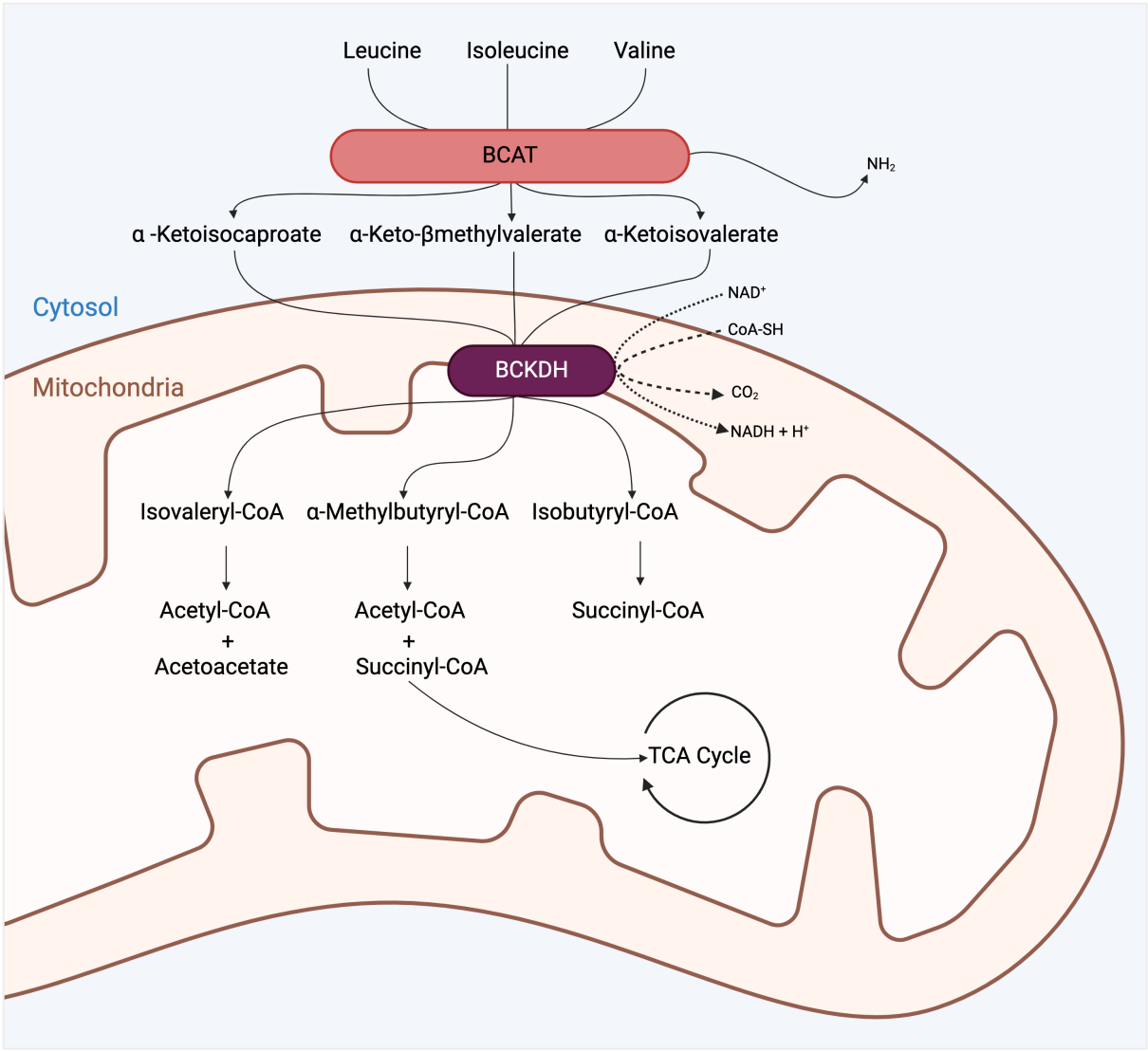

Figure 1-2 Cellular Metabolism of Branched Chain Amino Acids by cytosolic BCAT and the mitochondrial enzyme BCKDH. Abbreviations**:** BCAT, Branched chain Aminotransferase; BCKDH, Branched chain ketoacid dehydrogenase; Co-A, coenzyme-A, NAD^+/NADH, Nicotinamide adenine dinucleotide with and without hydrogen; NH_2, amine group. Figure made with BioRender.

1.2.3.4 Branched chain ketoacid dehydrogenase commits BCAA to the degradation pathway

BCKDH performs the second and irreversible step in BCAA metabolism, committing BCAA carbon skeletons to the degradative pathway [30]. The BCKDH complex is a 4-5 million Dalton (D) hetero-tetramer enzyme located on the inner mitochondrial membrane. The BCKDH hetero-tetramer consists a 24-meric cubic core of E2 (46.7 kD) subunits surrounded by approximately 6 to 12 copies of the E1 component (made up of two E1α and two E1β subunits, 45.5 kD and 37.8

kD respectively) and a dimeric E3 subunit (110 kD). A small number of E1 specific kinase and E1-phosphatase subunits also form part of the functional quaternary structure (Figure 1-3) [31, 32]. The catalytic subunits E1a, E1β and DBT are translated from genomic DNA as precursor proteins with a leading transit sequence of 44, 50 and 61 amino acids respectively, serving as a mitochondrial targeting signal [33]. These transit sequences are then cleaved to make mature peptides of 400, 342 and 412 amino acids long respectively. Once the subunit proteins are imported into the mitochondria, chaperonins are presumed to assemble the complex into the multienzyme BCKDH complex [34].

The catalytic subunits are held together through non-covalent interactions. Several important associated binding sites exist for each subunit with thiamine pyrophosphate acting as a prosthetic group for E1β with two additional potassium binding sites integral to the subunit structure [31]. Lipoic acid acts a prosthetic group for the E2 subunit, which contains three independently folded domains including an internal subunit-binding domain, an N-terminal lipoyl-bearing domain and a C-terminal inner core catalytic domain. The E2 domains associate through flexible hinge regions rich in proline, alanine and other charged residues [35]. Flavin adenine dinucleotidase acts as a prosthetic group for E3, however E3 is only loosely bound to DBT core, evidenced by the ready loss of this subunit during *in vitro* protein extraction and purification protocols [36].

Once assembled, BCKDH performs the rate limiting step in BCAA metabolism and irreversibly decarboxylates KIC, KMV and KIV producing Isovaleryl-CoA, α-Methylbuturyl-CoA and Isobutyryl-CoA respectively. These metabolites are then further metabolised to Acetyl-CoA, Acetoacetate and Succinyl-CoA feeding into the tricarboxylic acid cycle to generate the cellular energy currency, ATP. Each subunit performs critical steps in this process, with the E1 subunit, made up of E1α and E1β, decarboxylating the alpha-keto acids generated by BCAT. The remaining acyl group is then transferred to the lipoamide cofactor bound to E2. The complex core, made by

the repeat E2 subunits, catalyses the transfer of the acyl group from lipoamide to Coenzyme-A. This forms acyl-CoA and reduced lipoamide. Lipoamide is then regenerated by the E3 component by oxidation using bound FAD cofactor and the electron acceptor NAD^+ [31, 35, 37].

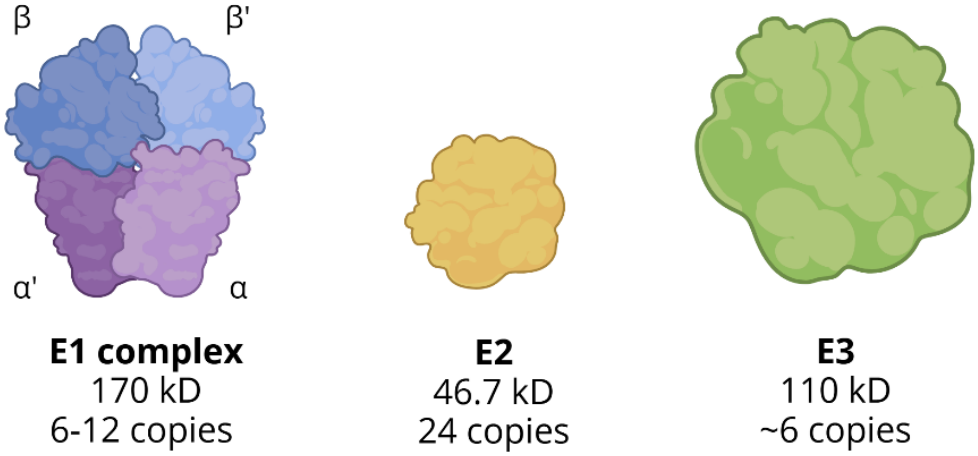

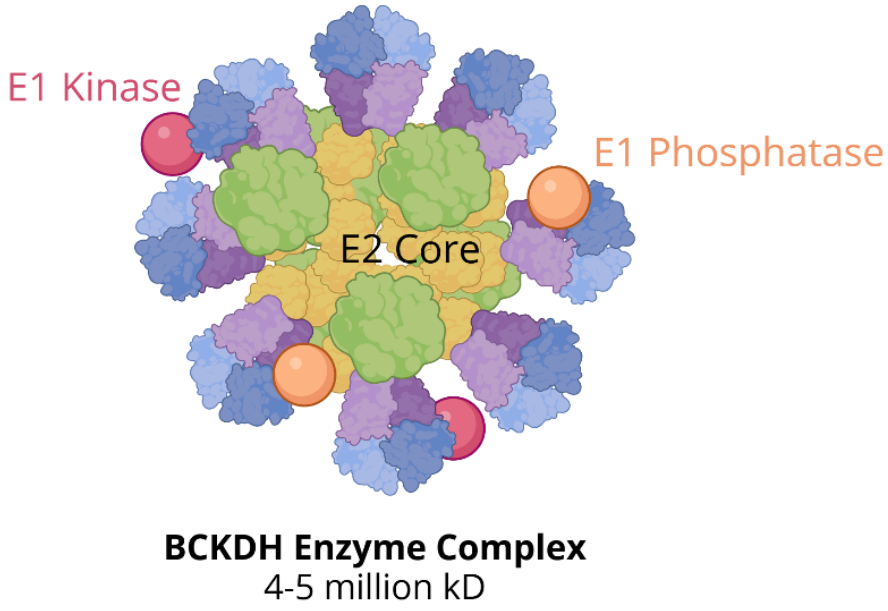

Figure 1-3 Protein structure of branched chain ketoacid dehydrogenase. The large complex branched chain ketoacid dehydrogenase complex (BCKDH) is made up of 6-12 copies of the E1 complex, which itself made up of two orthogonally oriented E1α units and two E1β subunits, 24 E2 units arranged in a central core and around 6 E3 dimers. E1 kinase (also known as PPMK1) activated the complex at several E1 complex attachment sites and E1 phosphatase (also known as BCKDHP) inactivated the BCKDH enzyme complex. Figure made in BioRender, adapted from Ævarsson *et al.* [31].

1.2.3.5 Branched chain ketoacid dehydrogenase enzyme is tightly regulated

Existing in both active and inactive forms, BCKDH activity is regulated by both covalent and allosteric interactions [38, 39]. BCKDH enzyme activity is primarily regulated by the phosphorylation state of the assembled E1 subunit. Phosphorylation by E1 Kinase (also known as BCKDHK) renders BCKDH inactive and conversely E1-phosphatase (also known as PPM1K) activates the complex [40] [41, 42]. E1 Kinase is allosterically inhibited by KIC and to a lesser degree by other α-keto acids and BCAAs, allowing for upregulation of BCKDH activity when substrate abounds.

BCKDH enzyme kinetics are linear and exhibit classical competitive substrate inhibition. The BCAA and their corresponding ketoacids all have similarly optimised pH and temperature activation curves [43, 44]. This mechanism provides rapid modulation of enzyme activity which can occur over seconds to minutes [4, 12]. As the most abundant subunit, *DBT* gene expression of the E2 subunit is also rate limiting for total BCKDH function although overexpression of a subunit does not translate to increased enzyme production due to the stoichiometric ratio requirements [45]. Additionally, during *in vitro* BCKDH activity assessment, the E3 subunit becomes functionally rate limiting due to the dissociation of this subunit from the BCKDH complex during protein purification and additional E3 must be added to BCKDH enzyme activity assays [46].

BCKDH enzyme activity is also influenced by various substrates, co-factors and other small molecules. The Michaelis constant, K_m, *i.e.,* the amount of substrate necessary for any enzyme to function at half the maximal velocity, for isoleucine, leucine and valines respective ketoacids KMV, KIC and KIV are 14, 15 and 28 μM respectively [47]. Rate limiting cofactors include NAD^+, co-enzyme A (CoA), thiamine pyrophosphate and magnesium, and an absence of any of these results in reduced enzyme activity [46]. Furthermore, the ratio NAD to $NADH^+$ and CoA to acyl-CoA

also contributes to flux of BCAA through BCKDH, with increasing concentration of the $NADH^+$ and acyl-CoA inhibiting BCKDH activity [26]. ATP also inhibits BCKDH activity, illustrative of the negative feedback of this metabolic pathway's end product and the dependant relationship BCKDH activity has with catabolism and anabolism [38, 48] (Figure 1-2).

Physiological states also influence BCKDH activity. Higher levels of dietary protein proportionally increase BCKDH activity [49]. Conversely, low protein diets correlates to increased BCKDH phosphorylation and thus a reduction in hepatic BCKDH activity [46]. Furthermore, studies in rats suggest that once 75% of leucine dietary requirement was met rates of leucine oxidation were found to have increased [4]. Extrapolating this concept in a teleological sense, this means that when leucine levels are low, the body is set up to conserve leucine for protein synthesis rather than catabolism [36]. Other physiological states that increase BCKDH activity include starvation and exercise. Endurance exercise increases BCKDH activity [11] which can be further augmented with repetitive exercise training leading to acute up-regulation. As this upregulation occurs so rapidly, it suggesting that post-transcriptional regulation of the BCKDH kinase is occurring, rather than increased genomic transcription [50]. Activating hormones of BCKDH include insulin, however this is thought to occur indirectly, as insulin increases protein catabolism and subsequently increases circulating BCAAs [51, 52]. Diurnal regulation of BCKDH has been observed in rats with overall activity highest during periods in darkness. It is not known if there are any diurnal changes in BCKDH activity in mice or humans. A gender difference was also observed with female rats having greater inactivation than male rates during light periods [53], however it is not known if this also occurs in humans or mice. It follows that these physiological states where BCKDH activity is upregulated also represent potential physiological triggers for metabolic decompensation in MSUD patients.

Physiological states that reduce the activity of BCKDH include resting [54], exposure to glucocorticoids and thyroid hormones [55]. This reduction in activity levels is brought about by increased kinase activity and thus downregulation of BCKDH activity [56]. Small molecule studies have shown the inducible nature of BCKDH also. Oxidation of BCAA also promoted by treatment of cells with carnitine due to mitochondrial acylcarnitine efflux [57]. Berberine, metformin and clofibric acid increase BCKDH activity states but their use has not been translated in a clinically significant manner applicable to MSUD patients [58] [59].

1.2.3.6 Alterative Leucine Degradation Pathway

Whilst the majority of leucine is metabolised via BCKDH, around 5% of leucine is oxidised via an alternative pathway catalysed by a cytosolic enzyme KIC-dioxygenase. KIC-dioxygenase converts KIC to β-hydroxy- β-methylbutyrate, which is then converted into a common metabolite with the main leucine degradation pathway and shuttled into the TCA cycle [60]. In the absence of BCKDH activity, the alternative leucine degradation pathway is not sufficient to maintain whole body BCAA homeostasis and unlikely to be able to be sufficiently upregulated with gene transfer technologies.

1.2.3.7 Accumulated leucine drives metabolic intoxication and neuronal damage in MSUD

BCKDH enzyme insufficiency results in disturbance of the normally tightly conserved stoichiometric ratio of leucine to isoleucine and valine to leucine, normally 2:1 and becomes grossly perturbed [25]. As a result, BCAA and their catabolic metabolites accumulate at biologically toxic levels leading to ketoacidosis and a characteristic clinical prodrome of muscle fatigue, lethargy, poor feeding leading to developmental delay, encephalopathy, coma and if untreated, death. Lactic acidosis occurs in E3-deficiency but is not usually observed in the other genetic types of MSUD.

Leucine is the culprit amino acid responsible for the deleterious neurological effects in MSUD [61]. Together with α-ketoisocaproate (KIC), leucine potentiates cerebral encephalopathy and critical brain oedema due to cerebral leucine influx via the *SLC7A5* transporter. Located on the blood brain barrier, *SLC7A5* is a selective transporter that is nominally saturated under standard physiological conditions. BCAAs compete with other neutral, zwitterionic amino acids, including alanine, phenylalanine, tryptophan and glutamine with uptake of individual amino acids directly proportional to their plasma concentration [62]. Thus, leucine concentrations are intimately linked with other essential zwitterionic amino acids and increased serum leucine levels lead to increased uptake into the CNS at the expense of other essential amino acids within the CNS (Figure 1-4).

For patients with MSUD, surges in plasma BCAA concentrations, such as after a dietary protein load or during a metabolic crisis, cause an exponential increase in cerebral uptake of leucine, isoleucine and valine, thereby displacing other critical amino acids from transport via *SLC7A5* into the brain. Acutely, this results in cerebral oedema, encephalopathy and if untreated permanent neurological injury or death. This imbalance is also precipitated by periods of catabolic stress, such as starvation, intercurrent infection or surgery. Indeed, infection was the most common precipitant of metabolic decompensation in a North American cohort study and most frequently occurring throughout childhood [20].

Leucine is also a neurotoxic molecule and affects the regulation of water homeostasis in the subcortical grey matter causing cell swelling and dysfunction. Toxic levels of leucine also increase oxidative stress, alter nitrogen homeostasis resulting in further depletion of glutamate, and compete with other amino acids such as tyrosine, which is involved in CNS protein signalling. Over time, this process is also thought to lead to chronic imbalances in brain amino acids and neurotransmitters, leading to heightened risk of intellectual disability, impaired executive function and risk of developing psychiatric disorders in MSUD affected individuals [63].

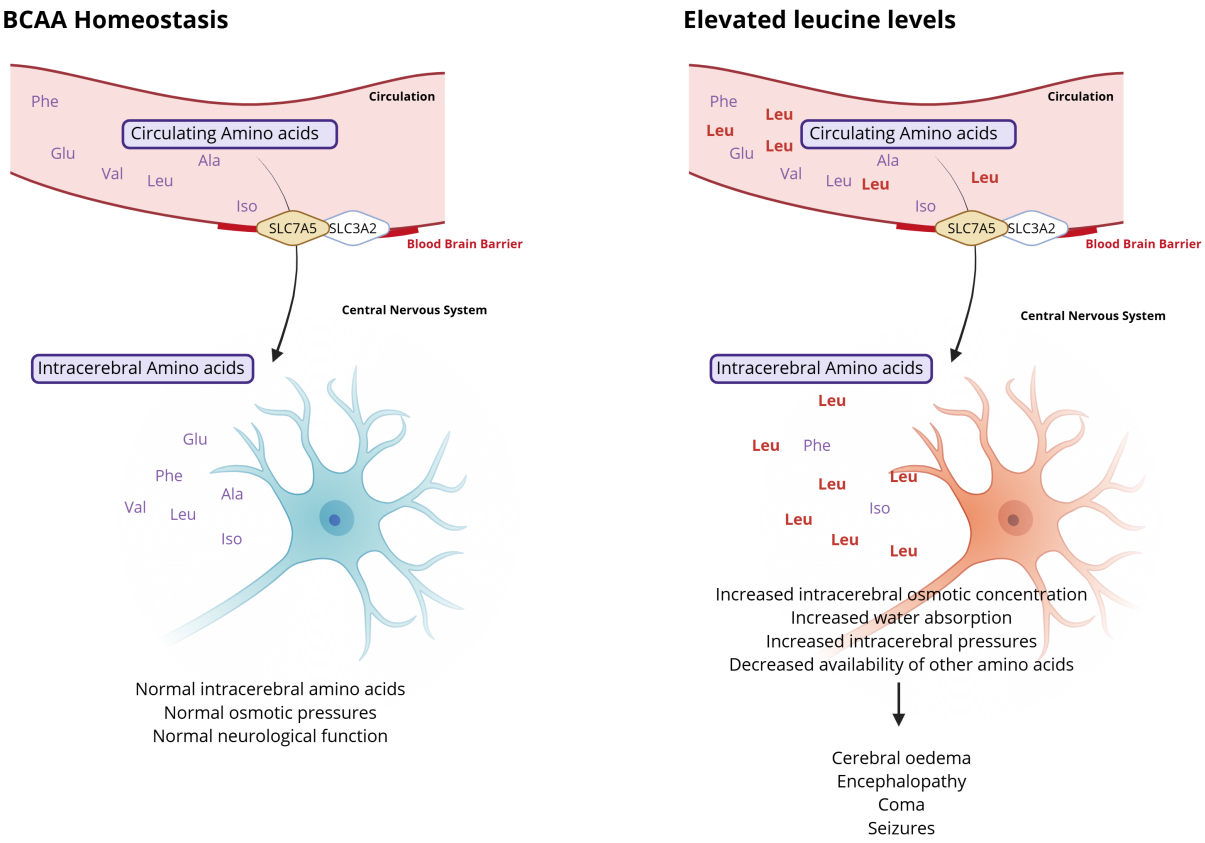

Figure 1-4 Leucine influx through the SLC7A5 transporter is implicated in the cerebral pathogeneiss of MSUD. SLC7A5 transports amino acids into the central nervous system. Increased concentrations of serum leucine levels result in heightened uptake of leucine by the central nervous system and lead to central nervous system symtpoms of encephalopathy, coma and seizures. Abbreviations Al (alanine), Glu (Glutamine), Iso (Isoleucine), Leu (leucine), Phe (phenylalanine), Val (Valine). Figure generated with BioRender.

1.2.4 MSUD clinical phenotypes, classification and presentation

There is a clear relationship between clinical presentation, severity and residual enzyme activities of the BCKDH complex. Definitive classification of MSUD patients with respect to clinical phenotype and underlying genotype as well as understanding the specific degree of enzyme deficiency in any individual will be critical for inclusion in gene therapy clinical trials. Important for numerous reasons, these metrics have proven critical in not only predicting potential therapeutic benefit of any new gene therapy strategy for MSUD but also allow for the effect of a gene therapy to be measured and will also inform the risk benefit profiles of these therapies.

1.2.4.1 Classical MSUD is the most severe and commonest MSUD phenotype

Classical MSUD is the most common form of MSUD and represents the most severe and metabolically volatile phenotype. Classical MSUD presents in the first few days of life in an otherwise normal infant and individuals with Classical MSUD typically have <4% of normal BCKDH enzyme activity [20]. With transition to extrauterine life and commencement of enteral feeding, the affected infant's capacity to metabolise BCAA is exceeded and ketonuria, dystonia, irritability, vomiting and feeding difficulties develop with the first 48 hours of life. As the ketoacidosis worsens, infants develop further neurological impairment characterised by increasing irritability, lethargy, opisthotonus, apnoea, seizures and without intervention can progress to brain herniation. This process has been designated "metabolic intoxication" and is a medical emergency. If untreated, and sometimes despite treatment, permanent neurological impairment ensures and if severe enough, leads to cardiorespiratory arrest and death [64, 65]. With the institution of a protein restricted diet and supportive therapy which aims to limit catabolism, BCAA levels can normalise. States which favour catabolism, such as exercise, fasting, illness or surgery, may disrupt this balance causing a metabolic decompensation.

1.2.4.2 Intermediate and intermittent MSUD

Intermediate MSUD presents slightly later in infancy and early childhood with enzyme levels approximately 5 to 30% of normal BCKDH activity [66]. Intermediate MSUD can present at any age with higher levels of residual BCKDH activity associated with later presentations [67]. This phenotype is less severe than Classical, and individuals present with milder spectrum of symptoms including irritability, dystonia, seizures and variable developmental delay. Rarely, intermediate MSUD patients have metabolic decompensations, however they can present with episodic ketoacidosis and life-threatening metabolic decompensation reminiscent of Classical MSUD. In between episodes, patients are well with normal growth and development. Intermittent MSUD is

characterised by episodic metabolic decompensation of variable severity ranging from mild to life threatening, usually in response to intercurrent illness presenting outside the neonatal period interspersed by periods of normal health [66, 68].

1.2.4.3 Rarer forms of MSUD

'Thiamine-responsive' MSUD is associated with mutations in either E1β or E2, with residual enzyme activity of 30-40% improved with thiamine supplementation [69]. These patients generally also require dietary management and rarely respond to thiamine supplementation alone. E3-deficient MSUD is equally rare and presents with lactic acidosis, raised liver transaminases, prolonged prothrombin time and myoglobinuria as well as the associated ketoacidosis and symptoms of intermediate MSUD [70]. Demonstrably, E3-deficiecny is a phenotypically distinct disease from MSUD with a highly variable disease course of persistent metabolic acidosis, elevated branched chain amino acids, progressive neurological injury and developmental delay. Affected infants typically present in the neonatal period with a variable clinical course, most often characterised by severe developmental delay and early demise [71].

1.2.4.4 Sotolone causes the characteristic urinary aroma in maple syrup urine disease

As the disease name suggests, a maple syrup odour was first observed in the index patients in the 1950's [24]. This urinary odour occurs due to the presence of 4,5-dimethyl-3-hydroxy-2[5*H*]-furanone, also known as sotolone [72]. Sotolone is an aromatic chiral substance formed from α-ketobutyric acid and at high concentrations is reminiscent of burnt sugar, maple syrup, fenugreek or curry leaves. Fenugreek seeds, from the plant *Trigonella foenum graecum L* are widely in Eastern and Mediterranean cultures as medicine and a galactagogue. Curiously, there have been multiple case reports of "spurious" or "pseudo" maple syrup urine disease in an infant's whose mothers had ingested fenugreek seeds during labour, leading to the presence of urinary sotolone and the

false suspicion of MSUD. Serum testing subsequently demonstrated normal BCAA and L-alloisoleucine levels however these cases served as excellent olfactory training tools for the involved clinical staff [73-75]. There are no reported cases of excessive maple syrup ingestion altering urinary aroma in BCKDH replete individuals.

1.2.5 Newborn screening allows for early diagnosis and improved prognosis in MSUD

MSUD is diagnosed clinically and with identification of supportive biomarkers. Patients with classical MSUD display characteristic symptoms and exhibit ketoacidosis with grossly elevated serum levels of leucine, valine and isoleucine early in life. The ratio of isoleucine:leucine:valine is normally tightly controlled in a 1:2:3 ratio, however in MSUD the gross elevations in leucine disturb this ratio such that leucine:valine is >1 [25]. Serum L-alloisoleucine concentrations are also elevated. L-alloisoleucine, a by-product of re-transaminated isoleucine metabolites [76] is the most sensitive biomarker of disturbed BCAA metabolism and elevation alone is sufficient for a biochemical diagnosis of MSUD [77]. L-alloisoleucine levels in neonates rise more slowly compared to the other BCAA however and may not be elevated until after six days of life. MSUD patient's also have a characteristic urinary organic acid profile with elevated ketoacids and succinate levels. Heel prick bloodspot testing via mass spectrometry for BCAA metabolites is the mainstay of early diagnosis and early intervention. With the opportunity for early intervention and a medical system that can provide intensive care support and monitoring required for MSUD patients, it follows that in countries with established newborn screening programs outcomes for MSUD patients are superior to those without [78]. If an advanced therapeutic such as gene therapy became available for paediatric MSUD patients, medical stabilisation would take precedence and then gene therapy could potentially be initiated.

1.2.6 Characterising the genetic basis of MSUD has implications for developing a genetic therapy

1.2.6.1 MSUD is genetically heterogenous

Understanding the underlying genetics of a disease such as MSUD is critical for informing the design of any novel advanced therapeutic intervention. MSUD is inherited in an autosomal recessive pattern and affects both genders equally. Affected individuals have biallelic defects in any of the four autosomal genes required to make protein subunits for BCKDH (*BCKDHA*, *BCKDHB*, *DBT* or *DLD*) or a fifth autosomal gene involved in BCKDH regulation *PPM1K*. Mutations must be biallelic and thus affected individuals are either homozygous or compound heterozygous in pathogenic mutations for one of the involved genes. The autosomal genes *BCKDHA*, *BCKDHB*, *DBT* and *DLD* correspond to the BCKDH protein catalytic subunits E1-α, E1-β, E2 and E3 respectively. *PPM1K* encodes for a mitochondrial serine/threonine phosphatase essential in the nutrient-induced upregulation of BCKDH activity [79, 80].

1.2.6.2 Genetic subtypes of MSUD

Genetic subtypes of MSUD are classified according to the underlying affected alleles, with MSUD Type 1a, 1b and 2 corresponding to mutations in *BCKDHA*, *BCKDHB* and *DBT* respectively (**Table 1-1**). Classification of genetic mutations has been undertaken, with the predicted pathogenicity of an underlying mutation, *i.e.,* large deletion or frame shift mutation or splice mutations causing non-functional subunit and thus non-functional BCKDH protein correlating with disease severity. There is no known whole genotype-phenotype correlation however between types 1a, 1b or 2, *i.e.,* type 1a does not have features distinct from type 1b, rather severity of clinical phenotype solely dependent on residual enzyme activity caused by the underlying mutation [81].

Table 1-1 Maple Syrup Urine Disease Genotypes

MSUD Type	Affected Gene	Affected Protein	Gene Location	Coding sequence length	Subunit affected
1a	*BCKDHA*	Branched chain ketoacid dehydrogenase E1, alpha polypeptide	19q13.1-2	1338 or 1335 bp	E1-alpha
1b	*BCKDHB*	Branched chain ketoacid dehydrogenase E1, β polypeptide	6q14.1	1179 bp	E1-β
2	*DBT*	Dihydrolipoamide branched chain transacylcase E2	1p21.2	1449 bp	E2
E3 deficiency	*DLD*	Dihydrolipoamide dehydrogenase	7q31-32	1530 bp	BCKDH - E3 subunit Pyruvate dehydrogenase alpha-ketoglutarate dehydrogenase
PPM1K deficiency	*PPM1K*	Activating kinase of the BCKDH complex	4q22.1	1941 bp	BCKDH complex
Thiamine responsive	*BCKDHB* or *DBT*	Branched chain ketoacid dehydrogenase E1 β polypeptide *Or* Dihydrolipoamide branched chain transacylase E2	6q14.1 *or* 7q31-32	1179 bp *or* 1449 bp	E1-β Or E2

Rarer MSUD genotypes E3-deficiency and *PPMK1*-deficiency have slightly different clinical phenotypes. E3 mutations have carrier rates of between 1:94 to 1:110 in Ashkenazi Jewish populations and a population incidence of around 1:35,000 to 1:48,000 and rarely outside these populations [82]. The E3 subunit is common to three mitochondrial enzyme complexes: BCKDH, pyruvate dehydrogenase and alpha-ketoglutarate dehydrogenase complex. Patients with E3-deficiency MSUD have raised BCAA alongside a metabolic lactic acidosis and typically die in early infancy [83]. *PPM1K* deficiency MSUD has also been reported to give a milder phenotype than classical MSUD and is very rare with only two case reports. In one case report total BCKDH enzyme activity was determined at 35% normal, inferring that a *PPMIK*-deficiency did not render the BCKDH enzyme entirely inactive [84]. There is also a thiamine responsive variant, involving

mutations in *BCKDHB* or *DBT* which presents similarly to typical MSUD, however responds to supplementation with thiamine.

1.2.6.3 MSUD Genotype prevalence

Excepting Mennonite populations in North America and a recent review from China [9], MSUD genotype prevalence has not been well characterised. One North American study, which excluded Mennonite Christians and thus a significant proportion of *BCKDHA* mutations, estimated that mutagenesis in *BCKDHB* accounted for 38% of cases, followed by *BCKDHA* at 33% and DBT at 19% and 10% unknown [5]. Reviewing the Human Gene Mutation Database demonstrated that *BCKDHA* with 122 listed mutations (34%), *BCKDHB* 144 mutations (40%), *DBT* 89 (25%) and *PPMK1* 6 mutations (2%) (Human Gene Mutation Database, https://www.hgmd.cf.ac.uk, accessed 29th March, 2025) [85]. Whilst useful, these databases do not account for frequency of these mutations in MSUD patients, representation within ethnic groups nor account for homozygosity or compound heterozygosity. Reviewing mutations across available published literature revealed 293 MSUD patients with a total of 212 allelic mutations across *BCKDHA*, *BCKDHB* and *DBT* [5-7, 69, 83, 86-114]. Across these reported genotypes, *BCKDHB* has the greatest number of reported mutations across the gene (n = 85, 40%), followed by *BCKDHA* (n = 83, 39%) and *DBT* (n = 44, 21%). Whilst not reflective of the population genotype prevalence or frequency, it is illustrative of the genetically heterogenous basis of MSUD and the need for novel treatments to either be mutation agnostic or tailored to specific patient genotype.

1.2.6.4 Genetic polymorphism in BCKDH subunits

The amino acid sequences of the mature catalytic E1α, E1β and E2 subunits have a high degree of conservation between species as well as between corresponding subunits of the α-ketoglutarate and pyruvate dehydrogenase mitochondrial complexes [115, 116]. There are several reported

polymorphisms in humans for BCKDHA genes corresponding to the E1α protein subunit, which has three variants. Two variants are 1338 bp in length (variant 1 and 3) and one 1335 bp (variant 2). Variant 3 has a point substitution at c.997C>T which conserves the amino acid residue, phenylalanine [117, 118]. Relative to variant 1 and 3, Variant 2 is shorted due to a missing alanine residue at codon 856 [119].

1.2.7 Tissue expression of Branched chain Ketoacid Dehydrogenase

Considering the tissue expression of BCKDH is imperative in understanding potential tissues targets and developing a targeted, clinically relevant gene therapy for MSUD. The genes corresponding to the BCKDH subunits are ubiquitously expressed in most cell types, though expression varies between species and organs (Figure 1-5) [30]. The exact percentage which various organs contribute to BCKDH activity and BCAA oxidation has only been characterised in a handful of papers, and data from the original study reviewing BCKDH activity in humans, rats and monkeys used to extrapolate organ contributions to total body BCKDH activity [10, 11, 30]. The relative tissue contributions to BCKDH enzyme activity in mice was not known until recently when C^{13} was used to measure relative organ contributions to isoleucine oxidation and infer total BCKDH activity [12] (Figure 1-5).

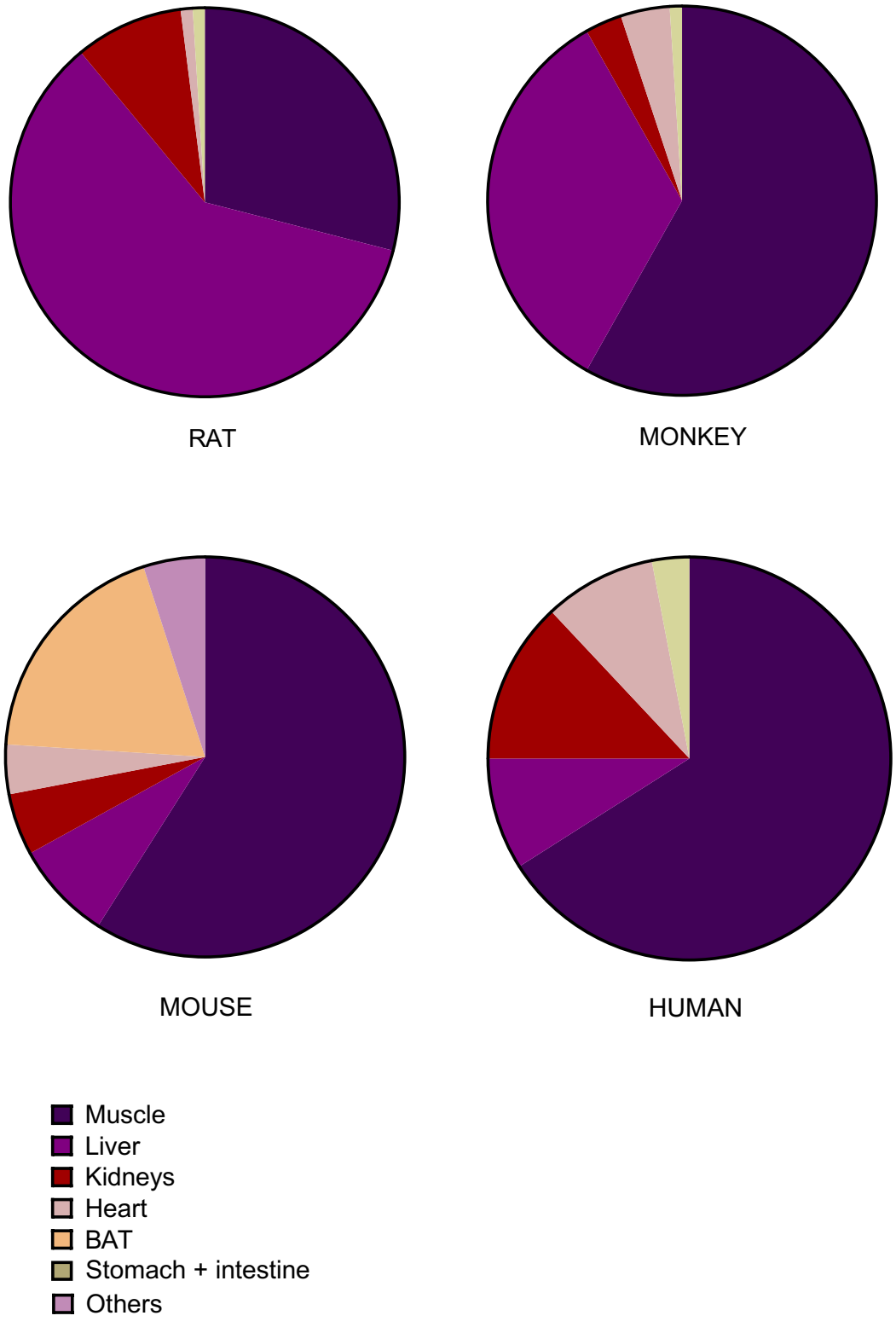

Figure 1-5 Interspecies differences in organ contributions to total body branched chain ketoacid dehydrogenase enzyme oxidation. Tissue distribution of BCKDH in monkey, rat, human [10, 30] and mouse [12]. Abbreviations: BAT, brown adipose tissue.

Organ specific BCKDH contributions varies considerably between humans, mice, rats and monkeys (Figure 1-5). In humans, monkeys and mice, skeletal muscle activity predominates, and accounts or 66%, 59% and 57% respectively of total body BCKDH oxidation. Conversely, in rats, only 29% of total body BCKDH activity is found in skeletal muscle. The liver accounts for approximately 9% in of total body BCKDH activity in humans, 8% in mice, 33% in monkeys and 60% in rats [12, 30]. Furthermore, in humans and mice, adipocytes, neural and renal tissue also contribute to BCKDH [10]. This inter-species variation led to speculation that significant inter-organ shuttling of BCAA metabolites occurs in order to maintain total body BCAA homeostasis [30].

Blood flow to organs and relative body weight also requires consideration when evaluating the relative activity of BCKDH across solid organs and the relative percentage of BCAA each organ accounts for. For example, skeletal muscle has lower activity but higher percentage overall body mass (35-40%) so metabolises relatively more of BCAA compared with cardiac tissue, where enzyme activity is much higher in a much smaller organ by mass [36]. It is likely that each organ contribution to BCKDH is also dynamic, with changes in blood flow and various regulatory metabolites changing relative amounts of active BCKDH in a particular organ in various physiological states [52].

This inter-species variation of organ contribution to BCAA oxidation and dynamic activation of the BCKDH enzyme may require careful consideration in the exploration of novel treatments, like gene therapies for MSUD. Testing novel gene therapies *in vivo* typically is undertaken in pre-clinical murine or rat disease models followed by non-human primate studies. MSUD gene therapy strategies which target the liver, for example, may have their potential success in humans over or underestimated depending on the model system they are using and any relative corrections across different organs.

1.3 Contemporary Maple Syrup Urine Disease treatments are not curative

Currently available therapies for MSUD are not curative with the primary aim to reduce toxic levels of leucine and improve quality of life. Available therapies include dietary restriction, liver transplantation and efforts to avoid catabolism, where possible.

1.3.1 Dietary Therapy for Maple Syrup Urine Disease

Dietary therapy is the mainstay of treatment for MSUD with the primary and immediate goal to normalise serum branched chain amino acids and toxic metabolites. Secondary and long-term goals are to limit catabolism whilst promoting anabolism, monitor complete nutritional status and intake to facilitate normal growth, development and health maintenance. In addition, thiamine responsiveness is evaluated and if responsive, the individual supplemented with thiamine [120].

Dietary sources of BCAA are mostly from animal proteins including poultry, red meat, fish, and cow's milk [121, 122]**.** Near total dietary elimination of enteral leucine by avoiding these foods and careful supplementation with alternative sources of protein or infant formula is commenced as soon as infants are diagnosed. Children are also supplemented with *SLC7A5* substrate-enriched formulas and other amino acids supplements to promote normal growth, neurotransmitter balance and development [123].

Tight metabolic control is pursued thorough intensive blood monitoring, with an average of 64 blood tests performed in the first year of life in a North American cohort [20]. Ideally, plasma leucine concentrations should be between 75 – 200 μmol/L for infants and children ≤ 5 years old and between 75 – 300 μmol/L for patients older than 5 years of age. Absolute leucine ingestion by each patient will depend upon their residual BCKDH enzyme activity and age, with infants suffering from classical MSUD recommended to consume 40 – 100 mg/kg/day, decreasing to 35

– 65 mg/kg/day at between 4 to 8 years of age and then 15 – 50 mg/kg/day upon reaching adulthood. Children with intermediate MSUD or other less severe forms may tolerate higher daily intakes of leucine, however the serum BCAA level targets remain the same. These limits were suggested in order to achieve favourable cognitive outcomes, however even with good dietary compliance serum leucine levels often remain approximately double the upper limit of normal and metabolic decompensations can occur, hence the need for a novel, curative therapy [20].

1.3.2 Metabolic decompensations are a major source of morbidity for Maple Syrup Urine Disease patients on dietary therapy

In MSUD, a metabolic decompensation refers to a clinical deterioration in a patient where the therapeutic threshold of their ongoing therapy, *e.g.*, dietary, is unable to maintain BCAA homeostasis leading to elevated leucine, or leucinosis. Metabolic decompensations are driven by physiological states that induce catabolism, such as fasting or caloric deficiency, intercurrent illness, trauma or surgery. The most common triggers tend to be febrile illness, especially when oral intake is not maintained, such as with vomiting or gastroenteritis illnesses [20, 124]. Metabolic decompensations require swift identification, aided by measuring urinary ketones at home and instituting sick day plans with increased enteral feeding. However, even with swift recognition of a metabolic decompensation and sick day management institution, MSUD patients can deteriorate quickly and often will require hospital-based therapy for several days. In-hospital treatment may include oral, nasogastric or IV fluid supplementation as well as intravenous nutrition or blood filtration to reverse any catabolism, restore leucine levels, and prevent cerebral encephalopathy.

These hospitalisations can have a big impact on patients, their families and result in numerous missed work or school days. A retrospective European study observed a mean admission duration of 6.6 days when oral or enteral supportive management was required, and 5.4 days when IV nutrition or fluids was required [124]. These patients often need high levels of specialist care, and

in one American centre, the advent of specialist clinics has reduced hospital days per patient-years from 7 prior to 1988 to 0.25 in the following 7 years. Furthermore, the estimated cost of dietary therapy and associated medical care is not insignificant. For MSUD patients in the U.S.A the estimated cost of care was estimated at $US80,000 per ten years of follow up, representing a significant cost to the family. For most individuals with the most severe form of MSUD, Classical MSUD, thus requiring the most intensive treatment, the lifetime cost of nutritional management greatly exceeds costs associated with liver transplantation [20].

1.3.3 Liver Transplantation in Maple Syrup Urine Disease

Liver transplantation is an established rescue therapy for many in-born errors of metabolism (IEM) including MSUD [125]. The utility of liver transplant for IEMs lies in the genetically normal allograft's ability to freely exchange any toxic metabolites from other disease affected organs through the systemic circulation. In this way, the allograft can stabilise the phenotype to near normal as seen for MSUD liver transplant recipients, or significantly improve the phenotype, such as in ornithine transcarbamylase (OTC) deficiency. Transplantation is often a second line therapy offered to patients who experience recurrent life-threatening metabolic decompensation in order to either avoid or effectively ameliorate serious health and neurodevelopmental risks associated with decompensations [126].

Originally, liver transplantation in IEM was limited to disorders with lethal outcomes, such as OTC deficiency. As the risks of transplant procedure have improved with advancement of surgical techniques and refinement of immunosuppressive regimens, the paradigm of suitable transplant candidates has evolved to include a wider range of IEM with heighted disease complexity and distinct risk benefit profiles [127]. Currently, in Australia and North America, IEM is the second most common indication for paediatric liver transplantation [128, 129]. Case studies of MSUD transplant series in Australia and North American centres describe 100% patient survival at 1 year

post-transplant, though complication rates, including re-transplantation for MSUD patients vary and longer-term studies are required to further understand long-term outcomes [20, 125].

For MSUD patients, clinical indications for liver transplant include brittle metabolic stability, difficulties with dietary compliance and poor patient quality of life secondary to recurrent hospitalisation [125]. For these patients, liver transplant is offered to both improve metabolic stability and with that, improve quality of life [130]. Whilst pre-transplant neurological injury is not reversible, transplant facilitates improvements in overall quality of life, dietary protein liberalisation and reduced hospitalisations from metabolic decompensation. In addition, chronic neurological impairment may also be arrested post transplantation [25]. In most cases, liver transplantation normalises serum levels of leucine, valine and isoleucine and prevents metabolic complications from typical precipitants. Whilst leucinosis can occur during metabolic stress post-transplant, the decompensations are milder and often respond to standard intravenous hydration therapy with no specific metabolic intervention, such as intravenous lipid therapy or haemofiltration, necessary [25].

Of particular interest, however, is that L-alloisoleucine levels fail to completely normalise in MSUD patients post liver transplant. In unaffected individuals, L-alloisoleucine levels are <2 μmol/L, contrasting the pathognomonic elevation in MUSD patients [77]. Whilst transplantation universally lowers L-alloisoleucine levels for MSUD patient's, serum L-alloisoleucine are often still elevated, albeit lower than pre-transplant [20, 131]. Conversely, in patients who receive a MSUD affected liver allograft, in a process known as a domino liver transplant, L-alloisoleucine levels remain undetectable. L-allosioleucine is a diastereomer of L-isoleucine and formed by the re-transamination of isoleucine metabolites. It is only present when there is a relative deficiency in total body BCKDH. This phenomenon suggests that whilst a liver graft does supplement total

body BCKDH and normalise serum leucine levels, subclinical abnormalities in BCAA metabolism persist in MSUD patients post transplantation.

Like any medical intervention, the benefits of transplantation also come with multiple risks. These risks include peri-operative metabolic decompensations, surgical complications, infection and life-long risk of organ rejection [132]. Rigorous immunosuppressive medication compliance is mandated, and the potential adverse effects of these medications are non-inconsequential, with heightened risk of skin cancer and post-transplant lymphoproliferative disease, a form of malignancy [131, 132]. Understandably, transplantation is limited to only the most unstable MSUD patients and benefits balanced carefully with the risks associated with this major surgery and ensuing life-long immunosuppression regimen. There is a clear opportunity to develop a novel therapy for MSUD which improves metabolic stability but avoids the associated risk of transplantation and associated immunosuppression. It is possible that gene therapy may be able to bridge this therapeutic gap.

1.3.4 Disease prognosis in individuals affected by MSUD

With adequate treatment, MSUD patients can live to adulthood and have normal life spans though are affected by the disease burden of a chronic condition [133]. Survival rates to adulthood in some centres have improved over the past half century, from around 70% to >95% and prognosis is described as good [20, 134]. Improvements in survival are nominally a reflection of successful newborn screening programs rather than any advances in actual therapies and has not been mirrored in other centres with developing health infrastructure. Childhood mortality rates from MSUD in resource poor countries such as the Philippines observed minor, if any, improvement over the past twenty years with 27% mortality rate improving to 24%-25% at two different centres [135, 136]. A study from China reported 77% mortality in MSUD patients with treatment non-adherence cited as the underlying cause [137].

Despite improvements in survival, care burden and disease-related morbidity remains significant for MSUD patients and their families and MSUD patients are at higher risk than many other patients with in-born errors of metabolism in developing permanent injuries from their disease [134]. Neurological injury is the most significant consideration with regards to morbidity and mortality in patients with MSUD and early detection and subsequent swift metabolic control of any and all metabolic decompensations is paramount to improve neurological outcome [64]. Some studies have demonstrated that neurological outcome is inversely proportional to the duration of elevated neonatal plasma leucine levels and also to the average leucine levels over the course of childhood: the higher the plasma leucine level, the poorer the neurological outcome [64, 138].

Again, newborn screening programs have contributed to early diagnosis and improved morbidity however in countries lacking the health infrastructure to support early detection programs, outcomes are undoubtedly worse with higher rates of mortality and intellectual impairment [21, 139]. Regardless of the health setting, MSUD affected patients score lower on IQ tests and are at high risk of developing affective psychiatric illnesses compared to age-matched siblings [20]. The emotional burden on families with a child with MSUD is high, with lower quality of life and associated high emotional and financial burden [140].

Pregnancy in classical MSUD females represents a significant physiological challenge secondary to the required growth and increased physiological stress on the mother's body resulting in heightened risk of metabolic decompensations. Multiple case reports have detailed successful pregnancy outcomes in women with Classical MSUD. Despite adequate medical support, a significant episode of metabolic decompensation with seizures occurred at the end of the first trimester in one MSUD pregnant patient. Psychometric and developmental testing on the infant 4 and 20 months of age was normal which suggested that maternal MSUD may not have a detrimental effect on developing unaffected foetuses [141].

Whilst prognosis has improved in resource-rich settings over the past half a century, significant morbidity remains with associated unacceptable mortality rates in resource poor settings. Clearly a therapeutic gap exists for MSUD and there is an opportunity and need to develop novel therapies which improve mortality and reduce burden of disease for patients and families.

1.3.5 Experimental therapies for MSUD have yet to prove clinically successful

The search for a novel treatment for MSUD has, as yet, been unsuccessful. Strategies including hepatocyte transplantation and small molecules therapy have been explored but none successfully translated to the clinic for MSUD patients. Hepatocyte transplantation in murine model has been explored as a way to circumvent transplant surgery. A single pre-clinical study demonstrated the utility of hepatocyte transplantation in the iMSUD disease model [142]. Affected mice received two injections of wildtype hepatocytes in the first ten days of life and had some improvements in serum BCAA but no change in serum leucine, improved survival, growth and liver BCKDH activity compared to saline injected affected mice. The overall effect was inferior compared to the phenotypic improvement provided by an autologous liver transplantation.

Metformin has been explored as an adjuvant therapy for MSUD, hypothesised to aid in the mitochondrial dysfunction caused by KIC accumulation. One study found metformin reduced KIC levels in patient derived fibroblasts and skeletal muscle of a murine MSUD disease model (iMSUD) with concomitant restoration of other mitochondrial metabolites, such as ATP [143]. There were also modest reductions in serum leucine in the metformin treated iMSUD mice, however the effect of metformin upon life span, which is shortened in disease affected mice, was not reported.

Berberine is another small molecule shown to interact with the metabolism of BCAA. In non-MSUD mice treated with berberine, BCAA catabolism was increased in liver and adipose tissue, however the exact mechanism by which berberine exerted this affect is not precisely known [144]. However, this small molecule has not been used in any pre-clinical MSUD disease models for comparison. It may be that utility of berberine lies in patients with normally functioning BCAT and BCKDH enzymes but who experience insulin resistance and life-style related dyslipidaemia. There are currently over 80 registered clinical trials exploring berberine and its effects on metabolic syndrome conditions like insulin resistance as well as general drug safety in humans (ClinicalTrials.gov).

Despite the above ventures in attempting to develop a novel therapy for MSUD, none have been translated clinically, and the unmet need for a definitive and curative therapy for MSUD persists.

1.4 Gene Therapy

Following the discovery of DNA by the Swiss scientist Friedrich Mieschner in 1869 [145], it would take almost another 75 years later until scientist Oswald Avery and his team unearthed DNA's critical role in encoding genes in 1943 [146]. In the application of DNA from one bacterial strain to another, Avery and his team demonstrated the "transforming" principle and this technique is still used by molecular biologists today. Russian scientist Phoebus Levene then discovered the components of a nucleotide (phosphate-sugar-base) [147] and Levene's work informed Erwin Chargaff and the development of "Chargaff's Rule" where the total number of purine bases in DNA equalled that of pyrimidines [148]. The exact structure of DNA as a molecule was still elusive until critical x-ray crystallography work undertaken by Rosalind Franklin and Maurice Wilkins [149] informed the discovery of DNA's structure, a three-dimensional double helix, published by James Watson and Frances Crick in 1953 [150]. These key sequential discoveries over almost a century finally confirmed the central role that DNA plays in molecular biology and inheritance.

Since the 1950's, advances in molecular biology and virology have helped conceptualise a new way to approach, diagnose and treat genetic conditions [150]. Dysfunctional genes account for 80% of the total 7136 diseases reported to date and more than 300 million people worldwide, over half of which are children, suffer from genetic diseases [151]. This gradual de-coding of the human genome, finally published in 2001 by Lander *et al.* [152] has resulted in an unprecedented opportunity to characterise individual genes and their respective roles in health and disease [152]. Whilst the way has been paved for increasing diagnostic sensitivity and specificity, advances in diagnostic sensitivity have yet to be met with a proportionate advancement in translational genomic therapies.

Contemporary gene therapy technologies are an evolving platform with the potential to meet this growing treatment demand. Gene therapy can be broadly classified by the vector delivery system, mechanism of therapeutic effect, *e.g.*, gene addition or gene editing, or the type of cells targeted, *e.g.*, *ex vivo* or *in vivo*. Vectors are used to package and deliver a genetic cargo of DNA or ribonucleic acid (RNA) and can encode genes or other genome manipulating machinery, including endonucleases. Coupled with a comprehensive understanding of a particular disease process, gene therapy represents an emerging biological therapy that has the potential to transform treatment approaches to genetic diseases currently considered incurable.

1.4.1 Origins of Gene Therapy

Gene therapy has origins in bacterial research from the early 1900s. Identification and refinement of the molecular biology principles of bacterial cell transformation [153] and transduction [154] led to the significant discovery that a genetic defect could be rescued through the transfer of foreign DNA in the 1940's [146]. This was the first time that gene transfer was shown to be potentially heritable and helped move the field towards the first human gene therapy trial in the 1970's, prior even to the development of recombinant DNA technology. This first gene therapy trial, differing vastly from contemporary rigorous pre-clinical testing standards, demonstrated that the Shope rabbit papilloma virus induced arginase expression *in vitro* and then attempted parallel experiments *in vivo* for three siblings with arginase deficiency [155]. Whilst ultimately unsuccessful due to protocol flaws and degraded virus, this paved the way to the first approved *ex vivo* human gene transfer study in 1989 [156].

The 1990's saw an explosion of gene therapy trials, however the relative knowledge gaps in scientific understanding of the viral vectors and host interactions were censured in a landmark report by Orkin-Motulsky in 1995 with a resounding recommendation to redirect funding towards basic research for this very purpose [157]. The emphasis on safety was further reinforced in 1999

after the devastating death of Jesse Gelsinger secondary to multiorgan failure 4 days post administration of an adenovirus vector in a clinical trial for ornithine transcarbamylase deficiency [158, 159]. The development of pre-malignant cellular proliferation reported in 2003 in two patients from the 2000 retrovirus SCID-X1 trial, only served to heighten safety concerns in the scientific and broader community [160-162]. Despite these relative setbacks, the field of gene therapy research persevered [163] and there are now 30 commercially available gene therapies and an ever-growing number of gene therapy clinical trials [13, 164].

The paradigm shift mandated by the Orkin-Motulsky report to increase research efforts into better understanding the disease and vector biology being exploited by gene therapy platforms highlighted several key challenges to overcome in order to improve the efficacy, safety and acceptability of these advanced therapeutics. Nominally, the development of improved vehicles, or vectors, as well as the development of animal models in which these experimental technologies and their effects could be studied. Orkin and Motulsky also called for researchers to further investigate the underlying disease mechanism that contributed to genetic disease, decrying the notion that simply replacing a faulty gene would be universally curative. They advocated for researchers to further characterise the genetic diseases and that all research should be undertaken with *"strict adherence to high standards of excellence"* [157]. Through this, extensive research efforts have focussed on gene therapy vector development as well as improving the precision of these vectors in achieving desired effects and understanding the acute and long-term risks of these technologies.

1.4.2 Vector Systems

Broadly, vectors can be classified as viral or non-viral in origin. Ideal vectors transduce desired target cells, *in vitro*, *in vivo* or *ex vivo*, and thereby successfully deliver genetic cargo without inciting pathogenic disease in the host organism. Vectors can be optimised for transduction efficiency, *i.e.,*

the rate of successful cell targeting and for maximal gene expression, depending on the target tissue type and model system used. Depending on the target tissue, vectors may also need to transduce quiescent or dividing cells. Considerable effort has been dedicated in the development of vectors with low immunogenic profiles, thus evading the host immune system, affording the flexibility of multiple doses for certain systems and also preventing the formation of neutralizing antibodies or life-threatening post treatment inflammatory syndromes [165].

1.4.2.1 Viral Vectors

The majority of gene therapy vectors are viral in origin, reflecting a naturally evolved, sophisticated delivery system capable of introducing foreign genetic material to human cells [166]. Through intensive research engineering, numerous viral genomes have undergone deliberate modification to generate recombinant, replication defective vehicles for packaging genetic therapies. By exploiting favourable biological properties, viral vectors can be designed to optimise tissue specificity, delivery location, genomic integration potential and immune system evasion. Viral vector systems can be DNA or RNA based and either single or double stranded in nature. Commonly used viral vectors in pre-clinical research include adenovirus, lentivirus, retrovirus, herpes simplex virus-1 and adeno-associated virus (AAV). These vectors have differences in the size of the genetic cargo that can be packaged as well as unique tropisms for tissue type and cell-cycle (Table 1-2).

Table 1-2 Commonly used viral vectors in pre-clinical and clinical research

Virus	Coating	Genome and packaging capacity (kB)	Infection status	Considerations
Adeno-associated virus (parvovirus)	Capsid	ss DNA or ds DNA <5 kB	Some emerging evidence AAV may be implicated in acute paediatric hepatitis [167].	Episomal [168]; neutralising antibodies on re-administration; dividing and non-dividing cells [166].
Adenovirus	Capsid	ds DNA 8 kB-36 kB	Inflammatory response	Episomal, dividing and non-dividing cells[166].
Herpes Simplex Virus-1	N/A	ds DNA >30 kB	Persistent latent state	Episomal loss after cell division; complex attachment and entry into cells [166].
Lentivirus (Complex retrovirus)	Lipid-enveloped	ss RNA <8 kB	Persistent	Integrating with long term transgene expression. Transduces non-dividing cells[169].
Simple retrovirus	Lipid enveloped	ss RNA <8 kB	Chronic infection	Transduction requires mitosis shortly after viral entry [166]. Latent disease risks insertional mutagenesis [160].

Abbreviations: ss (single strand), ds (double strand), kB (kilobases).

1.4.2.2 Non-viral vectors

Non-viral, or synthetic vectors have emerged as an alternative to viral vectors. In many ways these non-viral vectors replicate viral endocytosis to effectively 'transduce' a target cell and deliver a genetic product. These synthetic vectors are less immunogenic than viral vectors however their transfection efficiency is yet to prove superior [170]. Non-viral vectors currently being investigated include naked or plasmid DNA however these are often rapidly degraded and have low target tissue specificity [171]. More promising non-viral vectors include lipofection and a variety of lipid-based vectors such as cationic lipids, ionizable lipids and lipidoids, gene-lipid conjugates, and lipid

nanoparticles (LNP). These lipid based non-viral vectors transduce target cells through the enhanced permeability and retention effect [170]. This occurs over an extended period of time and thus engineered liposomes must have an enduring blood stream stability to allow for transduction events to occur [170]. LNP are functionalised particles engineered with modified tumour-specific ligands including anisamide [172], folic acid [173], iron-saturated transferrin [174] and arginyl-glycyl-aspartic acid (RGD) ligands [175] to enhance transduction and cell targeting efficiencies. Rational design strategies have been applied to enhance nuclear and cytoplasmic transgene delivery across these systems, similar to those seen in viral vector discovery and development [176].

1.4.3 Adeno-associated Virus Vectors

Recombinant adeno-associated virus (rAAV) vectors have emerged as a leading platform for *in vivo* gene therapy, spurred on by the landmark success in human clinical trials treating Haemophilia B [177]. Considered low risk of causing infection in humans, wildtype AAV is a *Dependovirus* of the Parvoviridae family and requires the assistance of a helper virus, such as adenovirus, herpes virus, human papilloma virus or vaccina virus, for replication [178-181]. Serendipitously discovered in laboratory adenoviral preparations in the early 1960's, AAV has since been found as a ubiquitous commensal in mammalian species including both human and non-human primates [182].

1.4.3.1 Adeno-associated viral vector Structure

AAV has a linear single stranded 4.7kb DNA genome, oriented both sense or anti-sense in equal frequency, packaged in a non-enveloped icosahedral protein capsid approximately 25 nm in diameter [181, 183]. AAV has two open reading frames (ORF), REP and CAP, flanked by two 145 base pair (bp) inverted terminal repeats (ITRs) (Figure 1-6). The REP ORF encodes four genes required for replication, Rep78, Rep68, Rep52 and Rep40 associated with the p5 and p19 promoters. The REP genes all have DNA helicase and ATPase activity and are also responsible for helping wildtype AAV to establish viral latency in host cells [184-187]. The CAP ORF encodes

the capsid proteins VP1, VP2 and VP3. Capsid proteins dictate tissue specificity and are transcribed in a 1:1:10 molar ratio of VP1:VP2:VP3. The CAP ORF also contains the assembly activating protein, which promotes virion assembly [188].

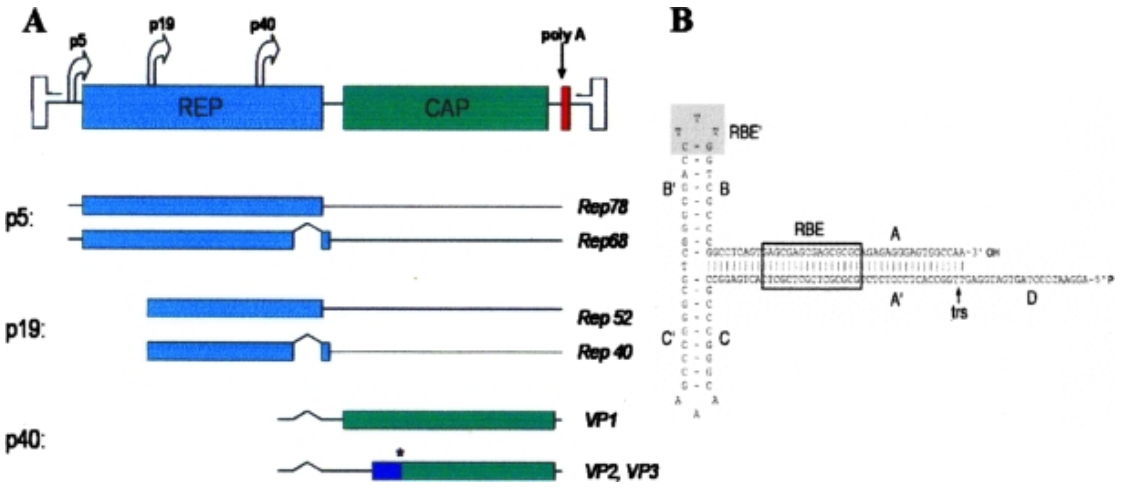

Figure 1-6 Genome of wildtype AAV. (**A)** Wildtype AAT genome demonstrating REP and CAP Open Reading Frames, the four replication genes Rep78, Rep68, Rep52, Rep40 and the three capsid genes VP1, VP2, VP3 and their respective promoters p5, p19 and p40. **(B)** Inverted terminal repeat secondary structure in AAV genomes. Figure adapted from Daya and Berns [188]

1.4.3.2 Adeno-associated virus as a gene therapy vector

Repurposing of AAV as a clinical vector has seen the replacement of the native viral genome with a therapeutic gene expression cassette and associated regulatory elements such as a Kozak consensus sequence [189], tissue specific promoters and a polyadenylation signal, flanked by the native AAV ITRs. Recombinant AAV (rAAV) can accommodate gene assemblies <5 kb, constraining vector design with regards to transgene and the requisite regulatory elements for gene expression. Subsequently, this packaging ceiling does limit the use of rAAV to transgenes and associated regulatory elements to a total size of <5 kB. Synthetic expression cassettes flanked by AAV ITRs can also be manipulated with standard molecular cloning techniques, such as bacterial

transfection, cloning into plasmids and bacterial transformations generating a highly versatile recombinant viral vector with enormous clinical potential [165].

The conservation the ITRs sequence is necessary for genome rescue, packaging, replication and vector persistence. Most contemporary recombinant AAV (rAAV) vector production platforms rely on the AAV2 wildtype Rep—ITR replication and packaging system, however other wildtype AAVs also exhibit unique sequence differences in their corresponding ITRs and REP genes. Despite the unique differences, all AAV ITRs have been shown to have inherent transcriptional activity which can drive transgene expression *in vitro* and *in vivo* independent of promoter selection [190].

The deliberate removal of the wildtype viral genome has also altered some of AAV's natural viral biology, including the removal of associated REP dependant viral latency. In wildtype AAV, viral latency occurs due to the similarity between the wildtype AAV ITR and Rep sequence with a human AAVS1 genomic locus on chromosome 19. This allows wildtype AAV to integrate into human cells establishing viral latency [184-186]. In contrast, REP deficient recombinant AAV vectors integrate at very low frequencies with limited therapeutic viability. Subsequently the majority of delivered transgenes persist in target tissue as non-replicating episomes. Of significance in target tissues with high mitotic rates, episomal DNA is not transcribed or conserved across daughter cells and so transgene expression does not endure indefinitely [168].

1.4.3.3 Adeno-associated virus capsid biology and considerations for gene therapy strategies

The effectiveness of rAAV as a vector is determined largely by interactions between the capsid and target cell surface receptors on a molecular level, with prevailing capsid pseudoserotypes able to recognise distinct cell surface glycoproteins and co-receptors conferring tissue specific tropism. There are eight naturally occurring AAV serotypes endemic to humans, AAV1, AAV2, AAV3,

AAV5, AAV6, AAV7, AAV8 and AAV9 [191-195] with multiple other pseudoserotypes isolated from non-human primates and mammals including bats and pigs as well as birds [196-199].

The pivotal role capsids play in vector efficacy has led to the aggressive pursuit of capsid optimisation through natural discovery, rational design and directed evolution over the past 25 years [165]. Through this process, key elements in the AAV capsid amenable to modification have emerged, including the 3-fold protrusions, which play important roles in directing tissue tropism and immunogenicity [200]. Additional modifications involve fusing specific peptide sequences including integrin-binding peptides [201], designed ankyrin repeat proteins (DARPins) [202] or single-chain variable fragments [203] to capsid proteins have also been shown to influence tropism though cell surface receptors and can promote immune evasion. Similarly, introducing single or multiple amino acid mutations in the capsid genomic sequences can also be harnessed to alter tissue tropism and reduce immune antigenicity [204]. Optimising favourable capsid properties can at times have negative consequences for other important vector qualities, including stability and packaging efficiency, highlighting the balance required in the ongoing search for clinically relevant capsids.

Species specific differences exist between many capsids, and capsid performance is not always translatable between different species (*i.e.*, human and mouse) or even at times different strains of the same species. This concept was illustrated elegantly with the AAV-PHP.B family of engineered adeno-associated viral vectors. The PHP.B capsid is a neurotrophic variant derived from AAV9. Historically, the central nervous system (CNS) has been difficult to transduce due to the blood brain barrier and the success of the PHP.B vector in the CNS was met with considerable enthusiasm. This success was not replicated across other mouse strains and led to interrogation of the vector transduction mechanism which showed LY6A as an essential receptor for the AAV-PHP.B vector transduction. Subsequently, inter-strain differences in LY6A expression were found

which affected vector transduction and rendered AAV-PHP.B capsid ineffective in certain mice strains [205]. Studies in non-human primates also confirmed the species-specific success of CNS transduction was limited to certain murine models [206, 207].

1.4.3.4 Tissue Tropism of recombinant AAV vectors

The exact mechanism of AAV tissue tropism and cellular entry remains largely enigmatic, but there is consensus that successful cellular transduction is first mediated by vector attachment to putative cell surface receptors followed by endocytosis [208, 209]. Broadly speaking, serotypes AAV1 through to AAV6 are capable of *in vitro* transduction of cell cultures, with serotypes AAV7 though to AAV13 better at *in vivo* cell transduction in animal models and clinical trials [208]. Heparin sulphate proteoglycan was the first cell surface receptor identified for AAV2 [210] and thought to be a consequence of *in vitro* viral propagation [193]. Multiple cell surface makers have subsequently been identified as important co-receptors including FGFR1 [211], αVβ5 [212], hepatocyte growth factor receptor (HGFR) [213] and more recently AAVR, which assists in rapid vector endocytosis and cytoplasmic trafficking to the trans-golgi network [209].

AAV naturally displays high tropism towards the liver and mammalian hepatocytes are a natural AAV reservoir [165]. Wildtype AAV serotypes with natural tropism to the liver include both AAV2 and AAV8. AAV8 belongs to the Clade E AAV family and was isolated from rhesus macaques in 2002 [214]. The AAV8 capsid serotype has been demonstrated to outperform AAV2 in several key areas including transduction efficiency, lower immunogenicity and improved commercial viability with regards to production yields [215] [194]. Deliberate capsid manipulation through the generation of capsid libraries has demonstrated the ability to change the tissue tropism of capsids and exploit vector properties [216]. This capsid shuffling has also contributed to the development of novel capsids with the emergence of LK03 representing a capsid with heightened *in vivo* human hepatocyte transduction demonstrated in a humanized mouse model and reduced immunogenicity

[217]. These advantages led the way for clinical recombinant AAV vector development, culminating in the successful intravenous treatment of patients with Haemophilia B via recombinant AAV8 mediated gene transfer to hepatocytes *in vivo*, of a recombinant factor 9 [218].

1.4.3.5 Designing recombinant AAV vector expression cassettes for therapeutic gene transfer

In the same way that capsid serotypes have been bioengineered to improve tissue transduction across a variety of cell types, the design of the AAV genome or expression cassette can be tailored to enhance vector efficacy in a disease and/or organ specific manner. Recombinant AAV vector genomes at a minimum must contain AAV ITRs, however the sequence and elements contained in between are limited only by the packaging limitation of <5 kB. Typical inclusions for a gene transfer expression cassette include a promoter with or without an enhancer, a Kozak consensus sequence, a transgene, a polyadenylation sequence and then any combination of regulatory elements.

In nuclear transcription, promoters are sequences upstream from a gene that aid in the binding of proteins required to initiate transcription and can vary from 100 – 1000 bp. Sections of these naturally occurring promoters have been appropriated for use in vector expression cassettes and synthetic promoters have also been created. The inclusion of promoter/enhancers upstream of transgene cassette is thus critical for nuclear transcription of the encoded transgene. Some promoters are used in conjunction with enhancer elements that improve their activity and also have tissue specific transcriptional activity. Some promoters have more tissue specific transcriptional regulation, such as human thyroxine binding globulin (TBG) or the LP1 promoter/enhancer. Both TBG and LP1 direct transcription predominately in the liver [218, 219]. Other promoters are active across a broader range of tissues and designated ubiquitous. Ubiquitous promoters include those taken from the cytomegalovirus (CMV) promoter region [220, 221], elongation factor 1α (EF1α) [222], chicken β -actin (CAG)[223], Ubiquitin C [224] and

phosphoglycerate kinase (PGK) [225] and can all induce transgene transcription and translation across a broad range of tissues and organs.

The transgene typically is situated downstream from the promoter and for most genes, will only be the intronic coding sequence, to accommodate the packing limitations of viral vectors. These sequences can also be codon optimised, where base nucleotides are changed to facilitate usage of more common codons for faster and more accurate translation, whilst still conserving the translated protein sequence [226]. This harmonisation of the coding sequence to frequent codons can also be species specific, and is used to increase the rate of protein translation and thus improve the expression of the transgene and enhance the effect of the vector [227].

Other elements can also influence transcription, such as introns and micro-RNAs (miRNAs). Introns, a major part of the non-coding sequence of genes, can be included in expression cassettes to improve transgene expression. Introns with demonstrated heightened transcriptional activity in mammalian cells include SV40, CHEFI, CMVI and hBG introns [228-231]. Enhancing expression after transcription can also be achieved by inclusion of moieties such the post transcriptional element in hepatitis B virus (PRE) and the more potent, tripartite woodchuck hepatitis post-transcriptional regulatory element (WPRE) [232]. These PRE's help to improve the termination of vector genomic transcripts thereby increasing transgene expression and improving the efficacy of vectors [233]. These PRE's are typically located downstream of the transgene where they are the most efficacious. Conversely, reducing expression in certain tissues can be achieved by the inclusion of miRNA targeting-sites which serve as a molecular tag upon transcribed RNA which are then bound to tissue specific microRNAs [234]. In binding the mRNA, the complex is tagged for degradation and not transcribed. As there are organ specific miRNAs, inclusion of miRNA-TS can allow for effective silencing of the transgene in some tissues which express the miRNA, but robust expression in those that do not.

In mammalian cells, a polyadenylation signal is imperative for the nuclear export, translation, and stability of transgene mRNA transcripts [235]. Subsequently, most AAV expression cassettes include a polyadenylation sequence to promote this process. Commonly used polyadenylation sequences in recombinant AAV vectors include a bovine growth hormone polyadenylation sequence (BGHpA) and a SV40 polyadenylation sequence [236, 237].

1.4.3.6 AAV vector genomes remain predominantly episomal

When used as a conventional gene addition vector, AAV predominates in transduced cells in an episomal manner [168]. AAV episomes are not replicated and so any cell division within a tissue leads to only one daughter cell retaining the therapeutic transgene and any therapeutic effect it confers. When persistent expression is desired, the episomal nature of AAV can be circumvented by targeting post-mitotic tissues or tissues with more stable cell populations. Other strategies designed to improve AAV-mediated transgene durability have included multiple dosing regimens, though these are often plagued by neutralizing antibodies, or the use of scaffold matrix attachment region sequences which maintain episomal interactions with the nuclear matrix [238, 239]. The most successful strategies for circumventing AAV episome loss, however, have been combining AAV with gene technologies that mediate permanent genomic integration, such as programmable endonucleases and transposon systems [240, 241].

1.4.4 Improving the durability of recombinant AAV Vectors

Durability of AAV therapies can be improved in several ways, most commonly by including genomic machinery to enact permanent changes in the genome such as editing nucleases or transposon systems.

1.4.4.1 Genomic Editing

Typically, gene editing uses a variety of technologies in a two-step process. First, a targeted break in genomic DNA strand, which can be single or double stranded, is created followed by the deliberate repair of the breakage leading to a desired DNA alteration [165]. DNA breakages are undertaken by programmable nucleases, including engineered meganucleases, zinc-finger nucleases (ZFNs) and transcription activator-like effector nucleases (TALEN) which rely on protein-DNA interactions and Clustered Regularly Interspaced Short Palindromic Repeats (CRISPR) technologies, such as CRISPR-associated (Cas) proteins which rely on RNA/DNA interactions. Due to the reliance upon RNA/DNA interaction, Cas proteins represent a highly versatile gene-editing system currently available for genetic research and therapeutics [165]. Cas endonucleases evolved as an adaptive immune system response against mobile genetic elements like bacteriophages and are found in most archaea and many bacterial cells, [242-244]. Cas endonucleases recognise CRISPR sequences and cut the genomic DNA accordingly. Combined with native cellular DNA repair mechanisms, therapeutic gene-editing can occur through either non-homologous end joining (NHEJ) or homology directed repair (HDR).

Exploiting the repair of these breakages can achieve a therapeutic gene-editing effect, through homology directed repair (HDR) or non-homologous end joining (NHEJ) (Figure 1-7). HDR occurs during the S-G2 phase of the cell cycle and relies on a donor DNA strand from a homologous chromosome or chromatid to repair a double-stranded break. Through supplying a short DNA template, HDR can be used to insert a site specific transgene, however *in vivo* efficiency is limited to cell cycle activity with a few notable exceptions in hepatocytes utilising ZFNs [245], recombinant AAV mediated transgene delivery combined with Lipid nano-particle (LNP) CRISPR delivery [246] and dual AAV transgene and Cas9 delivery [240].

NHEJ is a DNA repair mechanism which can be harnessed throughout the cell cycle [247], with editing efficiencies over 10 times higher than for HDR [248]. NHEJ processes and ligates cleaved DNA ends directly and because this repair is error prone can be exploited to disrupt genes and generate knock-outs. The creation of gene knock-ins has also successfully exploited NHEJ-mediated repair [249, 250] with this precision of *in vivo* transgene insertion further enhanced with homology-independent targeted integration (HITI) [248]. Other editing approaches include reframing protein-coding sequencing with splicing modulation [251], restoring a disrupted open reading frame through exon deletion [252] and allelic exchange for compound heterozygote autosomal recessive repair [253]. Independent of the exact approach, editing strategies are theoretically capable of inducing a permanent therapeutic effect, however translational therapies using CRISPR/Cas have been limited by sub-optimal transduction efficiencies and emerging genotoxicity concerns.

The complexity of executing an AAV gene editing strategy over gene replacement is arguably greater due to challenges with the transduction efficiency of dual vector systems [254]. Constrained by AAV packaging limitations, editing approaches require two vectors, one encoding the editing nuclease and the other encoding the repair templates. Thus, each cell requires transduction by both vectors for successfully editing to take place. In cells that are only transduced by the Cas endonuclease vector, double stranded DNA breaks without the repair can occur. Whilst the repair may be error free, most often inserts or deletions can occur, termed "indels". Target sites for editing are usually designed to limit the risk of these indels leading to pathogenic changes in the target genes, however these have been demonstrated to occur throughout the genome of transduced cells and risk insertional mutagenesis or further inhibit hypomorphic alleles leading to worsened disease phenotype. A recently published paper in 2024 documented frequent concatemeric insertions of Cas9 and AAV repair templates when co-transduced in viral vectors. These events were seen to occur across the genome and occurred independent of dose, locus,

vector concentration, or cell [255]. Whilst this study was *in vitro*, these data raised concerns about the actual specificity of the Cas nucleases, the potentially broad genotoxicity and the potential elevated oncogenic risk profile *in vivo*. Despite these drawbacks, the ability to target a particular genetic locus with high precision confers certain advantages in designing an enduring genetic therapy for monogenic disease which must be balanced by the barriers of primary cell transduction and integration safety concerns.

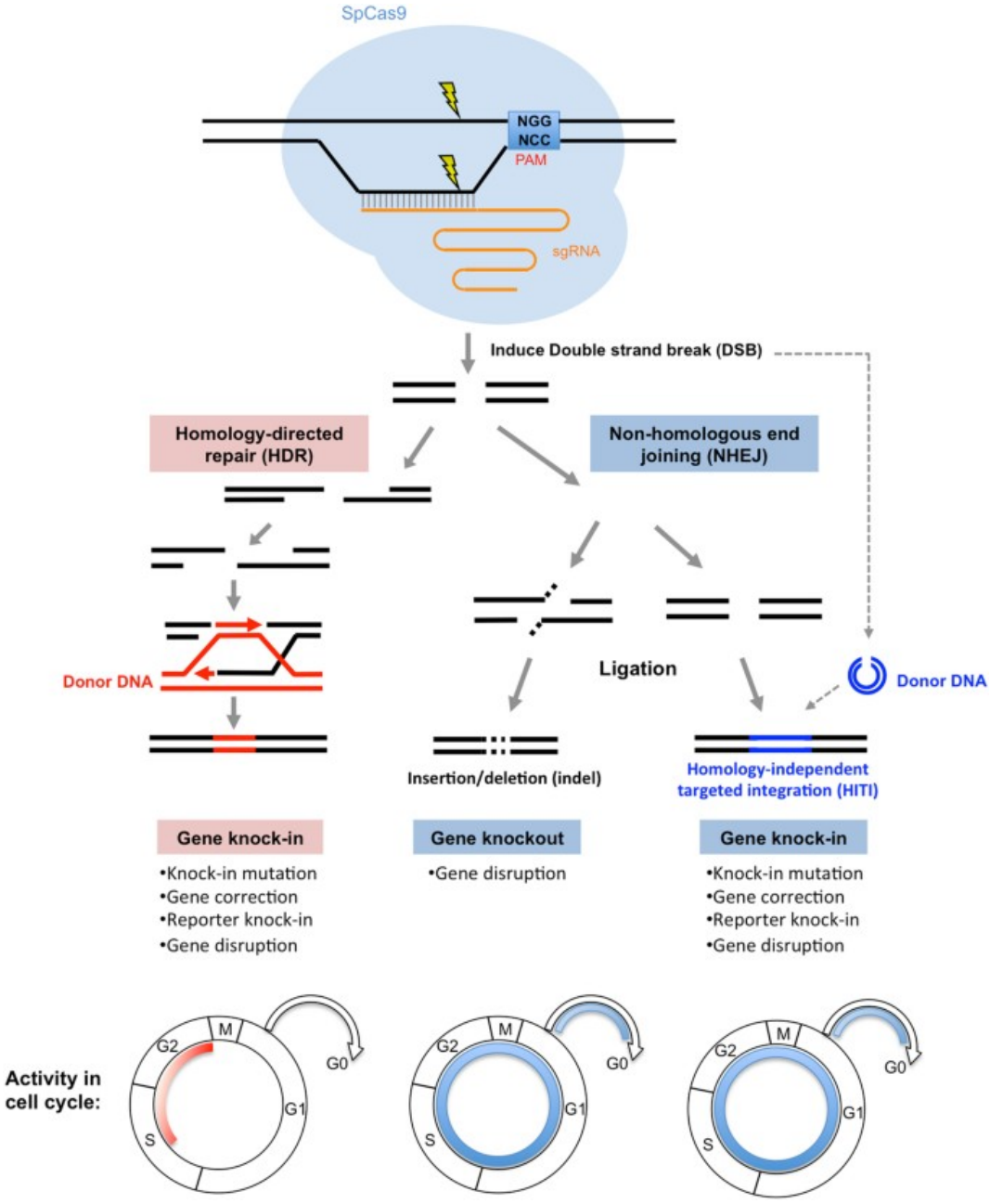

Figure 1-7 DNA repair mechanisms after double stranded DNA breakages. Targeted genome editing mediated by CRISPR/Cas9 homology directed repair (HDR) and non-homologous end joining (NHEJ) error prone and homology independent targeted integration (HITI) techniques. Figure adapted from Suzuki & Belmonte [254].

1.4.4.2 Hybrid Gene Addition with Transposases

Transposable elements are ancient genetic elements that have played pivotal roles in genome evolution and the development of novel signalling pathways and cellular functions [256]. Transposons, transposases, retro-transposons and transposable elements are all mobile genetic moieties that can positionally move within genomes or between host genome and foreign DNA [257]. 'Transposon' refers to the genetic material that is being inserted, 'transposases' refer to the nuclease enzymes or moiety that moves the DNA and 'transposable elements' refer to any moiety that is involved in this process [258].

Considered one of the most abundant and ubiquitous genes in nature, transposable elements make up large components of most eukaryotic genomes [259]. Whilst their movement in humans has been largely constrained, mostly by inactivation, transposons have been linked to the development of certain diseases including some colon cancers, neurofibromatosis type 1 and branchio-oto-renal syndrome [260]. These disease-causing instances are rare, and most transposable insertions do not detrimentally affect genomic fitness and are considered benign. Insertions that persist for long enough in populations, accompanied with genetic drift can eventually exist as gene polymorphisms and ultimately become fixed in a species [260]. In this way, transposons have proved critical in the genetic evolution of complex life.

Eukaryotic DNA transposon systems have also been exploited for specific gene therapy uses with the most commonly used DNA transposases being Sleeping Beauty transposase and *piggyBac* transposase [241, 261, 262]. These platforms can be used in AAV gene addition approaches to improve the persistence of transgenes by utilising the natural insertional ability of these transposase enzymes. By encoding a genomic sequence of interest between two transposase recognition sites to generate a hybrid AAV-transposase vector, transgenes can be inserted into a host cells genome, thereby rendering a permanent change and improve the durability conventional gene addition

vectors. The two most studied transposases, Sleeping Beauty and *piggyBac* have similar applications, however, differ in the genetic footprint they leave behind.

PiggyBac (*pB*) transposase was isolated from the cabbage looper moth, *Trichoplusia ni* [241]. As a "cut-and-paste" DNA transposase, *pB* is possibly evolved from the RNaseH-like or retroviral integrase superfamilyA [263]. A naturally occurring transposase, *pB* transposition is achieved through a series of transesterification and hydrolysis steps that generate an excised intermediate with transposon ends protected by DNA hairpins [264]. This process occurs at sites rich in a specific tetranucleotide repeat, TTAA. In this way, *pB* transposase can achieve, random, non-targeted integration in host genomes at sites with TTAA repeats [265]. Whilst integration is random and an acknowledged limitation of this platform, *pB* transposase excises and inserts DNA precisely, with no genomic insertions or deletions left behind. The lack of an excision footprint is highly desirable and had led to use in pre-clinical genetic therapies, non-viral vectors for transgenesis [266], insertional mutagenesis and genetic screening [267]. Alternative variants have been engineered through random sequence shuffling and include a hyperactive *pB* transposase [268] and another able to excise nucleotides without subsequent integration [269]. Sleeping Beauty transposase is a bioengineered synthetic transposase with a sequence drawn from transcriptionally inactive elements isolated from fish genomes [270] and considered a Tc1/mariner super family transposon [271]. Sleeping Beauty also follows a similar cut and paste mechanism of transposition to *pB* but leaves a TA dinucleotide duplication footprint at the site of integration and excision. This insertional TA is of course less desirable than excision achieved with *pB* transposase.

The integrating properties of transposases have been harnessed to enhance the durability of conventional episomal AAV gene addition strategies whilst also exploiting the episomal nature of gene addition. Theoretically, these platforms have the potential to integrate a desired transgene with accompanying loss of transposase cassette which remains in an episomal state. However there

has been some suggestion that the transposase can have prolonged transpositional activity, which may predict higher risks of oncogenesis due to double stranded DNA breaks. The main size limitation of using this system with AAV is the 5 kB packaging limitation of AAV. As a result, dual vectors are often required. The transposon vector carries the DNA to be inserted into the host genome, usually consisting of the promoter, transgene, polyA and any other elements flanked by transposases recognition sites. The transposon vector is then co-administered with a transposase vector, which encodes the sequence for the transposase enzyme, either *pB* transposase or Sleeping Beauty. The AAV packaging limitations are more restrictive than the integration limitations of the transposases and *pB* can integrate up to 9.1 kB. However with Sleeping Beauty, transposition efficiency declines in a size dependant manner and is reduced by 50% with 6 kB constructs [272]. Naturally, co-transduction with two vectors introduces an additional element of complexity to any therapy, however this technique allows for the exploration of durable gene addition therapies in pre-clinical models and avoids some of the undesirable complications associated with aforementioned genetic editing technologies.

The necessity of dual vectors for *pB* and Sleeping Beauty transposition does not set it apart from CRISPR/Cas9 editing techniques, but *pB* is more efficient than CRISPR and TALEN in effecting permanent genomic changes when used to generate novel transgenic rat models [273]. The liver has also been successfully targeted by *pB* transposase in numerous studies [274-276]. AAV co-transduction with *pB* transposase and an expression cassette has also affected enduring expression in neonatal murine livers, which undergo rapid mitotic expansion from birth to adulthood. In one pre-clinical model of progressive familial intra-hepatic cholestasis type 3 (PFIC3) dual hepatocyte transduction with a transgene vector encoding the causative gene *ABCB4* and *pB* transposase encoded on a separate vector led to durable expression of the transgene cassette and prevented the disease [275]. Other studies have used *piggyBac* to phenotypically correct haemophilia A in via gene transfer to mouse hepatocytes [277]. Another research group used hybrid *piggyBac* AAV

vectors to demonstrate sustained expression of the CFTR gene in murine models and in tissue cultures of primary human well-differentiated epithelial cells taken from cystic fibrosis patients [278].

Transposon systems have been used successfully in *ex vivo* clinical trials, most commonly in CAR-T Cell therapies. Similar to editing endonucleases, concerns about genotoxicity and insertional mutagenesis are relevant for these transposon systems which are not free of insertional mutagenesis risk. Two recent publications reported new malignancy in patients who received *pB* transposase *ex vivo* treated CAR-T cells in a B-cell lymphoma trial, however the study authors postulated that it was the unique CAR-T production methodology, rather than the use of *pB* transposase itself, that caused multiple integrated transposons and chromosomal rearrangements seen in the transformed malignant cells [279, 280].

Overall, the durability of a gene therapy is dependent upon numerous conditions, including the vector system used, the target cell type and the integrating potential of the platform. Nucleases such as CRIPSR/Cas systems and transposable systems like *pB* transposase and Sleeping Beauty have enormous potential but also significant limitations unique to each of these strategies. As with any novel therapeutic, balancing each of these limitations with the strengths of the system and the underling disease/gene of interest will likely be disease specific and thus highlights the utility of having numerous options for scientific medical research.

1.4.5 Challenges and barriers in AAV gene therapy

Regardless of the type of gene therapy strategy, the vector platform or the target cell, there are multiple challenges to overcome in order to optimise any therapeutic intervention. These include biological barriers, such intracellular, extracellular barriers, cellular barriers like the immune-vector

interactions and practical barriers to clinical translation such as financial viability, equity and ethical access questions (Figure 1-8).

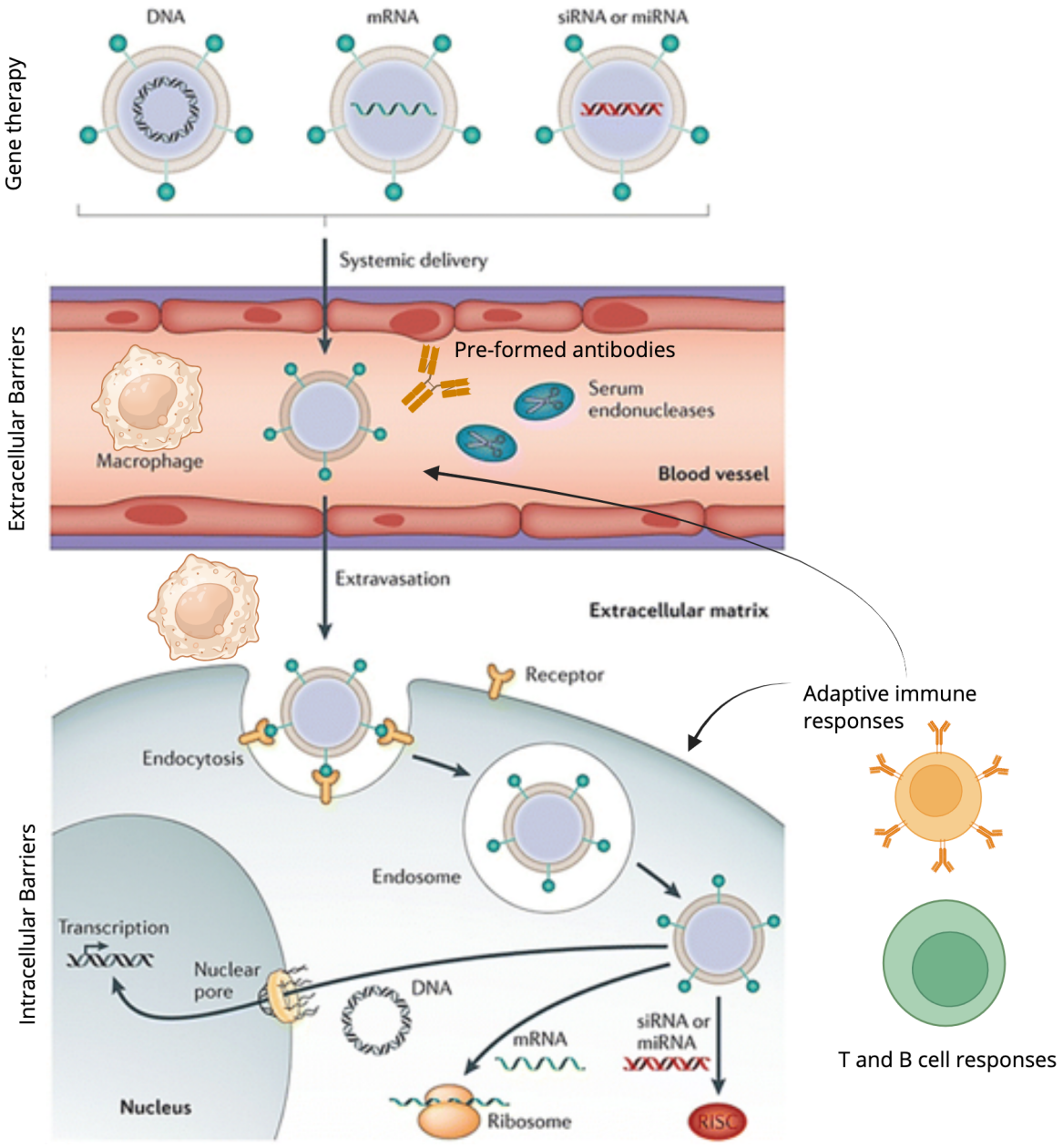

Figure 1-8 Biological barriers to successful gene therapy. Figure adapted from Chen *et. al* [281] and generated in BioRender.

1.4.5.1 Intracellular barriers to AAV gene therapy

Intracellular barriers which influence transduction are complex. As demonstrated with *in vitro* gene therapy models high transduction rates of up to 95% of a target tissue do not necessarily translate to transgene expression, which may occur in only a subset of the transduced cells [282]. Factors preventing transgene expression include endosome entrapment and escaping this vector-hostile environment along with clathrin and caveolae mediated endocytosis, represent major obstacles to nuclear trafficking of DNA vector cargo. Non-viral vectors such as LNP may be more advantageous in this regard, as they deliver their genetic cargo through endosomal escape but are not as efficient in delivering DNA to the nuclear compartment [283, 284]. Lysosomal degradation may also prevent expression of AAV delivered transgenes. Lysosomes can use a vacuolar-type H^+-ATPase to pump protons into the lysosomal lumen and maintain a pH of 4.5 which is hostile to AAV vector cassettes [285-287]. DNA based genetic therapies, inclusive of AAV vectors, need to travel across the nuclear membrane to allow for transcription whereas RNA vectors though inherently less stable than DNA only need to reach the cytoplasm [288, 289].

1.4.5.2 Extracellular barriers to AAV gene therapy

Extracellular barriers are similarly complex and numerous. Depending on the intended target site and administration route vectors may have distinct barriers to overcome before reaching their target. For vectors administered systemically, resistance to serum proteases and nucleases is critical. Naked DNA in the blood stream has a half-life of several minutes with rapid clearance by enzymes and removal by Kupffer cells, the liver's immune scavenger cells [290]. Tissues in immune privileged organs, such as tissues in the eye like the retina, are also difficult to transduce with systemic vectors due to tissue barriers. Similarly, the CNS is protected by the blood brain barrier. These tissue barriers can be overcome with high systemic doses or by direct injection into the tissue of interest - *e.g.,* retinal layers or intrathecally.

1.4.5.3 Host immune responses to AAV vectors

Preformed antibodies to AAV also represents a major barrier in accessing AAV therapies. The seroprevalence of AAV antibodies varies geographically and with age. Anti-AAV2 antibodies have been detected in 30-60% of study populations and are the most prevalent [291-293]. Antibodies to other capsid serotypes have also been reported with prevalence levels across study populations showing 45% positive for anti-AAV6 and AAV9 and 38% positive for anti-AAV8 antibodies [291]. Whilst not all cross reactive antibodies are neutralizing those that are often cross-react against multiple AAV pseudoserotypes [294] and have clinical implications in that high enough levels can preclude inclusion in AAV clinical trials [295, 296].

1.4.5.4 Maintaining off-target genomic integrity and AAV associated genotoxicity

Genotoxicity, the unintended disruption of functional chromosomal DNA secondary to the introduction of a transgene or viral DNA into a target cell, is of particular concern in the development of novel genetic therapeutics. Whilst any off-target effect is undesirable, of particular concern are those that occur in genes critical for tissue specific function and oncogenes including tumour suppressor genes. Whilst AAV vectors are considered episomal and do not integrate, there has been evidence to show long term, low level integration occurs with gene addition AAV vectors [297]. While insertional mutagenesis has not been observed with any *in vivo* AAV clinical trials these concerns were however illustrated by a retroviral clinical trial treating severe combined immunodeficiency disease through *ex vivo* retroviral mediated gene transfer in haematopoeic stem cells [298]. In this study, a tumour suppressor gene was disrupted and multiple patients developed leukaemia, demonstrating the ongoing balance between vector efficacy and safety.

The safety profile of a predominantly non-integrating vector such as AAV has been interrogated with numerous studies and clinical trials, and overall shown as more favourable with regards to

genomic insertion and potential native gene disruption [299, 300]. However, murine studies observing the development of hepatocellular carcinoma in AAV treated mice, highlighted the potential for genotoxicity even at the low levels of unsupervised integration typically seen with AAV [301]. This was later demonstrated to be secondary to preferential integration of AAV within the unique murine specific *Rian* genomic locus and of limited consequence in human studies where long term follow up has shown no integration in proximity to known hepatocellular carcinoma driver genes [302].

1.4.5.5 Immune Activation and Systemic Inflammatory Responses

Immune sensitivity reactions, such as generalised inflammation response and thrombotic microangiopathy after AAV vector administration is also of concern in clinical trials. Many clinical therapies include a discreet period of immunosuppression at the time of *in vivo* vector delivery to help reduce significant immune responses. The first death in a gene therapy clinical trial occurred due to an fatal inflammatory response secondary to immune activation after intravenous administration of an adenovirus vector treating OTC deficiency [303]. Clearly, ongoing attention to vector safety profiles, especially with evolution of new rAAV serotypes, is paramount in the development of effective genetic therapy.

Non-viral vectors also can incite concerning immune responses, with cationic lipids exhibiting severe toxicities [304, 305]. More immunogenic than anionic or neutral liposomes, cationic lipids have driven IL-6 mediated inflammatory responses in CF patients after inhalation of cationic liposome-DNA complexes [306] [170]. Furthermore, systemic therapies, such as the lipid oligofectamine nanosystems in human alveolar epithelial A549 cells induced gene expression changes with apoptotic and cell defence profiles [307], emphasising the importance of safety and immunogenicity profiling of any new potential gene therapy strategy [170].

1.4.5.6 AAV pathogenicity and immunogenicity

Traditionally, AAV was not thought to cause pathological infection in humans [208]. More recently emerging evidence has demonstrated that it may play a role in rare cases of paediatric acute hepatitis [167, 308]. Notwithstanding this rare occurrence, a growing body of research in epidemiological analysis demonstrates significant immunogenicity with potential immune interactions between the rAAV protein capsid, the DNA genome and the protein product of the transgene [309, 310]. Studies have demonstrated between 30 to 60% of people harbour neutralising antibodies (NAb) to AAV, predominantly immunoglobulin G (IgG), formed after co-infection with a helper virus [194, 311, 312]. The most prevalent NAb are directed towards AAV2, followed by AAV1 [194] with IgG antibodies the most prominent. Prevalence also varied by age, with the lowest NAb levels in children aged between 3 to 17 years of age. Optimising rAAV for maximal tissue transduction and reduced immunogenicity continues to be the goal of many gene therapy research teams. These antibodies are of clinical significance as their presence may preclude access to AAV based genetic therapies [313].

1.4.5.7 Considerations in the clinical translation of gene therapies

Successful translation of a gene therapy to the clinic represents a lengthy and rigorous process reliant upon on pre-clinical and clinical trials. Globally, the number of human gene therapy clinical trials is ever increasing, with over 3,700 clinical trials completed, ongoing or approved as of March 2023, an increase in over 1000 trials across the preceding 5 years with 2,597 trials in 2017 [13, 164]. The availability of new gene therapies is subject to approval by country specific drug regulatory processes, and in Australia this falls under the jurisdiction of the Therapeutic Goods Administration. In Australia there are 9 commercially available gene-based therapies currently available to patients, however patient access either through enrolment in phase 3 clinical trials or via the government funded Pharmaceutical Benefits Scheme (PBS) (Table 1-3). The only PBS

listed therapies in Australia to date are for Spinal Muscular Atrophy, and include Nusinersen (Spinraza), Risdiplam (Evysdi) and Onasemnogene abeparvovec (Zolgensma).

Table 1-3 Commercially available gene-based therapies available in Australia

Product	Company	Generic Name	Indication	Vector System
Imlygic	Amgen	Talimogene laherparepvec	Melanoma	Oncolytic gene modified viral gene therapy/HSV-1
Spinraza	Biogen	Nusinersen	Spinal Muscular Atrophy	RNA therapy
Evysdi	Roche Genentech	Risdiplam	Spinal Muscular Atrophy	RNA therapy
Kymirah	Novartis	Tisagenlecleucel	Certain B cell cancers	CAR-T cell therapy/Lentivirus
Yescarta	Kite Pharma	Axicabtagene ciloleucel	Certain B-cell cancers	CAR-T cell therapy/Lentivirus
Tecartus	Kite Pharma	Brexucabtagene autoleucel	Mantel cell lymphoma	CAR-T cell therapy/Lentivirus
Zolgensma	Novartis	Onasemnogene abeparvovec	Spinal Muscular Atrophy	AAV-9
Luxturna	Novartis	Voretigene neparvovec-rzyl	Inherited rentinal dystrophy	AAV-2
Elevydis	Sarepta	Delandistrogene moxeparvovec-rok	Duchenne Musclar Dystrophy	AAVrh74

Abbreviations: AAV (adeno-associated virus), CAR (Chimeric antigen receptor), HSV (Herpes simplex virus).

1.4.5.8 Commercial viability of Gene Therapies

Financial viability continues to influence the accessibility of novel post-trial gene therapies. The case of Glybera, designed to treat lipoprotein lipase deficiency via recombinant Adeno-associated virus mediated transduction of quiescent muscle cells with a hyperactive lipoprotein lipase, is illustrative of this principle [314]. Whilst now withdrawn from the market, Glybera (Alipogene tiparvovec, uniQure) was the first gene therapy approved by the European Medicines Agency in 2012 and represented the first commercially available genetic therapy [315]. However, Glybera failed to meet primary end points of decreasing triglyceride levels and only had modest effect on one manifestation of lipoprotein lipase deficiency (pancreatitis). Combined with the $1 million

treatment price tag, this ultimately led to market withdrawal. The case of Glybera highlights the requirement for translational research which is transformative, durable and economically sound [316]. Consideration of these principles, alongside the ethics accessibility are mandated in the development of a gene therapy strategy for MSUD. Three autosomal genes, *BCKDHA*, *BCKDHB* and *DBT* contribute to over 98% of known causative mutations for MSUD and the commercial viability in targeting less common mutations given current industry constraints will no doubt be less attractive financially than a strategy that targets more commonly occurring mutations.

1.5 Gene therapy for Maple Syrup Urine Disease

Currently available treatment options for MSUD are not adequate, and the search for alternative therapeutic options has broadened research efforts into genetic therapy. Gene therapy attempts to date have occurred in both cell culture and murine models.

1.5.1 *In vitro* maple syrup urine disease models and early gene therapy attempts

Prior to the widespread availability of small mammalian disease models, the first published gene therapy attempt for MSUD was in 1993. In this study, a retrovirus vector was used to deliver a human coding DNA (cDNA) transgene of *BCKDHA ex vivo* to patient derived lymphoblasts homozygous for the Mennonite *BCKDHA* mutation [317]. Another research group published a similar study in 1995, utilising retrovirus to restore BCKDH function, however worked with patient derived fibroblasts homozygous for *DBT* mutations [45]. This *ex vivo* study maintained stable expression of BCKDH enzyme activity in cultured fibroblasts for 7 weeks. Whilst these studies were *ex vivo* and a long way from treating a patient, they were the first to demonstrate the potential of gene transfer in MSUD.

1.5.2 Mammalian experimental models of maple syrup urine disease

In establishing the first murine MSUD disease model in 2006, Homanics *et al.* catalysed an important step in pre-clinical *in vivo* gene therapy research for MSUD. Murine BCKDH is similar to human BCKDH in that it is a multi-heterotertramer generated from E1α, E1β, E2, E3 and the associated regulatory proteins. This transgenic mouse was created through embryonal knock-out of the murine *DBT* gene with partial rescue provided by a knocked-in human *DBT* transgene. The human *DBT* transgene was complexed to an ultimately non-functional molecular switch with transgene expression detected in the murine liver and minimally in brain and kidney. Whilst the

molecular switch ultimately proved non-functional, the severity observed in this model was less severe than Classical MSUD, with the majority of affected mice surviving through weaning at 4 weeks, with progressive mortality over the next few months until all had died by 20 weeks of age. The levels of BKCDH activity in this hypomorphic model were reported at around 5-6% of normal, despite the human transgene E2 protein levels expressed at around the same levels as wildtype. The reduced activity was suggested to be secondary to a c-myc tag on the transgene interfering with BCKHD assembly and conferring reduced activity. As evidenced from the published thesis from a PhD student in the same research team that generated this transgenic model, *in vivo* gene therapy was attempted in this hypomorphic model with an AAV mediated gene transfer vector, however this was unsuccessful, and the results not published in any peer reviewed journals.

The hypomorphic model generated by Homanics *et al.* was used to generate the commercially available *Dbt*^{tm1Geh} Tg(Cebpb-tTA)5Bjd Tg(tetO-DBT)A1Geh/J model (The Jackson Laboratory). Other MSUD murine models are also available for the other genes encoding for the BCKDH protein subunits, including the E1α subunit (C57BL/6NCrl-Bckdha<em1(IMPC)Tcp>/Cmmr) and E1β unit (C57BL/6NJ-*Bckdhb*$^{em1(IMPC)J}$/Mmjax). There is also a bovine disease model characterised in 1992 by a research team in New South Wales, Australia after symptoms of neonatal metabolic intoxication were observed in Poll Hereford calves [318, 319]. Further characterisations revealed elevated BCAA and the neurological symptoms of classical MSUD. Subsequently, other *de novo* occurrences of MSUD in other cow breeds was reported in North and South America [320].

Chimeric human-animal models have also been used to increase the fidelity of pre-clinical gene therapy research. The FRG mouse model is a well-established mouse strain which can be used to generate chimeric disease models. Owing to the mutations conferring both immunodeficiency and tyrosinaemia, FRG mice can be engrafted with human hepatocytes which are then selectively

expanded in the murine liver through a murine hepatocyte injury cycle. This liver injury cycle is instigated through intermittent withdrawal of NTBC, the treatment for tyrosinaemia [321]. There have been no published attempts at gene therapy correction in chimeric human-murine models such as the $Fah^{-/-}/Rag2^{-/-}/Ilrg2^{-/-}$ (FRG) mouse, though engraftment of patient derived MSUD hepatocytes has been successfully demonstrated [322]. This model could be used to generate humanised MSUD mouse model with the opportunity to design, develop and test genetic therapy strategies for MSUD *in vivo*.

1.5.3 *In vivo* AAV Gene Therapy in pre-clinical animal models

Prior to 2021, there were no published pre-clinical studies exploring gene therapies for MSUD until Grieg *et al.* published the first exploration of an AAV gene therapy for a hypomorphic MSUD model, iMSUD (*Dbt*^{tm1Geh} Tg(Cebpb-tTA)5Bjd Tg(tetO-DBT)A1Geh/J) (The Jackson Laboratory). In this study, AAV8 or AAV9 capsids were used to deliver a codon optimised human *DBT* transgene gene addition vectors expressed under either a liver specific promoter (TBG), a muscle specific promoter (tMCK) or a ubiquitous promoter (CB7). The liver targeting vector AAV8.TBG.hDBTco worked only transiently and whilst overall survival of the iMSUD mice improved, mean leucine levels were over 3000 μmol/L (wildtype mean 150 μmol/L). The muscle targeting strategy employed both IV or direct IM injection of AAV9.tMCK.hDBTco into bilateral murine gastrocnemius muscles of iMSUD mice at 21 days of life. This saw improved growth but minimal improvements in survival and serum leucine levels. A final strategy using AAV9 and a ubiquitous promoter in AAV9.CB7.hDBTco was delivered either IV or IM. This vector saw the most convincing phenotypic rescue with comparable rescue between the IV and IM routes of administration. Both routes also had significantly higher amounts of hDBTco transgene expressed across liver and muscle compared to the other strategies. This study highlighted that a codon optimised human DBT transgene was able to complex with the murine BCKDH protein subunits and form a functional enzyme but was only able to meaningfully rescue the iMSUD model with

dual muscle and liver transduction. This study also demonstrated the difficulties in targeting a single organ system for a multi-organ disease like MSUD and quantifying how individual organ contributed to phenotypic rescue.

Following this pre-clinical study in the iMSUD *DBT* mouse model, an AAV gene therapy study in a previously unpublished murine MSUD model for *BCKDHA* was published by a French research group in 2022, followed by a study from the same research team using a *BCKDHB* murine model in 2024 [323, 324]. In the *BCKDHA* study, Pontoizeau *et al.* characterised a previously unpublished disease model (C57BL/6NCrl-Bckdha<em1(IMPC)Tcp>/Cmmr) and demonstrated that this model recapitulated severe, Classical MSUD. Homozygous affected pups died within the first two weeks, displayed pathognomonic elevations in BCAA and L-alloisoleucine and had minimally detectable E1α protein on western blot across liver, brain and heart. Two AAV vectors were generated, pseudoserotyped to the AAV8 capsid and contained an expression cassette with AAV2 ITRs, either a E1Fα promoter or an APOe/hAAT enhancer/promoter, human transgene for *BCKDHA*, WPRE and BGHpA and were administered via temporal-vein injection on post-natal day 0. Three doses were tested, from low (1×10^{13} vector genomes (vg)/kg), intermediate (3×10^{13} vg/kg) to high (1×10^{14} vg/kg) for both vectors to assess the liver restricted APOe/hAAT enhancer/promoter against the ubiquitous E1Fα promoter.

In the *BCKDHA* study, the highest degree of rescue was achieved with the high dose vector containing the E1Fα promoter and treated *BCKDHA* deficient mice survived to the experimental end point of 6 months. Growth and hepatic E1α protein expression was equivalent to wildtype, leucine levels roughly double that of wildtype mice and liver BCKDH enzyme activity approximated 12 ± 4 % of wildtype. In contrast, *BCKDHA* deficient mice treated with the liver restricted APOe/hAAT enhancer/promoter vector had statistically similar levels of BCKDH enzyme activity to the vector with the ubiquitous promoter. Despite this, these mice had less

robust growth and mean leucine levels approached ten times that of wildtype. These data illuminated the significant extrahepatic rescue provided by the vector with the ubiquitous promoter. Whilst molecular analysis was only undertaken in liver, brain and heart tissues, the similar levels of protein expression across these tissues for high dose vectors with either the ubiquitous or liver restricted promoters suggest that another organ was responsible for the improved rescue with the ubiquitous promoter, such as skeletal muscle.

The *BCKDHB* study utilised a commercially available model, C57BL/6NJ-Bckdhb$^{em1[IMPC]J}$/Mmjax (The Jackson Laboratory) backcrossed for 5 generations with BALB/cByJ (Charles River Laboratories). This backcrossing was undertaken to limit mother-associated infant cannibalism and the model also found to recapitulate severe, Classical MSUD. Privileged to knowledge regarding optimal dose and vector configuration from the *BCKDHA* study, the *BCKDHB* study treated homozygous affected pups with an AAV8 capsid containing an expression cassette with AAV2 ITRs, a ubiquitous E1Fα promoter, a human *BCKDHB* transgene, a WPRE and a BGHpA at 10^{14} vg/kg per mouse. Mice survived to two experimental end point of 6 months and 12 months, with leucine levels roughly double that seen in wildtype mice and hepatic BCKDH enzyme activity 16 ± 8% that of age matched wildtype mice.

These two studies by Pontoizeau *et. al.,* demonstrated that a single, high dose gene addition vector with a ubiquitous promoter provided stable, enduring, meaningful phenotypic rescue in two murine disease models of MSUD *BCKDHA* and *BCKDHB [323, 32*4]. However exactly which organs were contributing to the phenotypic rescue is not clear as these studies were limited in their molecular analysis to liver, brain and heart tissues. BCKDH is widely expressed in humans and mice and skeletal muscle contributes up to 59% of total body BCKDH oxidative activity, brown adipose fat 19%, liver 8%, kidney 5%, heart 4% and all other including brain contributing to the final 5% of oxidative BCKDH activity [12]. There was also no data exploring histological patterns

of correction in liver or heart tissue as the transduction efficiencies and transduction patterns for these murine models and vector is not known.

These three pre-clinical AAV gene therapy studies illustrate the potential for AAV gene therapies as a novel treatment for MSUD. Together they proved that human transgene proteins corresponding to BCKDH subunits when translated have activity with the murine BCKDH protein subunits. These studies also demonstrated how extra-hepatic transduction and transgene expression can contribute to phenotypic rescue. Therapeutic correction thresholds pertaining to clinically relevant organs such as the liver and skeletal muscle have yet to be definitively ascertained, and no study has yet demonstrated that hepatic transduction alone can provide meaningful levels of phenotypic rescue in murine MSUD disease models. Similarly, skeletal muscle as a sole target organ for recombinant AAV gene therapy in any of the neonatal lethal MSUD murine models has yet to be explored.

1.5.4 *In vivo* non-viral gene therapy for MSUD

Free of the packaging constraints of AAV, lipid nanoparticle mRNA platforms are attractive for conditions like MSUD where multiple affected genes cause the same condition. Instead of multiple different vectors required in an AAV platform addressing the various MSUD causative genes or editing technologies which also would need to be tailored to individual mutations, multiple mRNA transcripts corresponding to the three main causative MSUD genes could be encapsulated in a highly liver trophic LNP mRNA and co-delivered to any MSUD patient [325].

This mutation agnostic strategy was recently explored through encapsulating mRNA corresponding to three main human autosomal genes implicated in MSUD, *BCKDHA*, *BCKDHB*, and *DBT* into an LNP [325]. Murine models used were iMSUD, described above and three classical models corresponding to the *DBT*, *BCKDHA* and *BCKDHB* genes. The classical models used

were all neonatal lethal, with the *BCKDHA* and *BCKDHB* models generated via CRISPR mediated gene knock-out at the Jackson Laboratory. The *DBT* neonatal lethal model was generated by backcrossing the iMSUD model to C57BL/6J mice generating offspring lacking tTA and tetO transgenes for expression of h*DBT*.

In the iMSUD model, mice started IV LNP treatment on post-natal day 21-28 and then received weekly injections of 0.2 mg/kg, 0.5 mg/kg or 1mg/kg of LNP containing mRNA for *BCKDHA*, *BCKDHB* and *DBT* for ten weeks. Treated iMSUD mice had improved survival in a dose dependant manner, with mean serum leucine levels 1.5 times that of wildtype. Growth was similar across all treated iMSUD mice though the study made no comparison of the iMSUD mice with wildtype mice growth. *In situ* hybridisation of LNP encapsulated mRNA in liver sections from necropsied mice demonstrated the presence of *BCKDHA*, *BCKDHB* and *DBT* mRNA 24 hours after injection, with approximately 50% reduction over the following 7 days, giving insight into potential dosing intervals required.

In the DBT neonatal lethal disease models, LNP-encapsulated mRNA was administered by intravenous temporal vein injection of 2mg/kg of LNP containing mRNA for *BCKDHA*, *BCKDHB* and *DBT* on post-natal day 0 and 3 and then weekly thereafter via retro-orbital or tail vein. Homozygous affected *DBT-deficient* mice had improved survival, but none reach adulthood and all exhibited growth failure with serum leucine levels four times above wildtype. A lower dose of 1 mg/kg of the LNP containing mRNA for *BCKDHA*, *BCKDHB* and *DBT* administered to all three neonatal lethal models did not improve survival or growth for *BCKDHB* deficient mice, improved survival for *BCKDHA* mice by a few days and had a similar effect to the 2 mg/kg/dose for the DBT-deficient mice. Growth failure was seen in all the models treated with 1 mg/kg of LNP mRNA.

Mutation agnostic approaches such a LNP mRNA strategy remain attractive options for pre-clinical research with the potential for one treatment that could be administered to patients regardless of the underling mutation. Whilst this study highlights the potential for LNP and MSUD, it also is illustrative of the transient nature of mRNA gene replacement, and subsequently intensive dosing requirements were not optimised in this study and showed minimal therapeutic efficacy in the classical disease models. Classical MSUD occurs most frequently in humans, and an effective LNP therapy would still require regular doses throughout childhood, necessitating access to medical care. LNP could be used to deliver gene editing mRNA to effect a permanent change in the genome, however this would then negate the mutation agnostic benefits of mRNA. Whilst LNP avoids the immune neutralisation that is seen with AAV with repetitive dosing, it might be possible to use a bridge to more definitive gene therapy, especially for organs with high mitotic rates such as paediatric livers.

1.5.5 The Liver as a target for Gene Therapy in MSUD

At present, gene therapy for MSUD has only been explored in pre-clinical animal disease models using either AAV or LNP based strategies [324-326]. Translating these findings to the clinic requires consideration of many different, and at times competing, factors. Major considerations include the selection of a target organ or organs and within them target cell type. Furthermore, a precise understanding of the disease biology and any consequences on organ anatomy, anatomical or physiological barriers is imperative, as these may influence the success of *in vivo* tissue transduction. Most human organs have been the subject of AAV transduction research, and as AAV technologies have advanced so too has the precision with which certain organs and/or cell types, such as hepatocytes, are able to be transduced [217, 327]. AAV therapies are DNA based with the potential for stable gene transfer to the liver when integrated into genomic DNA or as episomes in non-dividing cells. By comparison LNP, whilst highly effective at transducing both

murine and human hepatocytes delivers transiently expressed mRNA and associated tissue biodistribution, optimal dose and dosing intervals are less well characterised than AAV [328]. The human liver is highly amenable to AAV transduction and is the metabolic hub of the body [329]. In conjunction with the significantly improved metabolic stability of MSUD patients post liver transplantation, this supports the liver as an attractive target organ for an AAV based gene therapy for MSUD.

1.5.5.1 Liver anatomy

The liver is the most metabolically active organ in the human body and performs many key cellular functions required to maintain homeostasis [330]. In humans, the liver is an intraperitoneal organ and is situated in the right upper quadrant of the abdomen, tethered to the diaphragm and anterior abdominal wall by the falciform ligament and round ligament respectively. Macroscopically, the liver consists of four lobes: the left, right, caudate and quadrate lobes. It can be further divided into eight segments with each segment delineated by separate systemic and portal blood supply as well as biliary outflow tract.

The liver receives two sources of blood, approximately 20% of which is supplied by the hepatic artery and the remaining 80% from the portal vein. The hepatic artery supplies oxygenated blood to the liver cells and is the dominant oxygen supply to the biliary tree. The portal vein carries oxygen depleted, nutrient rich blood from the intestinal veins, spleen and pancreas. Portal venules fuse with hepatic arterioles to form the liver sinusoids, a dilated leaky vascular bed which drains into central veins. These central veins then coalesce into larger hepatic veins and then drain into the inferior vena cava. The unique dual inflow of the hepatic artery and portal vein result in the liver receiving approximately 25% of cardiac output, despite representing only 3% of total body mass [331, 332].

The smallest functional unit liver is the hepatic lobule (Figure 1-9). Each lobule consists of 6 portal triads hexagonally arranged around a central vein. A triad contains a hepatic arteriole, portal venule and bile ductule with cells clustered around these structures. These cells include the liver's parenchymal cell's, the hepatocyte, and non-parenchymal cells including sinusoidal Kupffer and endothelial cells which play important roles in filtration and phagocytosis. Hepatocytes, which accounting for 80% of total liver cells and 70% of total liver mass, perform over 500 crucial cellular functions including vital metabolic, immune, haematological and detoxifying reactions, all which help to maintain physiological homeostasis [333].

1.5.5.2 Liver specific considerations for MSUD AAV gene therapy

Liver directed gene therapy represents a potentially curative therapy for many of these conditions with many theoretical advantages over current therapies. However, there are certain organ specific considerations that must be taken into account when designing an AAV gene therapy for MSUD. Firstly, the phenomenon of hepatic zonation is an important consideration in designing a liver directed genetic therapy. Due to the unique portal and arterial blood supplies, hepatocytes along the hepatic acinus are exposed to a nutrient and oxygen gradient. The hepatic acinus is a functional unit with regards to blood flow, illustrated by drawing a line between two portal triads from which it extends into the direction of the two adjacent central veins (Figure 1-9) [334]. Functional organisation of hepatocytes along this gradient results in dynamic speciation of several key metabolic functions including carbohydrate, lipid, amino acid, ammonia and drug metabolism [335, 336] . Non-parenchymal cells also exhibit zonation with regards to their location and cellular function [337, 338]. This speciation is dynamic, with gene expression patterns reactive to a variety of stimuli, including nutrition, xenobiotics, endogenous hormones with more general regulation undertaken by morphogens Wnt/β-catenin and hedgehog pathways as well as growth factors [334].

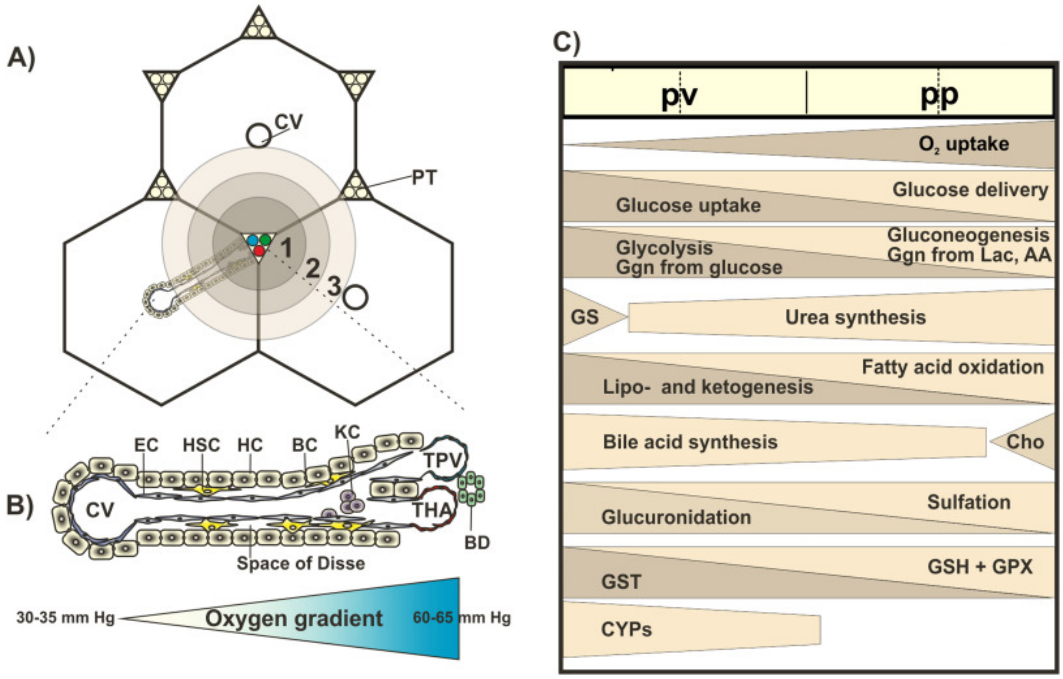

Figure 1-9 Liver microarchitecture and the hepatic acinus oxygen gradient and associated metabolic zonation. (**A)** Hepatic lobule and zonated hepatocytes from the portal trial (PT) to the central vein (CV) (dotted line represented hepatic acinus cross-section) indicating zone 1, 2, and 3. (**B)** Histology of hepatic acinus demonstrating TPV (terminal portal vein), TPA (terminal hepatic arteriole), BD (Bile duct), HC (Hepatocyte), BC (bile canaliculi), KC (Kupffer cells), EC (Endothelial cell), HSC (hepatic stellate cells). **C)** Zonated hepatic metabolic functions across the hepatic acinus. PP (peri-portal), PV (peri-venous), AA (amino acids), Cho (cholesterol synthesis), CYP (cytochrome p450 enzymes), Gng (Glycogen), GPX (glutathione peroxidases), GS (glutamin synthesis), GST glutathione transferase, Lac (Lactate). Figure adapted from Kieztmann, 2017 [334].

In certain monogenetic metabolic conditions, such as ornithine transcarbamylase deficiency (OTC), gene expression is expressed predominantly by periportal hepatocytes in zones 1 and 2 [339]. Thus, for OTC, periportal transduction is crucial to gain a therapeutic effect when native promoters are utilised by gene therapy strategies such as editing, whereas pericentral hepatocyte transduction is of lesser consequence [340]. It is not known if there is hepatic zonation with regards to BCKDH enzyme activity or expression of the corresponding subunit genes. Furthermore, zonal hepatocyte transduction has been demonstrated to be capsid specific, with AAV8 capsids in

murine gene transfer studies demonstrating preferential transduction of zone 3 hepatocytes adjacent to central veins [341-343].

Secondly, the nature of the hepatocyte cell cycle is also an important consideration in designing a liver based genetic therapy for MSUD. Hepatocytes are considered quiescent, originating from progenitor cells in the portal areas and biliary epithelium. Upon differentiation, hepatocytes centripetally migrate to the central vein over a life span of 200 to 300 days, then undergo apoptosis [344, 345]. Knowing the cell cycle state of target cells is an important consideration in vector selection and design as transduction can be cell cycle stage dependant. Viral vectors such as AAV have an established ability to transduce quiescent cells like hepatocytes, whereas simple retrovirus requires cellular division [165].

Whilst hepatocytes are quiescent cells, the rate of growth of the liver is dynamic and in paediatric organs, the growth rates much higher than in adults. Multiple pre-clinical gene therapy studies have demonstrated non-durable phenotypic correction with transduction of neonatal liver with AAV gene addition vectors secondary to episomal loss [341, 346]. Hepatocytes also have a remarkable ability to regenerate after a pathological stimulus such a liver resection, cellular insult causing injury and/or necrosis, or induced proliferative cell signalling with hepatocyte growth factor or peroxisome proliferators [347-350]. Should a patient undergo a liver insult after administration of an AAV gene therapy treatment, any interval growth and cell turnover would result in loss of episomal AAV transgenes and with it, loss of therapeutic effect [168].

Organ specific physicokinetic characteristics which require consideration in designing gene therapy approaches include the high proportion of cardiac output received by the liver, as well as the specialised sinusoidal vascular bed. The specialised sinusoidal vascular bed adds a unique element to AAV vector transduction in humans. In healthy human livers, these fenestrations are 107 ±

1.5 nm which is smaller than murine sinusoidal fenestrations of standard laboratory C57BL/6 mice, which are 141 ± 5.4 nm [351]. Designing vectors that are stable in the blood stream and of a size that can enter these sinusoidal fenestrations and cross the space of Disse to the hepatocytes allowing transduction, is critical.

Fenestration size has been demonstrated to directly impact transduction efficiencies in mice, with larger sinusoidal fenestrations associated with higher transduction efficiencies for adenoviral vectors in a rabbit model [352, 353]. The diameter of adenovirus approached that of the rabbit model with this simple physical barrier impeding target cell transduction. For smaller vectors such as AAV which is 25 nm in diameter this is less of a concern in healthy livers. However in monogenic liver disease where hepatic fibrosis and progressive cellular injury forms part of the natural disease history, hepatocyte transduction can be impeded by a barrier of connective tissue deposition in the space of Disse obliterating the sinusoidal fenestrations and preventing vector entry [354].

1.5.5.3 Liver targeted AAV therapy in the clinic

Exploitation of unique liver cellular biology and considered vector design have culminated in translational success of several liver directed gene therapies across multiple clinical trials. Notably for the condition Haemophilia B, where factor IX levels were improved from <1% up to 10% after human subjects with severe Haemophilia B received intravenous administration of serotype-AAV8-pseudotyped expressing a codon-optimised factor IX (FIX) transgene [177, 218]. Given the natural hepatic tropism of rAAV vectors, the critical metabolic role played by the liver and the phenotypic correction provided by liver transplantation in multiple metabolic liver diseases, the liver may be a promising target organ for recombinant AAV gene therapy for MSUD.

1.5.6 The Muscle as a Target for AAV Gene Therapy

Muscle cells, in particular skeletal and cardiac muscle tissues, have been an organ of interest for a growing number of gene therapies, including MSUD. Skeletal muscle accounts for approximately 50% of total body BCKDH in humans and thus stands as an attractive organ to target in the development of a novel genomic therapy for MSUD. Despite this, there have been no MSUD AAV gene therapy studies solely targeting muscle in the classical disease MSUD preclinical models.

1.5.6.1 Structure and Function of Mammalian Myocytes

Mammals have four types of muscle tissue cells, also known as myocytes: skeletal, cardiac, smooth and myoepithelial. They each have a specialise and unique function, structure and development and are supported by associated connective tissues and satellite cells. Unified by an ability to generate contractile forces through organised actin and myosin filament systems, the different myocyte cell types have specific differences with respect to actin and myosin amino acid sequences, cytoskeletal arrangements and alternative proteins involved in generating their contractile forces [355].

Skeletal muscle is one of the largest organs in the body, and comprises approximately 40% of human body mass and contains approximately 50-70% of body proteins [356]. Human tissues grow through either mitosis or by increasing their length or increasing their girth, however skeletal muscle cells only proliferate by mitosis *in utero* and the final number of multinucleated skeletal muscle cells an individual has is determined prior to birth. Skeletal muscle cells are thus a described as post-mitotic and the total number of myocytes remain relatively unchanged over an individual's lifetime [357]. Skeletal myocytes are also multi-nucleated cells and under the control of nuclear domains. These nuclear domains contain multiple cell nuclei and control protein synthesis, direct filament production and protein trafficking to the rest of the myocyte. As post-mitotic cells, skeletal muscle cells grow only through hypertrophy, increasing in length or girth [357]. Skeletal

muscle cells are large, and can be up to 2-3cm in size [358] compared to cardiac myocytes which range from 60 to 140 μm in length and 17 to 25 μm in diameter [359, 360].

Postnatally, the growth of skeletal muscle cells is directed by satellite cells, which are myocyte stem cells. These myocyte stem cells facilitate the maintenance of muscle fibres. Unlike the myocytes they manage, satellite cell populations are dynamic and can expand in response to exercise or muscle inflammation and have been seen to diminish in population size but not function with ageing [361, 362]. Satellite cells are situated between the basal lamina and the sarcolemma and function to repair damaged muscle fibres through regeneration and production of new myocytes which fuse with existing muscle fibres.

A single skeletal muscle, *e.g.*, a quadricep or bicep, consists of multiple tissues including contractile myocytes, blood vessels, lymphatics, connective tissue sheath and contractile muscle fibres (Figure 1-10). The basic functional, contractile subunit of muscle is the sarcomere. Multiple sarcomeres join to form individual muscle fibres which are surrounded by a connective tissue sheath, or endomysium. Muscle fibres, also known as myofibrils, group together to form fascicles. The whole muscle is then encased in perimysium. In skeletal muscle sarcomeres, actin and myosin are arranged in a striated pattern. Within the sarcomere a central M line anchors thick myofilaments of myosin which form dark A bands. The Z line borders the sarcomere which serves as the anchor point for the thinner actin filament. The actin and myosin project towards each other and partially overlap.

Skeletal muscle is also classified functionally as being fast or slow twitch based on shortening speeds. This simple definition corresponded to observed morphological differences, with fast twitch muscles appearing paler in some species, notably birds, and slow twitch muscles appearing darker due to higher myoglobin and capillary concentrations [356]. The higher concentration of

myoglobin and capillary content in red muscles also corresponds to the greater oxidative capacity in these slow twitch muscles compared with fast twitch. Histological analysis shows a correlation between myosin ATPase activity and shortening speeds [363]. The classification of muscle fibres has now expanded and includes 1) histochemical staining for myosin ATPase, 2) myosin heavy chain isoforms or 3) metabolic enzymes. Each of these classifications has relative merit depending on the outcome measures being assessed [364].

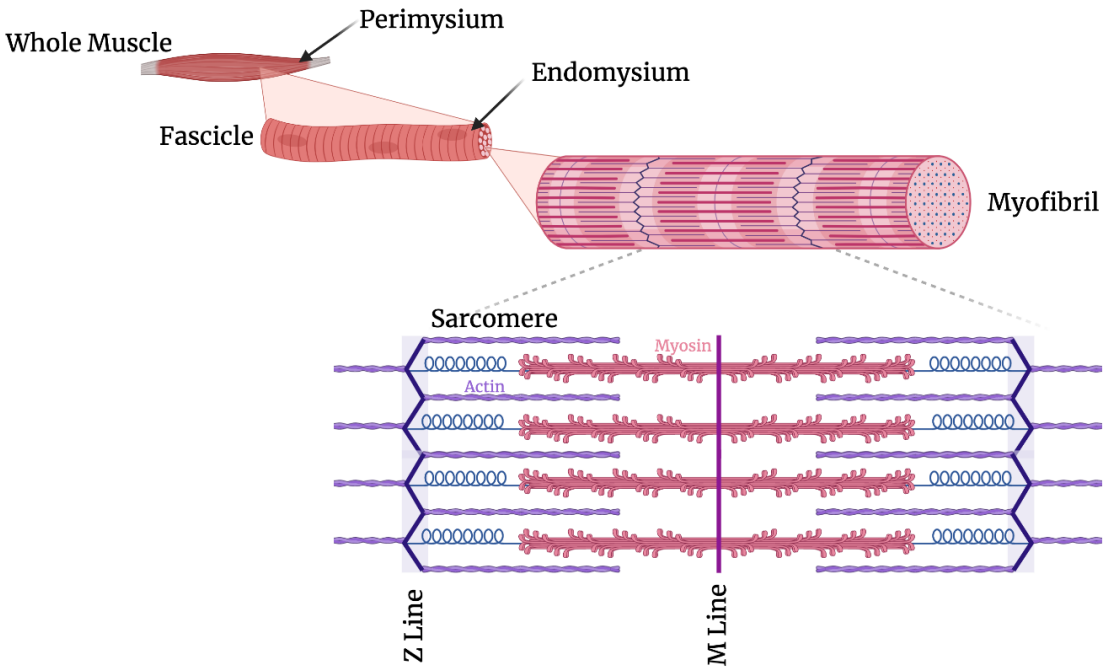

Figure 1-10 Structural anatomy of skeletal muscles. Whole muscle is covered in perimysium which contains bundles of fascicles covered with endomysium. Fascicles are made of groups of myofibrils which are in turn made up of multiple sarcomeres. Sarcomeres consist of central M line which anchors longitudinal myosin fibres (thick filaments), interlinked with actin (think filaments) which are anchored along the Z line. Figure made with BioRender.

1.5.6.2 Considerations in developing a muscle targeted AAV gene therapy for maple syrup urine disease

In humans, skeletal muscle contributes the largest total amount of BCKDH enzyme in BCAA catabolism. In MSUD patient's, there may be a muscle phenotype and muscle weakness presents

as a classical clinical feature but interestingly can also present with mixed signs of either hypotonia or hypertonia. The underlying pathophysiology of this is not well characterised but a small case study of 3 paediatric patients, one with good dietary control and two with poor outcomes demonstrated universal abnormalities in muscle biopsies assessed using electron microscopy including micro-fibrillary lysis, myocyte necrosis and auto-phagocytic vacuoles [365]. The exact mechanism for these changes are not known, though one hypothesis for these phenomena is mitochondrial dysfunction secondary to intracellular accumulation of KIC [143]. In this way, correcting muscle BCKDH enzyme activity with an AAV gene transfer strategy may be a way to both increase total body BCKDH activity and reduce myocyte mitochondrial dysfunction. Whilst is it not well characterised, if subtle muscle damage in MSUD is cumulative or indeed worsened with successive metabolic decompensations, early vector administration in the life of a MSUD patient may be important to ensure maximal vector efficacy and prevent muscle damage throughout childhood as vector transduction may be impaired if gene therapy is administered after muscle damage has occurred.

Like many organs considered for AAV gene therapy, a major challenge with skeletal muscle has been achieving even, widespread, systemic AAV vector delivery across skeletal and/or cardiac muscle cells. In humans, the two delivery routes for muscle gene therapy exist: intravenous or intramuscular. Generally, intravascular delivery allows for more widespread transduction, though vector losses to non-muscle tissue especially the liver, may reduce overall muscle transduction efficiencies whereas direct muscular injection improved individual muscle transduction efficiencies. However, certain significant muscles, such as the heart and diaphragm, are less accessible and direct injection carries higher risk. Intramuscular administration is often less practical, more invasive and overall, a less desirable route for clinical translation. Intravenous administration is the preferred route but necessitates balancing high vector doses required to

effectively transduce muscle with the associated safety concerns such as vector genotoxicity and severe immune and inflammatory responses.

The development of AAV capsids and promoters tailored for muscle expression is doing much to help balance efficacy with safety. Capsids with vastly improved myocyte tropism to skeletal and/or cardiac tissue and expression of muscle specific gene regulatory cassettes has not only assisted with improved biodistribution but also helped to reduce total vector doses required to achieve systemic delivery [366]. Capsid modifications such as glycated rAAV2 reduced heparin and monoclonal antibody A20 binding and also opportunistically resulted in remarkably improved transgene expression in muscles [367]. More deliberate muscle trophic vector discovery with directed evolution have recently delivered promising novel capsids, including AAV9 derived pseudoserotypes AAVMYO and Myo-AAV [368, 369]. These bio-engineered capsids were generated using directed evolution strategies. AAVMYO was assessed via massively parallel in vivo evaluation of barcoded capsid variants across three libraries in CB57BL/6J mice. Molecular analysis demonstrated AAVMYO to have superior transcriptional efficiency and specificity in murine muscle tissues including skeletal, cardiac and diaphragm compared to AAV9. Research into myotrophic AAV is ongoing and further optimisations in second generation capsids may further improve the transduction efficiencies and safety profiles across species including humans [370].

This improved biodistribution afforded by the current generation of muscle trophic capsids is clearly beneficial in considering clinical translation and vector safety profiles and is especially important in degenerative muscle conditions where muscle structure and function can be best preserved by improving tissue penetrance of therapies. In conditions like MSUD however, where a gene therapy vector predominantly would be used restore a non-structural metabolic function, this improved transduction efficiency is less important for overall muscle function, but no less important for overall vector efficacy.

1.6 Rationale for Gene therapy in Maple Syrup Urine Disease

Current treatment options for MSUD are non-curative and there is an unmet clinical need for superior therapeutic options. The success of liver transplantation in MSUD, essentially providing allogenic gene transfer with an organ, illustrates the potential for genomic technologies to do the same. Whilst the exact therapeutic threshold of cellular correction is not known for MSUD, the success of liver transplantation in achieving improved metabolic stability is illustrative of this organ as a potential target for genomic therapies. Of equal interest, skeletal muscle is the dominant organ contributing to total body BCKDH enzyme activity and may also represents an ideal target organ for a genetic therapy. Whilst the liver has traditionally experienced superior transduction efficiencies with recombinant AAV and thus is a prime target for many AAV-mediate gene therapy applications, the aggressive pursuit of novel myotropic capsids have led to ever increasing AAV myocyte transduction efficiencies. Three pre-clinical gene therapy studies using recombinant AAV published since this inception of this thesis have demonstrated the potential of AAV across the three main MSUD genotypes but failed to fully characterise organ contributions to phenotypic correction. No published study has yet proven successful in demonstrating full phenotypic correction of a murine MSUD disease model with an AAV mediated gene therapy, nor isolated rescue to a single tissue type. Targeting a single organ in pre-clinical models is important for vector safety considerations, both to narrow the window of off target effects and to direct understanding of vector biokinetics and so determine therapeutic thresholds for improved clinical translation.

The AAV vectors used in this project were configured based on currently available capsids and cassette elements selected for demonstrated efficacies in the intended target tissues. The AAV8 capsid [214] was selected to be used in experiments where murine liver tissue was the primary target and used in conjunction with a transgene cassette containing the strong putatively liver-specific enhancer/promoter APOe/hAAT. For the vectors used to target murine muscle tissue,

the capsid AAVMYO [368] was selected and the transgene expressed under the transcriptional control of the CK8e enhancer/promoter [371]. The overarching objective of this project is to develop a recombinant AAV-mediated therapy for MSUD using a neonatal lethal DBT-knockout murine model. The neonatal lethal DBT-knockout model was derived from a transgenic mouse and, whilst not formally characterised, anticipated to recapitulate Classical MSUD. Disease onset is expected to occur rapidly after birth and so a thorough understanding of host-vector interactions with respect to timing of vector administration will be necessary to aid assessments of vector durability in a MSUD disease specific context. In order to address these questions, the following hypothesis and corresponding aims were developed pertaining to the following chapters henceforth:

HYPOTHESIS 1: Highly efficient transfer of a human *DBT* transgene in an AAV8 pseudo-serotyped vector to livers of DBT-deficient mice in the newborn period will improve the survival and biochemical phenotype of MSUD.

Aim 1: to evaluate phenotype correction in DBT-deficient mice injected with a liver-directed recombinant AAV vector encoding a human DBT transgene using physical parameters including survival, growth, and blood branched chain amino acid levels during

i) a period of metabolic stability and,

ii) during a period of metabolic stress.

HYPOTHESIS 2: The exact hepatic therapeutic correction threshold of BCKDH activity in MSUD is not known and the phenotypic correction effects of neonatally administered liver-restricted recombinant AAV vectors have been shown to attenuate in concert with liver growth and hepatocyte cell division. The loss of AAV vector episomes from neonatally transduced livers of DBT-deficient mice will result in a re-emergence of the MSUD clinical phenotype before attaining adulthood.

Aim 2: To evaluate the durability of neonatally administered liver directed gene transfer with conventional AAV vectors in DBT-deficient mice.

HYPOTHESIS 3: Stable gene transfer to murine hepatocytes of DBT-deficient neonates with a hybrid AAV-piggyBac transposon system will improve the durability of phenotype rescue compared to conventional AAV-mediated gene transfer.

Aim 3: To evaluate the durability of neonatally administered liver directed gene transfer with a hybrid gene addition vector with *piggyBac* transposase in DBT-deficient mice.

HYPOTHESIS 4: The pattern of extra-hepatic expression of transgenes under the transcriptional regulation of the APOe/hAAT enhancer/promoter is influenced by cis-regulatory elements included in the expression cassette.

Aim 4: To evaluate the effect of cis-regulatory elements on the tissue expression patterns of a hDBT transgene, including the effect exerted by inclusion of

i) WPRE elements and

ii) pBTIRs.

HYPOTHESIS 5: Myocytes represent a relatively stable cell population and selective functional transduction of these cells in DBT-deficient mice with a highly expressed, myocyte-restricted AAV transgene expression cassette encoding a hDBT transgene will provide stable therapeutic correction of the MSUD phenotype.

Aim 5: To evaluate strategies which enhance the functional transduction of striated myocytes with an AAV encoded hDBT transgene including capsid pseudo-serotypes and micro-RNA targeting sites;

Aim 6: To evaluate phenotype correction in *DBT*-deficient mice treated with a muscle restricted recombinant AAV vector encoding a human *DBT* transgene.

Chapter 2
Materials and Methods

2.1 Materials

Chemicals used in this project were handled with the appropriate personal protective equipment (PPE) and all safety and environmental controls were adhered to as per material safety data sheets (MSDS) for each chemical. Waste products were disposed of safely in concordance with respective MSDS for each chemical. Overseas import of biological reagents and/or chemicals were undertaken as per Australian Government Department of Agriculture, Water and the Environment under current guidelines from the current (at time of purchase) permit to import conditionally non-prohibited goods issued to Children's Medical Research Institute by the Australian Government.

2.1.1 Chemicals and general reagents

Reagents used to make up solutions, buffers and bacterial media were all analytical grade or higher (Table 2-1). Solutions and buffers were made using MilliQ or molecular grade water (Table 2-2). Protocols were carried out at room temperature, unless otherwise stated.

Table 2-1 Chemicals and reagents

Chemical	Source
General reagents	
2-methylbuytane	Sigma-Aldrich (St. Louis, USA)
2 × TB Green Premix Ex Taq	TAKARA (Kyoto, Japan)
4-(2-hydroxyethyl)-1-piperazineethanesulfonic acid (HEPES)	Astral Scientific (Sydney, Australia)
Ampicillin Sodium Salt	AG-Scientific (San Diego, USA)
BioMix Red	Bioline (London, UK)
Calcium chloride	Sigma-Aldrich (St. Louis, USA)
Chloroform	VWR (Pennsylvania, USA)

Chloroform:isoamyl 24:1 (v/v)	Sulpeco (Sigma-Aldrich, St. Louis, USA))
Dimethylsulphoxide (DMSO)	Sigma-Aldrich (St. Louis, USA)
Dithiothreitol (DTT)	Sigma-Aldrich (St. Louis, USA)
Donkey Serum	Sigma-Aldrich (St. Louis, USA)
Ethanol 70% (v/v)	POCD Healthcare (New South Wales, Australia)
Ethanol 100% (v/v)	EMSURE, Merk Group (Darmstadt, Germany)
Ethylenediaminetetraacetic acid (EDTA)	Chem Supply (Gillman, Australia)
Glycerol	Chem Supply (Gillman, Australia)
Hydrochloric Acid	Merck (Rahway, USA)
Immu-Mount	Thermo-Fischer (Waltham, USA)
Isopropanol	Univar (Illanois, USA)
Kanamycin sulfate	Gibco (Waltham, USA)
Magnesium chloride	Sigma-Aldrich (St. Louis, USA)
Methanol	POCD Healthcare (New South Wales, Australia)
QX200 EvaGreen Supermix	BioRad (Hercules, USA)
Paraformaldehyde	Sigma-Aldrich (St. Louis, USA)
Phenol:chloroform:isoamyl 25:24:1	Invitrogen (Waltham, USA)
Phosphate buffered saline (PBS) Tablets	MP Chemicals (Victoria, Australia)
Polyvinyl alcohol	Sigma (St. Louis, USA)
Sodium Chloride	Sigma-Aldrich (St. Louis, USA)
RedSafe	iNtRON Biotechnology (Gyeonggi-do, South Korea)
Sodium Hydroxide Pellets	Sigma-Aldrich (St. Louis, USA)
Sucrose	Chem Supply (Gillman, Australia)
Tissue-Tek® Optimal Cutting Temperature (O.C.T.) Compound	Sakura (Osaka, Japan)
Tris Base	Amresco (Dallas, USA)
Trisaminomethane (Tris)	Chem Supply (Gillman, Australia)
Triton X-100	Sigma-Aldrich (St. Louis, USA)
TRIzol®	Invitrogen (Waltham, USA)
Tween-20	Sigma-Aldrich (St. Louis, USA)
Tissue Culture	
Dulbeccos Modified Eagle Medium (DMEM)	Gibco (Waltham, USA)
Dubecco's Phosphate Buffer Saline	Gibco (Waltham, USA)
Foetal Calf Serum (FCS)	Life Technologies (Carlsbad, USA)
Iscove's Modified Dulbecco's Medium (IMDM)	Sigma-Aldrich (St. Louis, USA)
Penicillin-Streptomycin	Gibco (Waltham, USA)
Trypan-Blue Solution 4% (w/v)	Amresco (Dallas, USA)
TrypLE™ Express Enzyme (1×)	Gibco (Waltham, USA)
Viral vector production	
Caesium Chloride	Invitrogen (Waltham, USA)
Polyethylene glycol (PEG) 8000	MP Chemicals (Victoria, Australia)

Pharmacological agents for Mice	
0.9% (w/v) Sodium chloride	Baxter (Deerfield, USA)
10% (v/v) Neutral Buffered Formalin	Sigma-Aldrich (St. Louis, USA)
4',6-Diamidino-2-phenylindole dihydrochloride (DAPI)	Sigma-Aldrich (St. Louis, USA)
Isoflurane	Abbott Australasia Pty Ltd (Macquarie Park, Australia)
Baytril® (Enrofloxacin)	Bayer Healthcare (Levekusen, Germany)
Buprenorphine	Reckitt Benckiser (Slough, UK)
Paraformaldehyde	BDH/Merck (Rahway, USA)

Table 2-2 Solutions and Buffers

Solutions	Composition and preparation
General Buffers and Solutions	
5× TBE	54 g Tris base, 27.5 g Boric acid, 10mM EDTA pH 8.0 in 1 L MilliQ. To make 1×, 5× diluted 1 in 5 parts MilliQ water; to make 0.5×, 5× diluted 1 in 10 parts MilliQ water.
6× Orange G Loading Dye (For agarose gel)	0.25% Orange G in MilliQ Water
Lysogeny Broth (LB) Agar	LB media containing 1.5% (w/v) Bacto-agar. Autoclaved
Lysogeny Broth (LB) Media	1% (w/v Bacto-tryptone, 0.5% (w/v) Bacto-yeast extract, 1% (w/v) NaCl. Autoclaved
Phosphate Buffered Saline (PBS)	1× PBS (no Ca^{2+}, no Mg^{2+}) tablet per 500mL of MilliQ Water
SOC Media	2% (w/v) Bacto-tryptone, 0.5% (w/v) Bacto-yeast extract, 10 mM NaCl, 2.5 mM KCl, 10 mM $MgCl_2$, 10 mM MgSO4, and 20 mM glucose. Autoclaved
Cell Culture	
Complete DMEM	DMEM + 10% (v/v) heat-inactivated FCS
Maintenance media	DMEM + 2% (v/v) heat-inactivated FCS
Transfection media	IMDM + 10% (v/v) heat-inactivated FCS
Transfection and AAV Purification	
0.15 M Na_2HPO_4	10.647 g in 500 mL dH2O, pH 7.10. Autoclaved
2M $CaCl_2$	29.404 g $CaCl_2$.2H2O in 100 mL MilliQ Water. Autoclaved
2× HEPES-buffered Saline (HBS)	280 mM NaCl, 50 mM HEPES, pH 7.10. Autoclaved
10% (v/v) TE	1 mM Tris, 0.1 mM EDTA, pH 8.0. Autoclaved
40% (v/w) PEG 8000/NaCl	200 g PEG 8000, 250 mL 5M NaCl with MilliQ to 500 mL. Filter sterilised (0.22 μm)
1000× (Ca^{2+}/Mg^{2+}) stock solution	0.90 M $CaCl_2$ anhydrous, 0.49 M $MgCl_2.6H_20$. Filter sterilised (0.22 μm). Diluted 1:1000 for dialysis and caesium chloride solutions
Benzonase Buffer	20 mL 1M Tris-HCl, Ph 8.5, 1 mL 1M $MgCl_2$, water to 500 mL. Autoclaved
Caesium Chloride solution (1.3 g/mL)	39.9 g to 100 mL PBS (Ca^{2+}/Mg^{2+}).
Caesium Chloride solution (1.37 g/mL)	50 g to 100 mL PBS (Ca^{2+}/Mg^{2+}). Filter sterilised (0.22 μm)
Caesium Chloride solution (1.5 g/mL)	33.75 g to 50 mL PBS (Ca^{2+}/Mg^{2+}). Filter sterilised (0.22 μm)
Dialysis Buffer	1× PBS (Ca^{2+}/Mg^{2+}) ± 5% (v/v) glycerol
HEPES/EDTA Resuspension Buffer	25mL 1M HEPES, pH 7.4, 15 mL 5M NaCL, 25 mL 0.5M EDTA, MillliQ to 500 mL. Autoclaved

Transfection solution A (per 10 cm tissue culture dish)	15 μg Plasmid DNA, 62.5 μL 2 M $CaCl_2$ made up to 500 μL 10% (v/v) TE
Transfection solution B (per 10 cm tissue culture dish)	54.5 mL 2× HBS, 550 μL 0.15 M Na_2HPO_4
Histology and Immunostaining	
4% (w/v) Paraformaldehyde (PFA)	8 g Paraformaldehyde in 100 mL, dissolved at 60ºC, adjust pH with NaOH until dissolved (pH 7.2-7.4). Made up to 200 mL with 2× PBS. Stored at -20ºC
5× Towbin	60.6 g Tris-base, 288 g Glycine and MilliQ water to 4 L.
10% (w/v) Sucrose	20 g in 200 mL 1× PBS. Filter sterilised (0.2μm). Stored at 4ºC
20% (w/v) Sucrose	40 g in 200 mL 1× PBS. Filter sterilised (0.2μm). Stored at 4ºC
30% (w/v) Sucrose	60 g in 200 mL 1× PBS. Filter sterilised (0.2μm). Stored at 4ºC
Gelvatol	15 mL MilliQ water with 30 mL 0.2M Tris HCl (pH 8.5) and 6 grams of polyvinyl alcohol
Luminol femto	1:1 of Luminol enhancer to peroxide buffer from the SuperSignal™ West Dura Extended Duration Substrate kit
Ponceau S Solution	0.1% (w/v) Ponceau S, 5% (v/v) Acetic galacial acid
PBST	1 x PBS, 0.1% (v/v) Tween 20
PBST/5% (w/v) skim milk	PBST as above with 5 g of skim milk power to 100mL
Running buffer	25 mL of NuPAGE Running Buffer to 475 mL of MilliQ Water
Transfer Buffer	200 mL 5× Towbin, 100 mL Methanol and 700 mL of MilliQ water
ddPCR	
Alkaline digestion buffer	1.25 mL of 1 M NaOH, 20 μL of 0.5 M EDTA, 48.73 mL H_2O
Neutralisation buffer	2 mL of 1 M Tris, 25 μL of Tween 20, make up to 50 mL with H_2O, pH 5, stored at 4°C

2.1.2 Kits and Antibodies

Commercially available kits used are listed (Table 2-3). Commercially sourced antibodies used are listed (Table 2-4).

Table 2-3 Commercial Kits

Item	Source
Isolate II Plasmid Mini Kit	Bioline (London, UK)
NucleoBond Xtra Maxi Kit	Macherey-Nagel (Düren, Germany)
NucleoBond Xtra Midi Kit	Macherey-Nagel (Düren, Germany)
On-column PureLink DNase treatment	Invitrogen (Waltham, USA)
pGEM-T Easy Vector System I	Promega (Madison, USA)
PureLink RNA Mini Kit	Invitrogen (Waltham, USA)
Qubit BR dsDNA Assay Kit	Invitrogen (Waltham, USA)
Superscript III First Strand Synthesis System	Invitrogen (Waltham, USA)
Superscript IV First Strand Synthesis System	Invitrogen (Waltham, USA)
SuperSignal™ West Dura Extended Duration Substrate	Thermo Scientific (Waltham, USA)
Wizard SV Gel and PCR Clean-Up System	Promega (Madison, USA)

Table 2-4 Antibodies

Antibody	Species raised in	Source, Cat No.	Conjugate	Concentration	Use	Dilution
Primary Antibodies						
Anti-DBT	Rabbit polyclonal	Sigma, #HPA026485	Nil	0.3mg/mL	Western blot	1:5000
Anti-Vinculin	Mouse Monoclonal	Sigma-Aldrich, #V9131	Nil	NA	Western blot	1:5000
Anti-DBT	Rabbit polyclonal	Invitrogen, #PA5-115097	Nil	1 mg/mL	IF	1:100
Secondary Antibodies						
Anti-Mouse	Goat Monoclonal	Biorad, #1721011	HRP	NA	Western blot	1:5000
Anti-Rabbit	Goat Monoclonal	Biorad #1721019	HRP	NA	Western blot	1:5000
Anti-Rabbit	Donkey polyclonal	Invitrogen #A32754	AF™PLUS594	2mg/mL	IF	1:500

2.1.3 Bacterial Strains

Bacterial host strains used in the construction of plasmids are detailed (Table 2-5).

Table 2-5 Bacterial Host Strains

Strain	Genotype	Source
DH5-α	F– φ80*lac*ZΔM15 Δ(*lac*ZYA-*arg*F)U169 *rec*A1 *end*A1 *hsd*R17(r_K^- , m_K^+) *pho*A *sup*E44 λ- *thi*-1 *gyr*A96 *rel*A1	Thermo Scientific (Massachusetts, USA)
JM109	*end*A1, *rec*A1, *gyr*A96, *thi*, *hsd*R17 (r_K^-, m_K^+), *rel*A1, *sup*E44, Δ(*lac-pro*AB), [F´ *tra*D36, *pro*AB, *laq*I qZΔM15]	Promega (Madison, USA)

2.1.4 Primers

Primers used in this thesis are listed (Table 2-6).

Table 2-6 Primers

Primer Name	Direction	Oligo sequence (5' to 3'))	Melting temperature (°C)
Genotyping primers			
km034	Anti-sense	GCTTCTTGCTTCACTGAACATCAA	62
km047	Sense	TCACCATCACCAGCCGTTAC	60.5
km053	Sense	GGCATTTACAGGAACATGCAAG	60.1
km058	Anti-sense	CAGGACATAGCGTTGGCTAC	60.5
Primers targeting DBT for PCR (RT-qPCR and ddPCR)			
km001	Sense	GCACCACTGATCTTACAGGAG	61.2
km020	Anti-sense	TTGATCCAAGGGCCCCAATG	60.5
Primers targeting murine albumin for PCR (RT-qPCR and ddPCR)			
mAlbF	Sense	AACTGCTACTCCCCTCCTAC	60
mAlbR	Anti-sense	TTTACCCCAGTGCAGGAAAG	58
Primers and probe targeting bovine growth hormone polyadenylation sequence			
SC277	Sense	GCC AGC CAT CTG TTG T	51
SC279	Anti-sense	GGA GTG GCA CCT TCC A	53
SC278	Probe	TCCCCCGTGCCTTCCTTGACC	67
Sequencing Primers			
km002	Sense	GCTTCTCCAATTTGTGGAAATCC	60.9
km003	Anti-sense	CGTTTAAAAAACCTCCCACACC	60.1
km004	Anti-sense	GCTTCAAAACATGAACATTACCACA	60.9
km005	Anti-sense	GCTGGAGGATGGGAACTGAG	62.5
km008	Sense	GCCCTGAAGATACCTCATTTTG	60.1
km009	Anti-sense	GCCTTATATACTTCTCCTTTCTGG	62
km016	Sense	AGTGTCTCAGTTTGATAGCATCTGT	62.5

km017	Anti-sense	CCCCAATGGCTACTTCAGGT	60.5
km018	Sense	AATGCGGGGAAGCTGATTTGT	59.5
km019	Sense	AAGGCTGCTTCCTTGGGATT	58.4
LP1 594R	Anti-sense	CGTATTTAAGCAGTGGATCCAG	60.1
SC035	Anti-sense	CGTCTAGATCAGTTCCAAAGGTTGGAATC	69
SC036	Sense	CGCGATATCTGCTTTATTTGTGAAATTTGTG	69
Gibson assembly primers			
km080	Sense	CCCCCGGGCTGCAGGAATTCGCGGCCGCTC TAGAGC	77
km081	Anti-sense	TCCAGAGGTTGATTATCGATAAGCTTGAATT CATCGATGTCGACTCATTTCAGATCTAGT	65

2.1.5 Plasmids

Plasmids used this thesis for cloning or vector production are listed (Table 2-7, Table 2-8).

Table 2-7 Parental Plasmids

Plasmid	Details	Source
pGEM®-T Easy	TA Cloning vector	Promega
pAd5	Addgene	Addgene [372]
pAVV2.APOe/hAAT.eGFP.pTIR	Plasmid with eGFP transgene with *piggyBac* TIR and AAV2 ITRs	Sharon Cunningham, CMRI
pUC-Kan.APOe/hAAT.hDBT.WPRE	Cloning plasmid with human *DBT* , WPRE under liver specific promoter	GenScript
pUC-Kan.APOe/hAAT.hDBT.pBTIR	Cloning plasmid with human DBT and pBTIR under liver specific promoter	GenScript
pUC-Kan.CK8e.hDBT.WPRE.miRNA-TS	Cloning plasmid with human DBT, WPRE and miRNA targeting sites under muscle restricted promoter	Azenta/GenWiz
pAAVMYO	Packaging plasmid for AAVMYO	Sourced from TVRU, CMRI. Original design from Dirk Grimm, University of Heidelberg [368]
pAAV8	Packaging plasmid for AAV8	Dr James Wilson, University of Pennsylvania [373]
pAAV2.APOe/hAAT.*piggyBac*	AAV2 plasmid encoding a *piggyBac* transposase transgene under liver specific promoter	Sharon Cunningham, CMRI

Table 2-8 Plasmids synthesised by candidate

Plasmid	Details	Source
pAAV2.APOe/hAAT.hDBT	AAV2 plasmid with human *DBT* transgene under liver specific promoter	Kathryn Mullany
pAAV2.APOe/hAAT.hDBT.WPRE.pbTIR	AAV2 plasmid with human *DBT* transgene WPRE and *piggyBac* TIR under liver specific promoter	Kathryn Mullany
pAAV2.APOe/hAAT.hDBT.pbTIR	AAV2 plasmid with human DBT transgene, *piggyBac* TIRs under liver specific promoter	Kathryn Mullany
pAAV2.APOe/hAAT.hDBT.WPRE	AAV2 plasmid with human DBT and WPRE under liver specific promoter	Kathryn Mullany
pAAV2.CK8e.hDBT.WPRE.miRNA-TS	AAV2 plasmid containing human *DBT* transgene WPRE and miRNA targeting sites under muscle restricted promoter	Kathryn Mullany

2.1.6 AAV Vectors

Vectors produced and used in this thesis are listed (Table 2-9). All vectors were produced by the candidate and purified via CsCl gradient purification.

Table 2-9 AAV Vectors

Vector	Description	Chapter
rAAV2/DJ.APOe/hAAT.eGFP	eGPF expression cassette with liver specific promoter, packaged in DJ capsid	4
rAAV2/8.APOe/hAAT.hDBT	hDBT expression cassette with liver specific promoter, packaged in AAV8.	4 and 5
rAAV2/DJ.APOe/hAAT.hDBT	hDBT expression cassette with liver specific promoter, packaged in DJ capsid.	4
rAAV2/8.APOe/hAAT.hDBT.WPRE.pbTIR **"Transposon encoding vector"**	hDBT expression cassette with liver specific promoter, WPRE and *piggyBac* transposase ITRs, packaged in AAV8.	5
rAAV2/DJ.APOe/hAAT.hDBT.WPRE.pbTIR	hDBT expression cassette with liver specific promoter, WPRE and *piggyBac* transposase ITRs, packaged in DJ capsid.	5
rAAV2/8.APOe/hAAT.*piggyBac* **"Transposase encoding vector"**	Expression cassette encoding the *piggyBac* transposase gene packaged in AAV8.	5
rAAV2/DJ.APOe/hAAT.*piggyBac*	Expression cassette encoding the *piggyBac* transposase gene packaged in DJ capsid.	5
rAAV2/8.APOe/hAAT.hDBT.WPRE	hDBT expression cassette with liver specific promoter and WPRE, packaged in AAV8.	5, 6
rAAV2/8.APOe/hAAT.hDBT.pBTIR	hDBT expression cassette with liver specific promoter and *piggyBac* transposase ITRs, packaged in AAV8.	5
rAAV2/AAVMYO.CK8e.hDBT.WPRE.miRNA-TS **"Muscle optimised vector"**	hDBT expression cassette with muscle restricted promoter CK8e, WPRE and miRNA-TS	6

2.1.7 Mouse strains

The $DBT^{-/-}$ neonatal lethal MSUD mouse model was kindly donated by Jenny Grieg (University of Pennsylvania)[325]. Heterozygous breeding pairs of $DBT^{+/-}$ mice were shipped from the University of Pennsylvania and bred to produce homozygous $DBT^{-/-}$ offspring. Heterozygous ($DBT^{+/-}$) and wildtype ($DBT^{+/+}$) littermates were also used in some experiments, where specified.

2.2 Methods

2.2.1 Molecular Biology

2.2.1.1 Small-scale plasmid purification

Commercial miniprep kits (Bioline/Meridan) were utilised for small scale plasmid DNA Isolation from bacterial clones through alkaline lysis. In brief, single bacterial colonies were selected from LB/ampicillin or LB/Kanamycin agar plates. Colonies were inoculated into 2 mL LB media supplemented with either ampicillin or kanamycin (working concentration 100 μg/mL or 50 μL/mL respectively) in 15 mL loosely capped, round bottom polypropylene tubes. Cultures were incubated at 37ºC overnight in a shaker (225 rpm, shaking orbit 19 mm) and 1 mL of culture was then pelleted in a 1.5 mL Eppendorf tube by centrifugation at 11,000 × *g* for 5 minutes. Plasmid DNA was isolated from the bacterial pellet according to manufacturer's instructions. In the final step DNA was eluted from column in 50 μL of Elution Buffer P, as provided in the kit. Purified plasmid DNA was stored at -20ºC.

2.2.1.2 Large-scale plasmid purification

Transfection-grade large scale plasmid DNA was undertaken using Nucleobond Xtra Midi or Maxi kits (Macherey-Nagel, Germany) for up to 500 μg or 2000 μg DNA per column, respectively. Plasmids were purified according to the manufacturer's instructions. Cultures for plasmid purification were generated by inoculating a single bacterial colony selected from LB/ampicillin or

LB/Kanamycin agar plates into 3 mL of LB/ampicillin or LB/Kanamycin medium and grown at 37°C in a rotary shaking incubator for 6 hours (225 rpm, shaking orbit 19mm). The culture was then diluted 1:500 into fresh LB media (300 – 500 mL depending on midi or maxi-prep) supplemented with either ampicillin or kanamycin (working concentration 100 μg/mL or 50 μL/mL, respectively). Cultures were incubated overnight in a rotary shaking incubator (225 rpm, shaking orbit 19mm) at 37°C. Purified plasmid DNA was stored at –20°C.

2.2.1.3 Restriction endonucleases

New England Biolabs restriction endonucleases were purchased and used for multiple protocols as detailed further in each section. These enzymes were used as per the manufacturer's instructions with corresponding enzyme buffers of either rCutsmart, NEB r1.1, NEB r2.1 or NEB r3.1.

2.2.1.4 Gel electrophoresis

Agarose gel electrophoresis was utilised to separate DNA fragments according to molecular weight. Agarose gels were prepared using 0.9-2% (w/v) Agarose (Meridian Bioscience) in TBE (either 1× or 0.5×) and heated until agarose melted. RedSafe Nucleic Acid Staining Solution (INtRON Biotechnology) was added 5 μL per 100 mL of molten gel. Gel was then poured into cases, combs inserted and allowed to set at room temperature prior to loading samples. Samples were supplemented with 6× Orange G loading dye before loading into gels. Voltages of 80 – 120 V were applied across the tanks using BioRad PowerPac™ Universal power pack and gels imaged with Gel Documentation System (AXYGEN) upon completion.

2.2.1.5 Purification of PCR amplicons and DNA products

DNA products from PCR or excised band from agarose gel electrophoresis was undertaken using Wizard SV Gel and PCR Clean-Up System (Promega). DNA was loaded onto a column, washed

and eluted according to manufacturer's instructions. DNA within agarose gel was dissolved with membrane binding solution at 50°C as per manufacturer instructions prior to loading on to the column. DNA was eluted with 30 µL of DNase/RNase free water.

2.2.1.6 A-tailing of PCR DNA fragments

Adenine bases were added to the 3' end of DNA fragments generated through PCR using *Taq* DNA Polymerase in ThermoPol Buffer (New England Biolabs). Reactions consisted of template DNA purified by Wizard SV Gel and PCR Clean-Up System (Promega), 5 µL 10× ThermoPol Buffer, 1 µL of 10 mM dATP, 1 µL of *Taq* DNA polymerase and nuclease free water to 50 µL and incubated in a thermocylcer at 72°C for 20 minutes.

2.2.1.7 DNA ligation

DNA ligation reactions were performed using the T4 DNA ligase kit from New England Biolabs. Reactions consisted of 1 µL T4 DNA ligase, 2 µL 10× DNA Ligase Reaction Buffer, and fragments at various ratios according to manufacturer's guidelines. Reactions were run overnight at 12°C. The reaction was inactivated by heat treatment at 65°C for 10 minutes.

2.2.1.8 Ligating clones with T4 DNA ligase

Ligation of vectors and DNA inserts was undertaken using the New England BioLabs T4 DNase Ligase protocol as per manufacturer's instructions (NEB, Cat# M0202). Ratios of 3:1 or 5:1 insert to vector were used. Final reactions were incubated either as per manufacturers protocol or at 4°C for 48 hours. Reaction mix was then heat inactivated at 65°C for 10 minutes and then chilled on ice. Competent cells, DH5α or JM109, were transformed with 5 µL of ligation products as described below.

2.2.1.9 Transformation of competent cells

Vials of 100 µL of competent cells (DH5α or JM109 (Promega)) were thawed on ice for 20 minutes. Cells were then gently pipetted up and down and transferred to 15 mL polypropylene round bottom tube. Material to be transformed were added and tubes flicked gently to mixed. Cells were then incubated on ice for 30 minutes and tubes then placed in 42°C water bath and heat shocked for 30 seconds. Tubes were then placed back on ice for 5 minutes. LB medium 2 mL was added to tube and incubated at 37°C for 1 hour in a shaking incubator (225 rpm, shaking orbit 19mm). Cells were then plated onto LB agar with appropriate antibiotic (*e.g.*, Ampicillin or Kanamycin at previously described working concentrations) at 37°C overnight.

2.2.1.10 Glycerol bacterial stocks

Glycerol stocks of bacterial harbouring plasmids of interest were made by taking 500 µL of saturated bacterial culture with 500 µL of 100% sterile glycerol (final concentration 50% (v/v)), frozen and stored at -80°C.

2.2.2 Sequencing

Sanger sequencing was outsourced to a private research company, Australian Genome Research Facility (AGRF Ltd, The Westmead Institute, 176 Hawkesbury Road, Westmead NSW 2145. Template was placed in a 1.5 mL Eppendorf tube with 1 µL of 9.6mmol primer and PCR standard water to 12 µL and then the reads analysed using SnapGene software. Amount of template added varied for different products, as follows: double stranded plasmid (600-1200 ng), 600-800 bp PCR product (18-30 ng), 400-600 bp PCR product (12-18 ng), 200-400 bp PCR product (6-12 ng) and 100-200 bp PCR product (3-8 ng).

2.2.3 Nucleic Acid quantification

Quantification of RNA and DNA was undertaken using either NanoDrop™ One/OneC Microvolume UV-Vis Spectrophotometer (Thermo Scientific) and/or Qubit. Nanodrop™ was used to quantify DNA PCR amplicons, plasmids and RNA for general molecular protocols. Sample purity was estimated by ratios of the following absorbances (260 nm/280 nm) and (260 nm/230 nm). The Qubit 4 Fluorometer (Thermo Scientific) was used to determine genomic DNA concentrations for use in digital droplet (ddPCR) protocols through binding targets with fluorescent dyes in the Qubit dsDNA BR Assay Kit (Invitrogen) as per manufacturer's instructions.

2.2.4 Tissue Culture

All tissue culture was undertaken within a class II biohazard safety cabinet using aseptic technique with sterile equipment and solutions. Cells were cultured with growth medium (DMEM, 10% FBS (v/v)), transfection medium (IMDM, 10% FBS (v/v)) and maintenance medium (DMEM, 2% FBS (v/v)). Foetal bovine serum (FBS) was heat inactivated at 56°C for 30 minutes prior to addition to culture medium or stored at –20°C. Disposable plastic flasks (Corning, New York, USA) were used to culture cells. Cells were maintained at 37°C with 5% (v/v) carbon dioxide humidified incubator. 1× PBS (-Ca^{2+}, -Mg^{2+}) was used to wash cells and 1× TrypLE™ Express Enzyme used to dissociate cells. Liquid reagents were warmed to 37°C in a water bath prior to use.

2.2.4.1 Cell passaging

Cells were passaged by first aspirating old cell media from the flask. Adherent cells were then washed with 10 mL of 1× PBS without magnesium and calcium (Sigma Aldrich). Cells were dissociated with 3 mL of 1× TrypLE™ Express Enzyme and incubated for 10 minutes in 37°C humidified incubator. Cells were then tapped to further dissociate cells. Cells were then recovered

from the flask, DMEM added to a final volume of 10 mL and pipetted up and down to disperse equally. If desired, cells were then centrifuged at 1,500 × *g* for 5 minutes, supernatant removed, and cell pellet resuspended in 10 mL of fresh cell medium. Suspended cells were then added to new flasks at the desired density and appropriate volume of cell medium added for the flask size (15 – 20 mL/150 cm^2 flask or 6 – 10 mL/10 cm dish).

2.2.4.2 Cell counting

Cells were counted by diluting 1:10 with trypan blue and applying 10 µL to a haemocytometer (Countess 3FL, Invitrogen). Living cells were counted and dead cells (stained blue), were excluded from counts.

2.2.5 Recombinant Adeno-Associated Virus Production

2.2.5.1 Viral packaging in HEK293 cells

Viral vectors were manufactured as per Synder *et al.* [374] as follows. Triple plasmid transfection with calcium phosphate of HEK293 cells was performed to produce recombinant AAV virions. Prior to seeding, HEK293s were passaged several times to 80% confluency in T_{150} flasks (Corning). Cells were then seeded at 4.24 × 10^6 cells per dish for 10 cm diameter culture dishes (Corning). Complete DMEM + 10% (v/v) FBS was used to grow the cells to 80% confluency over 24 hours in 37°C in 5% (v/v) CO_2 incubator using. Cell media was then aspirated, and transfection media was gently applied to each dish approximately 2 hours prior to transfection. Transfection solutions, A and B were prepared to a volume of 500 µL per dish per solution. Solution A contained plasmid DNA including 3 µg of transgene plasmid, 9 µg adenovirus packaging plasmid and 3 µg of an AAV capsid plasmid, 0.25 M $CaCl_2$ in 10% TE Buffer. Solution B consisted of 1× HEPES buffered saline and 0.0015 M Na_2HPO_4 as per table (Table 2-2). The calcium phosphate precipitate solution was generated by adding 2 mL of solution A in a dropwise manner to 2 mL of solution B and

stirring constantly. This solution was then incubated at room temperature for 15 – 20 minutes and then 1 mL was dropped across each 10 cm tissue culture dish. Cells were incubated for 18 – 24 hours in 37°C 5% (v/v) CO_2. Media was then aspirated and maintenance media gently applied and cells incubated for 24 – 48 hours depending on the vector production efficiency associated with each capsid plasmid. Cells and media were then harvested. Adherent cells were scraped from dishes with cell lifter (Corning) and both media and cells then transferred to 50 mL tubes (Falcon). Cells were pelleted by centrifugation at 1500 × *g*. Media was transferred to 500 mL flasks and frozen at –80°C. Cells pellets were resuspended in Benzonase Buffer and frozen at –80°C.

2.2.5.2 Caesium Chloride Gradient Purification of AAV Virions

Virions generated through recombinant AAV virus production were purified through the following method with all relevant steps performed in a biosafety cabinet [374]. Cells pellets were processed as follows. Pellets in benzonase buffer underwent three cycles of freezing at –80°C in an ethanol and dry ice bath and thawing at 37°C with cells homogenized by pipetting up and down after the first thaw. Benzonase (Sigma Aldrich) was added 6 µL per 30 mL of Benzonase buffer cell mixture, mixed well and then incubated with episodic mixing by inversion for 1 hour at 37°C. This solution was then centrifuged at 3,000 × *g* for 15 minutes to pellet any cellular debris. The cell supernatant was then measured and transferred to a new 50 mL falcon tube and 1/39th volume of 1M $CaCl_2$ added. This solution was then incubated on ice at 4°C for 1 hour and then centrifuged at 3,000 × *g* at 4°C for 30 minutes and the supernatant reserved. Media from recombinant AAV virus production was processed by spinning at 3,500 × *g* for 30 minutes and supernatant reserved.

The volume of the processed cell and media supernatants measured and transferred to new sterile containers and ¼ volume of 40% (w/v) PEG 8,000 in 2.5M NaCl was added, mixed by inverting gently several times and incubated in ice baths at 4°C overnight. Both cell and media solutions

were then centrifuged at 3,000 x *g* for 30 minutes at 4ºC and the pellet reserved. Cell and media pellets were resuspended in 20 mL each of NaHEPES/EDTA buffer and shaken in 50 mL Falcon tube on a nutator for a minimum of 4 hours or overnight.

The cell and media solutions were then prepared for CsCl gradient separation. Solution density was checked with a refractometer (60/70 ABBE, Bellingham & Stanley, Ltd) and 12 mL of 1.3 g/mL density CsCl was placed into a 5 × 89 mm Ultra-Clear ultracentrifuge tube (Beckman Coulter, California, USA) and then 1.5 g/mL density CsCl solution was pipetted slowly at the bottom of the tube to create a density interphase. At least one tube was prepared for each of the media and cell suspensions. The viral suspensions were then slowly loaded on top of the CsCl solutions and all tubes balanced to within 0.01 g by addition of NaHEPES/EDTA buffer. Tubes were then centrifuged at 106,800 × *g* under vacuum at 20°C for 20 – 24 hrs. Vector bands were extracted using a 10 mL syringe and 18-gauge needle by injecting the needle bevel up and horizontally into the junction between the round bottom and the side wall of the tube. 6 mL of fluid was then collected and placed into a 14 × 89 mm Ultra-Clear ultracentrifuge tubes (Beckman Coulter) and adjusted to a density of 1.37 g/mL, filled to 1mm from the top with 1.37 g/mL CsCl in PBS solution and balanced to within 0.01 g. Tubes were then centrifuged at 247,600 × *g* under vacuum at 20°C for a minimum of 48 and maximum of 60 hrs. Upon removal from ultracentrifuge, viral fractions were collected by creating a hole with an 18-gauge needle in the bottom of the tube and successive 1 mL fractions collected into 1.5 mL tubes (Eppendorf) and vortexed to mix. Fractions were stored at 4°C whilst undertaking quantitative assessment of fraction vector content with qPCR as per Chapter 2.2.5.3 below. Fractions identified with the highest vector titre (top three) were as determined by qPCR were pooled for further purification. Pooled fractions were loaded under sterile conditions into an appropriately sized dialysis cassette (Slide-A-Lyzer Gamma Irradiated Dialysis Cassette Extra-Strength, Thermo Scientific). The vector was placed in 4 L of dialysis fluid overnight at 4°C and then for a further 12 hours in a second 4 L of dialysis fluid and

finally overnight in 4 L dialysis fluid supplemented with 5% (v/v) glycerol. The vector was then transferred into a Vivaspin 20 100,000 molecular weight cut-off tube (Satorius) and concentrated by centrifugation at 3,700 × *g* to achieve a final volume of 300 µL – 800 µL and stored at 4°C.

2.2.5.3 Quantitative PCR analysis of AAV vector preparations with qPCR

Quantitative PCR (qPCR) analysis was used to determine vector concentration in crude vector preparations used for *in vitro* transduction and CsCl vector fractions. Primers were selected to bind the human DBT transgene (km001 and km020) or the bovine growth hormone polyadenylation sequence (BGHpA) with primer/probes (SC277, SC278 and SC279). Standard curves were created with linearised standards containing the corresponding primer target across concentrations from 10^2 to 10^8 copies per µL.

Amplification for qPCR targeting the DBT transgene was undertaken using 10 µL of 2× Takara SYBR, 1 µL of each 10 µM primer and 5 µL diluted template was made up to 20 µL per reaction with water. The qPCR conditions were 95°C for 30 seconds; 35 cycles of 95°C for 5 seconds, 58°C for 15 seconds, 72°C for 20 seconds; and then ramp from 58-99°C to melt holding for 5 seconds for each step. Amplification of BGHpA targets was undertaken using 10 µL 2× PrimeTime™ Gene Expression Master Mix, 2 µL of 10× primer probe master mix made to contain 10 µM of each primer and probe, and 5 µL of template DNA. The qPCR conditions were 95°C for 10 minutes; 40 cycles of 95°C for 15 seconds and 60°C for 1 minute.

2.2.6 Animal Work

All animal experiments were approved by the CMRI Animal Ethics Committee. All mice were kept in standard conditions with open air or individually ventilated cages under standard 12-hour light/dark cycles. Mice were given chow and water *ad libiutm*. Chows used were standard chow

(20% (w/w) protein, SF00-100, specialty feeds) or high protein chow (61% (w/w) protein, SF18-142, speciality feeds).

2.2.6.1 Genotyping DBT mice

Genotyping was performed on either toe, tail or ear tip tissue samples. DNA was extracted from tissue by HotShot method [375]. In brief mouse toes or tails were incubated in 0.2 mL Eppendorf tubes with 80 µL lysis solution (25 mM NaOH, pH 12) for 60 minutes at 95°C, then 80 µL of neutralizing buffer (100 mM Tris-HCl, 0.5 mM EDTA, pH 8) was then added to each tube, vortexed and then spun down for 3 minutes at 4,000 × *g*. 4 µL of this solution was then used as template for PCR. Amplification of the knockout (861 bp) and wildtype alleles (629 bp) was achieved by PCR amplification with two sets of primers, respectively km053 and km058, and km047 and km034 using the BioMix Red (Bioline) mastermix as per manufacturer's instructions. DNA fragments were amplified using the following cycling conditions: initial denaturation at 95°C for 5 mins, followed by 35 cycles of 95°C for 15 seconds, 58°C for 30 seconds and 72°C for 30 seconds. The reaction was then held at 72°C for 10 minutes. Bands were visualised on a 1.5% agarose gel with RedSafe staining.

2.2.6.2 Blood sampling

Blood was taken via either submandibular puncture or by intracardiac puncture as a terminal event. Submandibular puncture was performed via restraining the mouse securely and puncturing the left or right submandibular venous plexus, to remove 20 – 40 µL of blood. Cardiac puncture was undertaken under isoflurane anaesthesia. After the animal was fully anaesthetised with 4% isoflurane induction and 2% maintenance, blood was collected via needle and syringe passed sub-costally to puncture the heart and removed the circulating blood volume. The mouse was then

humanely euthanised with cervical dislocation. For neonatal mice, blood samples were collected by blotting after cervical decapitation.

2.2.6.3 Dried blood spots

Blood was collected via the above means and then placed on blotting card. Spots were dried for a minimum of 4 hours at room temperature, sealed in plastic and stored at -80°C until processing occurred.

2.2.6.4 Intraperitoneal injections

Day 0 pups was injected the requisite vector genome copies diluted in sterile saline to a final volume of 10 μL in a gastight 25 μL glass syringe (Hamilton, Nevada U.SA). Pups were held supine with downwards head tilt and gentle tension applied to abdominal skin. Hamilton 33 G needle was then inserted bevel up into the right lower quadrant and advanced towards the liver at an angle to the avoid the intra-abdominal organs. Vector was then injected and needle slowly withdrawn. s

2.2.6.5 Intrauterine surgery

Pregnant dams anaesthetised at day 15 of pregnancy (E15) using isoflurane inhalation anaesthetics and buprenorphine subcutaneous injection at standard doses. They were placed on a heat mat to ensure normothermia during the operation. Anterior abdominal hair was then trimmed and the surgical site disinfected with chlorhexidine solution. A laparotomy incision was made in the caudal to cranial direction to open the abdominal cavity approximating 1 cm. The gravid uterus was then exposed. The left uterine horn was first gently lifted out of the abdominal cavity and handled with a sterile gauze pad with soaked with warmed saline. The internal organs were bathed in warmed 0.9% (w/v) sodium chloride solution to prevent desiccation during the procedure. The viral vector was delivered to each pup by intra-peritoneal injection through the uterine wall using a 33 G needle

and Hamilton syringe. Viral vectors were made up to a total volume received by each pup was 5 μL with the requisite vector copies and sterile 0.9% (v/w) sodium chloride. Each foetus was injected with a sterilised needle to maximise sterility and minimise cross-contamination. The procedure was then repeated with the right uterine horn. The uterine horns were then returned to the abdominal cavity. The abdomen was irrigated gently with warmed sterile 0.9% (v/w) sodium chloride solution. The incision was closed in two layers, first the muscular abdominal wall, and then the skin with interrupted sutures. The surgical wound was then sterilised again with povidone-iodine or chlorhexidine solution. A subcutaneous dose of ampicillin was given and analgesia given as required. Each dam was then monitored carefully until fully recovered from the anaesthetic. Mice were maintained on carprofen 0.14 mL/250 mL sterile water for 7 days in drinking water, to minimise pain and inflammation following the surgical procedure and monitored twice daily for 7 days post-operatively.

2.2.6.6 High protein diet challenge protocol

Mice undertaking a high protein diet were first weighed, blood taken for baseline BCAA analysis via submandibular puncture onto bloodspot and then placed into new cages free of any other dietary sources. They were exclusively fed a 61% (w/w) protein diet for 48 hours, weighed every 24 hours and then sacrificed with a final blood collection by either submandibular puncture or terminal cardiac bleed.

2.2.6.7 Mouse weighing

Mice were weighed on the same standard scientific scale which were calibrated as per manufacturing instructions.

2.2.6.8 Humane euthanasia and terminal sample collection

All animals were culled humanely either via cervical dislocation or terminal cardiac blood sampling following by cervical dislocation. For mice < 2 weeks of age decapitation was undertaken for humane culling. For all experimental mice older than 8 days, terminal cardiac blood sampling was undertaken under inhalational anaesthetic (isoflurane) followed by cervical dislocation and organ harvest. The liver was harvested first, followed by heart and lungs, then intrabdominal organs followed by skeletal muscle, then brain. Tissues were snape frozen in liquid nitrogen or fixed in 4% (w/v) PFA or 10% (w/v) Neutral Buffered Formalin.

2.2.6.9 BCAA Quantitation

Branched chain amino acids were analysed using tandem mass spectrometry. BCAA were extracted from a 3 mm dried blood spot (DBS) punch with 100 μL of methanol containing D_8-L-Valine, D_{10}-L-Alloisoleucine, D_3-L-Leucine and $^{13}C_6$-L-Isoleucine. The spots were gently shaken for 30 minutes. The extracts were then dried at room temperature. This dried extract was then reconstituted in aqueous mobile phase comprising water with 0.2 mL/L heptafluorobutyric acid and 1 mL/L formic acid. Analysis was perform using the Waters Acquity TQS system (Waters Corporation, Rydalmere, NSW, Australia). 5 μL of sample was injected and the BCAAs were separated using an ACQUITY UPLC® HSS C18 1.8 μm 2.1 x 100 mm column and gradient elution. The instrument operates in multiple reaction mode looking at the following mass transitions for the native compounds and their internal standards: Valine (118.10 > 72.00), D_8-Valine (126.10 > 80.00), Leucine (132.10 > 86.00), D_3-Leucine (135.10 > 89.00), $^{13}C_6$-Isoleucine (139.10 > 92.00) and D_{10}-Alloisoleucine (142.10 > 96.00). Quantification was performed using the Target Lynx software. Three reads were taken for each sample with the average value for each branched chain amnio acid then being used as the final value.

2.2.7 Molecular Analysis

2.2.7.1 Viral titre determination with digital droplet PCR

AAV Viral Vector concentration was determined with BioRad's digital droplet PCR (ddPCR) system. Vector samples were first denatured by heating vector with alkaline digestion buffer (25 mM NaOH, 0.2 mM EDTA) in a 2:49 ratio vector to buffer at 99°C for 10 minutes. Samples were then chilled on ice for 1 minute and neutralisation buffer (40 mM Tris-HCl, 0.05% (v/v) Tween, pH 5) added to achieve a vector dilution of 1:50 concentration. Vectors were diluted to 1 in 4 million, 1 in 8 million and 1 in 16 million of the original vector concentration. Droplets were generated from 20.9 µL of a 22 µL reaction mix containing 1.1 µL of template DNA, 11 µL of 2× QX200TM EvaGreen® Supermix, 2.2 µL of 1 µM forward primer (km001), 2.2 µL of 1 µM reverse primer (km020) and 5.5 µL of water, as per manufacturer's instructions using BioRad QX200TM droplet generator, DG8 cartridges for QX200TM and BioRad gaskets. Droplets were placed in a 96 well semi skirted plate (Bio Rad Cat#12001925) sealed with pierceable foil heat seal (BioRad #1814040) using the BioRad PX1 PCR Plate Sealer. DNA targets were then amplified in BioRad C1000 Touch Thermal Cycler under the following conditions: 95°C for 5 minutes, 40 cycles of 95°C for 30 seconds, 60°C for one minute, signal was stabilised a 4°C for 5 minutes and run completed at 90°C for 5 minutes. Droplets were then read with BioRad QX200TM Droplet Reader and analysed using QX Manager Software (version 1.74.0917).

2.2.7.2 Using digital droplet PCR to analyse tissue vector copy number

Vector copy number was undertaken using genomic DNA extracted as per methodology for Pheno-Chloroform gDNA extraction. DNA (25 ng) was digested enzymatically using EcoRI (New England Biolabs Cat#R0101S) as per manufacturer's instructions for 2 hours at 37°C. Droplets were then generated as per manufacturer instructions outlined in the above methodology for ddPCR viral titre (BioRad, QX200^{TM}). Template DNA was amplified using the primers km001 and

km020. Signals were normalised for each sample with a parallel PCR targeting murine albumin using primers mAlbF and mAlbR (Table 2-5).

2.2.7.2 DNA Extraction

Genomic DNA was extracted from 10 – 50 mg of murine tissue. Tissue samples homogenised with a rotary pestle and electric hand-held homogeniser (BT LabSystems, Missouri, USA) with 400 mL of Lysis Buffer (10 mM Tris-Cl pH 8, 0.1 M EDTA pH 8, 0.5% (w/v) SDS and RNAse A to a concentration of 100 μg/mL). Samples incubated at 37°C for 60 minutes and then for 18 hours at 57°C after the addition of 5 μL Proteinase K (stock concentration 20 mg/mL). 500 mL of Phenol, Chloroform and Isoamyl (25:24:1 ratio) was added to each sample, mixed by inversion for 15 minutes and then centrifuged at 14,000 × *g* for 5 minutes. The aqueous phase was then collected and the preceding step repeated once. Residual phenol was then removed from the collected aqueous phase by adding 400 mL of chlorofrom:isoamyl to each sample, mixed by inversion for 15 minutes and then centrifuged at 14,000 × *g* for 5 minutes. The aqueous phase was collected, and the preceding step repeated once. The aqueous phase was then collected, and volume measured. DNA was precipitated by adding 2.5 × volume of cold ethanol 100% and 0.25 × volume of 10 M ammonium acetate. Samples were vortexed and stored at -20°C for a minimum of 30 minutes. DNA was pelleted by centrifugation at 14,000 × *g* for 30 minutes. Supernatant was discarded and DNA pellet washed in 75% ethanol and centrifuged at 14,000 × *g* for 10 minutes. The supernatant was then discarded. DNA pellet was air dried and resuspended in 10% TE Buffer (Tris 1 mM, EDTA 0.1 mM) and stored at -20°C.

2.2.7.3 RNA extraction

RNA was extracted from 10 – 50 mg of murine tissue first by homogenization with a rotary pestle and electric homogenizer with 500 mL of Trizol in a 1.5 mL Eppendorf tube. Tissues were

incubated for 5 minutes at room temperature. Chloroform 100 mL was then added to each sample and tubes shaken vigorously by hand for 15 seconds. Samples were then incubated at room temperature for 3 minutes. Samples were then centrifuged at 12,000 × *g* for 15 minutes at 4ºC. The colourless aqueous phase was then collected via pipette and an equal volume of 70% ethanol (v/v) was added in a new 1.5 mL Eppendorf tube. Each sample was then vortexed. The protocol was then continued using the PureLink™ RNA Mini Kit (Invitrogen) and each sample transferred into a spin cartridge with collecting tube. Sample were centrifuged at 12,000 × *g* for 15 seconds at room temperature and flow–through discarded. Each sample was washed with 350 µL of Wash Buffer 1 and centrifuged for 12000 × *g* for 15 seconds. The collecting tube was discarded and the column inserted into fresh collection tube. On column digestion of DNA was then performed by applying 80 µL of Purelink DNase mix to each column (8 µL of 10 × DNase I reaction buffer, 10 µL resuspended DNase (~3 U/µL) and 62 µL of RNase free water) and incubated for 15 minutes at room temperature. RNA was then purified according to manufacturer's instructions. Eluted RNA was stored at -80ºC.

2.2.7.4 cDNA Synthesis

RNA samples were used to synthesis cDNA using the SuperScript™ III First-Strand Synthesis System for RT-PCR (Invitrogen) or SuperScript™ III First-Strand Synthesis System (Invitrogen) or Superscript™ IV First-Stand Synthesis System (Invitrogen). 500 ng of template RNA was used in each reaction and the OligoDT method was used throughout following manufacturer's instructions. cDNA samples were diluted at 1:10 prior to use for RT-qPCR and stored at –20ºC. Each sample had an RT- control without addition of the reverse transcriptase enzyme added synthesised in parallel.

2.2.7.5 Protein Extraction

Tissue was homogenized with 300 μL of chilled homogenizing medium (0.25 M Sucrose, 5 mM HEPES, 1mM EDTA pH 7.5) using a teflon pestel and rotary homogenizer in 1.5 mL Eppendorf tube. Lysate was then centrifuged at 500 × *g* at 4°C for 10 minutes. Half of supernatant reserved as whole protein lysate and then remainder centrifuged at 9400 × *g* at 4°C for 10 minutes to isolate the mitochondrial pellet. Supernatant was removed and snap frozen in liquid nitrogen as the cytoplasmic protein lysate. Mitochondrial pellet was then resuspended 150 μL lysis buffer (0.5% Triton X-100, 10 mM HEPES pH 7.4, 2 mM DTT) and snap frozen in liquid nitrogen. All fraction were stored at -80°C. Weight of tissue varied with organ type, Liver (30 mg), Brain (40 mg), Heart (5 mg) Gastrocnemius muscle (2.5 mg), Kidney (10 mg).

2.2.7.6 Protein Quantitation

Protein lysates concentration was determined using the Protein Assay Kit (BioRad) utilising a colorimetric assay after sample detergent solubilisation. Protein lysates samples were diluted serially, minimum of three dilutions ranging between 1:5 to 1:240 depending on the tissue type. Protein standards were included with each assay ranging from 0 to 1.5 mg/mL. 5uL of protein standards and sample dilutions added in quadruplicate to a 96 well plate (Corning). Solution A^I was made by adding 20 μL of kit Reagent S to each mL of Reagent A and then 25 μL of Solution A^I added to each well using a multi-channel pipette. 200 μL of solution B was then added to each well and incubated at room temperature for 15 minutes to allow the spectrophotometic assay to develop. Plates were read at 650 nm with the Molecular Devices VersaMax Microplate Reader at room temperature. Average values were taken across the quadruplicate standards and a standard curve used to estimate the concentration of the samples accounting for dilution factors.

2.2.7.7 Western Blot

Protein sample concentration was determined as above. Samples were prepared in 10mM Tris, 140 mM NaCl and with equal volume of 2× Laemelli (BioRad) sample buffer supplemented with 0.05 µL/mL of 14.3 M Beta-mercaptoethanol. Samples were heated at 95°C for 10 minutes and chilled on ice for 2 minutes. Running buffer was prepared by adding 25 mL of NuPAGE™ MOPS Running Butter 20× to 475 mL of MilliQ Water per gel. Pre-cast NuPage™ 4-12% Bis-Tris Gel 1.0mm × 10 or 15 wells gels were then assembled in a Mini Gel Tank (Life Technologies), combes removed, running buffer poured to fill each chamber and wells flushed with 20 µL of running buffer. Samples were loaded at equal concentrations of protein in each well. A minimum of one protein ladder was loaded per gel, using 2.5 µL of the Precision Plus Protein Dual Color Standards (BioRad) and 140 V applied for 60 minutes or until the samples had run through the gel to completion. Gels were then transferred onto 0.2 µm nitrocellulose membrane (BioRad) in a transfer chamber and placed in an electrophoresis chamber submerged in cold degassed transfer buffer (200 mL 5× Towbin, 100 mL Methanol and 700 mL of MilliQ water) with an ice block. Transfer was undertaken for 60 min at 100V 4°C. Nitrocellulose membranes were then removed from the transfer chamber, stained with Ponceau S solution (0.1% (w/v) Ponceau S, 5% (v/v) Acetic glacial acid) to assess loading, cut at 75 kD, de-stained with milliQ and then blocked for 1 hour on a nutator with PBST/5% (w/v) skim milk powder. Membranes were incubated with primary antibodies at 1:5000 (v/v) with either mouse polyclonal anti-vinculin antibody (Sigma-Aldrich), or anti-DBT rabbit polyclonal antibody (Sigma) on a tube rotator at 4°C overnight. Membranes were washed five times with PBST for 5 minutes on a nutator and incubated with corresponding secondary antibody conjugated to HRP (goat anti-mouse or goat anti-rabbit) at 1:5000 (v/v) for 1 hour at 4°C. Blots were then washed five times for 5 minutes on a nutator with PBST. Blots were developed with luminal femto solution from the SuperSignal™ West Dura Extended Duration Substrate kit and imaged using ChemiDoc Imaging System (BioRad).

2.2.8 Histology

2.2.8.1 Tissue Fixation

Harvested tissues were placed at time of collection into 4% PFA Solution (w/v) and incubated at 4°C overnight on a nutator. PFA was then replaced with 10% (w/v) Sucrose in PBS and samples incubated overnight at on nutator 4°C. This step was repeated with 20% (w/v) and 30% (w/v) Sucrose in PBS. Samples were dried with a paper towel and placed into Tissue-Tek® Optimal Cutting Temperature Compound (OCT) (Sakura) in plastic casings. Samples were frozen by immersion in 2-methylbutane cooled with liquid nitrogen and stored at -80°C.

2.2.8.2 Tissue sectioning

Tissues block frozen in Tissue-Tek OCT were mounted onto cutting blocks and sectioned at 5 µm (liver and kidney) 10-15 µm (cardiac and skeletal muscle) or 20 µm (brain) sections using Leica Cryostat at –20°C. Sections were then mounted onto Menzel-Gläser Superfrost Plus Microscope Slides (Thermo Scientific) and stored at 4°C until required.

2.2.8.3 Immunofluorescence staining

Slides were first washed in phosphate buffer saline (PBS) 5 mins and permeabilised with pre-chilled methanol (-20°C) for 10 mins at -20°C and then rinse with PBS for 5 mins. Slides were then washed with 0.1% Triton X-100 in PBS for 10 mins. They were then washed PBS, 2× PBS/2% (v/v) FBS for 5 mins each. Blocking buffer (10% (v/v) foetal calf serum, 10% (v/v) Donkey Serum in PBS) and applied to each tissue slice for 30-60 minutes at room temperature. Primary antibody was then applied at 1:200 (Invitrogen) and sections incubated overnight at 4°C. Slides were washed 4 times with 0.1% (v/v) Tween-20/PBS on shaker (one minute, five minutes, 10 minutes, 15 minutes). Secondary antibodies were then diluted in PBS at 1:500 and spun at 21,000 × *g* for 5 minutes with the top $\frac{4}{5}$ of the supernatant collected and then spun again with the top ¾ supernatant collected and applied to the sections and incubated for 1 hour at room

temperature in the dark. Sections were then washed 3 times with 0.1% Tween-20/PBS for 5 minutes. Slides were then stained for DAPI, using 20 μL of 0.2 μg/mL in 50 mL of PBS for 5 minutes and then washed in PBS for 5 minutes. Sections were then dried and 3 drops of coverslip solution (either Immu-Mount or Gelvatol) applied prior to placing a coverslip on the section. Completed slides were then left to dry in the dark for 5 – 10 minutes prior to imaging and or stored at 4°C until required. Slides were reviewed using Zeiss Axio Imager A1 microscopes and Zeiss ZEN 3.8 software used for microscope setup, image capture and image processing.

2.2.9 Statistical analysis

GraphPad Prism (10.4.1) software was used to undertake all statistical analyses and generate graphs. Non-parametric statistical tests were utilised as data was not assumed to have a normal distribution due to small sample sizes. Values are graphed individual data points with median and standard error mean range displayed unless otherwise stated. Statistical significance was determined between two groups using the Mann-Whitney *U* test or when data paired the Wilcoxon matched-pairs signed rank test. Survival significance was determined using the log-rank (Mantel Cox) test. Statistical significance was defined as $p < 0.05$ for all statistical tests.

2.2.10 Figures

Some figures were created with Biorender.com, as noted where applicable.

Chapter 3

Characterising the neonatal lethal DBT$^{-/-}$ Murine Model of Maple Syrup Urine Disease

3.1 Introduction

This chapter describes the formal characterisation of a murine model of MSUD, the neonatal lethal DBT$^{-/-}$ mouse. The first murine model of Maple Syrup Urine disease was generated by Homanics *et al.* in 2006 [376]. Embryonal knockout of the *DBT* gene was achieved via insertion of a neomycin resistance transgene between exon 4 and 5, generating a neonatal lethal model. Partial rescue was achieved through knock in of a human DBT gene expressed under a complimentary "Tet-off" transgene intended to provide a molecular switch. However, this tetracycline molecular switch was not active, and the model characterised as an intermediately severe, or iMSUD, model. This iMSUD model was then crossed with the LAP-tTA transgenic mouse (background NMRI outbred; FVB; C57BL/6J) [377] to generate a triple mutant model of MSUD *Dbt^{tm1Geh}* Tg(Cebpb-tTA)5Bjd Tg(tetO-DBT)A1Geh/J. This triple mutant model does not express hepatic E2 protein and has BCKDH activity of around 5-6% of wildtype levels, equating to an intermediately severe MSUD phenotype (Appendix A, page 268).

To generate the DBT$^{-/-}$ model, Grieg and her colleagues had backcrossed *Dbt^{tm1Geh}* Tg(Cebpb-tTA)5Bjd Tg(tetO-DBT)A1Geh/J mice with CB57BL/6J mice to generate single mutant *DBT$^{-/-}$* mice without the recuse transgenes (Appendix A, page 268). Anecdotally, this recapitulated the severe phenotype described by Homanics *et. al.* to generate a severe form of MSUD akin to Classical MSUD in humans. As this rederived model had not been formally described in the literature, characterisation of both biochemical phenotype and genetic locus was warranted.

3.1.2 Homology between human and murine DBT genes

The *DBT* gene, encodes the E2 subunit and contains the catalytic domain for the BCKDH enzyme. This gene is found on chromosome 1 at the locus 1p21.2. Comprising 12 exons, DBT is constitutively expressed across most body tissues, the highest being skeletal muscle, liver, brain and kidney [10]. There is approximately 85% homology between human *DBT* and murine *DBT* and murine *DBT* is found on chromosome 3 at the locus 3 G1|3 50.37 cM. The open reading frame is 1449 bp in both species with the first 83 base pairs coding for a transit peptide which upon trafficking to the mitochondrial compartment, is cleaved.

The functional activity of human DBT in mice was first assessed by Homanics *et al.* when creating the iMSUD mouse model. By knocking in human *DBT* cDNA in a manner which induced hepatic expression, human E2 proteins levels in the iMSUD mice were comparable to WT murine E2 levels on western blot analysis. Despite this, the BCKDH activity was only around 6% of normal BCKDH enzyme activity, with the authors postulating that there may have been enzymatic interference caused by the inclusion of a c-myc tag at the carboxy terminus of the human E2 transgene. Another possibility for this reduced activity may have been that the human mitochondrial leader sequence worked poorly for import into the mitochondria [378]. It should be noted that the tetracycline switch in this model did not function as a molecular switch, as intended.

While Homanic's and his team did not manage to rescue their iMSUD model to wildtype levels, they did demonstrate that the homology between murine and human DBT was such that the BCKDH enzyme was functional and improved the phenotype. This observation implies that the hDBT underwent transcription and translation in a murine nucleus, was trafficked to the mitochondria and was then successfully assembled into the complex multi-hetero-tetramer

BCKDH along with the endogenous E1-alpha and E1-beta subunits, cofactors and regulatory elements.

3.1.3 Dietary rescue of the DBT$^{-/-}$ Model is impractical

Whilst dietary and supportive interventions such as intravenous therapy and haemofiltration are able to ameliorate the metabolic toxidrome that occurs in affected MSUD infant humans or when patients decompensate due to other measures, these treatment options are not readily accessible by our murine counterparts. Mouse pups are wholly dependent on suckling their mother's milk until weaning, which occurs around 3-4 weeks of age. Intravenous interventions are also impractical and unavailable. As such, standard treatment of MSUD in children, is not possible in MSUD mice.

3.1.4 Gender & developmental age-related changes to BCKDH activity

The BCKDH enzyme activity is closely tied to whole body catabolism and anabolism and as such can be greatly affected during a variety of physiological states, such as exercising, fasting or illness-related metabolic stress [52, 379]. There is also data in rodent and human studies that there is gender-based differences in BCAT and BCKDH activity and metabolites as well as between standard weight and obese individuals. Some studies have demonstrated that males have higher BCAA and alpha-keto acid metabolites and leucine is also elevated in obese adults compared to standard weight controls [380]. There may also be developmental changes in BCKDH enzyme activity in association with the transition from juvenile to more mature patterns of adolescent and adult adiposity patterns [381].

The aim of this chapter was to explore and evaluate hypothesis 1 and aim 1 (refer to Chapter 1.6).

3.2 Chapter Specific Methods

3.2.1 Sequencing the Mutant and WT DBT Locus

DNA was extracted from a small section of ear lobe taken from each of the 6 $DBT^{+/-}$ mice obtained from Jenny Grieg (University of Pennsylvania) to confirm the sequence of the DBT mutant and wildtype loci. The HotShot Jax method, as described in Chapter 2.2.6.1 was used to extract genomic DNA. Primer pairs (Table 3-1) were designed around the known junction of murine DBT exon 4 and the terminal region of the PGKneo (Neomycin Resistance) cassette, the direction of which was presumed to be knocked-in in reverse (later proven correct), however this was not 100% certain and primers were designed to confirm this (Figure 3-1).

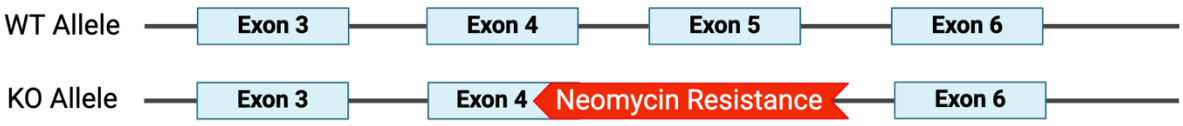

Figure 3-1 Described DBT Alleles in MSUD Murine Model. Wildtype (WT) and knock out (KO) allele of *DBT* gene in $DBT^{-/-}$ mouse model. Neomycin resistance gene knocked-in in reverse orientation. Figure adapted from Homanics *et al.* and created with BioRender.

3.2.2 Genotyping

Breeding pairs were set up from the original mice (female = 3), donated by Jenny Grieg and her team at the University of Pennsylvania. DNA was extracted using the HotShot Jax method, as described in Chapter 2.2.6.1. Mutant and wildtype DBT alleles were amplified via PCR using respective primers pairs km053 and km058, and km047 and km034.

3.2.3 Obtaining controls for relevant genotypes and retrospective genotyping

In order to obtain biological specimens for all genotypes a number of pups from several litters were humanely sacrificed on Day 0 of life as close to birth as possible. Pups were then retrospectively genotyped and end point assay results matched to their respective genotypes. As there were no surviving $DBT^{-/-}$ mice past 9 days of age, all $DBT^{-/-}$ untreated controls samples in this project were taken from pups in the first week of life. Where possible, specimens from aged matched untreated $DBT^{+/+}$ controls have been included for each experiment.

Mice were given individual numbers through toe clipping in certain patterns between day 8-12 of life. However, as there was a need to collect anthropometric and behavioural data on individual mice before this age, the following method was used to identify each mouse prior to toe clipping. Pregnant dams were house individually for the last week of their pregnancy. Upon birthing, all pups in each litter were marked over their back or abdomen when dorsal hair reduced the longevity of the marking. Each mouse was assigned a specific symbol (Figure 3-2A) and this was reapplied daily. Pups were then weighed daily and any behavioural changes noted (Table 3-2). When toe clipped, mice were then assigned a number as designated by the pattern of toe and ear clipping (Figure 3-2 B).

Table 3-1 Oligonucleotides use for sequencing wildtype and mutant DBT allele in MSUD mouse model

Primer	Sequence (5'-3')	Expected directionality	Details	T_m (C^o)
Mutant allele disrupted with Neomycine resistance Gene				
km030	GGGCGCCCGGTTCTT	Anti-Sense Neomycine ORF		54.2
km031	CCTCGTCCTGCAGTTCATTCA	Sense if Neomycine ORF reverse		61.2
km049	AAAGAACCGGGCGCCCC	Sense if Neomycine ORF reverse		59.8
km050	TGAATGAACTGCAGGACGAGG	Anti-sense if Neomycine ORF reverse		61.2
km055	GGGGCGCCCGGTTCTTTTT	Antisense if Neomycine ORF reverse		61.6
km056	GATCTGGACGAAGAGCATCAG	Antisense if NeoR ORF reverse		61.2
km057	CTCACCTTGCTCCTGCCG	Antisense if NeoR ORF reverse		60.8
km058	CAGGACATAGCGTTGGCTAC	Antisense if NeoR ORF reverse		60.5
km059	GGGTAGCCAACGCTATGTCC	Sense if NeoORF reverse	rev km058	62.5
km061	GTTCCTTGCGCAGCTGTGC	Antisense if NeoR in reverse		61.6
km062	CTGATGCTCTTCGTCCAGATC	Sense if NeoORF reverse		61.2
km070	CGTGTCGACGCGTTCCTTG	Sense if NeoORF reverse	Rev km061	61.6
Murine DBT Wildtype Allele				
km033	AGCAAAAACCTGTACAGTAAGACTTCA	sense	Intron 4	63.7
km034	GCTTCTTGCTTCACTGAACATCAA	anti-sense	Intron 4	62
km047	TCACCATCACCAGCCGTTAC	sense	Exon 4	60.5
km048	CAGGAGTTGACGGTAGTGGTT	antisense	Intron 5	61.2
km052	ATGTAAAAGAAGGAGATACGGTGT	sense	Exon 4 (more proximal to km047)	60.3
km053	GGCATTTACAGGAACATGCAAG	sense	Intron 3 (distal, almost at exon 4)	60.1
km054	GTGTGAAGTGTTATTAGGTGCC	antisense	Intron 5 (distal to km048)	60.1
km060	TTGACGGTAGTGGTTGCGAG	antisense	Intron 5	60.5

km071	GAAGTTTGCCAGCTGAGACC	antisense	Intron 5	60.5
km072	CCACCATGCCAGGCTTCTTT	antisense	Intron 5	60.5
km073	GGCTTCTTTTGTGAGTGCTGG	antisense	Intron 5	61.2
km074	CAGGGCTCCTGTAAGCTCTTC	antisense	Intron 5	63.2

Table 3-2 Mouse activity levels

Grade	Activity Level	Behaviours displayed
1	Moribund	Alive, no moving limbs, eyes closed, not eating or drinking, no response to stimulation.
2	Lethargic	Sleepy but respond to stimulation, can open eyes, some head and limb movement, reduced food intake.
3	Limited activity	Interruptions in movement with periods of rest, response to stimulus and environmental threats/changes, slightly reduced food intake.
4	Active	Strong, curious, occasional interruptions to movement/activity, normal food and water intake.
5	Highly active	Strong, curious, move around enclosure quickly and confidently, playful, normal food intake.

3.2.4 Timed mating to enhance birth detection and determine gestation duration

Timed mating was undertaken by housing harems (one male, multiple females) and assessing females daily for a vaginal copulation plug. A copulation plug is a hardened mixture of semen that forms in the vaginal tract after mating [382]. The presence of a copulation plug indicates mating but does not guarantee pregnancy. Upon detecting a copulation plug, females were housed separately and monitored for signs of pregnancy. Pregnant dams were identified with increasing abdominal girth visible between E10-15 and the start of the pregnancy was marked as the start of that day the plug was found 00:00 hours. Dams were reviewed in the morning and end of each day to check for parturition. The end of pregnancy was denoted as the day and time that newborns were first seen.

A

B

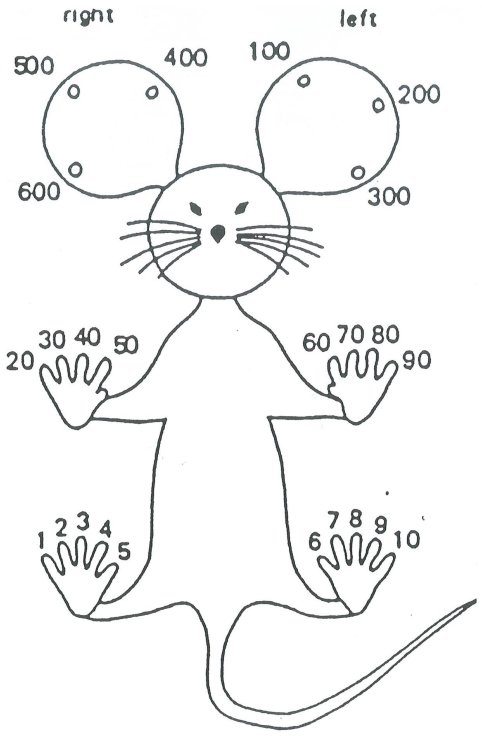

Figure 3-2 Murine identification systems (A) Pup designation in neonates form 0 to 9 days of age. Neonatal DBT pups from the same litter have been marked with symbols using permanent marker. Symbols used included ▲,■, |, X, O, and ┼ (pictured) as well as ||, |||, ◊ and H (not pictured) as dictated by litter size. **(B)** Ear and Toe clip sites with corresponding numerical value.

3.3 Results

3.3.1 Sequencing the mutant allele

The mutant allele junction between exon 4 and the neomycin resistance cassette was sequenced using primers designed to capture these two elements (Figure 3-3). A 1437 bp segment was sequenced corresponding to the end of intron 3, the start of native murine exon 4, through the junction of the truncated exon 4 with the neomycin resistance cassette to 47 bp beyond the end of the neomycin resistance cassette. This analysis confirmed that the Neomycin resistance cassette is in reverse orientation with respect to the reading frame of the murine DBT gene. The full elucidated sequence can be found in Appendix B, page 269.

Figure 3-3 Mutant Allele Sequence. Schematic of the mutant allele sequence obtained via Sanger sequencing and corresponding genetic elements. Generated using SnapGene and BioRender.

3.3.2 Genotyping

The WT and KO *DBT* alleles were captured using selected primer pairs. The WT primer pair km047 (forward annealing) and km034 (reverse annealing) and KO primer pair km053 (forward) and km058 (rev) were selected for all future genotyping experiments. These were chosen as the products generated by these primer pairs were different sizes (629 bp and 861 bp for WT and KO allele respectively), were readily distinguishable on gel electrophoresis and generated amplicons reliably under identical thermocycling conditions (Figure 3-4, n = 8 mice). The final thermocycling conditions were 95 deg for 5mins; 35 cycles of 95°C 15 sec, 58°C 30sec, 72°C 30sec; 72°C 10 mins; 4°C hold.

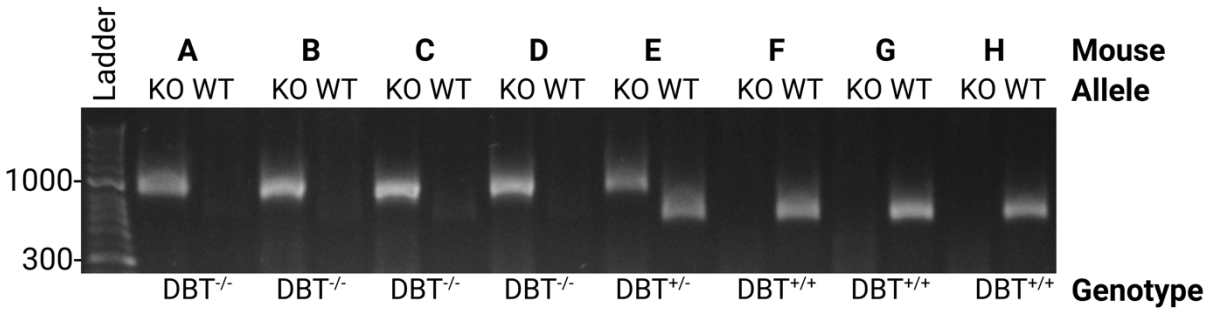

Figure 3-4 Genotyping Gel. Example of gel electrophoresis of Genotyping PCR for mutant (KO) allele and wildtype (WT) allele for n = 8 mice. Mice A-D illustrate the $DBT^{-/-}$ genotype, Mouse E a $DBT^{+/-}$ genotype and mice F-H the $DBT^{+/+}$ genotype.

3.3.3 Survival of *DBT*-deficient mice characterised as neonatal lethal

A breeding colony of DBT mice was established and during the first six months all mice born to the 3 known DBT+/- pairs were observed. A total of 160 mice were including in this survival study, (male = 55, female = 60, unsexed dead pups n = 45). Of these, 58% of pups born were $DBT^{+/-}$ (n= 93), 26% were $DBT^{+/+}$ (n = 41) and 16% (n = 26) were homozygous knockouts $DBT^{-/-}$. There was no significant difference between $DBT^{+/+}$ and $DBT^{+/-}$ survival ($p > 0.999$) and significantly reduced survival amongst the $DBT^{-/-}$ pups ($p < 0.0001$) (Figure 3-5). The majority of $DBT^{-/-}$ pups died within the first 48 hours of life apart from four, three survived to day 7 and one to 9 days, before dying.

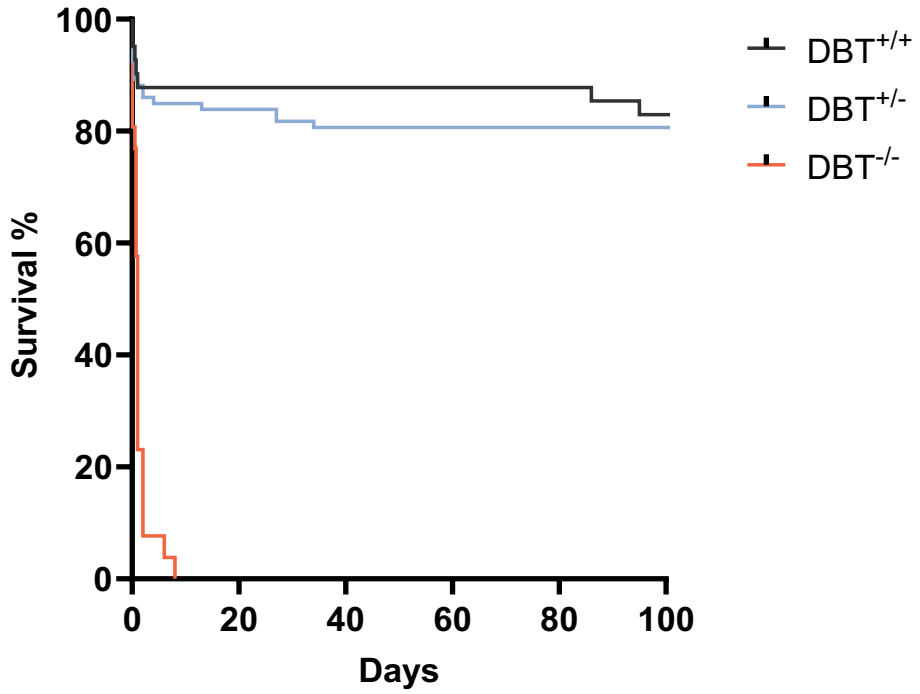

Figure 3-5 Survival in DBT MSUD Mouse Model. Dramatically reduced survival in neonatal lethal $DBT^{-/-}$ pups compared to wildtype ($p < 0.001$). $DBT^{+/+}$ and $DBT^{+/-}$ had equivalent long-term survival at 100 days ($p > 0.999$). Wilcoxon Log Rank test used to determine statistical significance. Demogrpahics of study population, male = 55, female = 60, unsexed dead pups n = 45, $DBT^{+/-}$ (n= 93), $DBT^{+/+}$ (n = 41) and $DBT^{-/-}$ (n = 26).

3.3.4 Growth failure in *DBT*-deficient mice

Pups in all litters used for genotyping the model were reviewed on day one of life. All pups in in each litter were noted to have milk spots in the abdomens, be moving normally at birth. Whilst most homozygous DBT-deficient mice died rapidly within the first 48 hours of life, those that survived beyond 2 days had comparable growth to wildtype until day 4 (Figure 3-6). After this time, weight plateaued and steadily declined until death. These *DBT*-deficient mice (n = 3) were also noted to be cachectic and moribund compared to their thriving wildtype and heterozygous siblings (Figure 3-7). Wildtype $DBT^{+/+}$ mice (n = 6) and heterozygote $DBT^{+/-}$ (n = 7) mice had comparable weights upon reaching adulthood at 56 days of age.

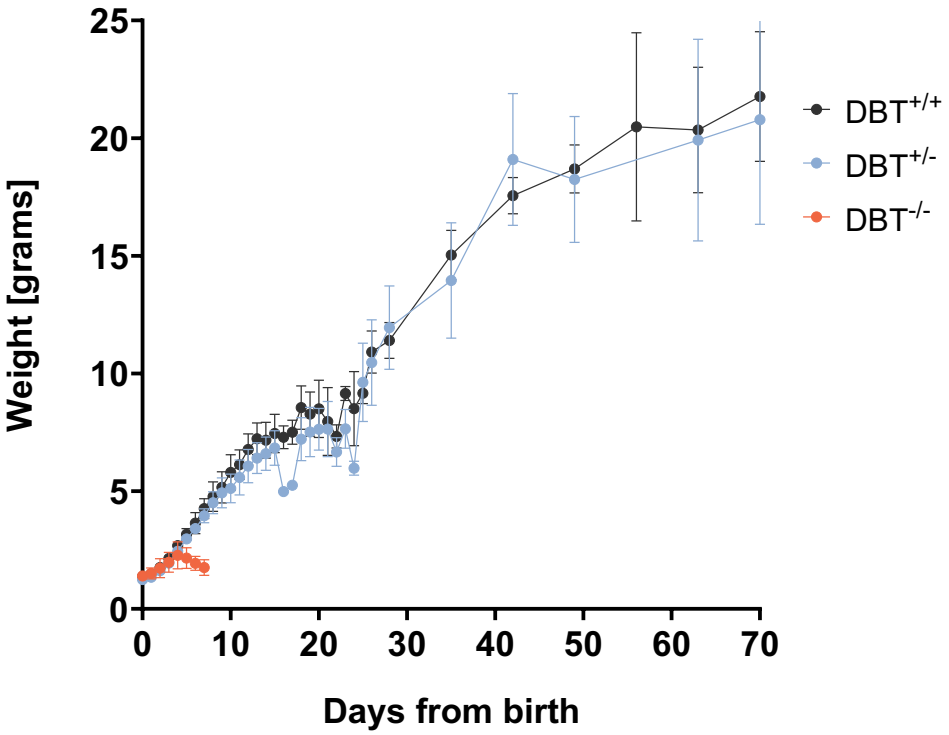

Figure 3-6 Growth of DBT MSUD Mouse Model. Growth from birth to 70 days of life in $DBT^{+/+}$, $DBT^{+/-}$ and $DBT^{-/-}$ mice. Error bars are mean and standard deviations.

Figure 3-7 Growth failure in $DBT^{-/-}$ Mice. Photograph of a $DBT^{-/-}$ mouse [left] with a $DBT^{+/+}$ littermate [right] at day 6 of life. Mice were identified by symbols applied with permanent marker prior to formal genotyping.

3.3.5 The *DBT* protein E2 is undetectable in *DBT*-deficient mice

Hepatic expression of the *DBT* protein E2 was assessed in neonatal $DBT^{+/+}$, $DBT^{+/-}$ and $DBT^{-/-}$ pups by western blot across a protein gradient of 2 ug, 4 ug and 10 ug. Signals were normalised to vinculin as described in aforementioned methods Chapter 2.2.7.7. No detectable E2 protein was expressed in the livers of $DBT^{-/-}$ mice on western blot analysis (Figure 3-8).

The cellular component of E2 protein was assessed in the whole tissue lysate, as well as cytosolic and mitochondrial fractions (Figure 3-9). Hepatic E2 protein expression was equivalent between $DBT^{+/+}$ and $DBT^{+/-}$ pups across all protein fractions. There was no E2 protein detected across any lysates for the $DBT^{-/-}$ pups. E2 protein concentration relative to vinculin was the highest in the mitochondrial fractions for both $DBT^{+/+}$ and $DBT^{+/-}$ pups.

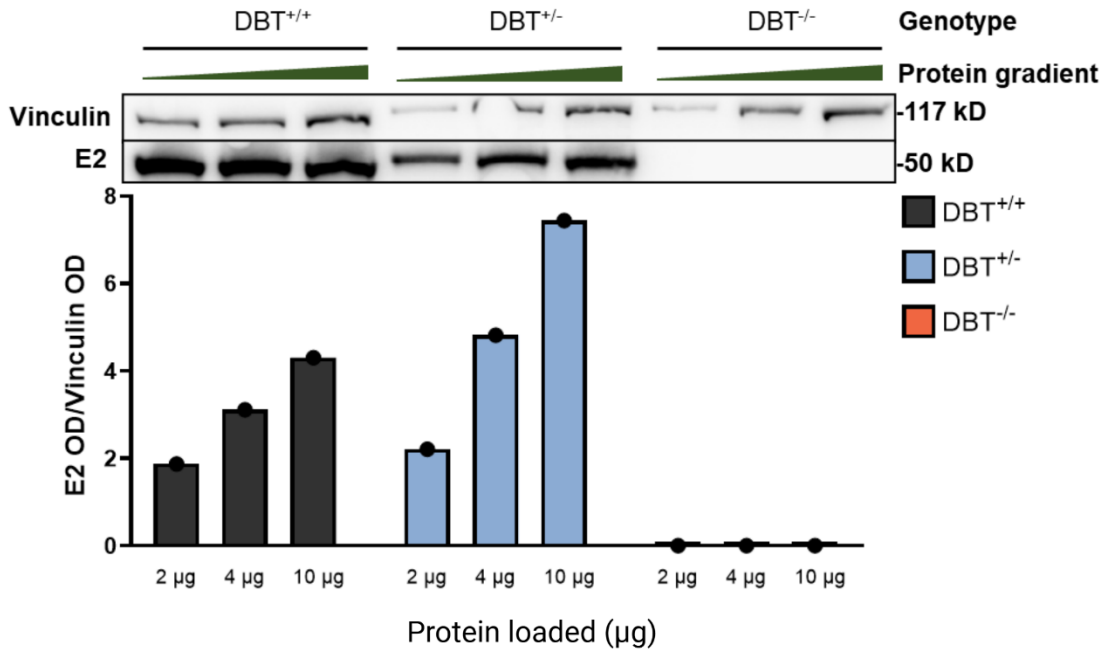

Figure 3-8 Hepatic E2 expression in MSUD DBT model. Hepatic E2 protein expression across $DBT^{+/+}$, $DBT^{+/-}$ and $DBT^{-/-}$ neonates. Blots were probed with polyclonal anti-DBT[Rabbit] antibodies (Invitrogen) and signals normalised to vinculin with anti-vinculin [Mouse] antibodies (BioRad). E2 protein optical density normalised to vinculin optical density as quantified with image J. Figure generated in BioRender.

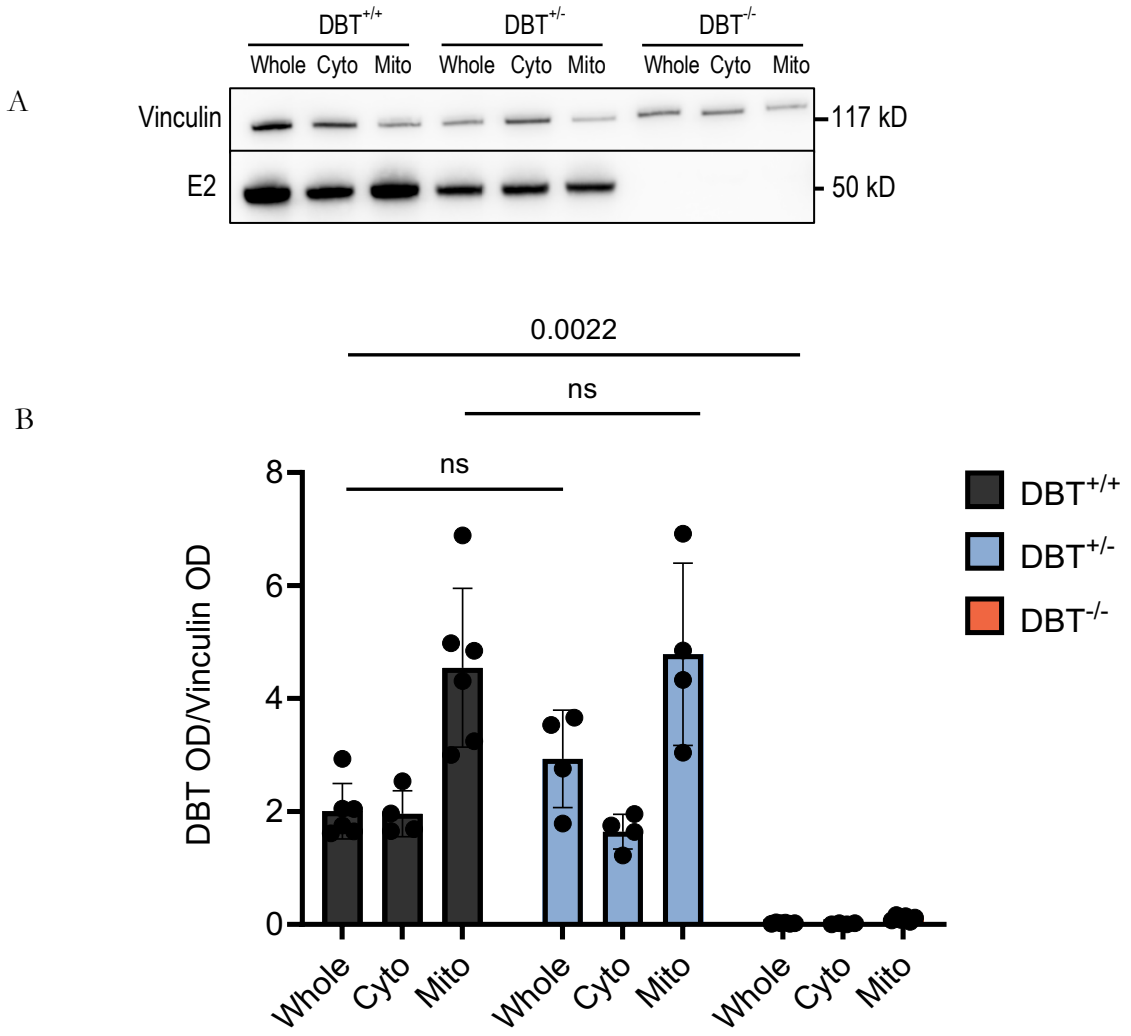

Figure 3-9 E2 protein expression across cellular compartments (A) Hepatic E2 protein expression across $DBT^{+/+}$, $DBT^{+/-}$ and $DBT^{-/-}$ neonates in the whole, cytosolic (Cyto) and mitochondrial (Mito) cellular compartments. Blots were probed with polyclonal anti-DBT[Rabbit] antibodies (Invitrogen) and signals normalised to vinculin with anti-vinculin[Mouse] antibodies (BioRad). **(B**) E2 protein optical density normalised to vinculin optical density as quantified with image J. Statistical analysis was undertaken using a Mann-Whitney test. Abbreviations: cyto (cytoplasmic lysate), mito (mitochondrial lysate). Figure generated in BioRender, n = 4 for each genotype.

E2 protein expression was also assessed in brain, heart and skeletal muscle (gastrocnemius muscle belly) using western immunoblotting. Expression of E2 was present across brain, heart and skeletal muscle in $DBT^{+/+}$ mice. There was relatively more DBT protein expressed in adult female skeletal muscle (n = 1) compared to male (n = 1), however, more replicates are required to confirm any trend. E2 was undetectable in DBT-deficient pups across these same tissues (Figure 3-10).

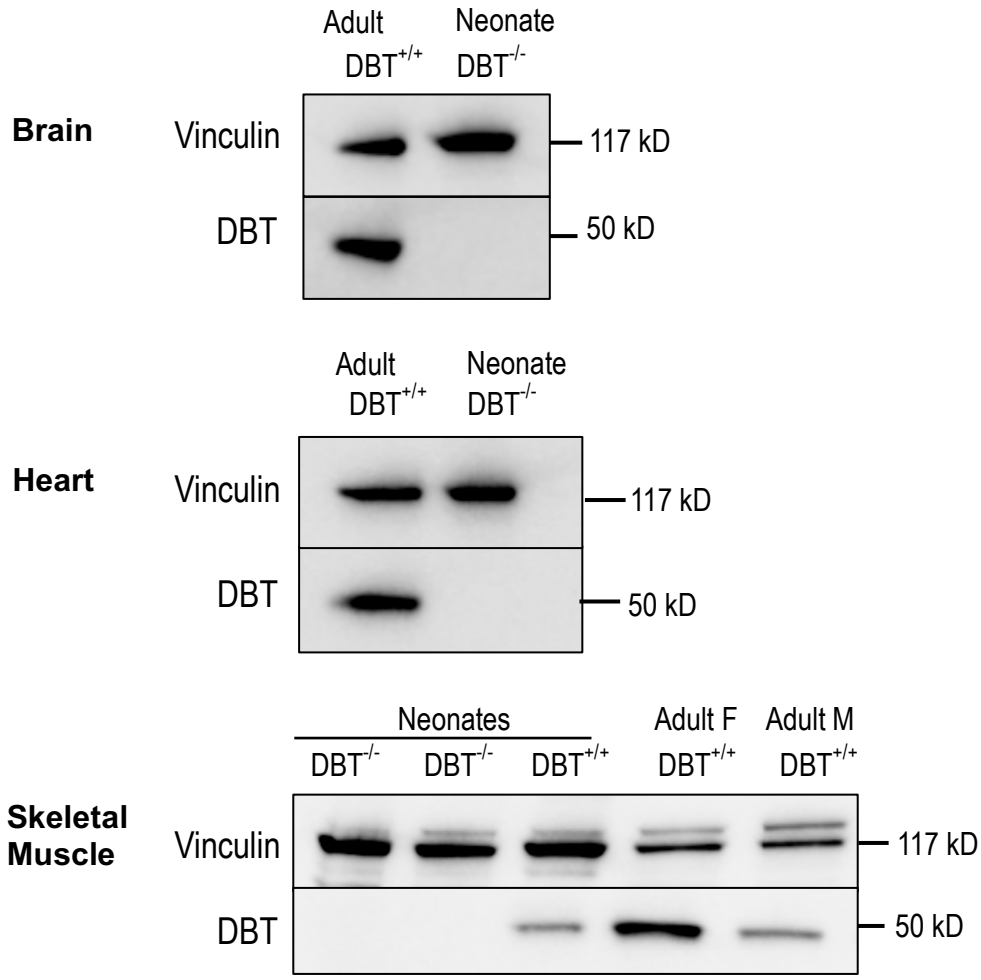

Figure 3-10 Tissue expression of E2 protein across brain, heart and skeletal muscle in $DBT^{+/+}$ neonates and adults and $DBT^{-/-}$ neonates. Blots were probed with polyclonal anti-DBT [Rabbit] antibodies (Invitrogen) and signals normalised to vinculin with anti-vinculin [Mouse] antibodies (BioRad). $DBT^{+/+}$ (neonate n = 1, adult male n = 1, adult female n = 1), $DBT^{-/-}$ (n = 1).

E2 protein expression was also detected by using immunofluorescence staining in PFA fixed hepatic sections as per Chapter 2.2.8. There was no detectable E2 protein in the $DBT^{-/-}$ mice. In $DBT^{+/+}$ neonates, there was E2 protein seen throughout the liver sections. In adult $DBT^{+/+}$ liver sections there appeared to be differentially expressed across the hepatic lobules of DBT, however this was not formally quantified (Figure 3-11).

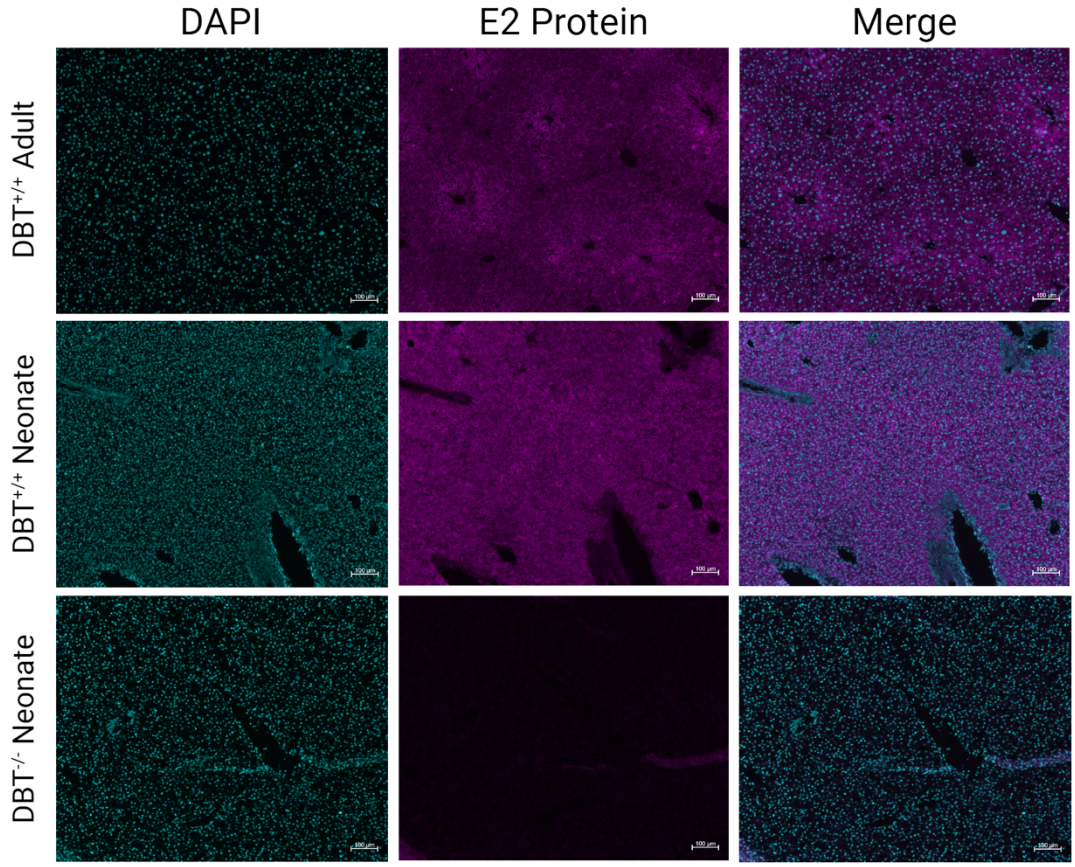

Figure 3-11 Hepatic E2 protein immunofluorescence in DBT Mouse Model. Hepatic tissue immunofluorescence of E2 protein (Purple) in $DBT^{+/+}$ neonate and adult and $DBT^{-/-}$ neonate. Cell nuclei are co-stained with DAPI (blue).

3.3.6 Biochemical phenotype in *DBT*-Deficient mice recapitulates Classical MSUD

Serum levels of L-alloisoleucine, isoleucine, leucine and valine were measured through tandem mass spectrometry performed on three dried whole blood spot samples, as described in Chapter 2.2.6.9. Branched chain amino acid levels were significantly higher in DBT-deficient neonates (n = 13) compared to $DBT^{+/+}$ (n = 6) and $DBT^{+/-}$ (n = 9) neonates (Figure 3-12). These blood spots were collected between 0-48 hours for 7 $DBT^{-/-}$ mice and after 72 hours for a subset of $DBT^{-/-}$ mice that lived past the first 48 hours. For $DBT^{-/-}$ pups that survived longer than 72 hours

(n = 6) the BCAA levels were significantly higher compared to levels observed during the first 48 hours (Figure 3-16). There was no statistical difference between the neonatal BCAA levels $DBT^{+/+}$ and $DBT^{+/-}$ with similar isoleucine ($p = 0.682$), leucine ($p = 0.7503$) and valine s blood levels ($p = 0.4371$) in neonates. This relationship persisted between $DBT^{+/+}$ and $DBT^{+/-}$ across all BCAA ($p = 0.1143$). BCAA were also assessed in male $DBT^{+/+}$ (n = 4) and $DBT^{+/-}$ mice (n = 3) upon reaching adulthood (>56 days) (Figure 3-13).

L-alloisoleucine levels in neonatal $DBT^{-/-}$ mice were significantly elevated compared to $DBT^{+/+}$ and $DBT^{+/-}$ ($p <0.0001$) and increased significantly further in the $DBT^{-/-}$ mice that survived to 7 days ($p = 0.0004$) (Figure 3-16). There was no significant difference in L-alloisoleucine between $DBT^{+/+}$ and $DBT^{+/-}$. Ratios of Leucine:valine were maintained <1 for $DBT^{+/+}$ and $DBT^{+/-}$ mice across their respective lifespans and equivalent between adult $DBT^{+/+}$ and $DBT^{+/-}$ (Figure 1-15) taken at 8 weeks of age. No $DBT^{-/-}$ mice attained adulthood, however the neonatal leucine:valine ratio was elevated at 1.461 (Table 3-3). Leucine levels in $DBT^{-/-}$ mice were 11-fold greater than those in $DBT^{+/+}$. L-alloisoleucine levels in $DBT^{-/-}$ mice were 364-fold higher than those of $DBT^{+/+}$.

Reliable gender determination at the time of neonatal blood collection was not possible and thus no gender-based analysis was performed for BCAA in neonates. Adult female data are not presented here as sample collection is ongoing.

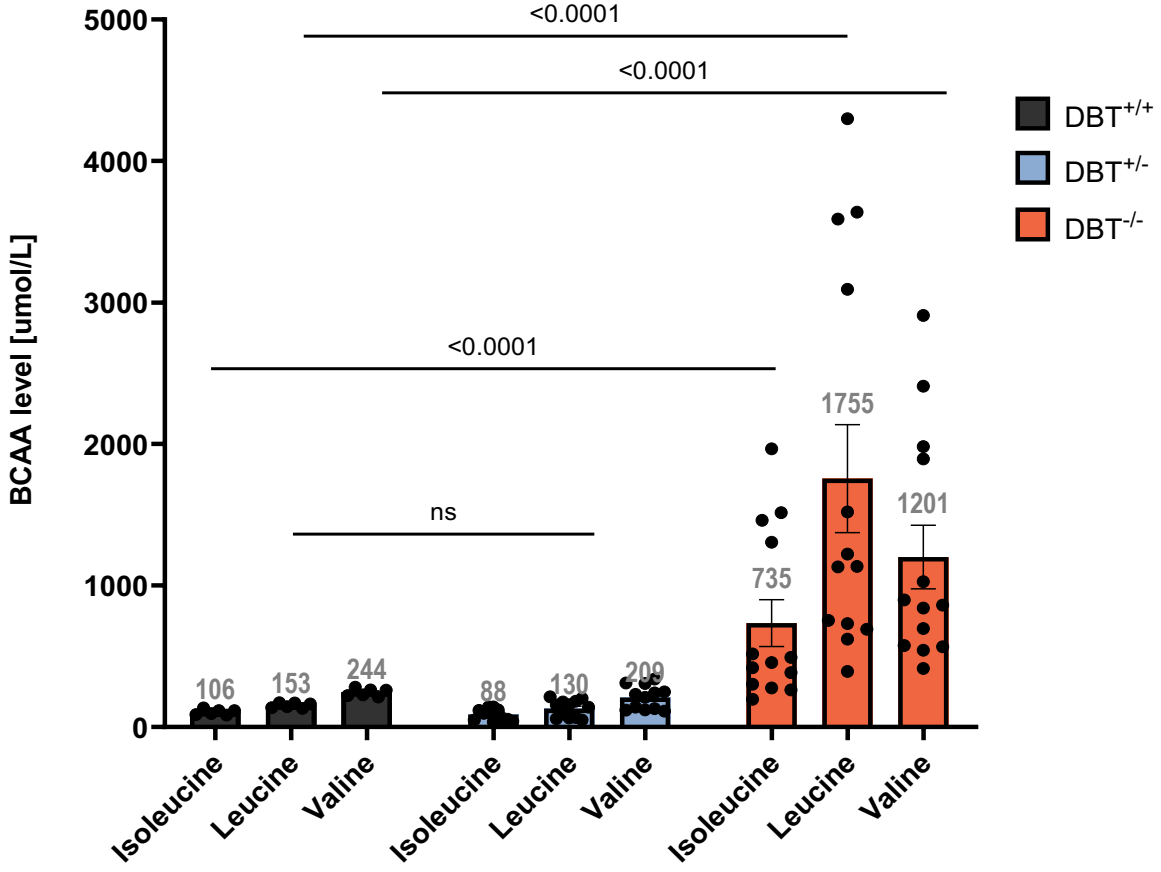

Figure 3-12 Branched Chain Amino Acid levels in DBT MSUD Model. Neonatal Branched chain amino acids in $DBT^{+/+}$ (n = 6), $DBT^{+/-}$ (n = 9) and $DBT^{-/-}$ (n = 13). Individual values are an average of three replicate measurements. Error bars represent mean (also displayed above each column) and standard error mean. Mann-Whitney test used to determine statistical significance.

Table 3-3 Age based Leucine:Valine ratios across genotypes in DBT MSUD murine model.

Leucine/Valine Ratio	$DBT^{+/+}$	$DBT^{+/-}$	$DBT^{-/-}$
Neonatal	0.627	0.622	1.461
Adult	0.575	0.529	N/A

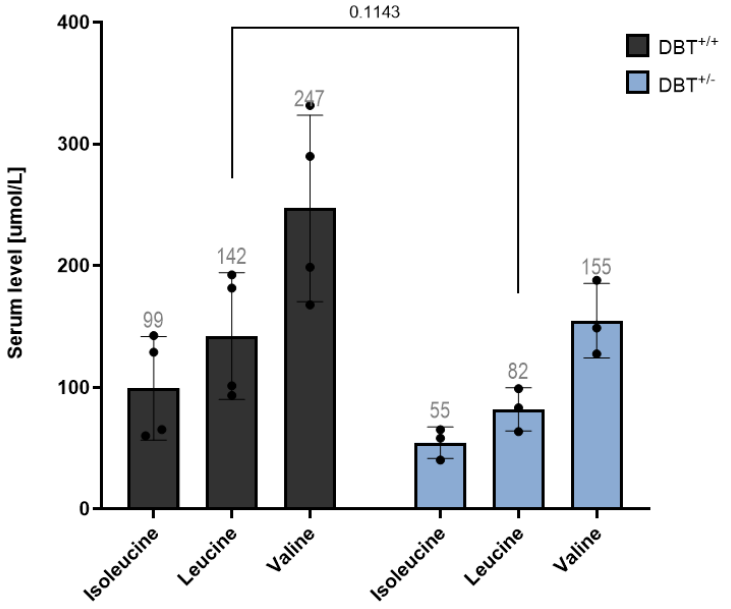

Figure 3-13 Branched Chain Amino Acids in WT and heterozygous adults. Adult BCAA measured in mice aged 56 weeks ($DBT^{+/+}$ n = 4, $DBT^{+/-}$ n = 3). Individual values are an average of three replicate measurements. Error bars represent mean (mean also displayed above each column) and standard error mean. Mann-Whitney test used to determine statistical significance.

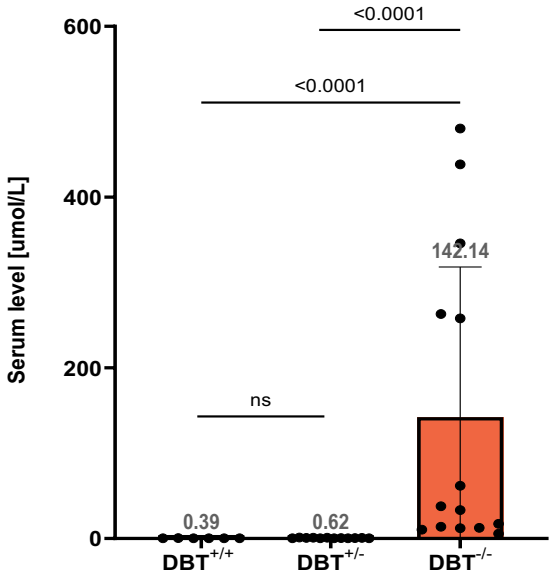

Figure 3-14 Neonatal L-alloisoleucine levels in DBT MSUD Mouse model. Neonatal L-alloisoleucine levels are significantly higher in $DBT^{-/-}$ (n= 13) compared to $DBT^{+/+}$ (n = 6) and $DBT^{+/-}$ (n = 9). Individual values are an average of three technical replicate measurements. Error bars represent mean (also displayed above each column) and standard deviation. Mann-Whitney test used to determine statistical significance.

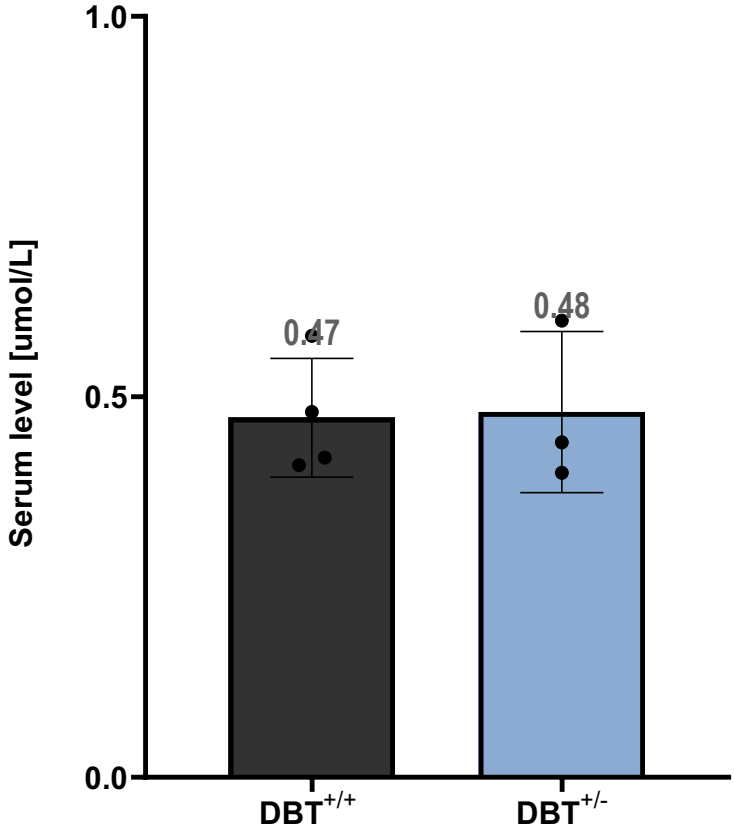

Figure 3-15 Adult L-alloisoleucine levels in DBT Murine Model. Adult L-alloisoleucine levels are comparable between adult male $DBT^{+/+}$ (n = 4) and $DBT^{+/-}$ (n = 3). Samples collected at 56 days of age. Individual values are an average of three replicate measurements. Error bars represent mean (also displayed above each column) and standard deviation. Mann-Whitney test used to determine statistical significance. No $DBT^{-/-}$ mice reached adulthood.

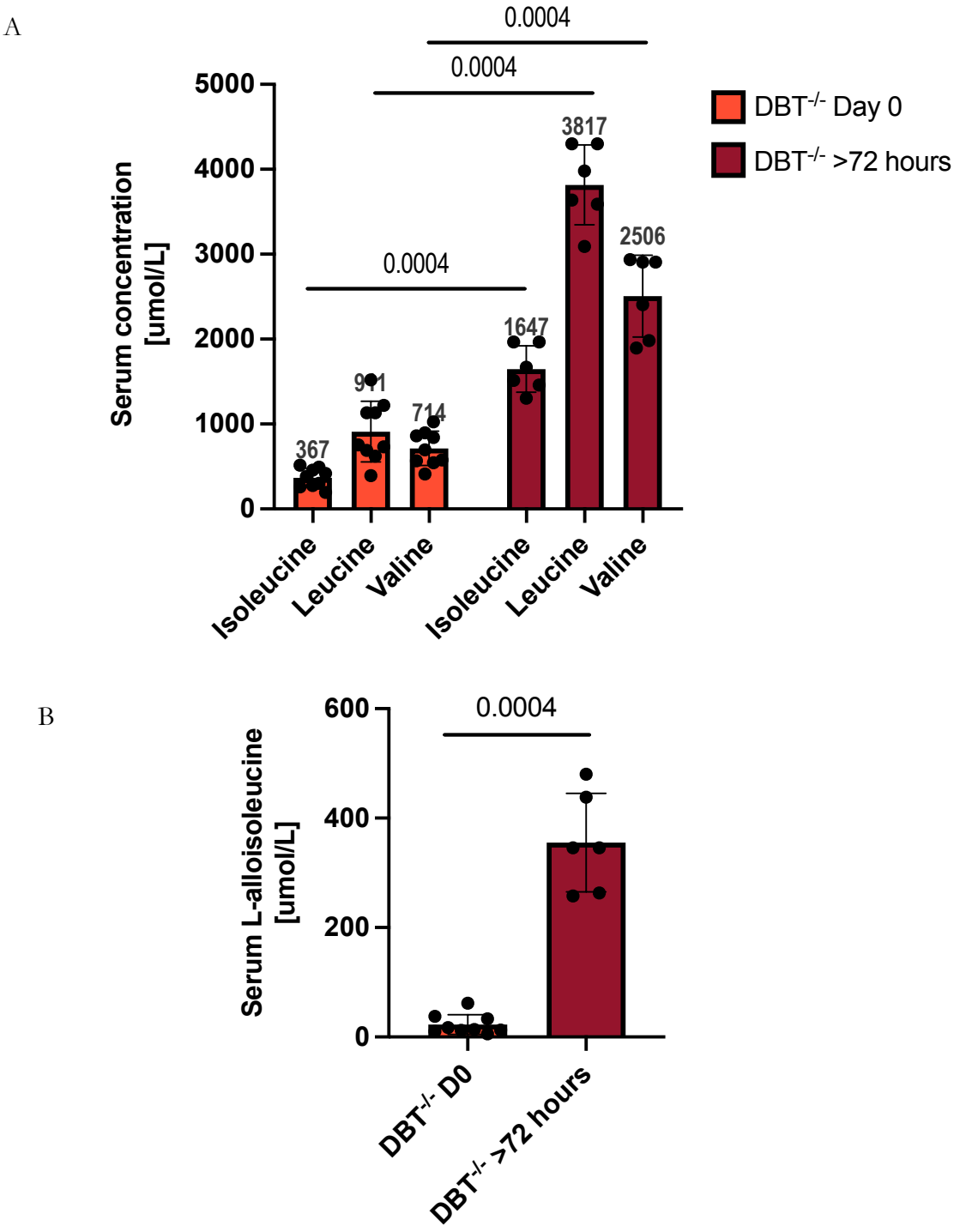

Figure 3-16 Biochemical Phenotype of DBT$^{-/-}$ progressively worsens over time. (A) Serum branched chain amino acid (BCAA) levels (BCAA) significantly increase in DBT$^{-/-}$ pups surviving past 72 hours of life (p = 0.0004). **(B)** Serum L-alloisoleucine levels in DBT$^{-/-}$ pups significantly increase in pups surviving past 72 hours (p = 0.0004). All DBT$^{-/-}$ pups had died by day 9 of life. Error bars represent mean with standard deviation and p value determined with Mann-Whitney two tailed test.

3.3.7 Gestational length and congenital abnormalities

In this study, litters to $DBT^{+/-}$ pairings were born on E19. This was deduced through a timed mating strategy where the female partner in heterozygous breeding pairs was plug checked daily (a mark of copulation). When a copulation plug was found females were then removed from the males and checked daily from 15 days post copulation allowing an estimation of the gestation.

Malocclusion occurred in 2% (n = 3) over the first 6 months (n = 160 mice born). Later in the colony development we observed an increased rate of malocclusion occurring in successive litters to certain dams or sires. When this occurred, the breeding pair was retired in an attempt to reduce the frequency of malocclusion in the colony. Other congenital abnormalities noted included glaucoma (n = 1), and there were two incidence of hydrocephalus (n = 2).

3.4 Discussion and Conclusions

The $DBT^{-/-}$ murine model was derived from the triple mutant iMSUD model Dbttm1Geh Tg(Cebpb-tTA)5Bjd Tg(tetO-DBT)A1Geh/J (The Jackson Laboratory) through backcrossing with C57Bl/6J mice to remove the Tet-Off DBT rescue gene and the Tg(Cebpb-tTa)5bjd transgene. As this strain development was undertaken by researchers external to our laboratory, it was important to formally characterise this model prior to designing and performing any phenotypic correction experiments. This model was characterised across relevant genotypes for survival, growth, E2 protein production and blood BCAA levels. Further behavioural characterisation could be undertaken in future studies, including righting reflex [383] open field testing, and dark light compartment testing to help further elucidate any behavioural or neuropsychometric phenotypes [384].

Phenotype characterisation data demonstrate that this model faithfully recapitulates a severe form of MSUD, or classical MSUD in $DBT^{-/-}$ pups. The genetic basis for the disease is similar to that in humans, with a mutation in the highly homologous *DBT* gene resulting in absent E2 protein and subsequently severely limiting the BCKDH enzyme activity.

3.4.1 $DBT^{-/-}$ is a neonatal lethal murine model

In this study the $DBT^{-/-}$ affected pups born to heterozygous breeding pairs died soon after birth, and most within the first 48 hours of life. There were a few $DBT^{-/-}$ affected pups that lived past 72 hours, and only that lived until 9 days (see Figure 3-5). Any $DBT^{-/-}$ pup that lived past 72 hours became very cachectic, with slowed movements and failed to develop some of the normal hair growth patterns that occur during the first week of life [385]. They also experienced extreme growth failure and became moribund with slowed movements and intermittent myoclonic movements (see Figure 3-7). The observed growth failure and motor function characteristics is

reflective of the known clinical toxidrome that occurs in humans with untreated MSUD where poor feeding, muscle weakness, seizures and encephalopathy occur once newborns start feeding [20].

The model's BCAA levels were also comparable to levels seen in humans with classical MSUD [386]. Furthermore, BCAA levels in $DBT^{-/-}$ pups that survived past 72 hours were much higher than those taken from $DBT^{-/-}$ on day 0 of life, reflective of the ongoing pathological accumulation of isoleucine, leucine and valine as they continue suckling (see Figure 3-16). BCKDH stoichiometry of isoleucine:leucine:valine was approximately conserved in an 1:2:3 ratio in DBT replete mice as seen in humans. In $DBT^{-/-}$ mice, the ratio of leucine to valine was elevated at >1. A similar leucine-to-valine ratio is also seen in affected human's with MSUD.

L-alloisoleucine was the bio marker that rose the most compared to the levels found in DBT sufficient genotypes. From this it can be concluded that L-alloisoleucine is the most sensitive biomarker of perturbed BCAA metabolism in this murine model, which again is consistent with human MSUD biochemistry [77].

An attempt to measure BCKDH enzyme activity was undertaken using the spectrophotometric assay however was ultimately unsuccessful in replicating the published assay methods [40]. There is one alternative published assay with which to measure BCKDH activity with liquid scintillation chromatography, however ready access to specific equipment required for this was not available in the centre the candidate was working in [387]. Whilst BCKDH enzyme activity was not measured directly, BCAA levels are inversely proportional to BCKDH enzyme activity with the grossly elevated BCAA in this murine model reflective of very low BCKDH enzyme activity. The $DBT^{-/-}$ model is more severe than the iMSUD model, which was reported to have a residual 6-10% total body BCKDH activity. Subsequently, whilst the exact level of BCKDH activity in the

DBT model was not quantified, the level is lower than 6% and the universal neonatal lethality in $DBT^{-/-}$, growth failure and pathognomonic elevation in BCAA are demonstrative of a model that recapitulates the natural history of classical MSUD in humans.

3.4.2 Autosomal recessive inheritance pattern and genotype incidence

From the early on during DBT colony establishment it became apparent that the affected $DBT^{-/-}$ mice died rapidly and sick or dead mice were often found cannibalised by their mothers. Neonatal deaths within in-bred murine species are not uncommon, and may occur for a variety of reasons including both *in utero* issues such as placental issues leading to post-natal issues like lower birth, poorer feeding or other congenital abnormalities and other unknown reasons [388]. In this project it was found that the incidence of homozygous unaffected, heterozygous and homozygous affected births (26%, 58% and 16% respectively) did not approximate that expected for an autosomal recessive inheritance pattern, which should be closer to a 1:2:1 ratio or 25%/50%/25%. Possible reasons for this could be that some $DBT^{-/-}$ mice were never accounted for due to the early deaths and cannibalisation occurring prior to litter discovery. Mice have highly evolved olfactory senses and if the $DBT^{-/-}$ pups smelled different due to the build-up and excretion of toxic metabolites it could be that the mothers cannibalised close to birth and prior to them being found by the animal biotechnicians. There may also be some unaccounted *in utero* or alternative post-natal reason which conveyed a selective disadvantage to $DBT^{-/-}$ pups. Irrespective of the underlying cause, $DBT^{-/-}$ pups births rates at levels below expected for autosomal recessive conditions and rapid neonatal deaths are illustrative of the known difficulties in working with neonatal lethal models [389].

There were also a number of early neonatal $DBT^{+/+}$ and $DBT^{+/-}$ deaths, the cause of which was not obvious, but may have related to undetectable abnormalities affecting feeding or behaviours leading to hypothermia or starvation and early death, as is seen in other in-bred laboratory mice [390].

3.4.3 Gestation length for DBT$^{-/-}$ mouse similar to that of background strain C57Bl/6J

Mating characteristics, including pregnancy length were important to characterise for this neonatal lethal model for multiple reasons. As the majority of affected DBT$^{-/-}$ pups died within the first 48 hours, it was suspected there would be a narrow treatment window for administering any therapeutic interventions. As such, knowing when pups would be born was vital for ensuring early therapeutic interventions and increasing opportunities for biophysical observations. Furthermore, *in utero* vector administration had been proven successful in other neonatal lethal models [391]. Thus, understanding the pregnancy length in this murine model was vital to understand appropriate surgical windows for *in utero* injections should this strategy be utilised in future experiments.

There were major public building works adjacent to the animal house facility for the duration of this project, including the construction of two multi-story new hospitals and a light rail. There was some anecdotal evidence in other mouse strains housed in the same facility that gestational lengths had shorted possibly due to the tremors and vibrations from the construction. However the gestation length of our colony was consistent with published lengths of 462 hours or 19.2 days [392]. Genetic and environmental factors are known to affect pregnancy lengths in several mouse strains including C57Bl/6J, with gestation length being shorted in Autumn and longest in spring, despite living in a highly controlled environments with regards to temperature, food availabilities and diurnal light cycles. We also acknowledge that vaginal copulation plugs as a proxy for conception start date is an imprecise measurement and assumes that copulation results in conception. Whilst imperfect, it is widely used in research and is the most easily accessible, non-invasive and utilised the pre-existing expertise of our team.

3.4.4 Congenital and developmental abnormalities

The DBT colony experienced malocclusion, glaucoma and one case of hydrocephalus. Congenital abnormalities are not uncommon in inbred mouse strains and the background strain of the DBT model is C57Bl/6J and FBV. C57Bl/6J is most widely used laboratory mouse strain, multiple congenital/developmental abnormalities are known to occur in this model and are well documented [393]. These include a high susceptibility to type 2 diabetes, diet-induced obesity, and atherosclerosis, microphthalmia and other associated eye abnormalities, decreased bone density, resistance to audiogenic seizures, hereditary hydrocephalus at rates including 1-4%, hair loss associated with exuberant grooming, portosystemic shunts (~5%), late-onset hearing loss, and increased incidence of hydrocephalus and malocclusion, spontaneous calcaneal luxation in adult males (approx. 1%) causing ankylosing enthesopathy in the corresponding tarsal joint, and vaginal septa [394].

3.4.5 Model Limitations

This model has high fidelity to the natural history of classical MSUD in humans which is useful for assessing neonatal treatment efficacy and durability in developing organs, however this also results in a narrow therapeutic window. This mutant gene in this model also only reflects one of the known genotypes of MSUD. Whilst the clinical phenotypes across the most common MSUD genotypes in humans are analogous, this model can only be used to explore DBT related genetic therapies. This also would be true for MSUD in humans and any human clinical genetic therapy would need to consider the underlying patient mutation. The $DBT^{-/-}$ mouse model however faithfully recapitulates classical MSUD and is a useful and important pre-clinical model to study MSUD.

Chapter 4

Liver directed AAV-mediated Gene Addition for Maple Syrup Urine Disease in a neonatal lethal DBT$^{-/-}$ murine model

4.1 Introduction

The treatment of Maple Syrup Urine Disease has remained largely unchanged, with dietary therapies the mainstay of treatment for the past 60 years and more recently liver transplantation however both of these options are suboptimal. Even with good compliance MSUD patients on dietary therapies remain at risk of serious life-threatening metabolic decompensations during periods of catabolic stress (fasting, surgery, intercurrent illness) and patients with disease severe enough to warrant a liver transplant remain on life-long immunosuppression with the associated long-term risks. Clearly, there is a need for novel therapeutics that avoid the short-comings of current MSUD therapies. One such strategy for a novel therapeutic approach for MSUD could be liver-directed AAV gene therapy.

The liver is an attractive target when conceptualising a clinically translatable MSUD gene therapy for numerous reasons. Foremost, the success of liver transplantation in providing a near complete metabolic cure for MSUD coupled with the availability of highly human hepato-trophic AAV vector technology proffers it a natural target to explore [25]. In humans, hepatocytes contribute to approx. 15% of total body BCAA metabolism activity, and a gene replacement therapy targeting the liver has the potential to improve BCKDH activity in MSUD individuals. Whilst there are no current clinical trials for MSUD, there has been recent success with simple AAV gene addition

vectors in the pre-clinical neonatal lethal MSUD murine models, *BCKDHA*, *BCKDHB* models [323, 324] and an iMSUD model [326]. These studies all used either AAV8 or AAV9 to target the liver or muscle, respectively, and used a variety of liver specific and ubiquitous promoters. There have not yet been any published studies investigating rescue of the neonatal lethal murine $DBT^{-/-}$ model with AAV alone or stand-alone hepatic rescue.

The liver also stands as an attractive target in the practical sense with an ever-growing number of human hepato-trophic AAV capsids available for human use, some already validated in clinical trials and with an established path for translating success in murine model systems to non-human primates and on to human clinical trials [395]. Targeting the liver in neonatal mouse models is also well documented, with established vector delivery routes in neonatal mice of both IP and IV injections simple and effective in transducing hepatocytes [396, 397]. This is an important consideration as the $DBT^{-/-}$ murine model is neonatal lethal, and as such, vector will need to be given as close to birth as possible to rescue neonatal $DBT^{-/-}$ affected pups.

Undoubtably, the biggest inherent challenge when targeting neonatal tissues like the liver is the major developmental changes that occur during late embryogenesis until adulthood which directly influence the concentration of AAV episomes in transduced neonatal cells. Hepatocytes are one of a few terminally differentiated cell lines that can replicate [398] and in murine studies the neonatal liver grows over 100-fold in mass until reaching adulthood. During this time, the hepatocyte compartment expands as haematopoietic cells present in the liver at birth migrate to the bone marrow [399]. Strategies for overcoming this challenge have included multiple vector dosage regimens or passing by the neonatal liver completely and limiting liver directed treatments to adults who have a more stable hepatocyte population [400]. In conditions like MSUD which present in the neonatal period and most severely impact paediatric populations, limiting novel therapeutics to adult cohorts precludes a group of patients who arguably have the most to gain

from early therapeutic intervention. Thus, any novel therapeutic for MSUD would ideally be designed for early neonatal or paediatric dosing and endure for the rest of the patient's life.

In the two pre-clinical studies exploring gene addition strategies for the *BCKDHA* [323] and *BCKDHB* [324] MSUD neonatal lethal models, both of these studies had success in phenotypic rescue with a single dose of a AAV8 gene addition vector with a human transgene under transcriptional regulation of a liver enhancer/promoter APOe/hAAT at a dose of 10^{14} VGC/kg. This APOe/hAAT enhancer was selected for the reported liver specificity this enhancer/promoter provides. The durability of phenotypic rescue, to 180 days of age was unanticipated given that the AAV vectors were administered neonatally and hepatic vector effects were expected to attenuate with time. AAV gene addition has never been explored in the neonatal lethal $DBT^{-/-}$ murine model.

This chapter describes a proof of concept for a hepato-trophic AAV gene addition vector to treat MSUD in a $DBT^{-/-}$ neonatal lethal model of MSUD. We assess the efficacy of neonatal intraperitoneal vector administration with regards to tissue transduction, transgene protein production and therapeutic durability. The AAV8 vector capsid (rAAV8) was selected for initial exploration into a liver targeted AAV gene therapy for the $DBT^{-/-}$ murine model as this capsid serotype has demonstrated efficiency in transducing neonatal hepatocytes [401]. A liver specific combination of an apolipoprotein-e (APOe) enhancer element and a human Alpha-1-Antitrpsin promoter (APOe/hAAT) were used to drive expression of the human transgene. This enhancer/promoter combination has been demonstrated to drive strong transgene expression in hepatocytes [402].

The purpose of this chapter was to explore and evaluate hypothesis 2 and aim 2 (see Chapter 1.6).

4.2 Chapter specific methods

4.2.1 Construction of a rAAV vector plasmid containing human *DBT*

The coding sequence of human DBT was synthesised by generating human cDNA from RNA extracted from Huh7 cells using superscript first strand synthesis III as per manufacturer's instructions (Invitrogen). Primers were designed to capture the hDBT coding sequence from exon 1 (DBT.For 5'-GGAGCTAGTACTGCCGCCACCATGGCTGCAGTCCGTATGC-3') to exon 12 (DBT.Rev 5'-GTAGCAGTCGACTCATTTCAGATCTAGTAGCATAAAAGC-3'). Additional features added in included a Kozak sequence (GCCGCCACC [403]) and ScaI restriction digest sites in DBT.For and a SalI restriction digest site in DBT.Rev. The hDBT sequence was amplified in a thermocycler using Phusion HotStart kit as per manufacturer's instructions (Thermo Scientific). Products were isolated via gel electrophoresis 1% (wt/v) agarose at 90 V for 60 minutes and then purified by Wizard gel purification kit as per manufacturer's instructions Wizard SV Gel and PCR Clean-Up system (Promega). The product was then ligated into pGEM-T Easy plasmid as per manufacturer's instructions. The hDBT sequence integrity was then cross-referenced to published reference sequences of the human DBT gene [404].

JM109 cells were transformed with the ligation products with appropriate controls and plated on LB Agar + ampicillin + X-Gal and incubated overnight at 37°C. Colonies were picked, grown, purified and then sent for Sanger sequencing at AGRF (Westmead Institute of Medical Research, Australia) and aligned to reference sequences using SnapGene. The human DBT sequence was then cloned into a plasmid backbone containing recombinant AAV ITRs (Figure 4-1) by restriction digest of the pAAV2.APOe/hAAT.PCCA plasmid backbone with ScaI and SalI. Products were separated using gel electrophoresis and purified using Wizard SV Gel and PCR Clean-Up system.

Ligation of backbone and insert was then undertaken using T4 DNA Ligase (New England Biolabs) as per manufactures instructions and JM109 cells transformed with plasmid constructs. Colonies were then picked, grown and purified and screened with both restriction digest to assess ITR integrity (MscI) and presence of the other elements and Sanger sequencing at AGRF. The resultant AAV vector plasmid was called pAAV2.APOe/hAAT.hDBT (Figure 4-1) and packaged with the AAV8 capsid plasmid and pAd5 helper plasmid via methods described in Chapter 2 to generate the recombinant AAV vector rAAV2/8.APOe/hAAT.hDBT

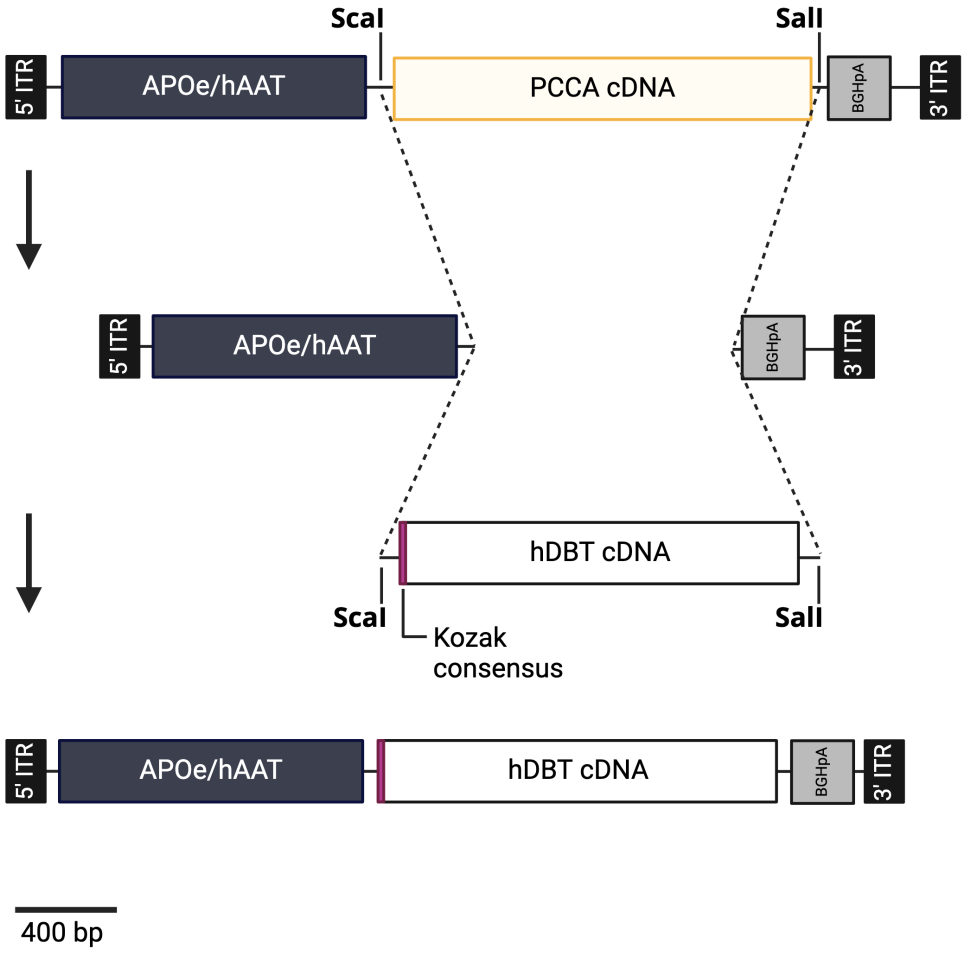

Figure 4-1 Molecular sub-cloning history of pAAV2.APOe/hAAT.hDBT. Detailed explanation of subcloning is described in Section 4.2.1 and parental plasmid details in Table 2-7. The expression cassettes are flanked by AAV2 ITRs (black boxes). Digest sites are marked with corresponding restriction enzymes. Other DNA components illustrated are the APOe/hAAT promoter enhancer (charcoal box), PCCA transgene (yellow box), human *DBT* coding sequence (hDBT cDNA white box) preceded by Kozak consensus sequence (magenta bar) and bovine growth hormone polyadenylation signal, BGHpA (light grey boxes). Scale bar = 400 bp. Figure generated in BioRender

4.2.2 *In vitro* validation of pAAV2.APOe/hAAT.hDBT expression cassette

The transgene plasmid pAAV2.APOe/hAAT.hDBT was used to generate an AAV vector pseudo-serotyped with the DJ capsid [216] to make AAV2/DJ.APOe/hAAT.hDBT as per methods in chapter 2.2.5. Vector genomes were quantified prior to the CsCl purification steps and this preparation used in the crude formulation for cell application. Cell lines for transduction were selected from human liver derived immortal cell lines (Huh7 and HepG2) as well as a cell line with low endogenous expression of BCKDH enzyme and E2 subunit, U2-OS cells, derived from an osteosarcoma cell line. Cells were transduced with the AAV2/DJ.APOe/hAAT.hDBT crude vector preparation over a range from 1×10^3 to 1×10^5 VGC per cell in 10 cm tissue culture plates at approximately 80% confluency (4.25×6^{10} cells). Cells were seeded on day 1 in DMEM, transduced day 2, media changed with DMEM on day 3 and harvested on day 4. Cells were then assessed for vector genome copy and DBT transgene RNA expression via qPCR, and E2 protein production via western blot.

4.2.3 Neonatal injections and experimental design

Two cohorts of mice were used to validate the hepatic transduction efficiency, transgene expression of the rAAV2/8.APOe/hAAT.hDBT vector as well as the durability of this strategy. Whole litters of mice born to heterozygous breeding pairs ($DBT^{+/-}$) mice were weighed and marked on day 0 as in Chapter 3.2.3. Thereafter each pup was administered 5×10^{11} VGC of rAAV2/8.APOe/hAAT.hDBT via intraperitoneal injection as close to birth as possible. Due to the overt phenotype of the murine disease model, this study was non-blinded and non-randomised. All mice were monitored daily for growth and physical condition. The short-term cohort, ($DBT^{-/-}$ n = 9) were sacrificed on post-natal day 7. A long-term cohort of $DBT^{-/-}$ mice (n = 18) were followed until either they became unwell or reached adulthood (Day 56). Mice were sacrificed if they became unwell, displayed features of metabolic intoxication (ataxia, weakness, seizures, weight loss, poor feeding) lost more than 20% of their body weight or reached the experimental endpoint

(Day 56). Any pup that was found dead within the first 48 hours after injection was genotyped only with no other specimens collected due to the *post mortem* state affecting the integrity of the biochemical end-point assays.

4.2.4 *In utero* AAV Gene Addition

In utero injections were undertaken on E15 as described in Chapter 2.2.6.5. Foetuses were identified through the uterine horns and vector administered in a total volume of 5 μL via intraperitoneal injection. All foetuses were treated with rAAV2/8.APOe/hAAT.hDBT at either high dose (5×10^{11} VCG/foetus) or low dose (2.5×10^{11} VCG/foetus). Dams were monitored daily until birth and then for the subsequent fortnight *postpartum*. Pups were marked at birth, weighed and monitored daily until they became unwell or reached adulthood.

4.2.5 Vector biodistribution

Vector biodistribution was assessed with digital droplet PCR (ddPCR) and per Chapter 2.2.7.2, targeted to the human DBT transgene and genomic albumin copies to determine the vector copy number (VCN) per diploid cell in each tissue. For the short-term cohort, only mice that survived to 7 days (n = 5) were used and only their livers were assessed. For the long-term cohort, liver, brain, kidney, cardiac and skeletal muscle tissue was taken from the 8 randomly selected mice who survived beyond 15 days.

4.3 Results

4.3.1 Functional validation of rAAV2/DJ.APOe/hAAT.hDBT *in vitro*

In vitro transduction of Huh7, HepG2 and U2-OS cell lines with DJ.APOe/hAAT.hDBT was undertaken to assess if the transgene expression cassette was functional. These cell lines were transduced in parallel to assess if transgene derived E2 protein would detectable above endogenous levels. In Huh7 cells, a dose dependant expression was demonstrated with vector $\leq 5 \times 10^3$ VGC per cell. There was a reduction in expression at 1×10^4 VCG per cell expression equivalent to 1×10^3 VCG per cell (Figure 4-2). There was no increase in E2 protein expression above baseline in the HepG2 or U2-OS cell lines reflective of either poor transduction with the DJ capsid and/or tissue restricted expression under the APOe/hAAT enhancer/promoter (Figure 4-2).

As the Huh7 cells were the only cell line to have E2 expression above baseline and demonstrated dose-dependent transduction we transduced these cells again at higher levels 1×10^5 , 1×10^4 and 5×10^3 VCG per cell and assessed E2 protein expression, vector copy number (Figure 4-3). The highest dose had the lowest vector VGC and E2 protein expression, potentially suggesting cell death and toxicity associated with the highest MOI.

These *in vitro* experiments demonstrate that our transgene expressed under the transcriptional control of the liver specific promoter-enhancer APOE/hAAT in Huh7 cells. There appeared to be some dose-dependent toxicity in Huh7 cells and no expression in HepG2 or U2-OS cell lines.

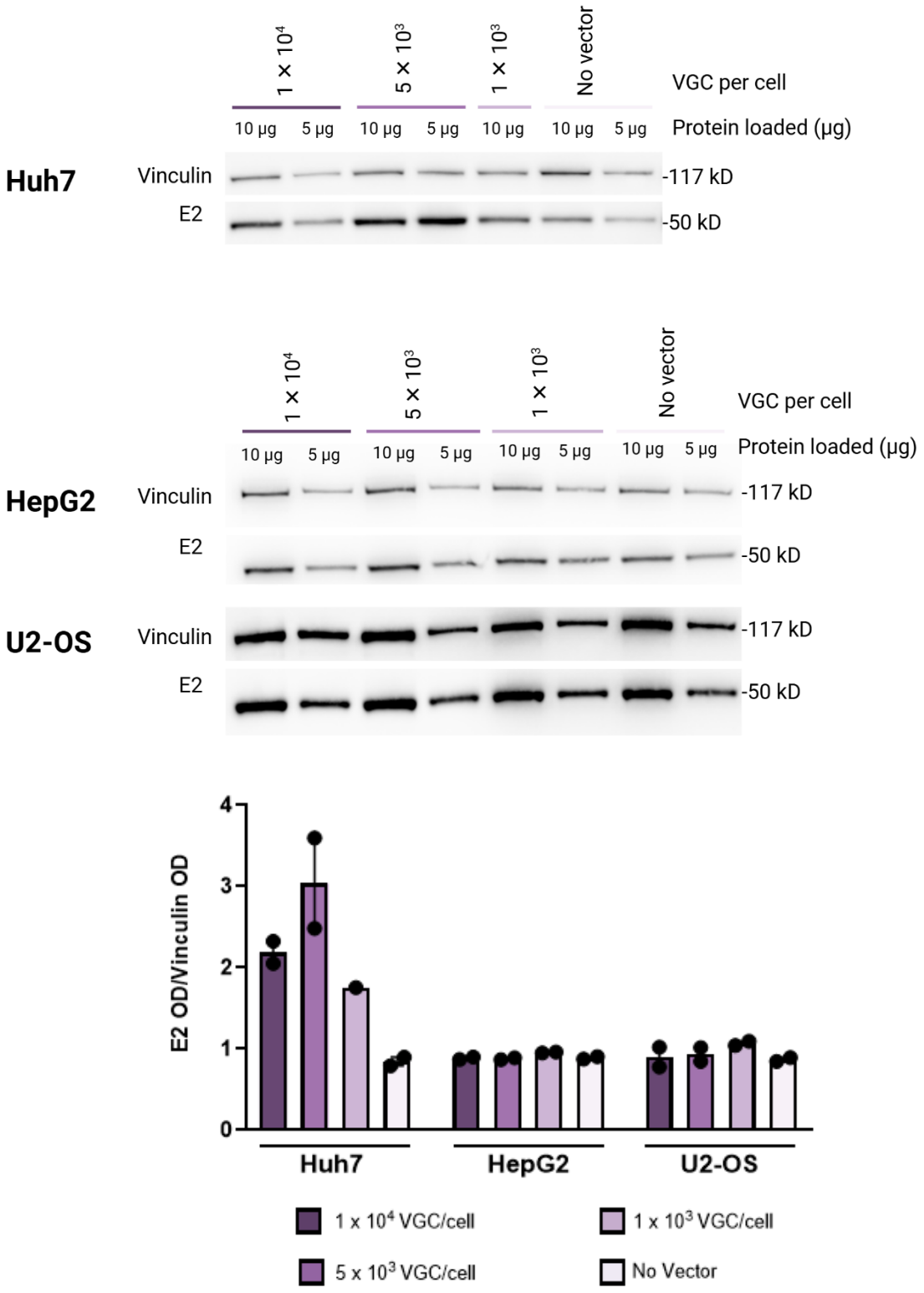

Figure 4-2 Functional Transduction of hDBT expression cassette. Western blot quantitation of E2 protein expression from Huh7 cells transduced with rAAV2/DJ.APOe/hAAT.hDBT vector across three different MOIs (10,000, 5000, 1000 vector genomes/cell), (n = 2 wells for each MOI). Quantitation undertaken using Image J. Membranes were cut at 100kD and then probed individually for vinculin and E2 protein. Figure generated in BioRender. Mean of n = 2.

A.

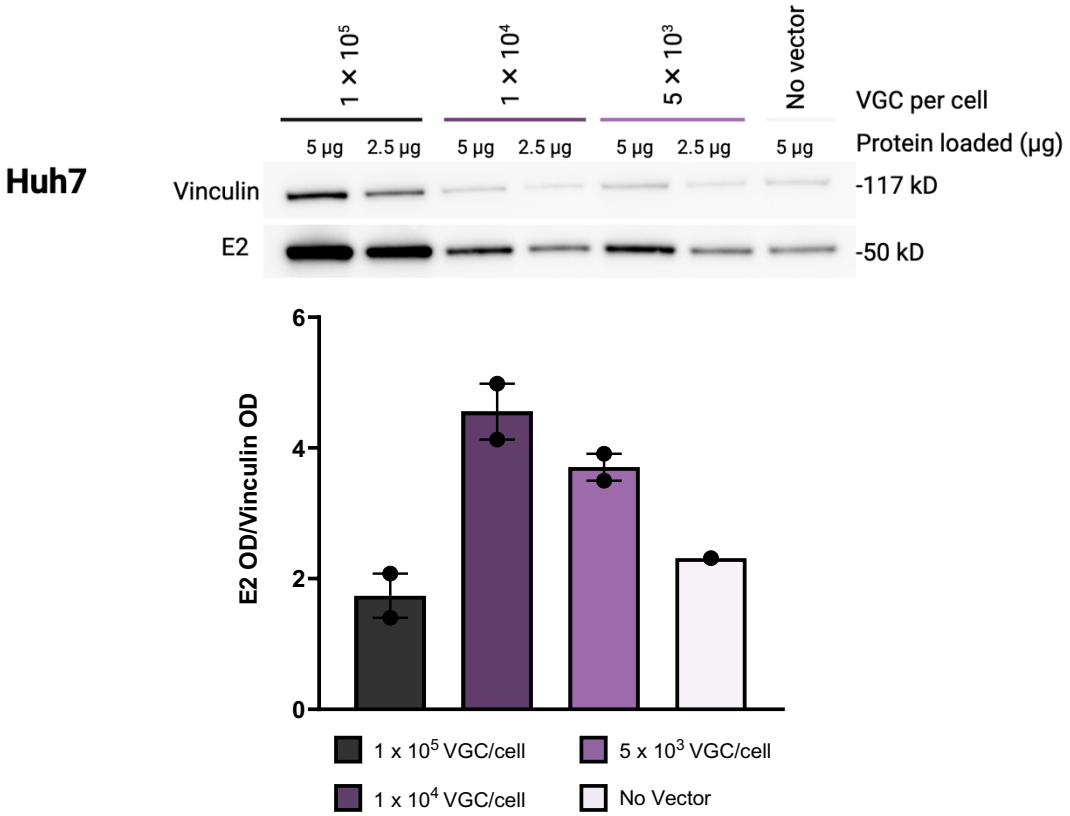

B.

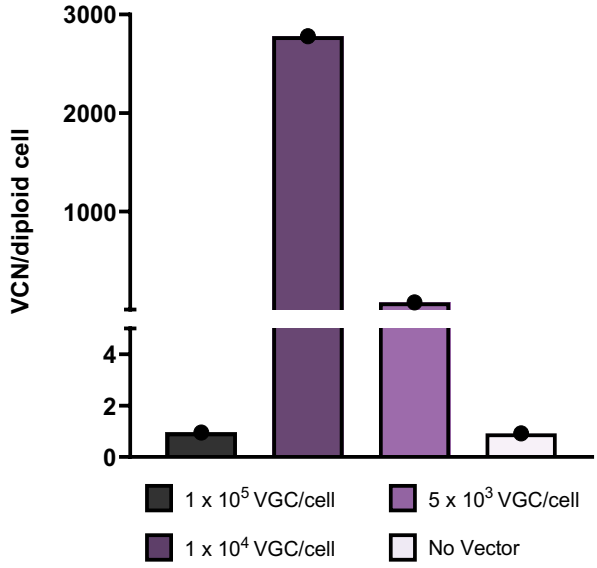

Figure 4-3 Functional transduction of hDBT expression cassette in Huh7 over increased range of MOIs. (A) Dose titration experiment of Huh7 cells with rAAV2/8DJ.APOe/hAAT.hDBT vector demonstrating E2 protein expression. Quantitation undertaken using Image J. Membranes were cut at 100kD and then probed individually for vinculin and E2 protein. **(B)** vector genome copy in Huh7 cells 48 hours after vector transduction signals were normalised to human albumin. Figure generated in BioRender.

4.3.2 Liver directed gene addition provides transient biophysical phenotypic rescue with rAAV2/8.APOe-hAAT.*DBT* viral vector

Survival was significantly improved in both the short and long-term cohorts in rAAV8.APOe/hAAT.hDBT vector treated $DBT^{-/-}$ pups. For the short-term cohort (n = 9) survival at 7 days for $DBT^{-/-}$ mice was 56%, which was significantly longer than untreated $DBT^{-/-}$ (n = 26) (p = 0.0008). In the long-term cohort, $DBT^{-/-}$ pups (n = 18) were treated with rAAV2/8.APOe/hAAT.hDBT vector at 5×10^{11} VGC. Whilst the intended experimental end point was 56 days, none of these mice survived past 20 days with a mean survival of 9.2 days (SD ± 8.7 days) (Figure 4-4). This survival was still significantly improved compared to untreated $DBT^{-/-}$ which have a 100% death rate by 9 days ($p < 0.0001$). Ten of these mice died quickly, within 48 hours of injection, however 8 mice survived with a mean life span of 18.6 days (± 1.9 SD) before developing features of metabolic intoxication (ataxic, wight loss, poor balance, poor grooming and cycling leg movements potentially indicative of seizures) and were humanely euthanised between 17 to 20 days of age.

Growth was comparable between the short-term $DBT^{-/-}$ cohort and $DBT^{+/+}$ (Figure 4-6). For the 8 $DBT^{-/-}$ long-term mice that survived past 48 hours, their growth was also similar to $DBT^{+/+}$ mice until around three days before death, whereupon they demonstrated faltering growth and then weight loss (Figure 4-5). The mean weight loss in these mice was 14.6% ± 6.9 SD of maximum body weight (Figure 4-5). During this time of growth failure features of metabolic intoxication were observed. Prior to this, as were all the $DBT^{-/-}$ mice in the short-term cohort, they were seen to be ambulating normally, interacting and feeding in a normal manner and were indistinguishable from their DBT sufficient litter mates.

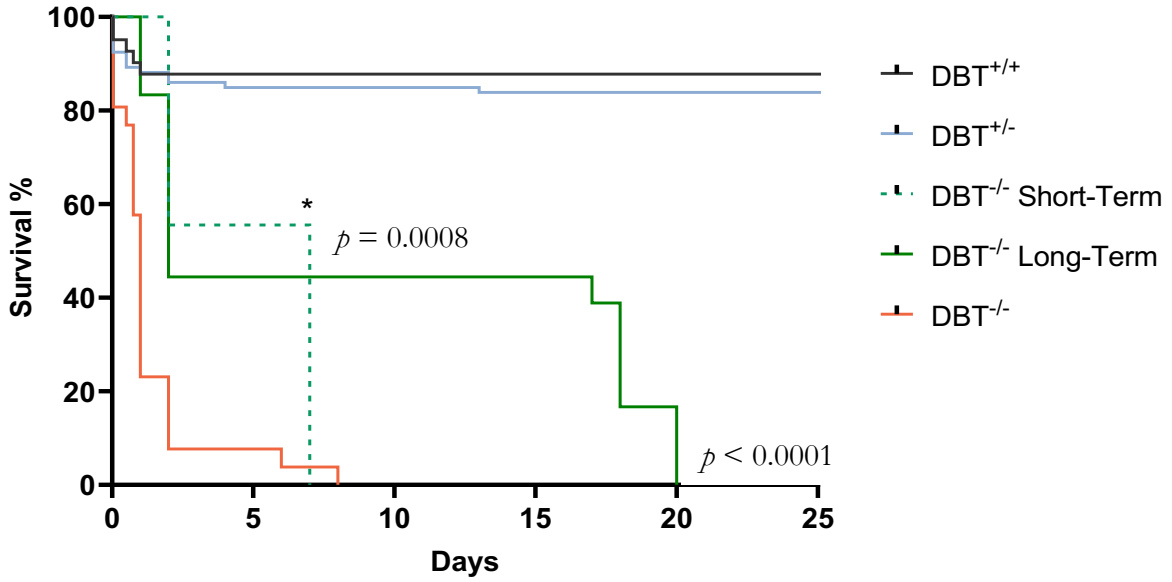

Figure 4-4 Survival of DBT$^{-/-}$ rAAV8.APOe/hAAT.hDBT vector treated mice. Survival curve of untreated DBT$^{+/+}$ and DBT$^{+/-}$ and short-term and long-term vector treated DBT$^{-/-}$. Surviving DBT$^{-/-}$ short-term cohort were culled humanely at day 7 (*) (day 7 survival 57%, $p = 0.0008$, Log-rank (Mantel Cox) test compared to DBT$^{-/-}$ survival). The DBT$^{-/-}$ long-term cohort were followed to assess long term survival and all became unwell requiring humanely euthanised (Day 15 survival 44%, $p < 0.0001$, Log-rank (Mantel Cox) test, compared to DBT$^{-/-}$ survival).

A

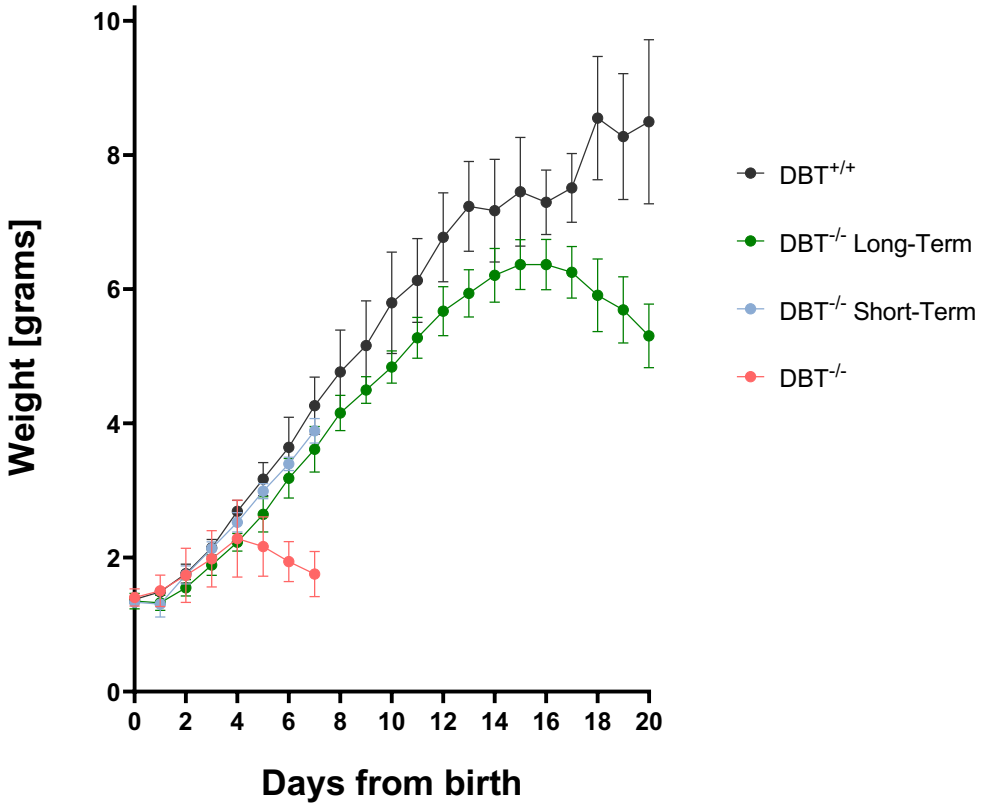

B

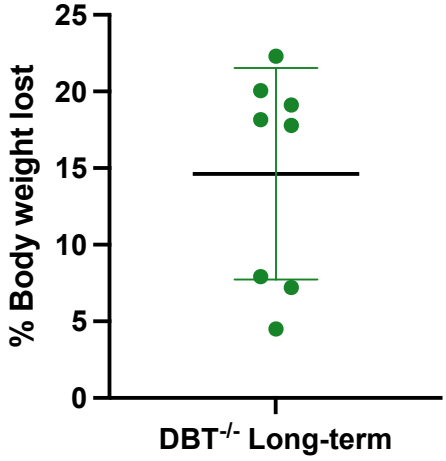

Figure 4-5 Growth in DBT$^{-/-}$ Mice treated with rAAV2/8.APOe/hAAT.hDBT vector (A) Daily weights of untreated DBT$^{-/-}$, DBT$^{+/+}$ and vector treated DBT$^{-/-}$ pups. Growth **(B)** % weight loss in Long-term cohort of DBT$^{-/-}$ mice surviving past 14 days after treatment with rAAV8.APOe/hAAT.hDBT. Final body weight was divided by maximum body weight attained during lifespan to achieve % weight lost.

4.3.3 rAAV2/8.APOe-hAAT.DBT vector biodistribution following neonatal intra-peritoneal vector administration

VCN was significantly higher in the hepatic tissue of the short-term cohort compared with the long-term cohort for the same vector dose of 5×10^{11} VCG/pup (Figure 4-6A). A wider assessment of vector biodistribution was undertaken for the long-term cohort and vector was also detected in the brain, kidney, cardiac muscle, skeletal muscle (gastrocnemius) and lung. Within the tissues assessed for the long-term cohort, cardiac tissue had the highest cellular concentration of vector followed by liver (Figure 4-6B).

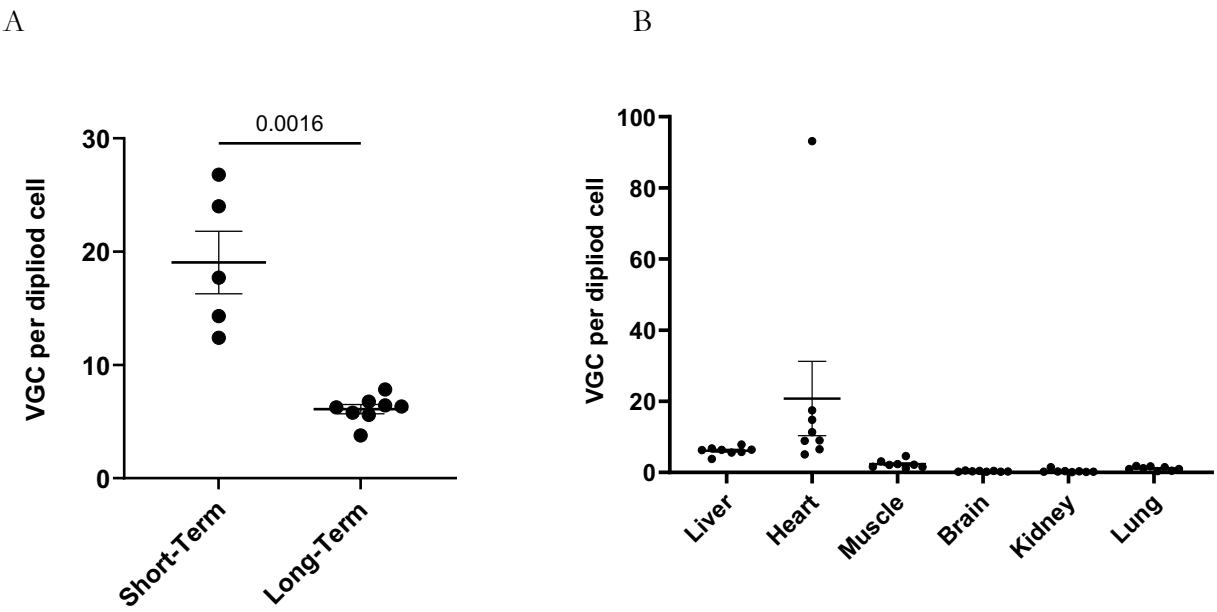

Figure 4-6 Vector Biodistribution following neonatal administration of rAAV2/8.APOE/hAAT.hDBT. (A) Hepatic tissue from the short-term cohort (n = 5, culled at day 7) demonstrated had significantly higher vector concentration than the long-term cohort (n = 8) ($p = 0.0016$). (B) Vector biodistribution across select tissues in the long-term cohort. Vector Biodistribution was determined with digital droplet PCR (ddPCR) Mann-Whitney test used to determine statistical analysis. Error bars represent standard error mean.

4.3.4 rAAV2/8.APOe-hAAT.DBT viral vector drives supraphysiological expression of human E2 protein across whole murine livers

DBT transgene expression was assessed in the long-term cohort via qPCR of cDNA generated from purified RNA transcripts in liver, brain, cardiac, renal, lung and skeletal muscle tissue (Figure 4-7). Hepatic tissue had the highest transgene RNA expression, and this was significantly more than cardiac, which was the second highest transgene expressing tissue. The lung demonstrated the lowest RNA expression, and this was significantly lower than liver.

E2 protein expression was also assessed using western blot across multiple tissues in the long-term cohort and in hepatic tissue in the short-term cohort (Figure 4-8). Hepatic E2 expression in vector-treated $DBT^{-/-}$ was approximately 7-fold higher than wildtype expression at 7 days post injection, as seen in the short-term cohort. However, over the following two weeks, hepatic E2 expression had reduced to near wildtype levels and all $DBT^{-/-}$ became unwell despite the E2 expression levels being equivalent to $DBT^{+/+}$. Extra-hepatic E2 protein expression in the long-term cohort was assessed in brain, kidney, heart and skeletal muscle (Figure 4-9). E2 expression was detected cross these extra-hepatic tissues, the most being in cardiac tissue, but only minimal amounts detected in brain, kidney and skeletal muscle.

Liver sections for the short-term and long-term cohort were stained for the E2 protein and co-stained with DAPI to highlight cell nuclei (Figure 4-10). At 7 days post transduction, immunofluorescence (IF) showed homogenous, widespread expression of E2 protein in hepatocytes. This reflects highly efficient hepatic transduction of the gene addition vector with approximately 90% of cells transduced in the vector treated $DBT^{-/-}$ pups at 7 days post vector administration. The IF pattern of E2 protein seen in the long-term cohort is more patchy and not as homogenous, reflective of the interval hepatocyte compartment expansion with subsequent AAV episomal loss and approximately 50% of cells strongly positive for E2 expression. The E2

protein brightness appeared to be more intense in the short-term treated DBT$^{-/-}$ cohort at 7 days compared to DBT$^{+/+}$ adults.

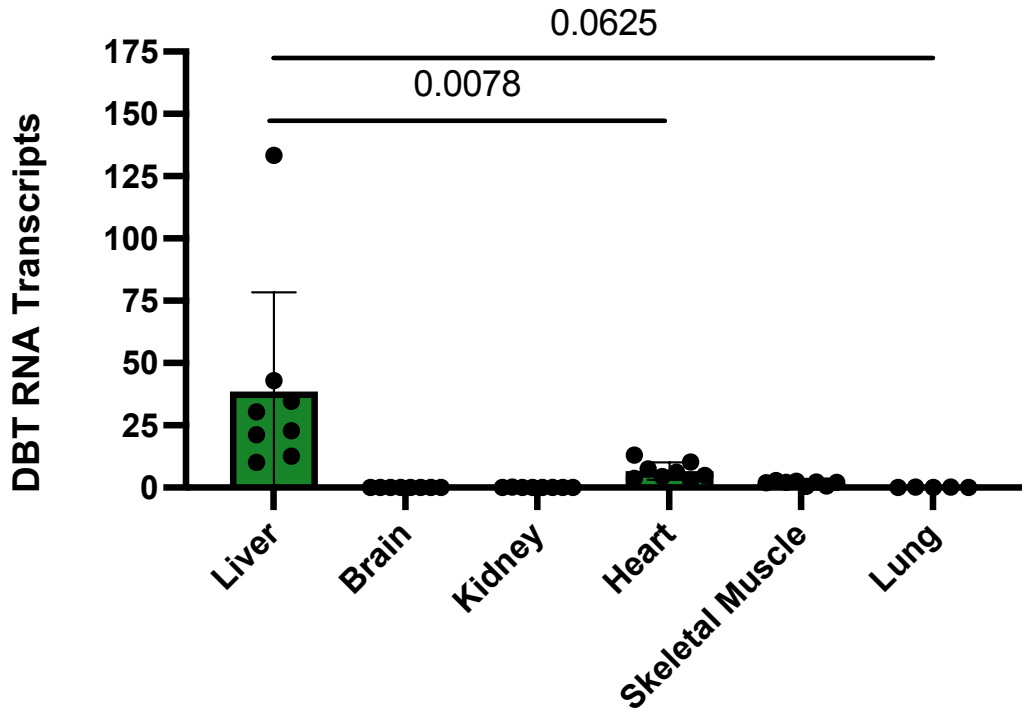

Figure 4-7 Transgene RNA transcripts quantified with qPCR. Signals were normalised to murine B-actin across liver, brain, kidney, heart, skeletal muscle and lung tissue in DBT$^{-/-}$ mice (n = 8) treated with rAAV8.APOe/hAAT.hDBT at 5x10^{11} VGC/pup on D0 of life via IP injection. Mann Witney test used to determine statistical significance.

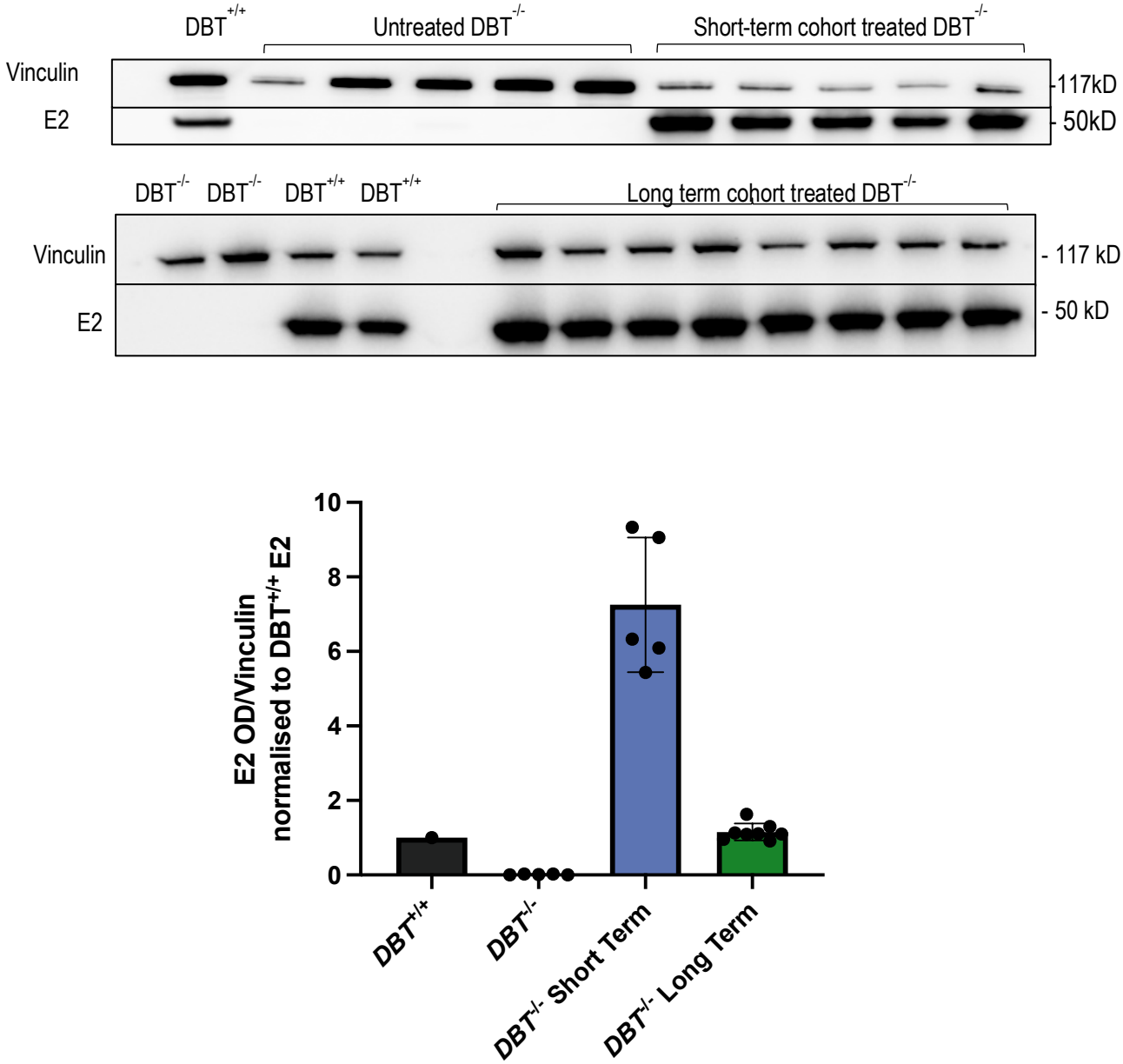

Figure 4-8 Hepatic E2 protein expression in vector treated in short- and long-term cohorts of DBT $^{-/-}$. Short-term cohort was culled at 7 days and long-term cohort mice used in this analysis (n = 8) lived for 18.6 days (± 1.9 SD). **(A)** Western blot of untreated neonate DBT$^{+/+}$ (n = 1) and DBT$^{-/-}$ (n = 5) with treated DBT$^{-/-}$ mice short-term (n = 5) and long term (n = 8) cohorts. **(B)** E2 protein expression was quantified with Image J, E2 signals were first normalised to vinculin optical density and then again to the E2/Vinculin OD of the average DBT$^{+/+}$ control signal in individual blots.

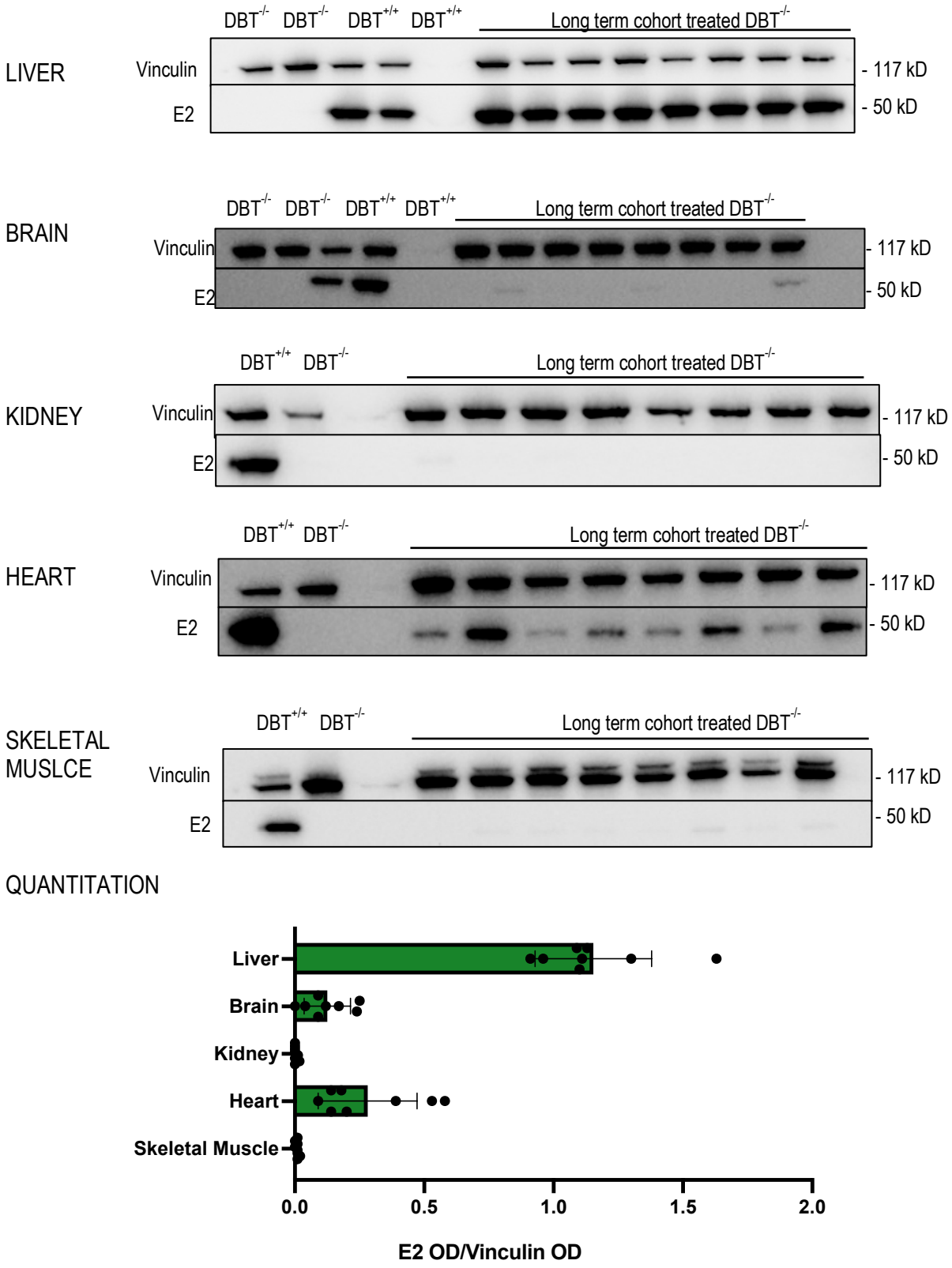

Figure 4-9 E2 protein expression in long-term cohort of vector treated DBT$^{-/-}$ mice. DBT$^{-/-}$ (n = 8) were treated with 5x10^{11} VC of rAAV8.APOe/hAAT.hDBT vector. E2 protein was assessed via western blot across various tissues (liver, brain, kidney, heart and skeletal muscle) and quantitated with Image J.

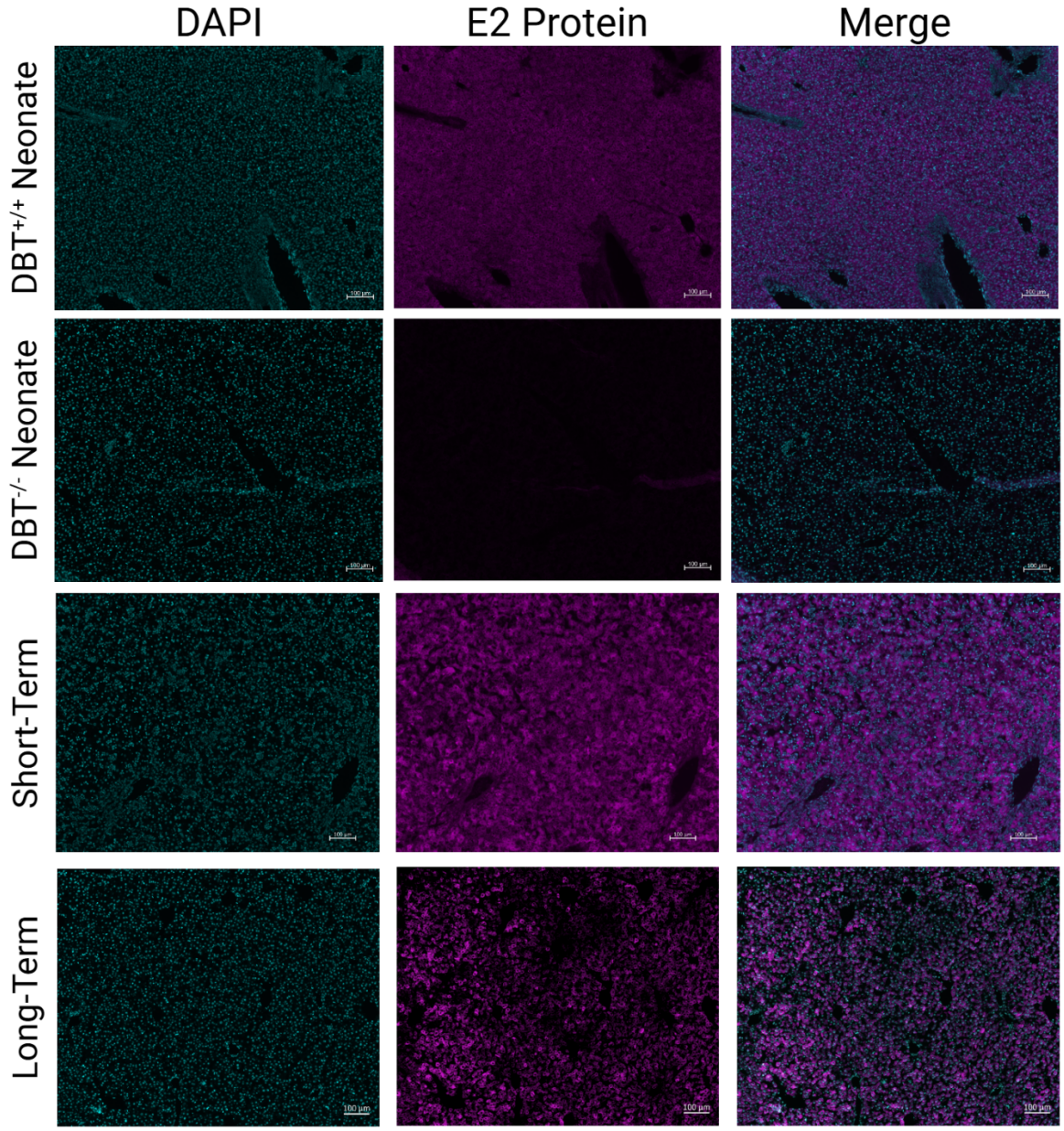

Figure 4-10 Representative Hepatic E2 protein immunofluorescence in vector treated DBT$^{-/-}$. Liver sections of pups treated with rAAV2/8.APOe/hAAT.hDBT vector in the short-term and long-term cohorts were probed for E2 protein (Polyclonal Anti-DBT (Rabbit) Invitrogen, Purple) and cell nuceli (DAPI, Blue). Magnification was 10x and scale bars 100 μm. Figure generated in BioRender.

4.3.5 Human E2 expression provides transient biochemical phenotype correction

Branched chain amino acid (BCAA) levels were assessed by using tandem mass spectrometry in dried blood samples taken at the point of euthanasia for both short-term and long-term cohorts of $DBT^{-/-}$ vector treated mice (Figure 4-11). At 7 days post IP injection of rAAV2/8.APOe/hAAT.hDBT, leucine and valine levels were significantly improved compared to untreated $DBT^{-/-}$ mice, however leucine levels were still significantly higher than levels in $DBT^{+/+}$ mice. The biochemical phenotype improvements seen at 7 days were not sustained in long-term cohort mice which lived past 15 days (n = 8). The BCAAs at death in the long-term cohort were higher than those seen in untreated $DBT^{-/-}$ with significant elevations in leucine and valine, but not isoleucine. L-alloisoleucine levels were measured at the same timepoints as BCAA (Fig 4-11). At 7-days post vector injection, L-alloisoleucine levels were significantly improved in vector treated $DBT^{-/-}$compared to untreated $DBT^{-/-}$ however still significantly higher than $DBT^{+/+}$. For the long-term cohort L-alloisoleucine levels has become significantly more elevated compared to treated $DBT^{-/-}$ at 7 days and equivalent to untreated $DBT^{-/-}$.

The average leucine:valine ratio in the vector treated $DBT^{-/-}$ pups was 0.07 at one week post treatment, however this had increased to an average of 1.13 in the long-term $DBT^{-/-}$ cohort, reflective of grossly disturbed total body BCKDH homeostasis in these mice. There was a positive association between hepatic VCN and hepatic E2 protein expression (Figure 4-12). Conversely, there was an inverse association between serum leucine levels and both hepatic VCN and E2 protein expression (Figures 4-13, 4-14).

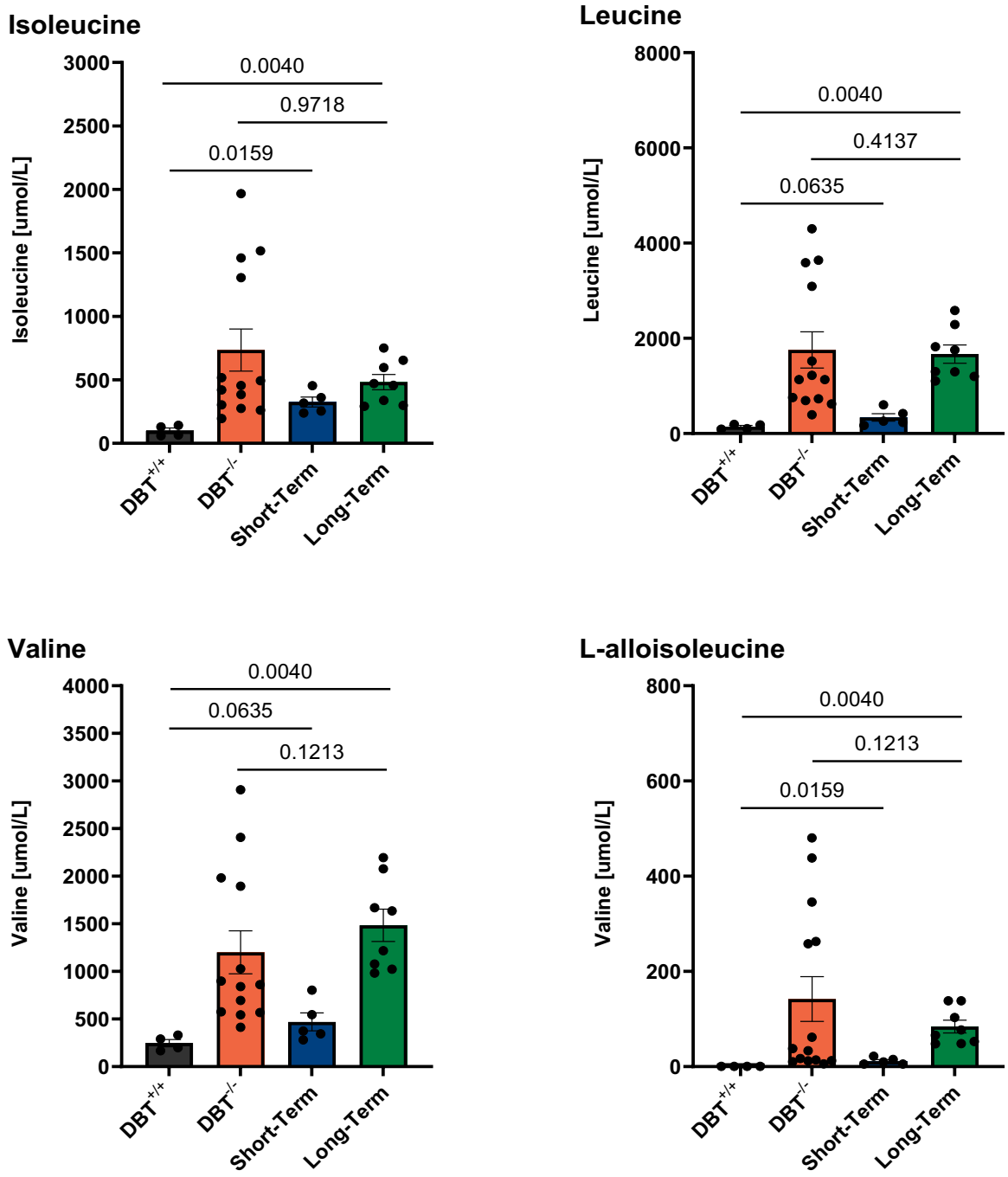

Figure 4-11 Branched Chain Amino Acid levels in rAAV8.APOe/hAAT.hDBT vector treated DBT$^{-/-}$. The DBT$^{-/-}$ short-term cohort (n = 5) was humanely euthanised at 7 days and blood collected at this time and DBT$^{-/-}$ long-term cohort (n = 8) had blood collected prior to humane euthanasia due to metabolic intoxication (average life span 18.6 days). Statistical significance was determined with Mann Witney two tailed test and error bars represent standard error mean.

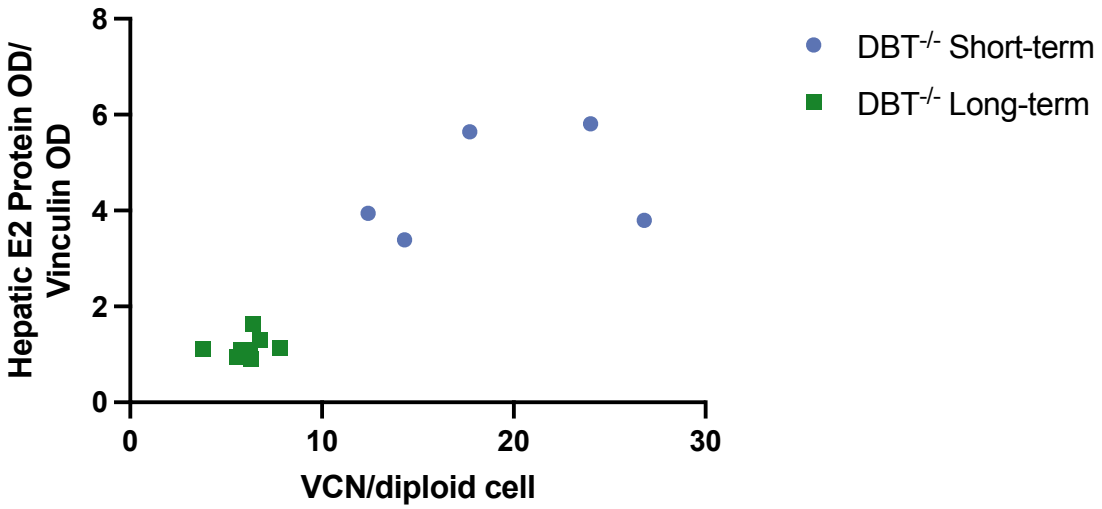

Figure 4-12 Hepatic vector copy number positively correlates with Hepatic E2 protein expression. Hepatic vector copy number was determined using digital droplet qPCR with transgene signals normalised to murine albumin. Hepatic E2 protein expression was determined with western blot probing for E2 protein with signals normalised to vinculin and quantitated with Image J.

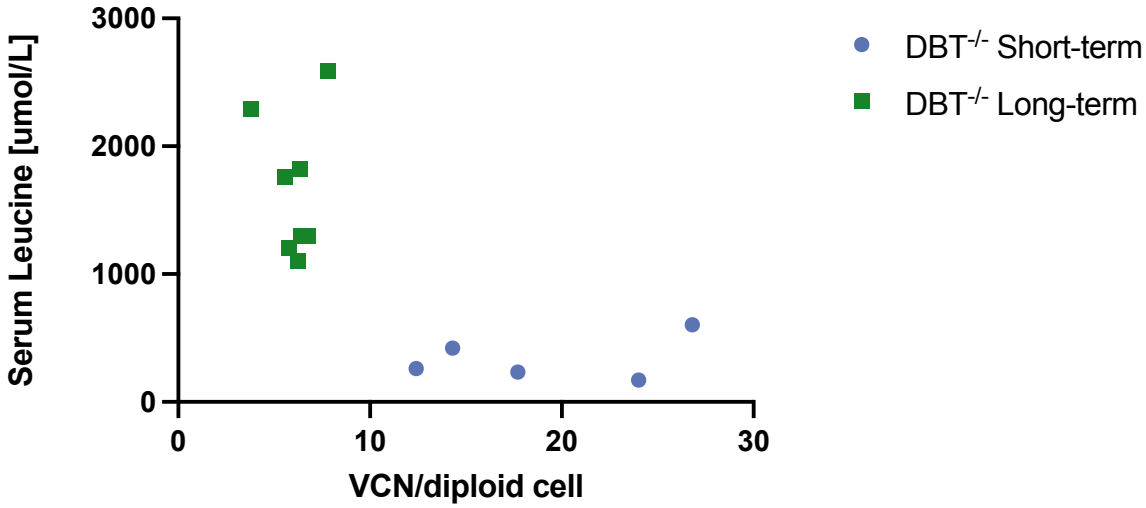

Figure 4-13 Serum leucine inversely proportional to hepatic vector copy number. Hepatic vector copy number was determined using digital droplet qPCR with transgene signals normalised to murine albumin. Serum leucine levels were determined using tandem mass spectrometery on blood samples taken during euthanasia of the short-term (n = 5) and long-term (n = 8) DBT$^{-/-}$ treated cohorts.

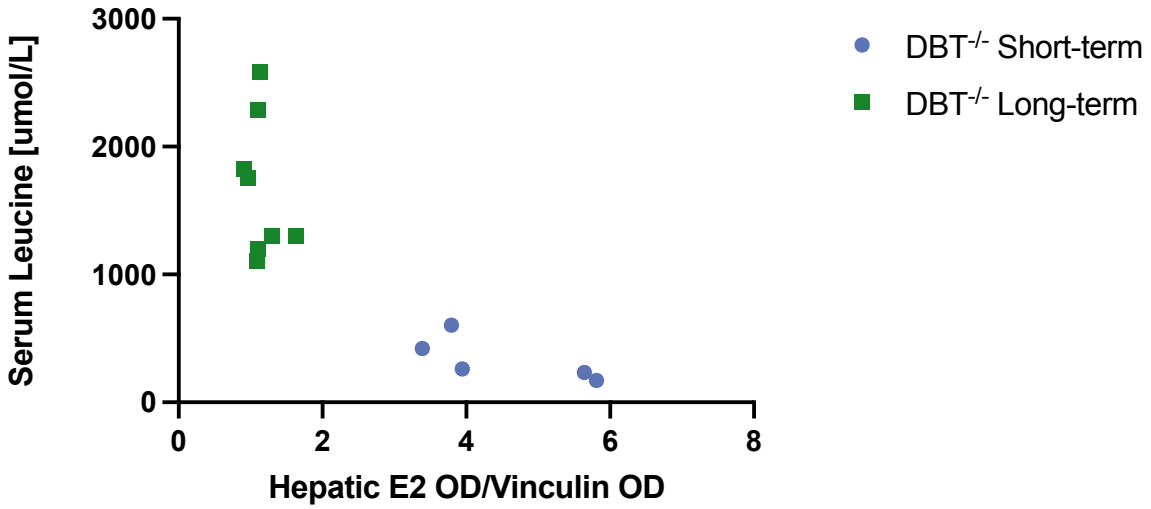

Figure 4-14 Serum leucine inversely proportional to hepatic E2 protein expression. Serum leucine levels were determined using tandem mass spectrometery on blood samples taken during euthanasia of the short-term (n = 5) and long-term (n = 8) DBT$^{-/-}$ treated cohorts Hepatic E2 protein expression was determined with western blot probing for E2 protein with signals normalised to vinculin and quantitated with Image J.

4.3.6 *In utero* gene therapy with gene addition did not confer survival advantage in DBT$^{-/-}$ model

In an attempt to improve the early phase rescue of DBT$^{-/-}$ pups, *in utero* IP injections of rAAV2/8.APOe/hAAT.hDBT were administered at high dose (5×10^{11} VGC/foetus) to 4 DBT$^{-/-}$ foetuses and at low dose (2.5×10^{11} VGC /foetus) to 1 DBT$^{-/-}$ foetus. Survival for all the *in utero* treated DBT$^{-/-}$ mice was limited to less than 10 days. Two of the high-dose treated DBT$^{-/-}$ were found to be still-born (Figure 4-15), one mouse treated with high dose was found dead on day 9 of life, another found dead on day 1. A single DBT$^{-/-}$ pup treated with low dose rAAV2/8.APOe/hAAT.hDBT became unwell requiring humane euthanasia on day 8. Overall survival rate of all *in utero* treated DBT$^{-/-}$ was not significantly different compared to untreated DBT$^{-/-}$. These precipitous deaths made biospecimen collection difficult and coupled with the small physical size of these DBT$^{-/-}$ mice resulted in insufficient tissue for all end point assays to be performed in each mouse, as outlined in Table 4-1. Furthermore, as parallel experiments described

in chapter 5 were proving successful in durable phenotypic rescue, *in utero* gene addition was not pursued further than these data below.

Table 4-1 End point assays performed on *In utero* vector treated DBT$^{-/-}$

Mouse	*In Utero* Vector Dose	Tissue status	BCAA	VGC	RNA	Western Blot	IF
V100	High 5×10^{11} VGC	Harvested post mortem on P9	No	No	No	Yes	No
V114	Low 2.5×10^{11} VGC	Harvested at euthanasia on P8	Yes	Yes	No	No	Yes

All *in utero* treated DBT$^{-/-}$ mice exhibited growth failure over the first week of life (Figure 4-16). Hepatic vector copy number determined by ddPCR was similar to that seen in the long-term cohort around (Figure 4-17). The branched chain amino acid levels collected from the low dose mouse treated with *in utero* low dose vector were all at levels similar to untreated DBT$^{-/-}$ (Figure 4-18). There was minimal hepatic E2 expression detected on western blot analysis (Figure 4-19) with similarly minimal levels of hepatic E2 seen with immunofluorescence on frozen liver sections (Figure 4-20).

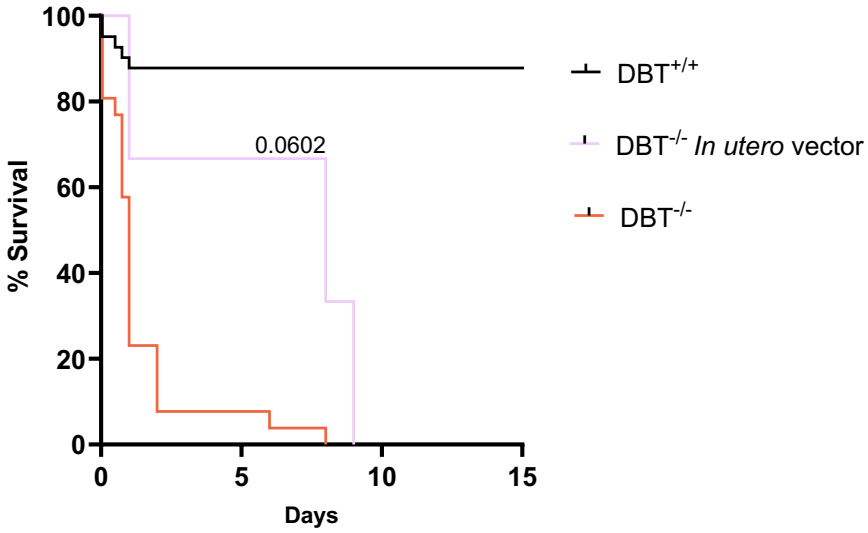

Figure 4-15 Survival in DBT$^{-/-}$ mice treated with *in utero* rAAV8.APOe/hAAT.hDBT. DBT$^{-/-}$ pups were injected at embryonal day 15 with the gene addition rAAV8.APOe/hAAT.hDBT a high dose (5x10^{11} VGC transposon/foetus) or low dose (2.5x10^{11} VGC/foetus). Survival statistical analysis with Wilcoxon test and *p* values displayed on curves compare vector treated DBT$^{-/-}$ to untreated DBT$^{-/-}$.

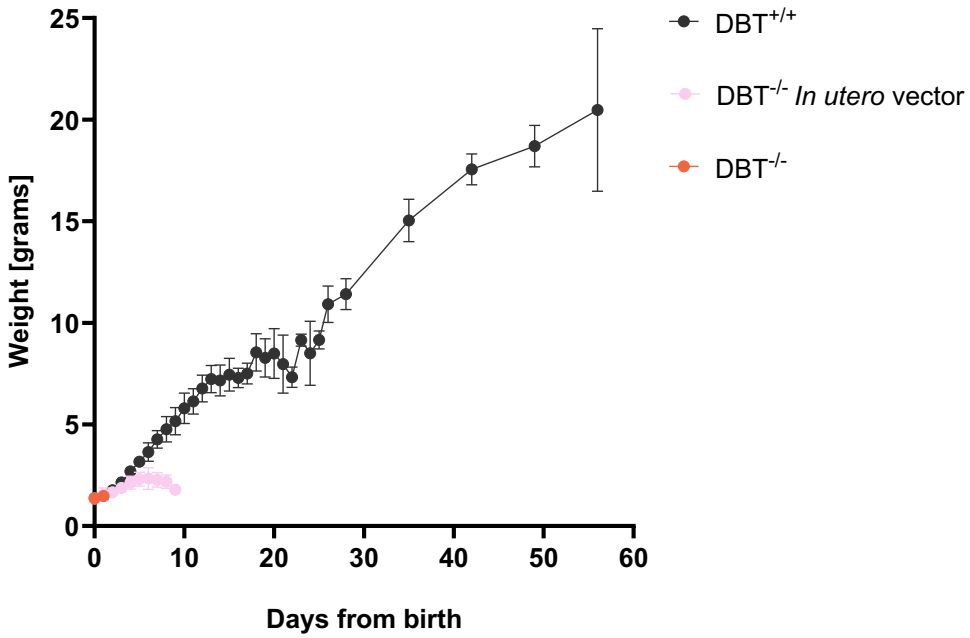

Figure 4-16 Post-natal growth in DBT$^{-/-}$ mice treated with *in utero* AAV Gene Addition vector. DBT$^{-/-}$ pups were injected at embryonal day 15 with the gene addition rAAV8.APOe/hAAT.hDBT a high dose (5x10^{11} VGC transposon/foetus) or low dose (2.5x10^{11} VGC/foetus). Growth curve represents data combined from both high and low dose vector treated mice.

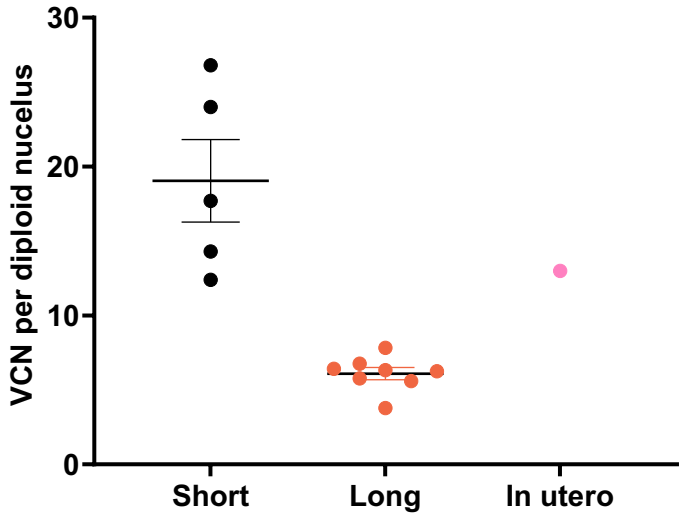

Figure 4-17 Hepatic vector copy number in DBT$^{-/-}$ mouse treated with *in utero* AAV Gene Addition vector. DBT$^{-/-}$ pup was injected at embryonal day 15 with the gene addition rAAV8.APOe/hAAT.hDBT at the low dose (2.5x10^{11} VGC/foetus). Short (short-term cohort treated DBT$^{-/-}$), Long (long-term cohort treated DBT$^{-/-}$) hepatic vector copy number (VCN) data presented previously in figure 4-6(A). Error bars represent SEM.

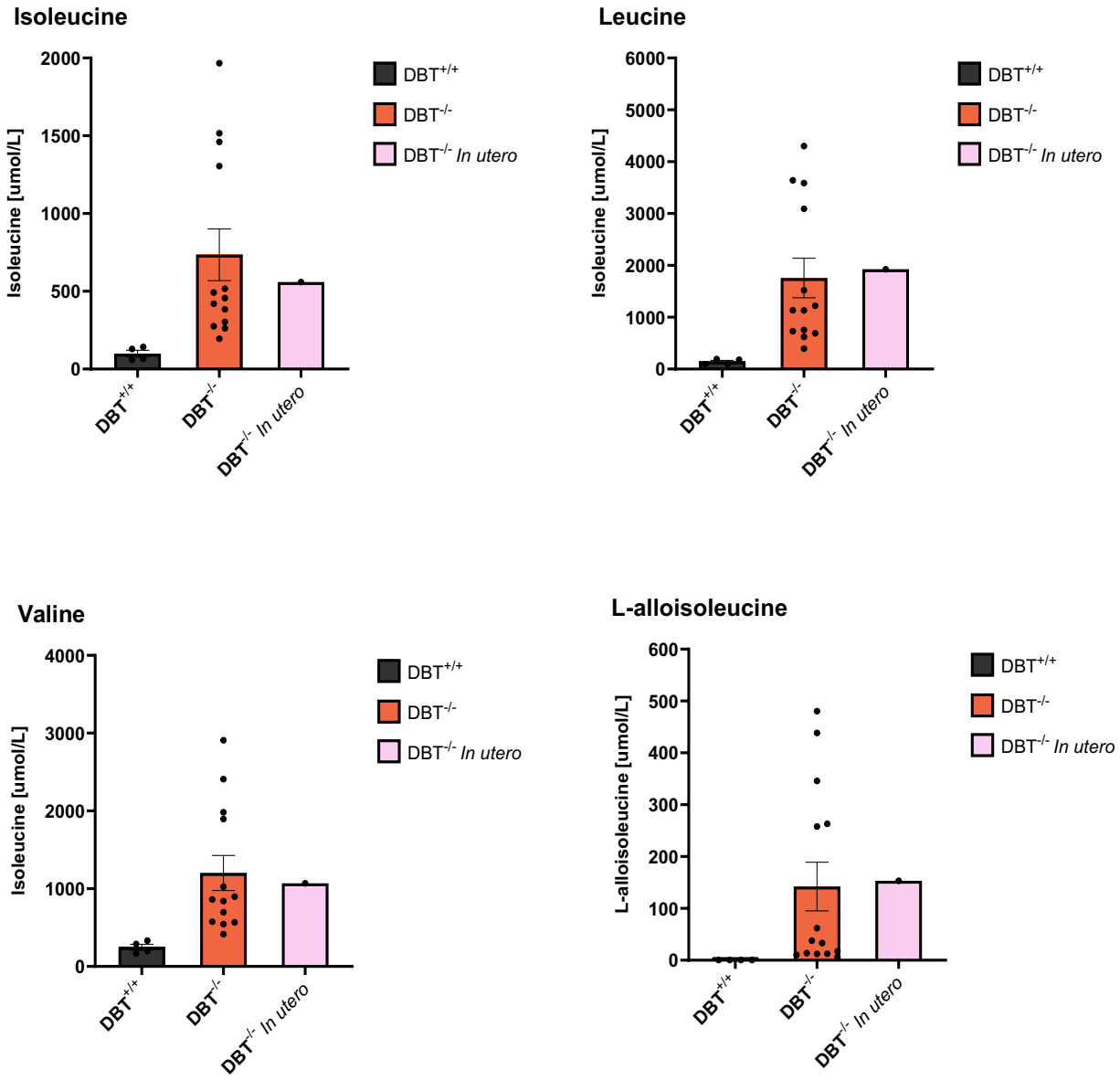

Figure 4-18 Serum branched chain amino acids in DBT$^{-/-}$ treated with *in utero* AAV Gene Addition vector. DBT$^{-/-}$ *In utero* (n = 1) was injected at embryonal day 15 with the gene addition rAAV8.APOe/hAAT.hDBT a low dose (2.5x10^{11} VGC/foetus). Serum levels of leucine and L-alloisoleucine were assayed with tandem mass spectrometry. Error bars represent standard error mean.

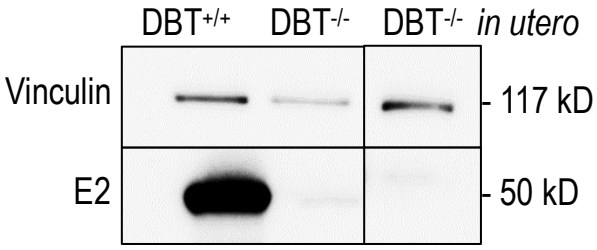

Figure 4-19 E2 protein expression in DBT$^{-/-}$ treated with *in utero* AAV Gene Addition vector. DBT$^{-/-}$ *In utero* (n = 1) was injected at embryonal day 15 with the gene addition rAAV8.APOe/hAAT.hDBT a high dose (5x10^{11} VGC/foetus). Samples all imaged on same western blot, but membranes cut for clarity.

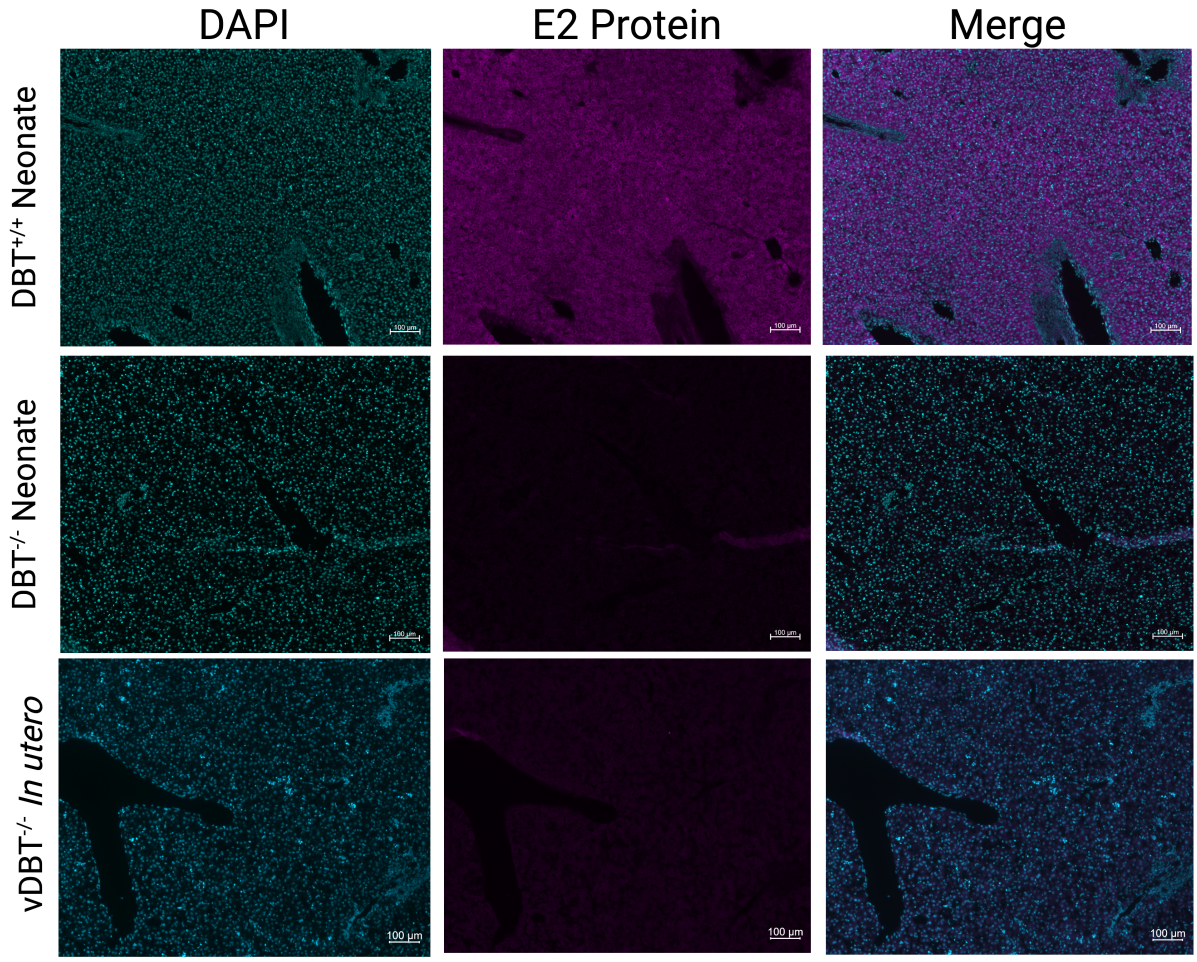

Figure 4-20 Hepatic E2 Immunofluorescence of DBT$^{-/-}$ treated with *in utero* AAV Gene Addition vector. DBT$^{-/-}$ (n = 1) in this image was injected at embryonal day 15 with the gene addition rAAV8.APOe/hAAT.hDBT a low dose (5x10^{11} VGC/foetus). Liver sections were fixed in 4% paraformaldehyde and sectioned at 5 µm before staining cell nuclei with DAPI (blue) and E2 protein (purple). All images taken at 10x magnification and scale bars represent 100 µm. Figure generated in BioRender.

4.4 Discussion

4.4.1 rAAV2/8.APOe/hAAT.hDBT provides transient rescue of DBT-deficient pups

Neonatal administration of a murine liver trophic vector rAAV2/8.APOe/hAAT.hDBT provided transient phenotypic rescue of the $DBT^{-/-}$ MSUD mouse model. In this neonatal lethal model, the DBT-deficient phenotype was significantly improved at one week post vector injection across all biological endpoint measures of survival, growth, E2 protein production and BCAA levels compared to untreated $DBT^{-/-}$. However, the vector effect waned after two weeks with universal growth failure, BCAA levels equivalent to untreated homozygous knockouts and metabolic intoxication necessitating euthanasia.

The non-enduring nature of a neonatally administered, liver-targeted. gene addition vector has been observed in other neonatal lethal metabolic conditions with a loss of vector effect around 21 days of age [391]. This loss of effect was most likely secondary to gradual clearance of episomal vector in cells undergoing mitotic divisions during organ growth [401]. The liver undergoes dramatic growth and development in the neonatal period, and as such hepatocytes transduced with vector at birth, can lose episomal vectors during each cell division, thereby diminishing the therapeutic effect [341]. This episomal loss likely explains the significant 3-fold reduction of vector genomes per diploid cell in liver tissue between the short and long-term cohorts, as well as the proportional reduction in hepatic E2 protein expression over the same time frame. The changes in E2 detected via immunofluorescence in hepatocytes also reflects this episomal loss. Sections from livers in the short-term cohort, showed a homogenous, bright signal pattern of E2 protein expression whereas liver sections of mice injected at birth and sacrificed between 14-21 days, E2 protein distribution was less uniform. This changing pattern is most likely reflective of vector loss and reduction from nearly 100% of hepatocytes producing E2 protein to approximately 50%.

4.4.2 Insights into the hepatic phenotype correction threshold in the DBT$^{-/-}$ MSUD Model

The loss of phenotypic correction observed between the short-term and long-term cohort of DBT$^{-/-}$ mice provides insight into a potential hepatic correction threshold in the DBT$^{-/-}$ murine model. Western blot demonstrated DBT$^{-/-}$ treated mice had hepatic E2 protein levels 6-fold higher than wildtype and widespread hepatocyte transduction with E2 expression detected in over 90% of hepatocytes on immunofluorescence. In the time intervening between the short-term cohort and the metabolic intoxication of the long-term cohort, hepatic E2 levels had reduced to approximately those of wildtype and the E2 protein expression seen on immunofluorescence was more heterogenous with around 50% of cells positive for E2 protein expression. Together, these observations demonstrate that physiological levels of human E2 protein expression in the DBT$^{-/-}$ liver alone, does not provide sufficient BCKDH activity to meet total body metabolic demand during weeks 2-4 of life. Weaning may have also increased the metabolic stress in the DBT$^{-/-}$ mice as the protein concentration is 12% (w/v) in C57Bl/6J breastmilk compared to 21% (w/w) protein in standard chow. This may have placed additional metabolic demands and pressures on these juvenile mice during early growth and development in the first 3 weeks of life [405, 406].

There also seemed to be a potential phenotypic correction threshold pattern emerge around 10 vector genomes per diploid cell in liver tissue. In the short-term cohort, vector genomes in the liver ranged from 12.4 to 26.8 VGC/diploid cell with no convincing correlation between the serum leucine level and tissue vector concentration. This may reflect a ceiling of correction able to be affected by the rAAV8.APOe/hAAT.hDBT vector. It may also reflect delivery of non-functioning or partial transgene cassette or alternatively transgene toxicity with excessive DBT. There was also correlation between E2 protein expression and serum leucine levels suggesting that when E2 protein expression was less than 2 times the levels seen in wildtype mice, metabolic intoxication occurs.

4.4.3 Timing of metabolic intoxication may offer insight into dynamic metabolic pressures in developing DBT$^{-/-}$ neonates

The timing at which the DBT$^{-/-}$ mice became unwell may reflect an increased metabolic demand experienced during weaning and transitioning to chow may have placed additional physiological pressures on the DBT$^{-/-}$ pups and accelerated the point at which tissue demands exceeded residual BCKDH activity provided by the vector transgene. It was interesting, however that in studies published by Pontoizeau *et al.* investigating AAV gene therapy in the BCKDHA and BCKDHB murine MSUD models, single dosing with a gene addition vector in the neonatal period conferred a durable phenotypic rescue. These studies compared AAV gene addition vectors with both liver specific and ubiquitous promoters, with the ubiquitous promoter out-performing the liver specific promoter. It is likely that the ubiquitous promoter allowed for extra-hepatic expression in transduced tissues an approach which has been used in other in born errors of metabolism, including methylmalonic acidaemia [407].

However published studies exploring single-dose neonatally administered gene addition in other MSUD murine models BCKDHA$^{-/-}$ and BCKDHB$^{-/-}$ with the same AAV capsid (AAV8) and equivalent enhancer promoter (APOe/hAAT) used in our study had an enduring effect on survival with rescue to adulthood in the treated homozygous knockout pups. The major difference in these vectors however these vectors was the presence of a WPRE element, absent in the vector used in this chapter, rAAV2/8.APOe/hAAT.hDBT. In the same studies, additional vectors were also tested in parallel, with corresponding transgenes under the transcriptional regulation of a ubiquitous E1Fa promoter. These vectors outperformed the liver targeted vectors across all measured parameters, suggesting that extra-hepatic transgene expression may be necessary to overcome the increased metabolic demands occurring during weaning and development.

4.4.4 Limited extra-hepatic contribution of rAAV2/8.APOe/hAAT.hDBT in phenotype rescue

This vector was designed to be liver specific, and our data confirm that the phenotype correction was largely due to E2 expression in liver. Interestingly, in the tissues assessed for vector genome copies, the rAAV2/8.APOe/hAAT.hDBT vector was seen to have the highest vector concentration in cardiac tissue and with liver tissue second highest, whereas RNA transcripts and E2 protein expression was highest in liver. AAV8 is known to transduce murine cardiac tissue and has been detected at stable vector copy numbers after neonatal injection over 16 weeks in heart tissue in both murine and canine pre-clinical studies [408, 409]. Whilst we did not measure the VCN in extra-hepatic tissues for the 7-day cohort, cardiac, skeletal muscle and central nervous system tissues are mostly post-mitotic and do not undergo the rapid growth seen in hepatic tissues [410]. The apparent difference in targeting between the heart and liver is at least in part explained by the difference in mitotic activity between these two tissue types. Episomal vector loss in tissues with high rates of mitosis, like juvenile mouse livers is well reported and after neonatal vector administration, dramatic reductions in vector copy number occur over just the first week of life [341]. Thus, at the time of sacrifice for the long-term cohort, which occurred when the mice became unwell after entering the second week of life, there has been episomal loss in the liver, but this would not have occurred in the cardiac tissue thus accounting for the apparent higher rates of transduction in cardiac tissue compared to hepatic tissue in the long-term cohort.

Furthermore, it is difficult to compare RNA transcripts between tissues, as these signals require normalisation by housekeeping genes which can have variable expression across different tissues. Murine β-actin was chosen as it has the most consistent levels of expression across the tissues of interest [411], and the RNA levels largely mirrored the E2 protein expression found on western blot analysis, further supporting this. The RNA and protein expression profiles support the selectivity of APOe/hAAT enhancer-promoter to predominantly facilitate hepatic transcription

and that the liver was the dominant tissue in which the rAAV28.APOe/hAAT.hDBT vector exerted an effect.

4.4.5 Bi-modal survival pattern reflects limitations of AAV vector onset of action in neonatal lethal model

With regards to the delivery route and timing of treatment, neonatal IP injection was effective in improving $DBT^{-/-}$ survival rates, however there was a subset of treated $DBT^{-/-}$ mice that still perished rapidly. In both the short-term and long-term cohorts, there appeared to be two distinct survival patterns, where $DBT^{-/-}$ mice either died within 48 hours or lived beyond this time point to the experimental endpoint. Whilst every attempt was made to inject neonates as close to birth as possible, the exact time between delivery and vector injection was unable to be accounted for. In addition, the time required for rAAV8.APOe/hAAT.hDBT to transduce target tissues, which then must be trafficked to the nucleus, undergo uncoating and then the cassette transcribed, translated and transported into mitochondria, and begin metabolising BCAA in an assembled BCKDH complex, is not known. It is possible that neonatal delivery may not be sufficiently early to rescue all $DBT^{-/-}$ pups and *in utero* transgene delivery may be required to address this variable of time of vector administration.

There is precedence of *in utero* administration of liver targeted gene addition vectors successfully rescuing other neonatal lethal metabolic murine models [346], however i*n utero* administration of rAAV2/8.APOe/hAAT.hDBT, described herein, did not confer equivalent survival rates in the $DBT^{-/-}$ MSUD model. Whilst vector genomes were still detectable in liver tissue, RNA expression and E2 protein expression was below the limit of detection. This may have been due to the clearance of vector episomes with the rapid *in utero* and post-natal growth and development of the liver. There also may have simply not been enough vector given and higher doses may be required. Conversely, it is possible that there may have been some cellular toxicity associated with *in utero*

vector exposure, exerting negative selection pressure on transduced cells, which may also have accounted for the low vector copy number in liver tissue. The sample size for the *in utero* gene addition experiments was also limited, and it is possible that unaccounted for technical and biological reasons may have influenced the failure of these experiments, including failed injections outside the foetal peritoneum, excessive maternal stress or vector irregularities. These experiments were not pursued further as parallel experiments, described in chapter 5 were proving successful in durable phenotypic rescue.

4.4.6 Overcoming AAV Episome Loss in tissues with high rates of mitosis

These data demonstrate that liver targeted simple gene addition with a human DBT transgene expressed under an APOe/hAAT enhancer promoter can rescue a neonatal lethal model of MSUD, however this effect is transient due to progressive loss of episomal vector genomes. Potential ways to overcome this episome loss could be to use an integrating strategy, such as piggyBac Transposase or editing nucleases like Cas9 with template repair [241, 248]. Multiple dosing strategies may also work, however AAV neutralising antibody development post vector injection is common and risks the efficacy of any subsequent doses using the same or similar AAV capsid serotype [412].

In summary, these results demonstrate that a liver targeted AAV vector can rescue a neonatal lethal $DBT^{-/-}$ model, albeit a non-enduring rescue. The loss of phenotypic correction was most likely due to hepatic episome loss in a growing organ and the residual vector and human E2 protein produced incommensurate to total body BCKDH requirements during a physiological period of high demand during growth and weaning. Exploration of integrating strategies, such as piggyBac transposase or gene editing is necessary to improve the durability of a liver targeted gene therapy rescue for the MSUD $DBT^{-/-}$ neonatal lethal knockout model.

Chapter 5

Gene addition with a hybrid AAV/*piggyBac* transposase system in a neonatal lethal DBT$^{-/-}$ MSUD model

5.1 Introduction

Paediatric patients with MSUD have the most to gain AAV gene therapies with enduring effects. For a liver-directed gene therapy to have maximum utility in this patient group it must provide stable gene transfer in an organ that undergoes significant growth across childhood, most notably in infancy, and then to adulthood and beyond. This is a major challenge for conventional, predominantly non-integrating AAV gene therapy vectors which predominate as episomes in transduced cells. Technologies developed to overcome AAV episome loss include either multiple dosing strategies which are fraught with immune-mediated vector neutralisation or genomic editing tools including user-targeted endonucleases such as Cas9 [413], prime editors [414], base editors [415] or through the use of transposable elements including *piggyBac* transposase [241].

Hybrid AAV/*piggyBac* vectors have been used to effectively integrate transgene cassettes into host cells thereby achieving stable transduction and disease rescue in tissues including juvenile livers in pre-clinical studies [274, 275]. Due to the packaging limitations of AAV, the *piggyBac* transposase gene requires packaging into a separate AAV vector to the transgene being "inserted". Therapies that require dual vector transduction are inherently more complex than single vector strategies, however *piggyBac* transposase does not leave an excision footprint nor exhibits over-expression inhibition like Sleeping Beauty transposase systems [416]. Whilst the dual vector system and less

specific integration pattern of *piggyBac* [417] represent relative downsides in this platform, dual AAV vector cassettes are also often mandated due to cassette size in other more precisely integrating strategies. Furthermore, genomic editing technologies, such as Cas9 and other endonucleases lauded for the precision with which they achieve stable genomic effects have complexities which are still being characterised. In order to edit a locus like *DBT* in MSUD with an endonuclease like Cas9, two AAV vectors are required to deliver the Cas9 nuclease and template repair guides strands with successful co-transduction of a target cell required for any effect to take place [418]. Also, target tissue editing rates seen with Cas9 vary depending on the type of editing strategy used and stage of the cell cycle the target tissue is in, and *in vivo* can vary from 1-30% [419, 420]. Cas9 is also a bacterial protein with the potential to cause an immune response in treated individuals [421]. Furthermore, the insertional mutagenesis risks of Cas9 vectors are of growing concern with off target integrations, large on target deletions [422] and concatemeric insertions reported raising concerns over the oncogenic risk profile as well potentially affecting residual target gene function [255].

Liver targeted gene addition using a hybrid AAV/*piggyBac* system for MSUD represents a novel strategy with the potential to improve the stability of transgene expression in a neonatal tissue with high rates of mitotic growth whilst circumventing some of the less desirable side effects of editing approaches addressed above. This chapter describes the rational design of a liver targeted hybrid gene addition vector (transposon vector) compatible for transposition with a vector encoding *piggyBac* Transposase (transposase vector). These vectors were tested in the $DBT^{-/-}$ murine model with an accompanying investigation into dose titration and the vector elements that confer tissue expression and specificity.

The results in this chapter explore hypothesis 3 and 4 and aim 3 and 4 (see Chapter 1.6).

5.2 Chapter 5 materials and methods

5.2.1 Construction of *piggyBac* transposon expression plasmid encoding the human DBT cDNA

The coding sequence of human cDBT was amplified via PCR from pAAV2.APOe/hAAT.hDBT generated in section Chapter 4.2.1 using NEB HiFi primers (km080 5' CCCCCGGGCTGCAGGAATTCGCGGCCGCTCTAGAGC 3', T_m 77°C) and km081 (5' TCCAGAGGTTGATTATCGATAAGCTTGAATTCATCGATGTCGACTCATTTCAGATC TAGT 3', T_m 65°C), products separated by gel electrophoresis and purified by Wizard SV Gel and PCR Clean-Up system as per manufactures instructions (Promega). The hDBT fragment was then subcloned using HiFi Assembly (New England Biolabs) into an AAV/*piggyBac* transposon expression plasmid (pAAV2.APOe/hAAT.eGFP.WPRE.pBTIR) which contained AAV2 ITRs and *piggyBac* transposase inverted repeats (TIRs) as recognition sites for *piggyBac* transposase-mediated excision. Chemically competent DH5α *E. coli* cells were transformed with the ligation products and cells cultured at 37°C for 1 hour, plated on LB-Ampicillin and incubated at 37°C overnight. Colonies were then selected, grown for 18 hours, purified with Mini-prep Plasmid purification Kit (Bioline) as per manufactures instructions and sequence confirmation undertaken via Sanger sequencing at AGRF (Westmead Institute of Medical Research, Australia). The resultant plasmid was designated pAAV2.APOe/hAAT.hDBT.WPRE.pBTIR and the cloning history documented (Figure 5-1). This plasmid was then used to make the transposon vector rAAV2/8.APOe/hAAT.hDBT.WPRE.pbTIR as per the methods described in Chapter 2.2.5. The transposase vector plasmid encoding the *piggyBac* transposase enzyme sequence was donated by Dr Sharon Cunningham, with thanks, and packaged into the AAV8 capsid as per the methods in Chapter 2.2.5. The AAV8 serotype selected for the high murine tropism and was used for all vectors made in this Chapter. Components included in each vector in Chapter 5 can be found in Appendix C, page 271.

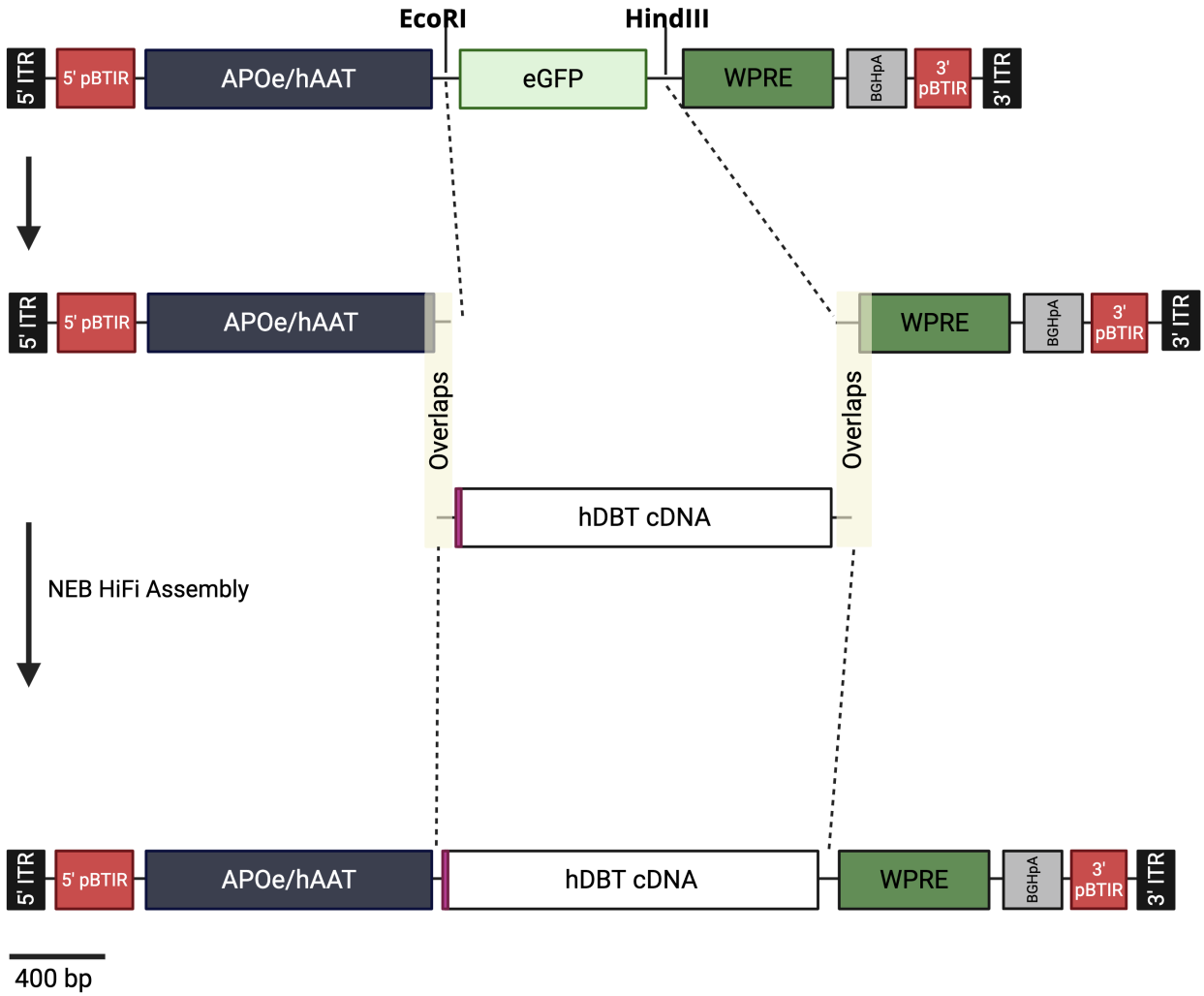

Figure 5-1 Cloning history of pAAV2.APOe/hAAT.hDBT.WPRE.pBTIR. Detailed explanation of subcloning using NEB HiFi assembly is described in Section 5.2.1. The expression cassettes are flanked by AAV ITRs (black boxes). Digest sites are marked with corresponding restriction enzymes. Other DNA components illustrated are the APOe/hAAT enhancer/promoter, human *DBT* coding sequence, hDBT cDNA (white box) and bovine growth hormone polyadenylation signal, BGHpA (light grey boxes), pBTIRs (red boxes) and Kozak consensus sequence (magenta box). Regions of sequence overlap between the backbone and insert generated by PCR with km080 and km081 are designated with light yellow highlighting. Scale bar = 400 bp. Figure generated in BioRender.

5.2.2 Generation of vectors to explore the effects of the WPRE and pBTIR elements on tissue expression

Vectors were designed to explore the effect of *piggyBac* transposase inverted repeats (pBTIR), and woodchuck hepatitis protein regulatory element (WPRE) on the hDBT transgene tissue expression profile. These new AAV expression cassettes were designed *in silico* to be the same as the AAV *piggyBac* transposon hDBT expression plasmid, pAAV2.APOe/hAAT.hDBT.WPRE.pBTIR (Figure 5-1) with or without the pBTIR or the WPRE elements (Figure 5-2). These AAV expression plasmids were designated pAAV2.APOe/hAAT.hDBT.WPRE, pAAV2.APOe/hAAT.hDBT.pBTIR and the results from the rAAV8.APOe/hAAT.hDBT gene addition experiments used as a historical control for both the pBTIR and WPRE elements. These expression cassettes were designed *in silico* using SnapGene, synthesised externally by GenScript and were then subcloned into the backbone of pAAV2.APOe/hAAT.eGFP.pBTIR via restriction digest to completely remove of the eGFP expression cassette and pbTIRs. New vector inserts were ligated with T4 DNA ligase (New England Biolabs), transformed into Dh5α cells, colonies grown and screened with mini-prep and sequenced confirmed with sanger sequencing (AGRF, Westmead Institute of Medical Research, Australia).

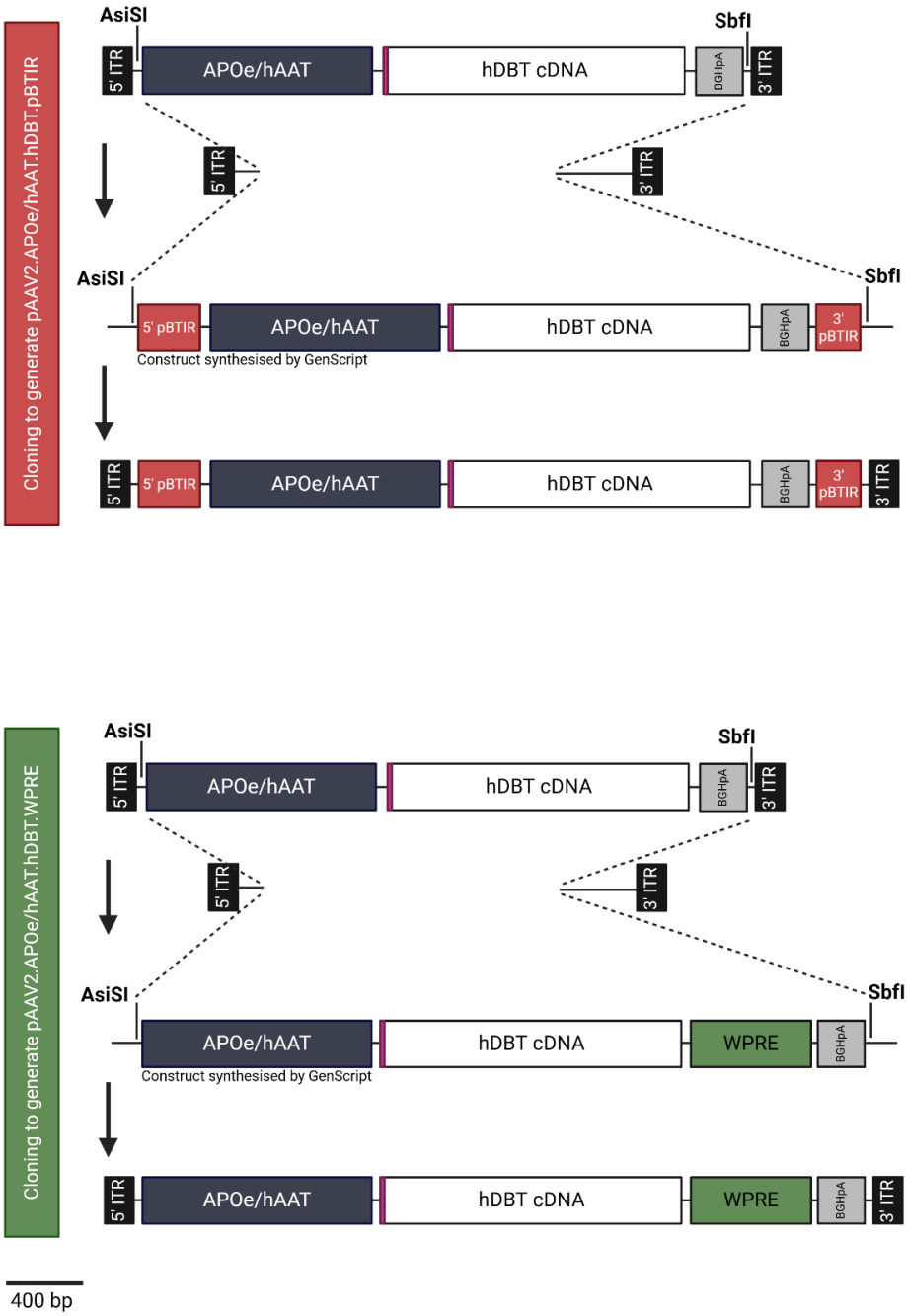

Figure 5-2 Cloning history of pAAV2.APOe/hAAT.hDBT.pBTIR and pAAV2.APOe/hAAT.hDBT.WPRE. Detailed explanation of subcloning is described in Section 5.2.2. The expression cassettes are flanked by AAV ITRs (black boxes). Digest sites are marked with corresponding restriction enzymes. Other DNA components illustrated are the APOe/hAAT enhancer/promoter, human *DBT* coding sequence, hDBT cDNA (white box) and bovine growth hormone polyadenylation signal, BGHpA (light grey boxes), pBTIRs (red boxes) and Kozak consensus sequence (magenta box). Regions of sequence overlap generated by PCR with km080 and km081 are designated with light yellow highlighting. Scale bar = 400 bp. Figure generated in BioRender.

5.2.3 *In vitro* validation of transposon vectors in Huh7 cells

Transposon vector constructs were functionally validated in Huh7 cells lines. Hybrid AAV/*piggyBac* vectors were generated through triple transfection of HEK293 cells with plasmids carrying either the eGFP transgene (pAAV2.APOe/hAAT.eGFP.WPRE.pBTIR) or the hDBT transgene (pAAV2.APOe/hAAT.hDBT.WPRE.pBTIR), DJ capsid [216] and pAd5 to generate two viral vectors rAAV2/DJ.APOe/hAAT.eGFP.WPRE.pBTIR and rAAV2/DJ.APOe/hAAT.hDBT.WPRE.pBTIR. Theses vectors were prepared as per the methods in Chapter 2.2.5 however were used in the crude formulation for cell application and VG quantitated prior from whole non-purified virus.

Huh7 cells were transduced with the crude preparations at 10,000 vector genome copies (VGC) per cell of a transposon vector carrying a hDBT or enhanced GFP (eGFP) transgene, with or without 5000 VGC of transposon vector in 6 well tissue culture plates (Corning). On Day 1 Huh7 cells were seeded at a density of 3.75×10^5 cells on day 1 in DMEM + 10% (v/v) foetal calf serum. Huh7 cells were then transduced on Day 2, media changed on Day 3 and then passaged 1:10 (cells to new media) every 4-5 days for a total of 3 passages to remove any non-transduced vector. Cells were harvested 15 days after initial transduction. Cells transduced with the eGFP encoding transposon vector were assessed for eGFP expression by flow cytometry and cells transduced with the hDBT encoding transposon vector had RNA transcripts and E2 protein expression levels measured using qRT-PCR and western blot analysis, respectively.

5.2.4 Neonatal Hybrid AAV/*piggyBac* gene addition experiments

For the experiments using hybrid AAV/*piggyBac* transposon vectors, whole litters of mice were given IP injections as close to birth as possible on post-natal day 0 with either a high dose (5×10^{11} VGC/pup) or low dose (5×10^{10} VGC/pup) of the transposon vector rAAV2/8.hDBT.WPRE.pbTIR with or without the *piggyBac* transposase vector. The *piggyBac*

transposase vectors were administered at were one tenth of the dose used for the transposon encoding vectors such that 5×10^{10} VGC transposase was used with high dose transposon and 5×10^{9} VCG of transposase used with low dose transposon. Total injection volumes were 10 μL/pup. All vector treated $DBT^{-/-}$ mice were weighed daily for the first 21 days of life and weekly thereafter. If mice displayed any features of metabolic intoxication after 21 days of life, daily weighs were reinstituted as part of close monitoring. $DBT^{+/+}$ controls were included and gender parity conserved where possible. Experimental end points were reaching 56 days of life or becoming unwell for any reason. Upon reaching an experimental end point, mice were humanely sacrificed and liver, heart, brain, kidney and gastrocnemius muscles were harvested for biochemical end-point assays, as previously described in Chapter 2.2.6.8.

In experiments exploring the effect of cis-regulatory elements in the expression cassette, whole litters were injected via IP injection as close to birth as possible on post-natal Day 0 with a vector dose of 5×10^{11} VGC/pup. Additional vectors used in this experiment were rAAV2/8.APOe/hAAT.hDBT.pBTIR and rAAV2/8.APOe/hAAT.hDBT.WPRE. Total injection volumes were 10 μL/pup. Mice were weighed daily, observed for any features of metabolic intoxication and followed until they either became sick or reached day 56 (adulthood). Tissues were then harvested for biochemical end-point assays, as described above. Tissues for biochemical end-point assays were only harvested in mice surviving past 7 days of life.

5.2.5 Inducing a metabolic stress with a high protein chow

Vector rescued $DBT^{-/-}$ mice that attained adulthood (56 days of age) were given a high protein chow (61% protein, Speciality Foods, Perth, Australia) challenge for 48 hours. Standard chow contains 21% protein. Directly prior to starting, mice were weighed and whole blood spot collected for BCAA analysis. Mice were supplied a high protein chow exclusively for 48 hours, weighed

every 24 hours and observed carefully. Mice were then humanely sacrificed at 48 hours, whole blood spots collected and tissues harvested for endpoint molecular analyses.

5.2.6 Assessing reproductive status in two vector-rescued male DBT$^{-/-}$ mice

Two male vector-rescued DBT$^{-/-}$ mice that attained adulthood were paired with an adult heterozygous DBT$^{+/-}$ female with demonstrated breeding success. Females paired with the DBT$^{-/-}$ males had not been housed with another male mouse in the 4 weeks prior to pairing. Pairs were monitored and females checked for signs of pregnancy. Pups alive at 8 days were genotyped and carefully monitored. Any pups found to be dead were removed and also genotyped.

5.2.7 Statistical analysis

All statistical analysis was performed using GraphPad Prism (10.4.1). Non-parametric statistical testing was used as normal distribution of our data could not be assumed due to sample size. The Mann Whitney two-tailed statistical test was used to generate *p* values unless otherwise stated and Log-Rank (Mantel-Cox) statistical test was used to assess the significance of survival curves. Calculated *p* values were determined significant if <0.05.

5.3 Results

5.3.1 *In vitro* validation of the hybrid AAV/*piggyBac* Transposon vectors in Huh7 cells

Transduction of Huh7 cells with the eGFP transposon encoding vector, rAAV2/DJ.APOe/hAAT.eGFP.WPRE.pbTIR demonstrated functional transduction with the eGFP transgene (Figure 5-3). Transduction of Huh7 cells with the hDBT encoding transposon vector, rAAV2/DJ.APOe/hAAT.hDBT.pbTIR, yielded significantly higher level of DBT mRNA transcripts and E2 protein expression than that observed in untreated Huh7 cells (Figures 5-4 and 5-5). The highest concentration of E2 protein was in the mitochondrial protein fraction across all experimental conditions, which is in keeping with the BCKDH enzyme complex localising to the inner mitochondrial membrane.

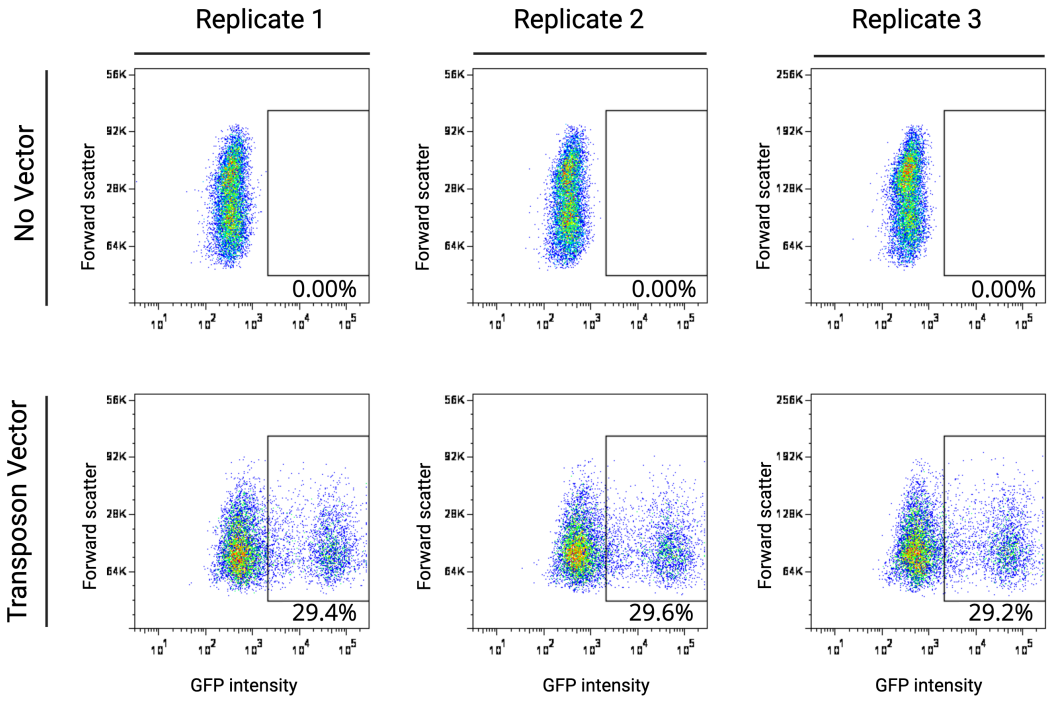

Figure 5-3 Evidence of functional transduction with eGFP transposon vector in Huh7 cells. Huh7 cells were transduced with rAAVDJ.APOe/hAAT.eGFP.WPRE.pbTIR at a multiplicity of infection of 10,000 VCG/cell. Boxed cells represent eGFP positive cells, percentage of positive cells is displayed below each box. The experiment was conducted with three biological replicates. Y axis represents forward scatter and X axis eGFP intensity.

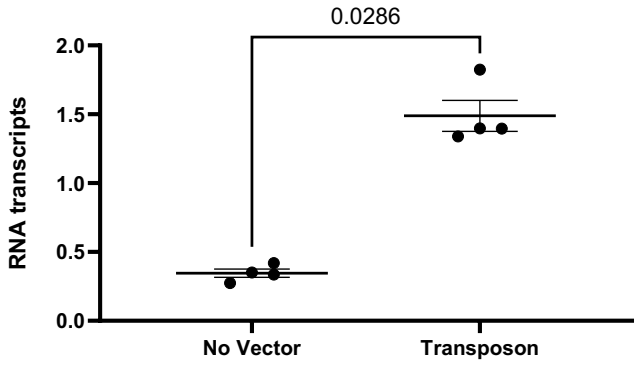

Figure 5-4 RNA transcripts from *in vitro* vector validation of hDBT AAV/*piggyBac* transposon vector in Huh7 cells. Transposon vector rAAVDJ.APOe/hAAT.hDBT.WPRE.pbTIR (10,000 VCG/cell) was applied to Huh7 cells in tissue culture and passaged 3 times over 15 days. Data represent PCR analysis undertaken from cDNA synthesised from RNA transcripts isolated from whole Huh7 cell pellets. Error bars represent standard error mean. Signals were normalised to human albumin and Mann Witney two tailed t-test used to determine statistical significance.

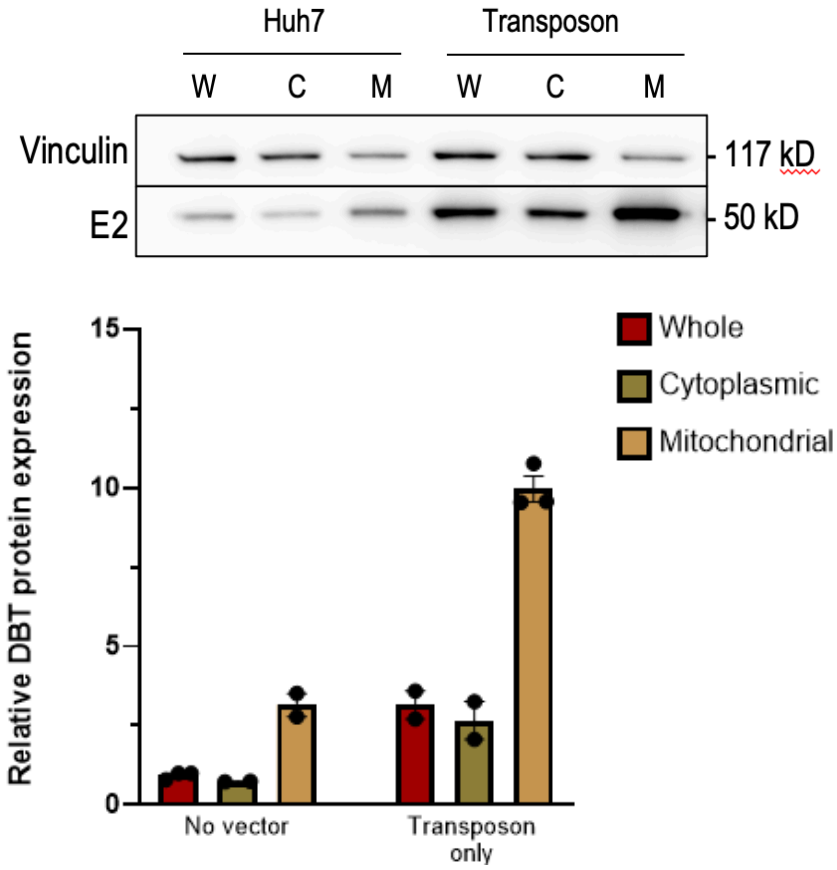

Figure 5-5 Protein expression from hDBT AAV/*piggyBac* transposon vector in Huh7 cells across cellular compartments. Huh7 cells were transduced with rAAV2/DJ.APOe/hAAT.hDBT.WPRE.pbTIR at an MOI of 10,000 and harvested after 3 cell passages and 15 days (n = 2 wells for each MOI). Data represent western blots (top) and quantification of signal with Image J (bottom). Blots were cut at 100kD and probed with either anti-Vinculin antibody or anti-DBT antibody. E2 protein signal for each sample was determined by (Sample E2 optical density (OD)/ vinculin OD for same sample)/(E2 OD for Huh7 cell of same fraction)/vinculin OD for that sample). Abbreviations: W (protein fraction from whole cell), C (cytoplasmic protein fraction) and M (protein fraction isolated from mitochondria). Error bars represent Standard Error Mean.

5.3.2 Survival to adulthood following neonatal administration of *piggyBac* transposon encoding vector independent of transposase encoding vector co-administration

Throughout Section 5.3.2, the vector rAAV2/8.APOe/hAAT.hDBT.WPRE.pbTIR will be referred to as the transposon vector, and rAAV2/8.APOe.hAAT.*piggyBac* referred to as the transposase vector. Treatment cohorts are detailed below (Table 5-1).

In the high dose cohorts, 11 $DBT^{-/-}$ pups were treated with both high dose transposon vector (5×10^{11} VCG/pup) and transposase vector (5×10^{10} VGC/pup) vector and 10 $DBT^{-/-}$ pups were treated with high dose transposon vector alone. All vectors were administered via IP injection on post-natal Day 0 (D_0). In the low dose cohorts, 14 $DBT^{-/-}$ mice were treated with both low dose transposon vector (5×10^{10} VGC/pup) and transposase vector (5×10^{9} VGC/pup), and 13 $DBT^{-/-}$ mice with low dose transposon alone administered via IP injection on D_0. The mice that received both transposon and transposase vectors are referred to as "dual vector treated mice" or $dvDBT^{-/-}$. The mice that were treated with only the transposon vector only are referred to as $tDBT^{-/-}$. Dosage level, high or low, is denoted as required.

Survival rates of high dose dual vector treated $DBT^{-/-}$ mice ($dvDBT^{-/-}{}_{High}$) and high dose transposon only treated $DBT^{-/-}$ mice ($tDBT^{-/-}{}_{High}$) were 58% and 80% respectively at 56 days (Figure 5-6). Survival rates of both groups were significantly improved compared to untreated $DBT^{-/-}$ mice. For both low dose cohorts, survival rates were 0% at 56 days. In the low dose cohorts, an early rescue was observed in four $dvDBT^{-/-}{}_{Low}$ mice (29%) and one $tDBT^{-/-}{}_{Low}$ mice (8%) with these mice living beyond 2 weeks and demonstrating normal growth and behaviour, until they became unwell, lost weight and developed features of metabolic intoxication between 21 and 31 days of life. Despite the rescue only being transient, the survival of $dvDBT^{-/-}{}_{Low}$ mice was

significantly better than untreated DBT$^{-/-}$ mice whereas the survival of tDBT$^{-/-}{}_{\text{Low}}$ mice was equivalent to untreated DBT$^{-/-}$ mice (Figure 5-6).

In all groups, early deaths of DBT$^{-/-}$ occurred within the first 48 hours following vector injections after which survival rates were observed to plateau. For tDBT$^{-/-}{}_{\text{High}}$ mice, 2 out of 10 died in the first 48 hours, with long term survival of the remaining mice out to 56 days when the experiment was then terminated. For the dvDBT$^{-/-}{}_{\text{High}}$ cohort, 4 out of a total 12 DBT$^{-/-}$ mice died within the first 48 hours, one DBT$^{-/-}$ mouse died at 5 days post-injection and the remaining 7 lived to 56 days when the experiment was terminated. For the tDBT$^{-/-}{}_{\text{Low}}$ cohort, there were high rates of early deaths with 12 of the 13 treated DBT$^{-/-}$ pups dying within the first 48 hours and the sole surviving pup developing metabolic intoxication at 30 days post-injection. The dvDBT$^{-/-}{}_{\text{Low}}$ cohort also exhibited high rates of early loss with 10 of 14 DBT$^{-/-}$ pups dying within 48 hours and the remaining 4 developing metabolic intoxication between day 23 of and 31 days post injection.

Table 5-1 Cohorts of DBT$^{-/-}$ mice treated with Hybrid *piggyBac*/AAV Vectors

Treatment group	Vectors administered	Vector Dose (vector genome copies/mouse)	Number in group
dvDBT$^{-/-}{}_{\text{High}}$	Transposon vector	5×10^{11}	11
	Transposase vector	5×10^{10}	
tDBT$^{-/-}{}_{\text{High}}$	Transposon vector	5×10^{11}	10
dvDBT$^{-/-}{}_{\text{Low}}$	Transposon vector	5×10^{10}	14
	Transposase vector	5×10^{9}	
tDBT$^{-/-}{}_{\text{Low}}$	Transposon vector	5×10^{10}	13

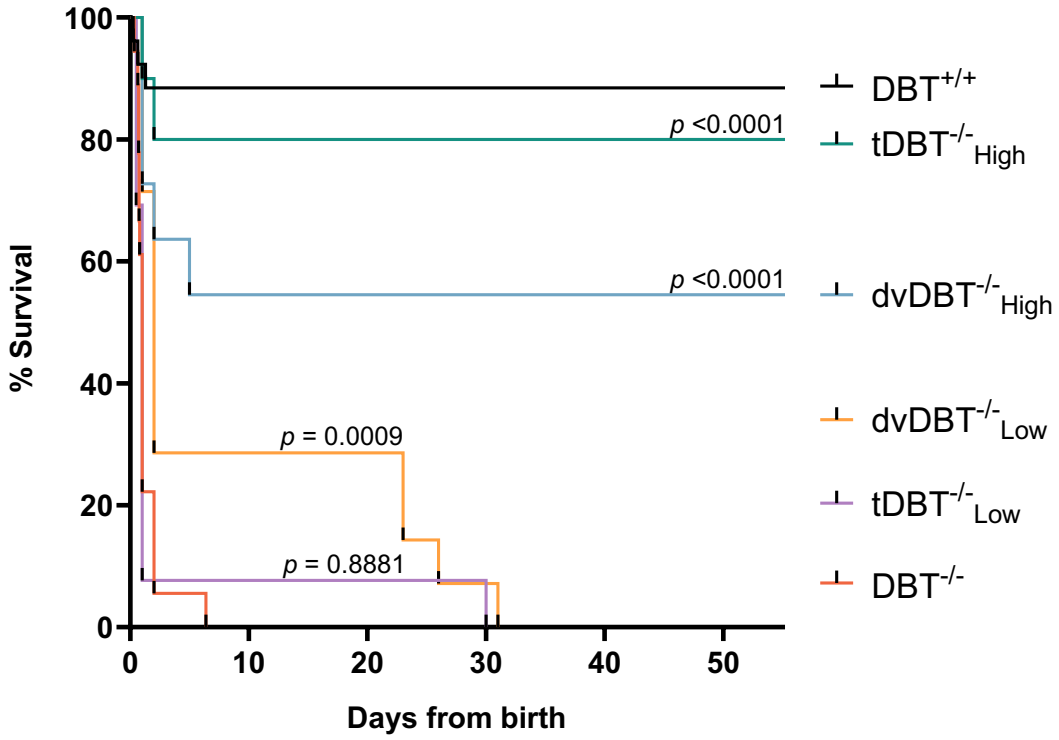

Treatment Group	Cohort size (n)	Survival % at 48 hours (n)	Survival at 56 days (n)
dvDBT$^{-/-}$$_{\text{High}}$	11	64% (n = 7)	55% (n = 6)
tDBT$^{-/-}$ $_{\text{High}}$	10	80% (n = 8)	80% (n = 8)
dvDBT$^{-/-}$ $_{\text{Low}}$	14	29% (n = 4)	0% (n = 0)
tDBT$^{-/-}$$_{\text{Low}}$	13	8% (n = 1)	0% (n = 0)

Figure 5-6 Survival in DBT$^{-/-}$ mice treated with hybrid AAV/piggyBac vectors in the newborn period. Survival curve of the treatment groups (top) and statistical analysis with Log-Rank (Mantel-Cox). The *p* values displayed on curves compare vector treated DBT$^{-/-}$ mice to untreated DBT$^{-/-}$mice. Table of treatment group cohort sizes and survival rates at 48 hours and 57 days (bottom). DBT$^{-/-}$ pups were injected at birth with high dose transposon vector rAAV2/8.APOe/hAAT.hDBT.WPRE.pBTIR at a dose of 5×10^{11} VCG/pup with (dvDBT$^{-/-}$$_{\text{High}}$) or without (tDBT$^{-/-}$$_{\text{High}}$) the transposase vector rAAV2/8.APOe.hAAT.*piggyBac* at a dose of 5×10^{10} VCG/pup. Low dose cohorts were treated with transposon vector rAAV2/8.APOe/hAAT.hDBT.WPRE.pBTIR 5×10^{10} VCG/pup with (dvDBT$^{-/-}$$_{\text{Low}}$) or without (tDBT$^{-/-}$$_{\text{Low}}$) the transposase vector rAAV2/8.APOe.hAAT.*piggyBac* 5×10^{10} VCG/pup.

5.3.3 Growth improvements in vector treated DBT$^{-/-}$ mice are independent of co-administration of *piggyBac* transposase vector

Growth observed in all treated DBT$^{-/-}$ mice cohorts was below that observed in wildtype mice (Figure 5-7). Both high dose treated DBT$^{-/-}$ cohorts continued to demonstrate steady weight gain over the course of experiment until 56 days and co-administration of the transposase encoding vector did not significantly affect body weight at 56 days of age. Both cohorts of high dose vector treated mice weighed significantly less than wildtype mice at 56 days of age (Figure 5-8).

The low dose cohorts displayed steady growth which better approximated DBT$^{+/+}$ mice compared to the high dose cohorts over the first few weeks of life. Both the low dose cohorts succumbed to metabolic intoxication after entering the third week of life however, with faltering growth and weight loss in the days prior to humane euthanasia (Figure 5-7).

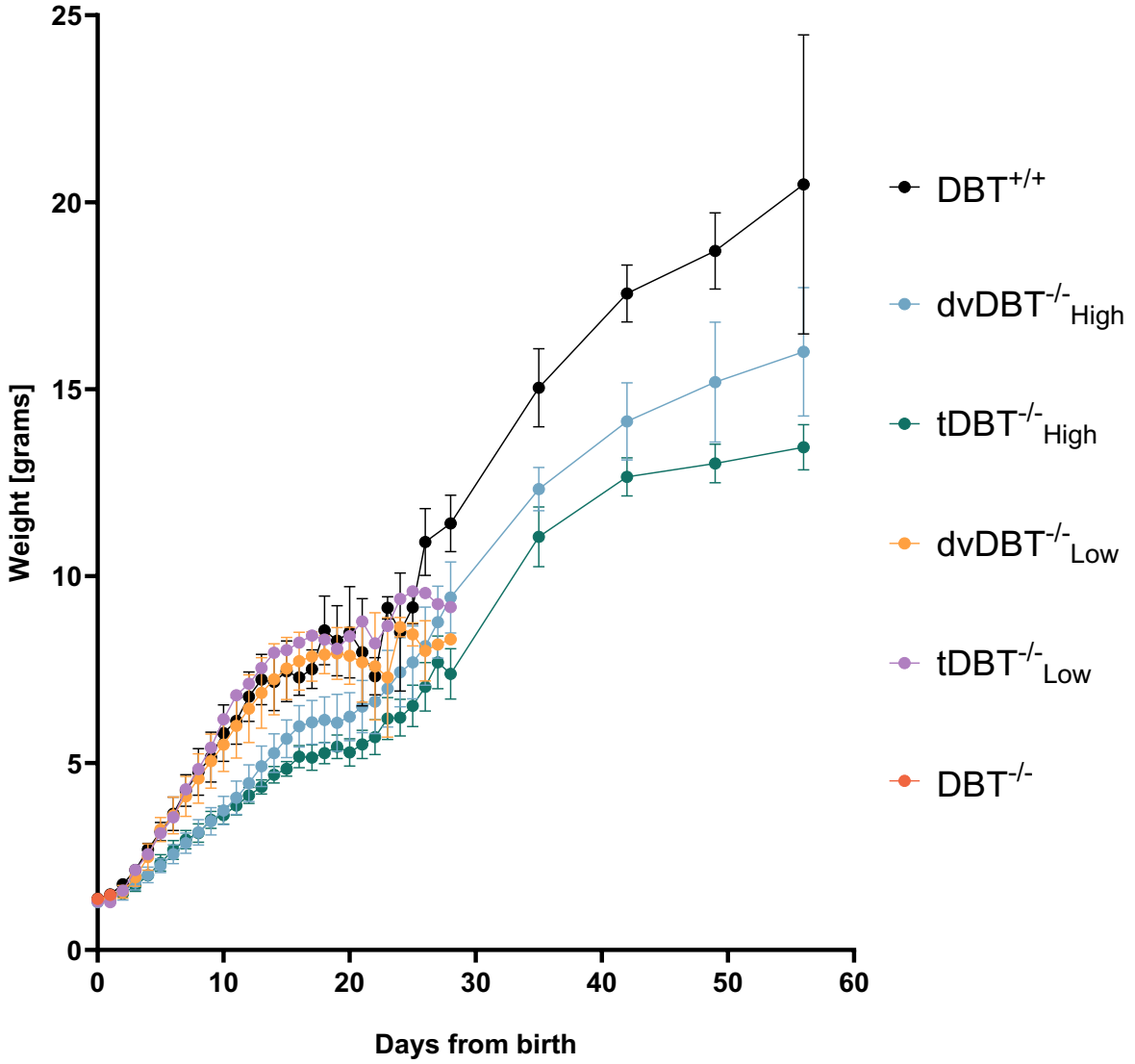

Figure 5-7 Growth of DBT$^{-/-}$ mice treated with hybrid AAV/piggyBac vectors. DBT$^{-/-}$ pups were injected at birth with high dose transposon vector rAAV8.APOe/hAAT.hDBT.WPRE.pBTIR 5×10^{11} VCG/pup with (dvDBT$^{-/-}{}_{\text{High}}$) or without (tDBT$^{-/-}{}_{\text{High}}$) the transposase vector rAAV2/8.APOe.hAAT.*piggyBac* 5×10^{10} VCG/pup. Low dose cohorts were treated with transposon vector rAAV2/8.APOe/hAAT.hDBT.WPRE.pBTIR 5×10^{10} VCG/pup with (dvDBT$^{-/-}{}_{\text{Low}}$) or without (tDBT$^{-/-}{}_{\text{Low}}$) the transposase vector rAAV2/8.APOe.hAAT.*piggyBac* 5×10^{10} VCG/pup. Data point represent average growth of mice in each cohort and error bars represent standard deviation within that group.

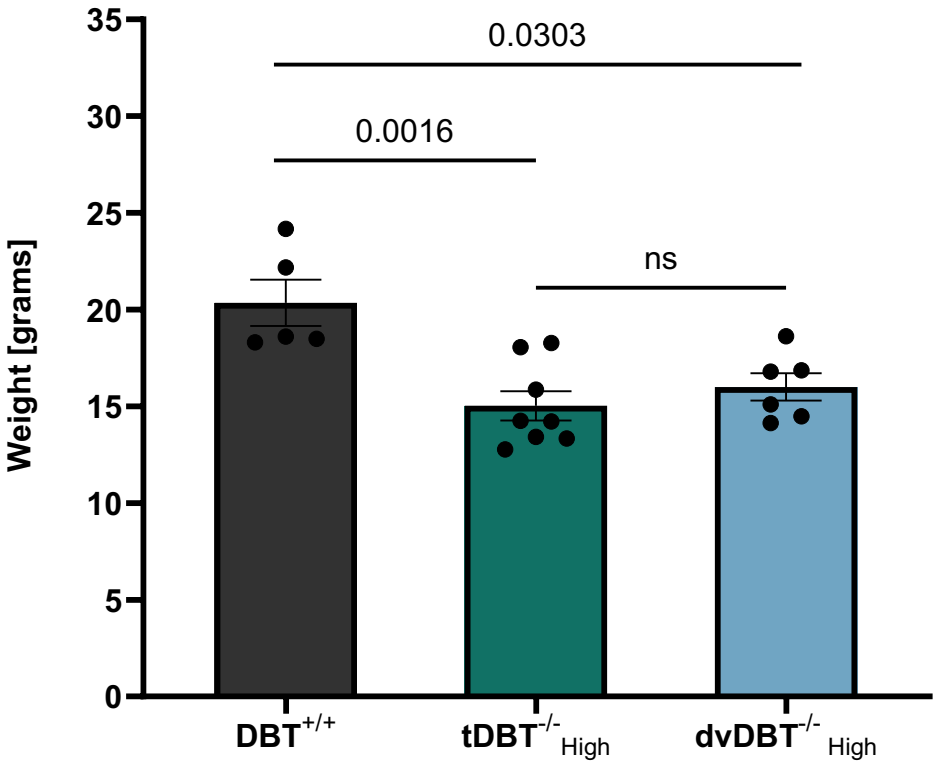

Figure 5-8 Average weight of DBT$^{-/-}$ mice treated with high dose piggyBac transposase AAV hybrid gene addition vectors at 8 weeks post injection. DBT$^{-/-}$ pups were injected at birth with high dose transposon vector rAAV2/8.APOe/hAAT.hDBT.WPRE.pBTIR (5×10^{11} VCG/pup). Mice in the dvDBT$^{-/-}{}_{High}$ cohort also received co-administration of the transposase vector rAAV2/8.APOe.hAAT.*piggyBac* 5×10^{10} VCG/pup. Mice in the tDBT$^{-/-}{}_{High}$ cohort received the transposon vector alone. Weights represent the mouse weight on day 56 of life. Statistical analysis was performed with Mann-Whitney t-test and *p* values between different treatment groups are labelled. Significant if $p < 0.05$. Error bars represent standard error mean. Abbreviations: ns (not statistically significant).

5.3.4 Hybrid AAV/PiggyBac transposon conferred no advantage to vector retention in DBT$^{-/-}$ murine model

Vector copy number (VCN) analysis was undertaken to assess the vector concentration of the transposon encoding vector in treated DBT$^{-/-}$ mice that survived past the first 7 days of life for each experimental condition. Tissues assessed included liver, skeletal muscle (gastrocnemius), heart and brain. The vector concentration in each tissue type was equivalent between tissues assessed high dose cohorts, tDBT$^{-/-}{}_{\text{High}}$ and dvDBT$^{-/-}{}_{\text{High}}$. In both these cohorts, cardiac tissue had the overall highest concentration of vector (Figure 5-9A). In the low dose vector treated cohorts, tDBT$^{-/-}{}_{\text{Low}}$ and dvDBT$^{-/-}{}_{\text{Low,}}$ VCN was lower across all tissues compared to the high dose cohorts and most concentrated in cardiac tissue (Figure 5-9B).

A

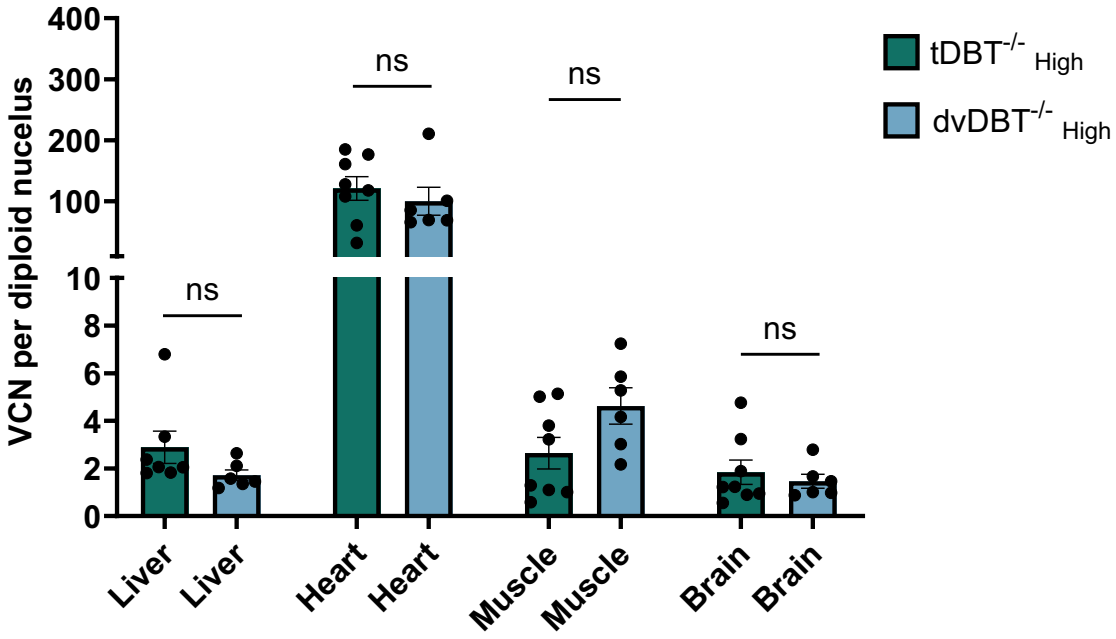

B

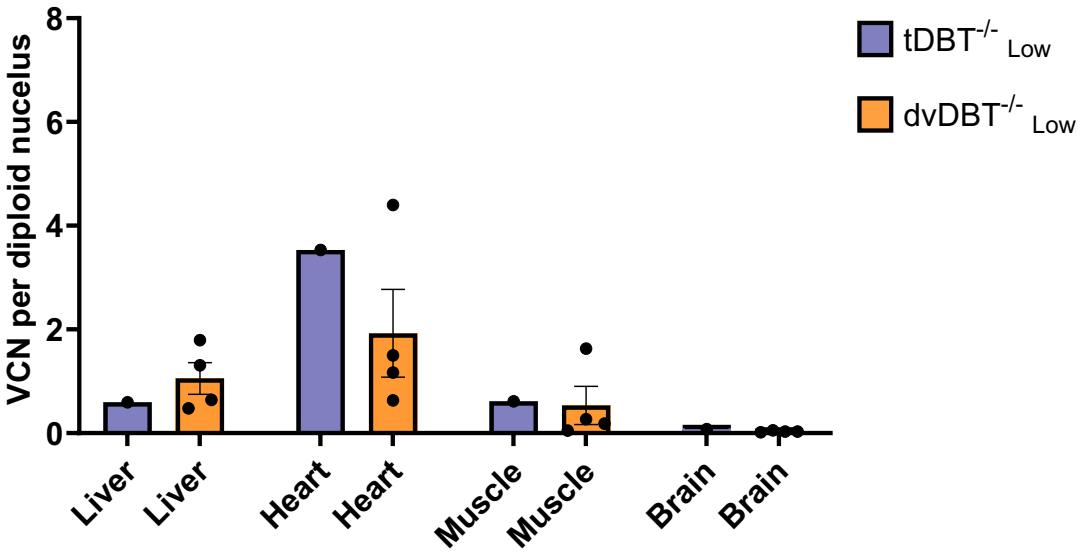

Figure 5-9 Vector biodistribution in DBT$^{-/-}$ mice treated with high and low dose hybrid AAV/piggyBac vectors. Vector genome copies (VGC) were quantitated with ddPCR and signals normalised to the number of murine albumin gene copies/2 to give VGC per diploid nucleus. **(A)** VGC in high dose cohorts. **(B)** VGC in low dose cohorts. Error bars represent standard error mean. P values calculated with Mann-Witney double sided test, significance if p <0.05.

5.3.5 Improved hepatic transgene expression in DBT$^{-/-}$ mice treated with high dose hybrid AAV/*piggyBac* transposon system

At 8 weeks post vector administration, hepatic RNA transcripts of the hDBT transgene were significantly higher in DBT$^{-/-}$ mice treated with both transposon and transposase vectors, compared to mice treated with transposon vector alone (Figure 5-10A). The improved durability of hepatic transgene expression in dvDBT$^{-/-}{}_{High}$ was also observed using western blot analysis with higher liver E2 expression in dvDBT$^{-/-}{}_{High}$ cohort compared to the tDBT$^{-/-}{}_{High}$ cohort (Figure 5-11). Hepatic immunofluorescence also demonstrated more E2 detected on PFA fixed frozen liver sections for mice in the high vector dose cohorts compared to those in the low dose cohorts. In the dvDBT$^{-/-}{}_{High}$ cohort's murine liver sections, there were also more hepatocytes positive for E2 protein compared to sections tDBT$^{-/-}$ murine livers. The presence of discrete clusters of more intensely purple cells in dvDBT$^{-/-}{}_{High}$ murine liver sections is supportive of clonal expansion of hepatocytes that underwent successful transposition. These clusters were not observed in tDBT$^{-/-}{}_{High}$ liver sections (Figure 5-12).

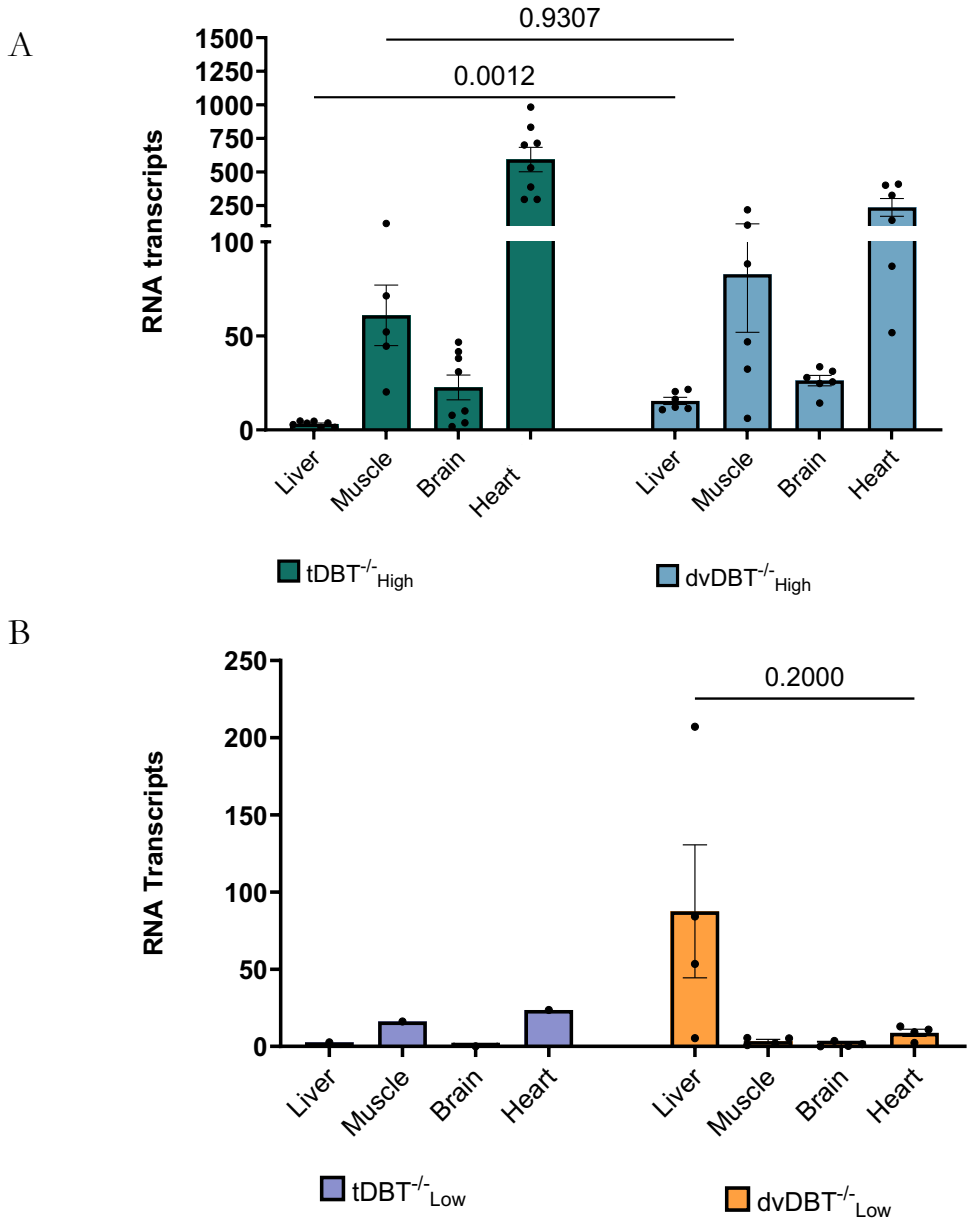

Figure 5-10 RNA transcripts of hDBT transgene for neonatal DBT$^{-/-}$ mice treated with neonatal piggyBac AAV Hybrid Gene Addition vectors. (A) High dose cohorts were injected at birth with high dose transposon vector rAAV8.APOe/hAAT.hDBT.WPRE.pBTIR 5 × 10^{11} VCG/pup with (dvDBT$^{-/-}$$_{High}$) or without (tDBT$^{-/-}$$_{High}$) the transposase vector rAAV8.APOe.hAAT.*piggyBac* 5 × 10^{10} VCG/pup. **(B)** Low dose cohorts were treated with transposon vector rAAV8.APOe/hAAT.hDBT.WPRE.pBTIR 5 × 10^{10} VCG/pup with (dvDBT$^{-/-}$$_{Low}$) or without (tDBT$^{-/-}$$_{Low}$) the transposase vector rAAV8.APOe.hAAT.*piggyBac* 5 × 10^{10} VCG/pup. RNA transcripts were assessed via qPCR from cDNA generated from snap frozen tissue and signals normalised to murine β-actin/1000. Two-tailed Mann Whitney test used to generate *p* values. Error bars are standard error mean.

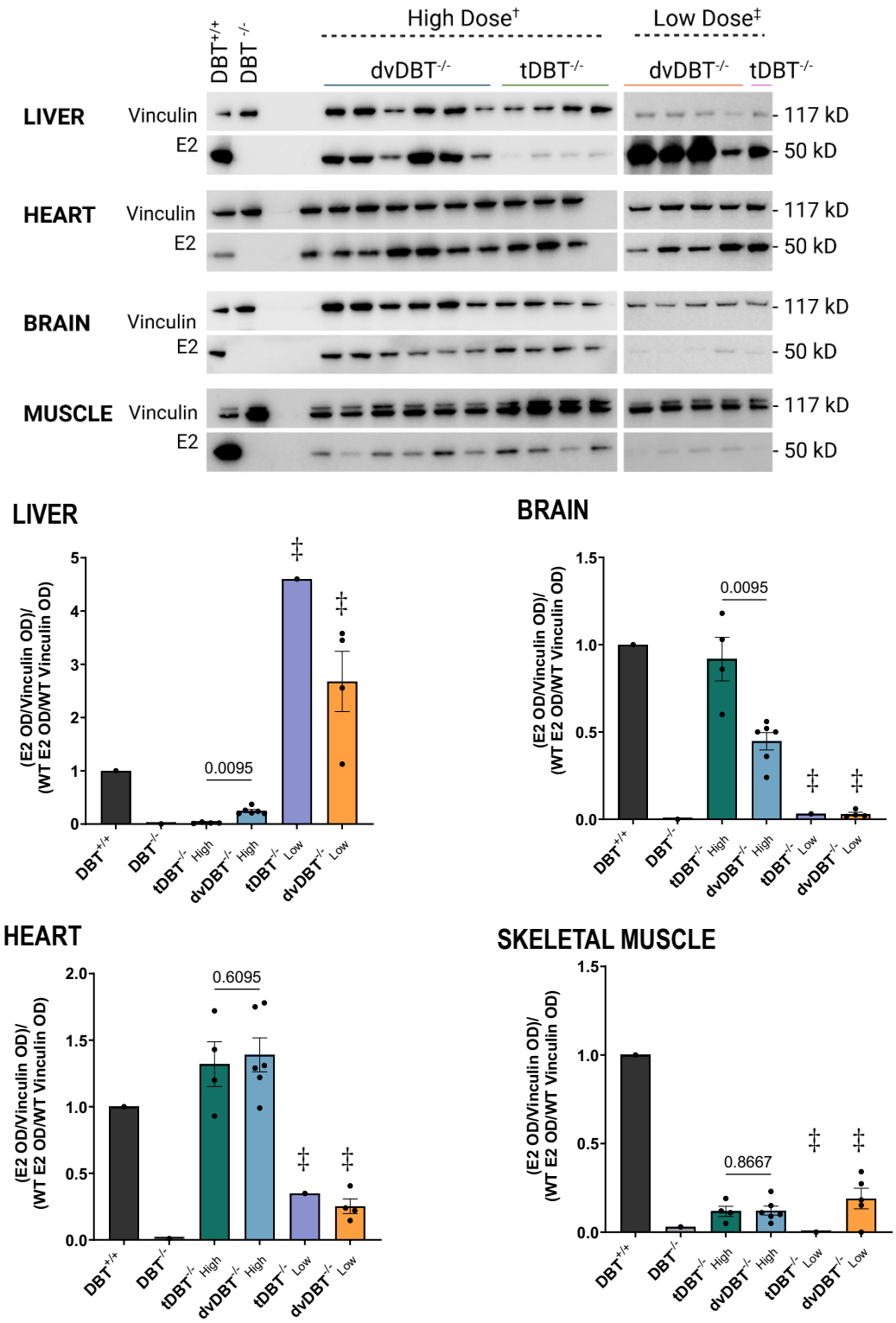

Figure 5-11 E2 protein expression as detected on western blots in DBT$^{-/-}$ mice treated with high or low dose neonatal piggyBac AAV Hybrid Gene Addition vectors. DBT$^{-/-}$ pups were injected at birth with high dose transposon vector (dvDBT$^{-/-}{}_{High}$) with transposon vector or without (tDBT$^{-/-}{}_{High}$). Low dose cohorts were treated with transposon vector with (dvDBT$^{-/-}{}_{Low}$) or without (tDBT$^{-/-}{}_{Low}$) the transposase vector. Expression was quantified with image J. E2 protein in vector treated samples normalised to E2 protein in DBT$^{+/+}$ for the same tissue type with n = 1 used for the control. Two-tailed Mann Whitney test used to generate *p* values. Error bars are standard error mean. † Tissues harvested at 8 weeks; ‡ Tissues harvested when mice became unwell, as per Figure 5-6. Figure generated in BioRender.

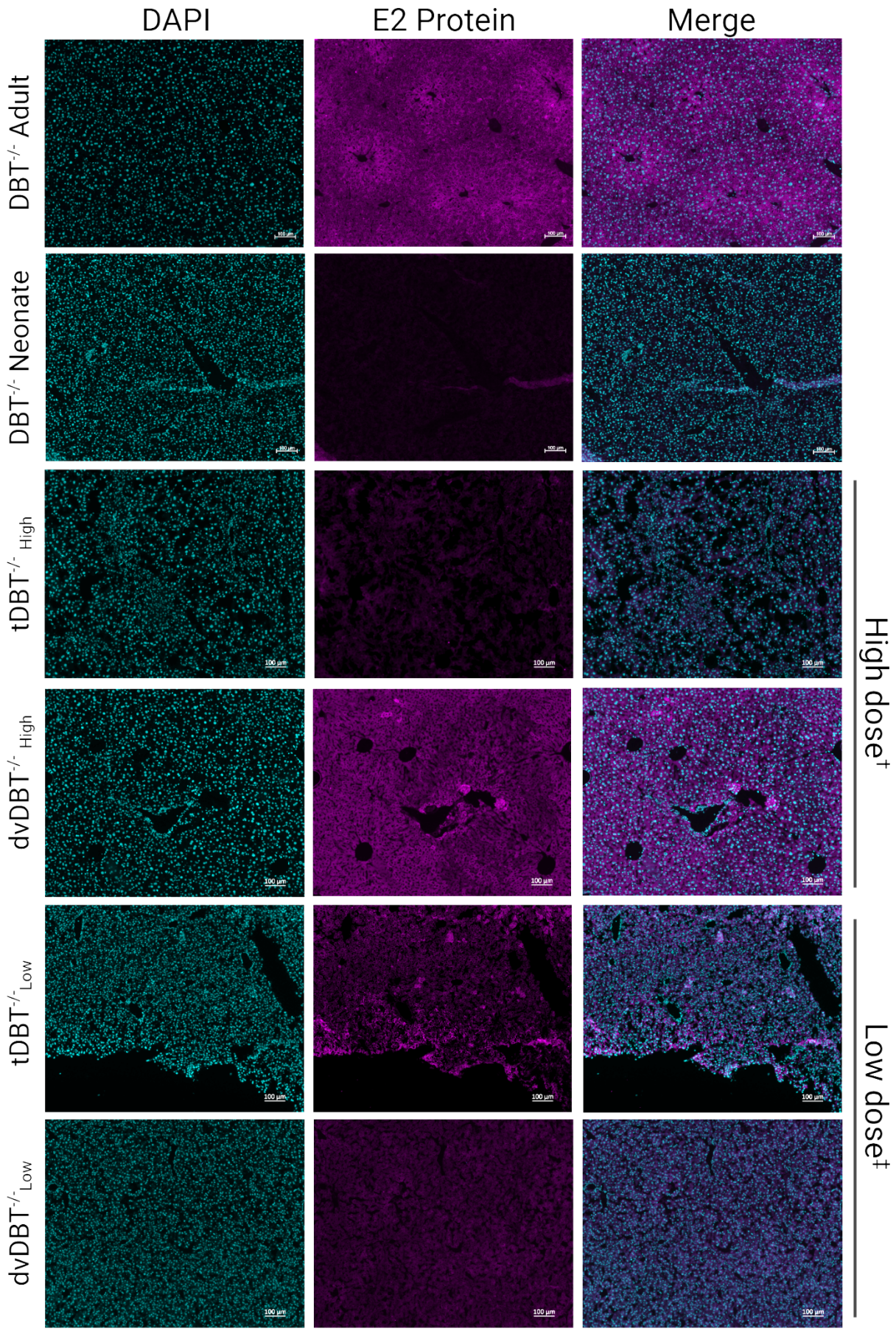
DAPI
E2 Protein
Merge
DBT-/- Adult
DBT-/- Neonate
tDBT-/- High
dvDBT-/- High
tDBT-/- Low
dvDBT-/- Low
High dose+
Low dose+
100 µm

Figure 5-12 (PREVIOUS PAGE) Immunofluorescence of Hepatic E2 expression in neonatal DBT$^{-/-}$ mice treated with high and low dose Hybrid AVV/*piggyBac* vectors. DBT$^{-/-}$ pups were injected at birth with high dose or low dose transposon vector rAAV8.APOe/hAAT.hDBT.WPRE.pBTIR with or without the transposase vector rAAV8.APOe.hAAT.*piggyBac* 5 × 10^{10} VCG/pup. Liver sections were fixed in 4% paraformaldehyde and sectioned at 5 μm before staining cell nuceli with DAPI (blue) and E2 protein (purple). Abbreviations: dvDBT$^{-/-}{}_{\text{High}}$ (high dose transposon vector and transposase vector treated DBT$^{-/-}$ mice), tDBT$^{-/-}{}_{\text{High}}$ (high dose transposon vector treated DBT$^{-/-}$), dvDBT$^{-/-}{}_{\text{Low}}$ (low dose transposon vector and transposase vector treated DBT$^{-/-}$ mice) and tDBT$^{-/-}{}_{\text{Low}}$ (dose transposon vector treated DBT$^{-/-}$). † Tissues harvested at 8 weeks for high dose; ‡ Tissues harvested when mice became unwell in all low dose cohorts, as per Figure 5-6. Figure created in BioRender.

5.3.6 Correction of biochemical phenotype in DBT$^{-/-}$ mice treated with high dose hybrid AAV/*piggyBac* system was independent of hepatic transgene expression

The *piggyBac* transposon expression cassette was designed with a putatively liver specific enhancer/promoter APOe/hAAT to maximise transgene expression from transposase mediated integration into hepatocytes. Co-administration of the transposase encoding vector with the transposon encoding vector achieved significantly higher hepatic expression in the dual vector treated cohort, however the biochemical phenotype between the high dose cohorts was equivalent (Figure 5-13). The biochemical phenotype of DBT$^{-/-}$ treated in both high dose cohorts was observed to have significantly improved levels of leucine and L-alloisoleucine at 56 days post vector administration and moreover, the degree of biochemical correction was statistically equivalent between the dual vector treated mice and the transposon only treated DBT$^{-/-}$ mice. This demonstrated that the biochemical correction was due to the high dose transposon vector itself and was independent of transposase vector co-administration. Whilst DBT$^{-/-}$ mice in both high dose cohorts showed significant improvements in blood leucine and L-alloisoleucine levels compared to untreated DBT$^{-/-}$, the levels of these metabolites did not reach those observed in wildtype mice (Figure 5-13). Despite this, the treated the high dose cohorts DBT$^{-/-}$ leucine:valine ratios were statistically equivalent, pointing to an improved stoichiometry of BCAAs (Figure 5-14). The equivalent biochemical correction between the DBT$^{-/-}$ mice treated with dual transposon and transposase encoding vectors with the DBT$^{-/-}$ mice treated with transposon encoding vector alone, despite different levels of hepatic E2 expression, implied that the transgene under the APOe/hAAT enhancer/promoter was being expressed in in extra-hepatic tissues (Figure 5-11).

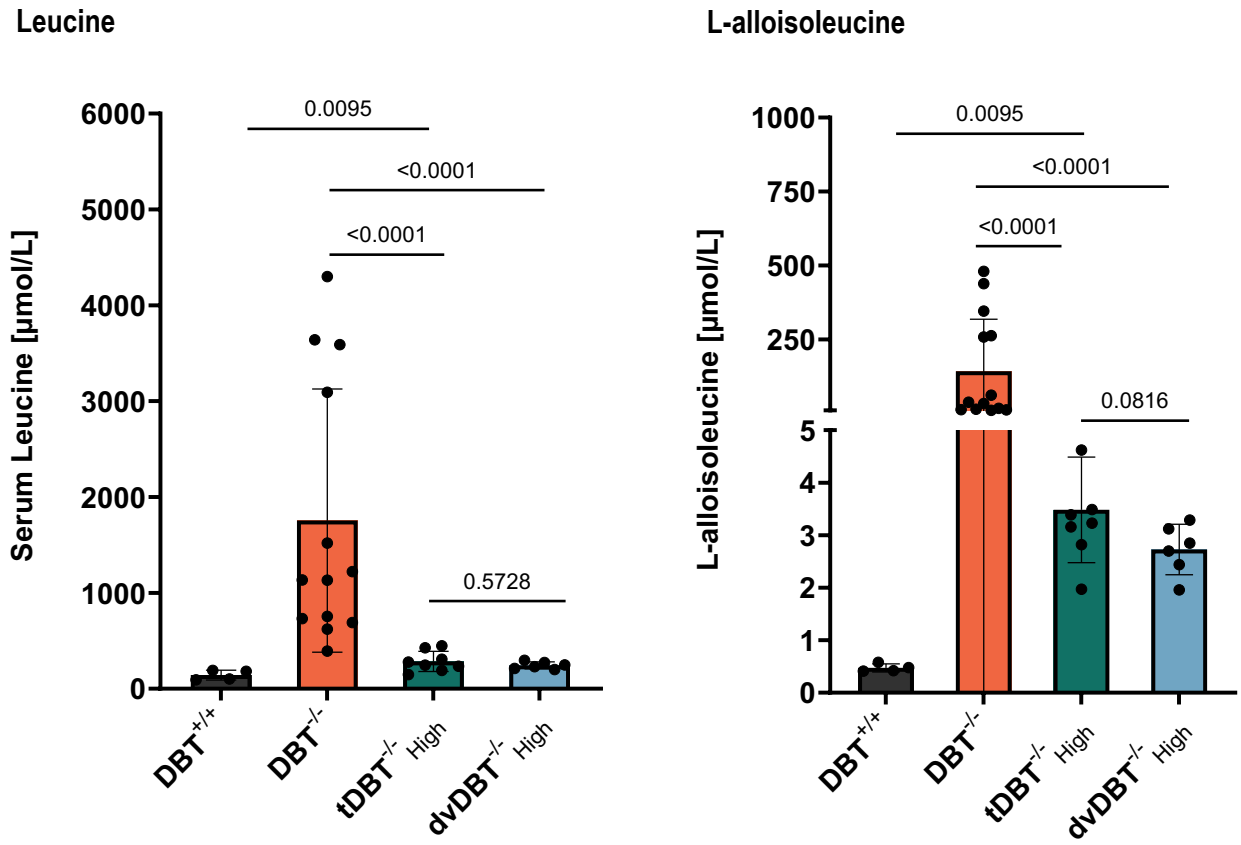

Figure 5-13 Biochemical phenotype in DBT$^{-/-}$ treated with high dose hybrid AAV/piggyBac vectors. DBT$^{-/-}$ pups were treated at birth with high dose transposase vector ± transposon (5×10^{11} VGC/pup transposon vector, 5×10^{10} VGC/pup transposase vector). Whole blood spots were taken on Day 56 of life and analysed via tandem mass spectrometry leucine and L-alloisoleucine levels determined (µmol/L). P values were determined using Mann-Whitney t test. Error bars represent standard error mean. Abbreviations: dvDBT refers to mice that received both transposon and transposase, tDBT refers to mice that received the transposon vector alone.

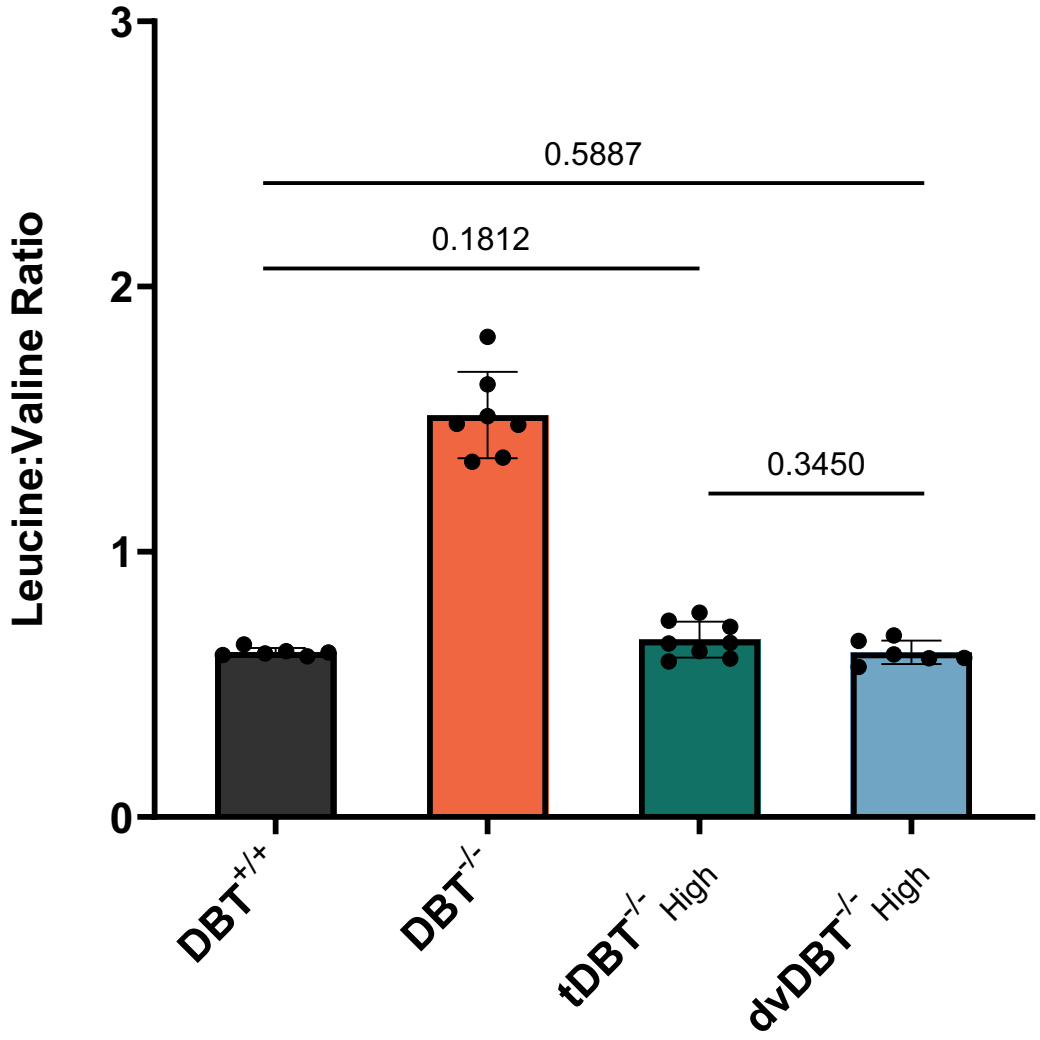

Figure 5-14 Leucine:Valine serum concentration ratio in neonatal DBT$^{-/-}$ mice treated with high dose neonatal piggyBac AAV Hybrid Gene Addition vectors. DBT$^{-/-}$ pups were injected at birth with high dose transposon vector rAAV2/8.APOe/hAAT.hDBT.WPRE.pBTIR 5×10^{11} VCG/pup with (dvDBT$^{-/-}{}_{\text{High}}$) or without (tDBT$^{-/-}{}_{\text{High}}$) the transposase vector rAAV2/8.APOe.hAAT.*piggyBac* 5×10^{10} VCG/pup. Leucine level was divided by valine level to give a ratio. P values were determined using Mann-Whitney t test. Error bars represent standard error mean. Abbreviations: dvDBT refers to mice that received both transposon and transposase, tDBT refers to mice that received the transposon vector alone.

5.3.7 Quantitating extra-hepatic expression in DBT$^{-/-}$ mice treated with the high dose hybrid AAV/piggyBac transposon expression cassette

Extra-hepatic expression of the hDBT transgene in vector treated DBT$^{-/-}$ mice was assessed by quantitating the RNA transcripts of the hDBT transgene and E2 protein expression using western blot analysis. In the high dose cohorts, RNA transcripts were highest in cardiac tissue followed by skeletal muscle, brain, and liver (Figure 5-10). Western blot analysis for both the high dose vector treated cohorts, tDBT$^{-/-}{}_{High}$ and dvDBT$^{-/-}{}_{High,}$ showed that E2 protein was expressed in extra-hepatic tissues under the APOe/hAAT enhancer/promoter (Figure 5-11). In cardiac tissue, E2 expression was equivalent between both the high-dose treated cohorts, tDBT$^{-/-}{}_{High}$ and dvDBT$^{-/-}{}_{High}$ and detected at levels 1-1.5 times greater than the levels seen in wildtype mice. For brain tissue, E2 expression in tDBT$^{-/-}{}_{High}$ approximated wildtype and was significantly higher than dvDBT$^{-/-}{}_{High}$ which was detected at roughly half of wildtype E2 expression. Expression of E2 protein in skeletal muscle of DBT$^{-/-}$ mice was equivalent between both high dose vector treated DBT$^{-/-}$ cohorts and approximated one tenth of the level seen in wildtype mice.

5.3.8 DBT$^{-/-}$ mice treated with low dose hybrid AAV/*piggyBac* transposon system cohorts died early despite high levels of hepatic expression

In the low dose cohorts, all vector treated DBT$^{-/-}$ that survived past 48 hours became unwell in the 3rd or 4th week of life necessitating tissue harvest at this time after humane euthanasia. The low dose cohorts tDBT$^{-/-}{}_{Low}$ and dvDBT$^{-/-}{}_{Low}$ had BCAA levels taken just prior to euthanasia. Blood levels of L-alloisoleucine blood levels were statically similar to untreated DBT$^{-/-}$ in the dvDBT$^{-/-}{}_{Low}$ cohort and statistical analysis was not able to be performed for the tDBT$^{-/-}{}_{Low}$ cohort due to sample size (Figure 5-15).

In both the low dose treated cohorts, RNA transcripts were detected in heart, muscle and brain at levels lower than those seen in the high dose treated cohorts (Figure 5-10). In the low dose treated

mice, hepatic RNA hDBT transcripts were higher in $DBT^{-/-}$ treated with both low dose transposon vector and transposase vector compared to the mouse treated with low dose transposon alone (Figure 5-10). Hepatic E2 protein expression as detected using western blot analysis was higher in the $dvDBT^{-/-}{}_{Low}$ than the high dose cohort $dvDBT^{-/-}{}_{High}$ reflective of the timing of tissue harvest (Figure 5-11). Both the low dose cohorts had higher hepatic E2 levels on western blot analysis at the time they became unwell and were culled compared to high dose cohorts at 8 weeks. The main difference in the E2 protein tissue expression pattern between the high dose and low dose cohorts was that the low dose cohorts had much lower levels of brain and cardiac expression, likely secondary to the lower vector dose resulting in lower rates of tissue transduction (Figure 5-9).

The E2 protein expression in these low dose cohorts as seen on the western data did not align with the levels of immunofluorescence seen on fresh frozen liver sections probed with anti-E2 antibody to detect transduced hepatocytes expressing the E2 protein. Areas of E2 positive hepatocytes were seen in PFA fixed frozen liver sections in mice from the $dvDBT^{-/-}{}_{Low}$, $tDBT^{-/-}{}_{Low}$ cohorts, however the immunofluorescence observed across these sections showed some scattered positive cells, compared to the strongly positive E2 protein bands in transduced cells were seen scattered throughout sections and E2 protein expression in hepatocytes was not detectable for these low dose cohorts (Figure 5-12).

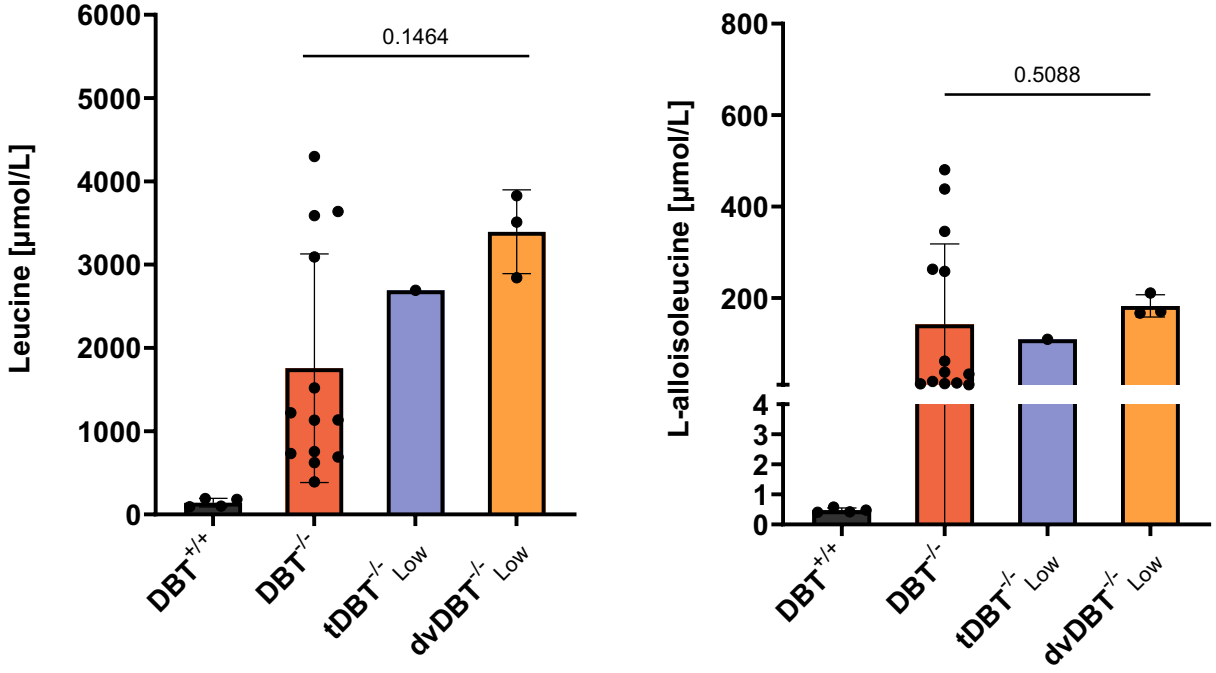

Figure 5-15 Biochemical phenotype in DBT$^{-/-}$ treated with low dose hybrid AAV/piggyBac vectors. DBT$^{-/-}$ pups were treated at birth with low dose transposase vector ± transposon (5×10^{10} VGC/pup transposon vector, 5×10^{9} VGC/pup transposase vector). Whole blood spots were taken prior to human euthanasia after all treated DBT-/- became unwell. Blood spots were analysed via tandem mass spectrometry and leucine and L-allisoleucine levels determined. P values were determined using Mann-Whitney t test. Error bars represent standard error mean. Abbreviations: dvDBT refers to mice that received both transposon and transposase, tDBT refers to mice that received the transposon vector alone. Abbreviations: dvDBT$^{-/-}{}_{\text{High}}$ (high dose transposon vector and transposase vector treated DBT$^{-/-}$ mice), tDBT$^{-/-}{}_{\text{High}}$ (high dose transposon vector treated DBT$^{-/-}$), dvDBT$^{-/-}{}_{\text{Low}}$ (low dose transposon vector and transposase vector treated DBT$^{-/-}$ mice) and tDBT$^{-/-}{}_{\text{Low}}$ (dose transposon vector treated DBT$^{-/-}$).

5.3.10 Metabolic stress unmasks persistent deficiency in total body BCKDH activity in hybrid AAV/*piggyBac* vector rescued DBT$^{-/-}$ mice

Part of each high dose cohort (tDBT$^{-/-}{}_{High}$ n= 4, dvDBT$^{-/-}{}_{High}$ n = 4) and male wildtype controls (n = 3) were subjected to metabolic stress induced with a 48-hour hour period of dietary restriction to a high protein chow. The high protein diet is relatively unpalatable compared to standard chow and it is possible that the caloric intake of the mice overall was lower than otherwise normally would have been. All mice survived this high protein challenge despite significant weight loss experienced across all cohorts (Figure 5-16). Blood leucine and L-alloisoleucine levels rose in all mice, and this with significant elevations in the treated DBT$^{-/-}$ mice but not in the wildtype mice (Figure 5-17). The levels of leucine, if seen in humans would warrant clinical concern and likely hospitalisation. Despite these elevations, there was no observation of physical signs of metabolic intoxication in the vector treated DBT$^{-/-}$ mice such as seizures or altered physical state. Wildtype mice were observed to have non-significant elevations in leucine, but stable L-alloisoleucine levels (Figure 5-17).

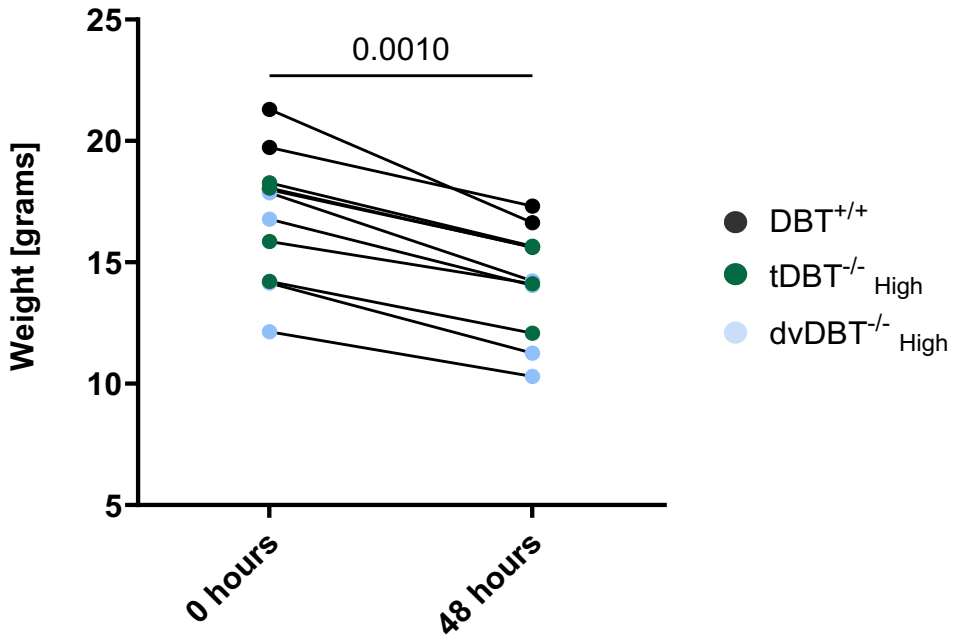

Figure 5-16 Weight loss during a simulated metabolic stress in neonatal DBT$^{-/-}$ mice treated with high dose neonatal piggyBac AAV Hybrid Gene Addition vectors. Body weight was measured at the start and end of a 48-hour high protein dietary challenge. P values calculated with Wilcoxon matched-pairs signed rank test. Abbreviations: dvDBT$^{-/-}{}_{High}$ (high dose transposon vector and transposase vector treated DBT$^{-/-}$ mice), tDBT$^{-/-}{}_{High}$ (high dose transposon vector treated
DBT$^{-/-}$).

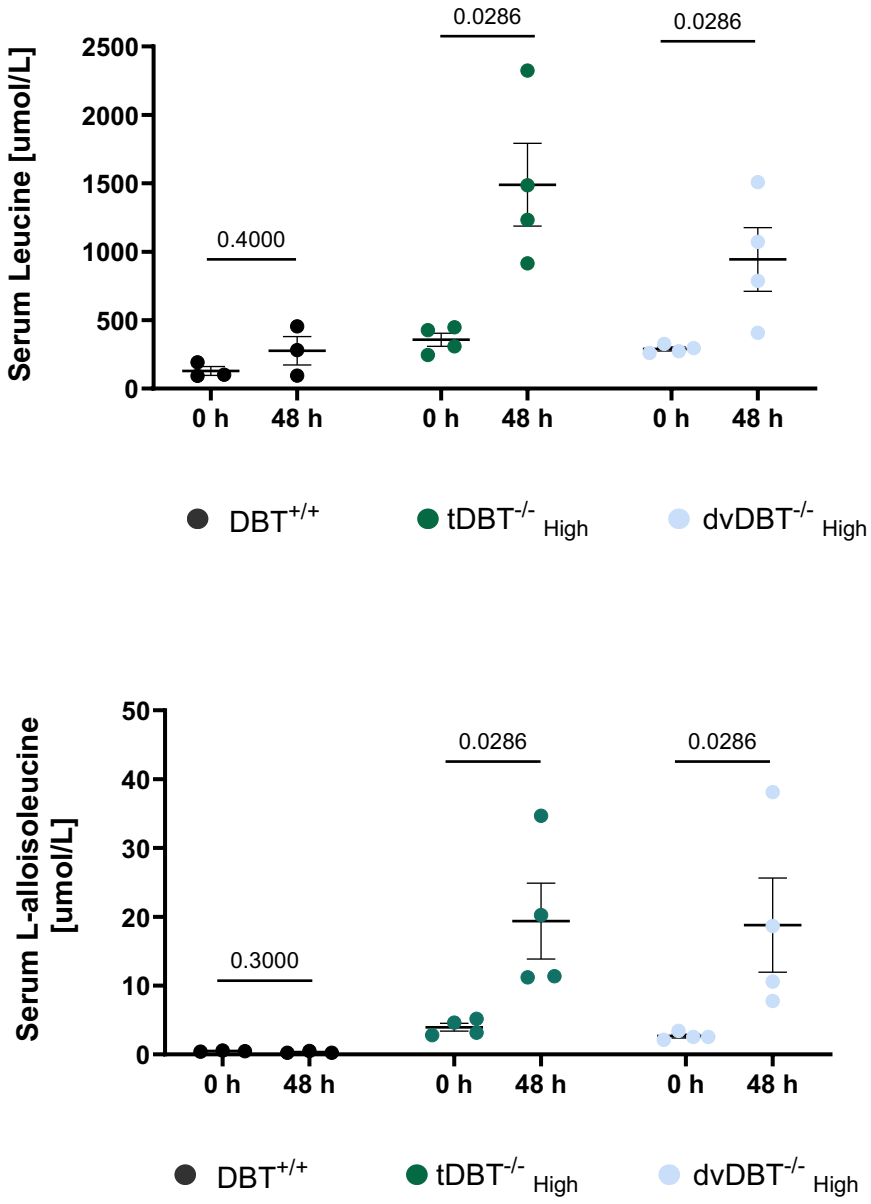

Figure 5-17 Biochemical phenotype of vector treated DBT$^{-/-}$ mice when exposed to severe metabolic stress. Observed increases in Leucine and L-all isoleucine were significantly higher in vector treated DBT-/- mice after 48 hours on a high protein diet. Leucine and L-alloisoleucine whole blood samples were taken at the start and end of a 48-hour high protein dietary challenge. P values were determined using Wilcoxon signed rank test, significant if p <0.05. Error bars represent standard error mean. Abbreviations: dvDBT$^{-/-}{}_{High}$ (high dose transposon vector and transposase vector treated DBT$^{-/-}$ mice), tDBT$^{-/-}{}_{High}$ (high dose transposon vector treated DBT$^{-/-}$).

5.3.11 Cis-regulatory elements in the transposon encoding expression cassette postulated to influence expression profile of transposon encoding vector

The biochemical correction in DBT$^{-/-}$ mice treated with high dose transposon encoding vector (rAAV8.APOe/hAAT.hDBT.WPRE.pbTIR) was equivalent with or without co-transduction of the *piggyBac* transposase encoding vector. Whilst the use of the transposase vector did increase hepatic expression of the hDBT transgene 8 weeks post vector administration compared to that seen in mice treated with transposon alone, the extent of hepatic transposition described in other model systems that used *piggyBac* transposase in neonatal livers was not observed in study [274, 275]. Regardless of the level of hepatic transposition achieved with the *piggyBac* system in this study, the equivalent biochemical phenotypes of transposon encoding vector treated DBT$^{-/-}$ with or without coadministration of transposase encoding vector demonstrates that the extra-hepatic tissue expression of the transgene cassette was critical in conferring the improve durability of this treatment. In this way, the configuration of the transposon encoding vector itself, rather than co-administration of transposase encoding vector, contributed to the improved biochemical phenotype and survival and thus durability of the treatment. This was interesting as the transposon encoding vector, rAAV2/8.APOe/hAAT.hDBT.WPRE.pbTIR achieved more robust rescue of the DBT$^{-/-}$ mouse when compared to an equivalent dose of the gene addition vector rAAV2/8.APOe/hAAT.hDBT described in Chapter 4, despite having the same transgene and transcriptional enhancer/promoter.

The key differences between the transposon encoding vector and the gene addition vector were the inclusion of pBTIRs and a WPRE element in the transposon encoding vector. To better understand which, if any of these elements were contributing to the significant difference in phenotypic rescue and extra-hepatic tissue expression, two new vectors were generated, rAAV2/8.APOe/hAAT.hDBT.**WPRE** and rAAV2/8.APOe/hAAT.hDBT.**pBTIR**. These

vectors were administered to DBT$^{-/-}$ neonates on D_0 of life under the same experimental conditions as the previous experiments.

It should be noted that the following data presented includes data already presented pertaining to DBT$^{-/-}$ mice treated with rAAV2/8.APOe/hAAT.hDBT in Chapter 4 and mice treated with rAAV2/8.APOe/hAAT.hDBT.**WPRE** earlier in this Chapter. A comparison of various vector elements can be found in the appendix.

5.3.12 Evaluating the effects of cis-regulatory elements on DBT$^{-/-}$ mouse survival and growth

The inclusion of a WPRE element in the expression cassette of rAAV vectors encoding a hDBT transgene was associated with significantly improved survival compared to vectors carrying a pBTIR. (Figure 5-18). The inclusion of a pBTIR in the rAAV expression cassette significantly prolonged the survival of DBT$^{-/-}$ compared to an expression cassette with the hDBT transgene alone, however the rescue was only transient when there was no WPRE, and no DBT$^{-/-}$ mice reached 8 weeks of age without the inclusion of a WPRE in the vector expression cassette (Figure 5-18).

Growth in DBT$^{-/-}$ treated with rAAV2/8.APOe/hAAT.hBDT.**WPRE** and rAAV2/8.APOe/hAAT.hDBT.**pBTIR** was equivalent until the third and fourth weeks of life when mice treated with the latter became unwell and required humane euthanasia (Figure 5-19). Growth of DBT$^{-/-}$ treated with rAAV2/8.APOe/hAAT.hBDT.**WPRE** at 8 weeks was equivalent to that seen with rAAV8.APOe/hAAT.hDBT.WPRE.pBTIR.

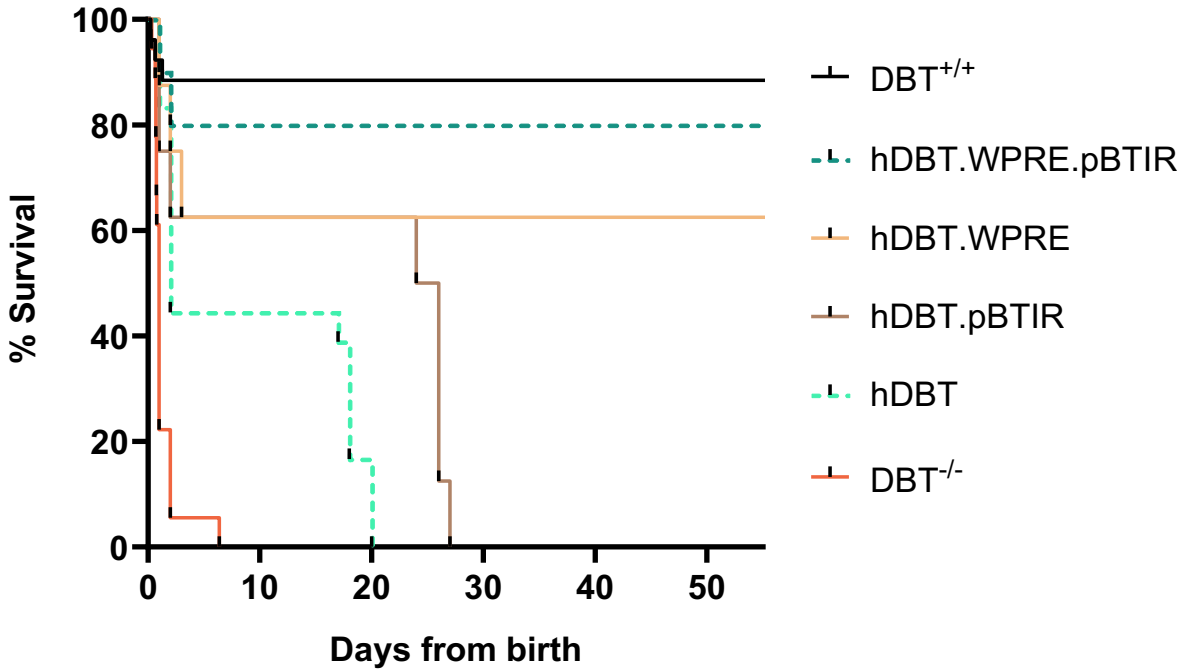

Comparative *p* values	hDBT.WPRE	hDBT.pbTIR	hDBT
hDBT.WPRE.pBTIR	0.4551	0.0019	0.001
hDBT.WPRE	-	0.0394	0.0068
hDBT.pbTIR	0.0394	-	0.0100
hDBT	0.0068	0.0100	-

Figure 5-18 Survival data from DBT$^{-/-}$ treated with AAV hDBT transgene vectors containing WPRE and/or pBTIR. All mice were treated at birth with 5 × 10^{11} VGC/pup of either the transposon vector rAAV2/8.APOe/hAAT.hDBT.WPRE.pBTIR (hDBT.**WPRE.pBTIR,** data from earlier in Chapter 5), rAAV2/8.APOe/hAAT.hDBT.WPRE (hDBT.**WPRE**), rAAV2/8.APOe/hAAT.hDBT.pBTIR (hDBT.**pBTIR**) or rAAV2/8.APOe/hAAT.hDBT (**hDBT**, data from Chapter 4). Log-Rank (Mantel-Cox) statistical analysis test was used to compare each of the vector groups.

A

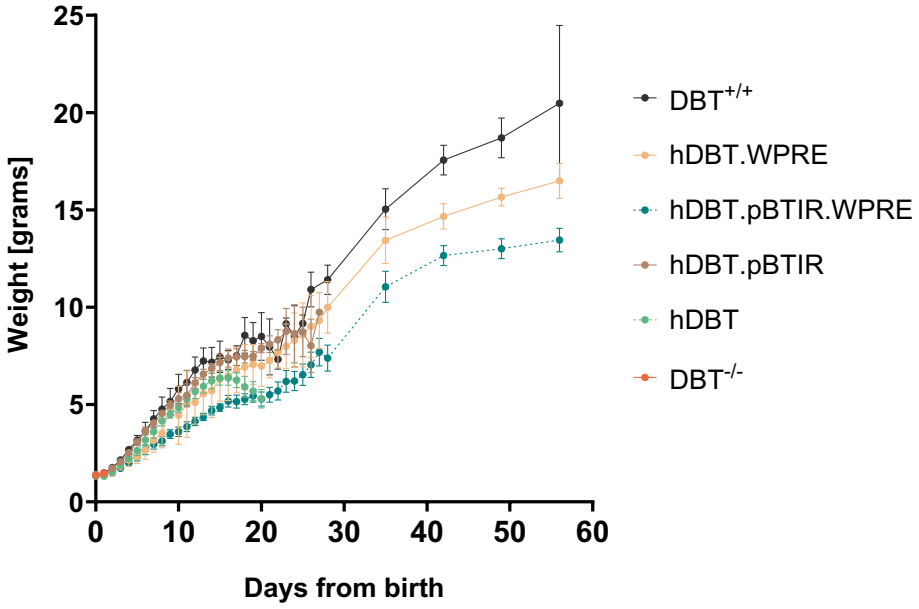

B

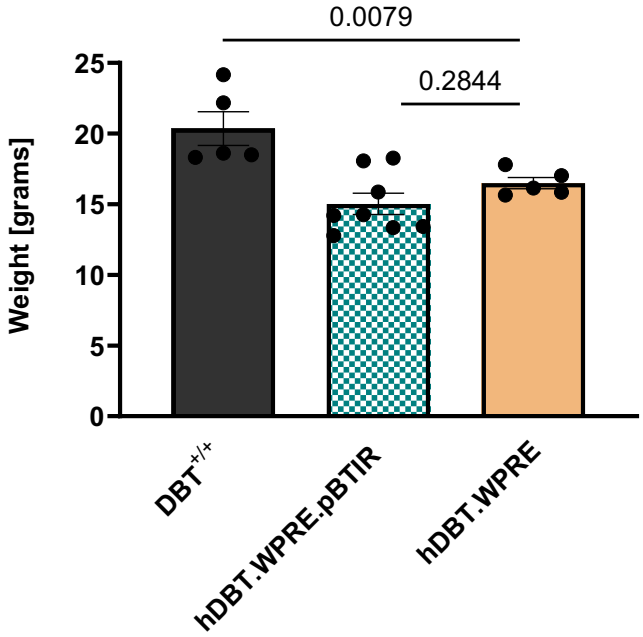

Figure 5-19 Growth data from DBT$^{-/-}$ treated with AAV hDBT transgene vectors containing WPRE and/or pBTIR. (A) Growth comparison of DBT$^{-/-}$ mice treated at D_0 of life with 5×10^{11} VGC/pup of either the transposon vector rAAV2/8.APOe/hAAT.hDBT.WPRE.pBTIR (hDBT.**WPRE.pBTIR,** data from earlier in Chapter 5), rAAV2/8.APOe/hAAT.hDBT.WPRE (hDBT.**WPRE**), rAAV2/8.APOe/hAAT.hDBT.pBTIR (hDBT.**pBTIR**) or rAAV2/8.APOe/hAAT.hDBT (**hDBT**, data from Chapter 4). Error bars represent standard deviation. of mice. **(B)** Weight of mice at experimental end point of 8 weeks. Error bar represent standard error mean and column height mean. Statistical significance was determined with Mann-Witney two tailed t-test and significant if $p < 0.05$.

5.3.13 Interpreting biodistribution in vectors with different *cis*-regulatory elements

As the survival of $DBT^{-/-}$ mice treated with the vectors used to explore the effect of the cis-regulatory WPRE and pBTIR elements differed, tissues were harvested at differing time points, subsequent molecular analysis end point assays were undertaken on tissue collected at different time points and needs to be interpreted accordingly. Analysis of kidney tissue was also undertaken as this organ is biologically relevant with regards to BCKDH activity, as was not assessed in the molecular analysis undertaken in Chapter 4 or earlier in Chapter 5.

The presence or absence of pBTIR did not significantly change the tissue transduction patterns between the rAAV2/8.APOe/hAAT.hDBT.WPRE.pBTIR vector and rAAV2/8.APOe/hAAT.hDBT.WPRE vector at 8 weeks post injection (Figure 5-20). Similarly, the tissue transduction pattern in mice treated with rAAV2/8.APOe/hAAT.hDBT and rAAV2/8.APOe/hAAT.hDBT.pBTIR was similar and all mice in these treated groups experienced metabolic intoxication before or with a few days of the 4th week of life.

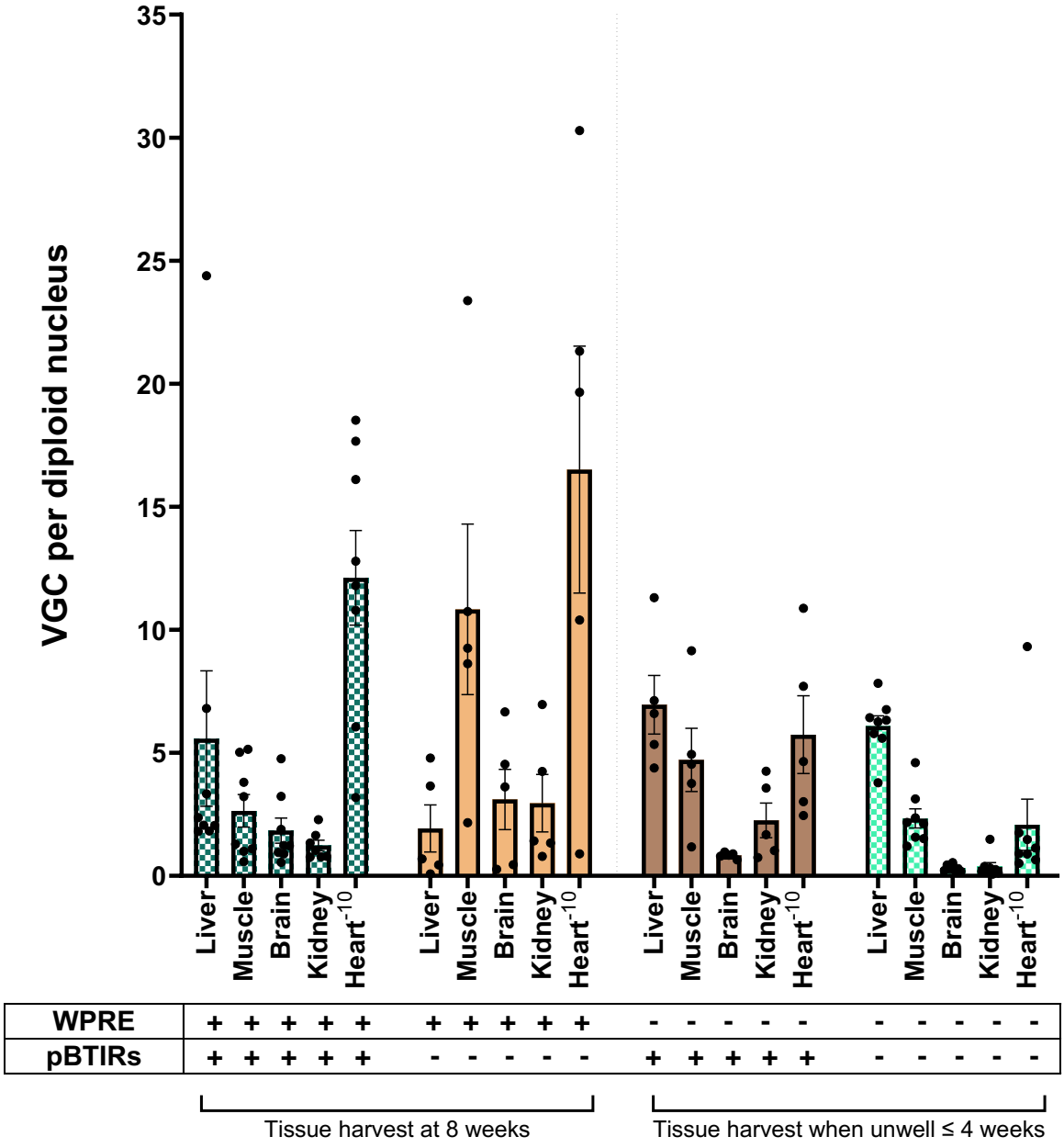

Figure 5-20 Vector biodistribution of vectors with differing *cis*-regulatory elements in DBT$^{-/-}$ mice. DBT$^{-/-}$ mice were treated at D_0 of life with 5×10^{11} VGC/pup of either the transposon vector rAAV2/8.APOe/hAAT.hDBT.WPRE.pBTIR (hDBT.**WPRE.pBTIR,** data from earlier in Chapter 5), rAAV2/8.APOe/hAAT.hDBT.WPRE (hDBT.**WPRE**), rAAV2/8.APOe/hAAT.hDBT.pBTIR (hDBT.**pBTIR**) or rAAV2/8.APOe/hAAT.hDBT (**hDBT**, data from Chapter 4).

5.3.14 Effect of cis-regulatory elements on the tissue expression of AAV transgene cassette in DBT$^{-/-}$ mice.

DBT$^{-/-}$ mice treated with vectors containing a WPRE element had higher RNA transcripts in the brain and cardiac tissues compared to those mice treated with vectors that did not contain WPREs (Figure 5-21). Transgene protein expression as detected using western blot analysis also demonstrated more protein in the brain, heart and skeletal muscle in mice treated with vectors that had expression cassettes containing a WPRE (Figure 5-22).

Hepatic expression was the highest in mice treated with the hDBT transgene cassette without either the WPRE or pBTIR (Figure 5-22). This is likely a reflection of the timing of when these mice were sacrificed, as they all became unwill around 16 days of life and were all euthanised before 21 days of life and this high hepatic expression was not associated with a survival advantage.

One mouse treated with rAAV2/8.APOe/hAAT.hDBT.WPRE.pBTIR had higher renal E2 expression as detected on western blot analysis than any other mouse in this experiment (Figure 5-22). It is possible that the IP injection may have been intrarenal. The RNA and vector copy data did not correlate with this observation which may have been due to the manner in which the tissue was collected and different section of kidney used for VCN and RNA to the sample reserved for protein extraction.

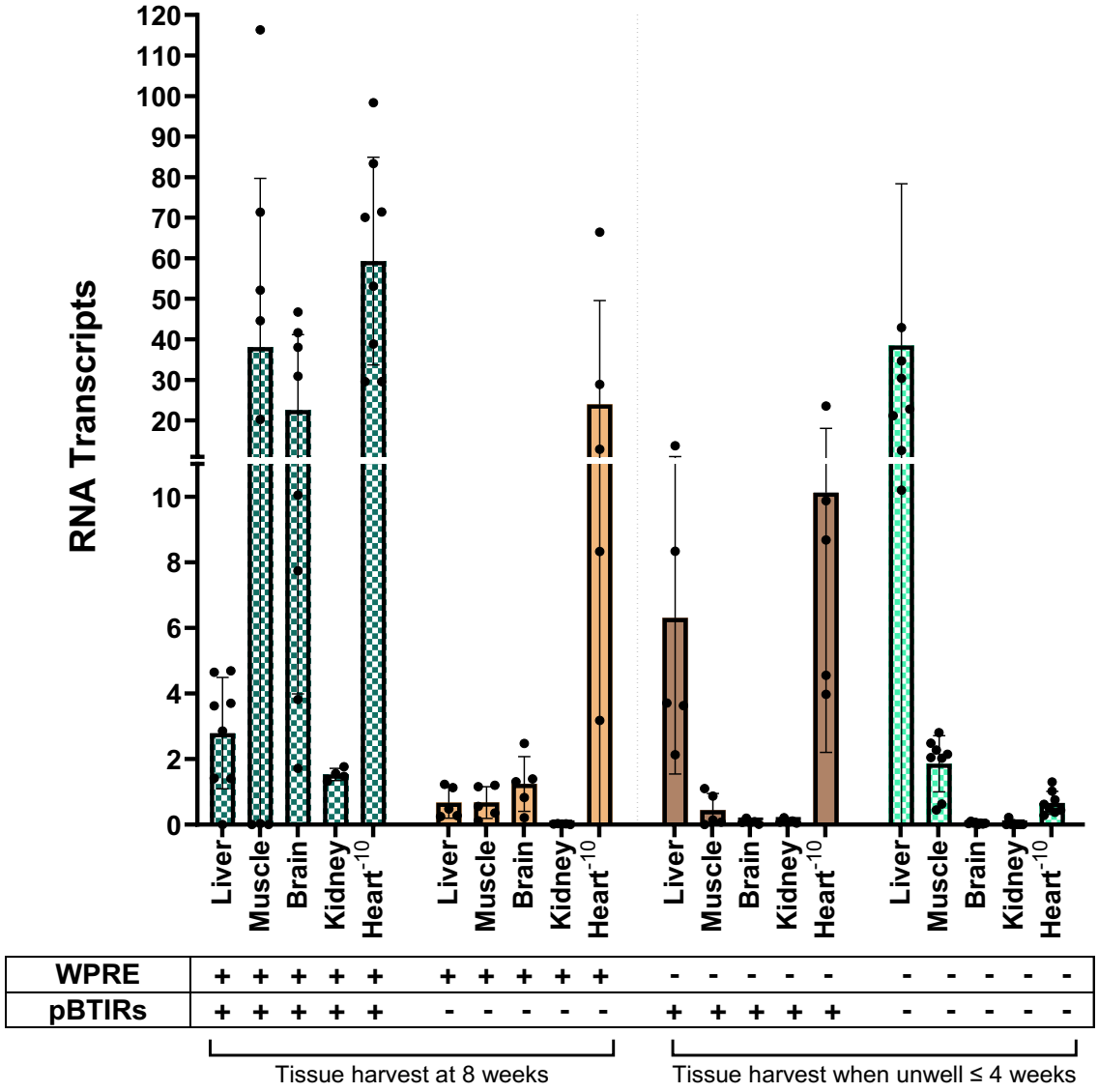

Figure 5-21 Transgene RNA expressed across tissues in DBT$^{-/-}$ treated with rAAV vectors with different *cis*-regulatory elements. DBT$^{-/-}$ mice were treated at D_0 of life with 5×10^{11} VGC/pup of either the transposon vector rAAV2/8.APOe/hAAT.hDBT.WPRE.pBTIR (hDBT.**WPRE.pBTIR,** data from earlier in Chapter 5), rAAV2/8.APOe/hAAT.hDBT.WPRE (hDBT.**WPRE**), rAAV2/8.APOe/hAAT.hDBT.pBTIR (hDBT.**pBTIR**) or rAAV2/8.APOe/hAAT.hDBT (**hDBT**, data from Chapter 4). RNA transcripts were detected via qPCR and each signal normalised to murine β-actin/1000.

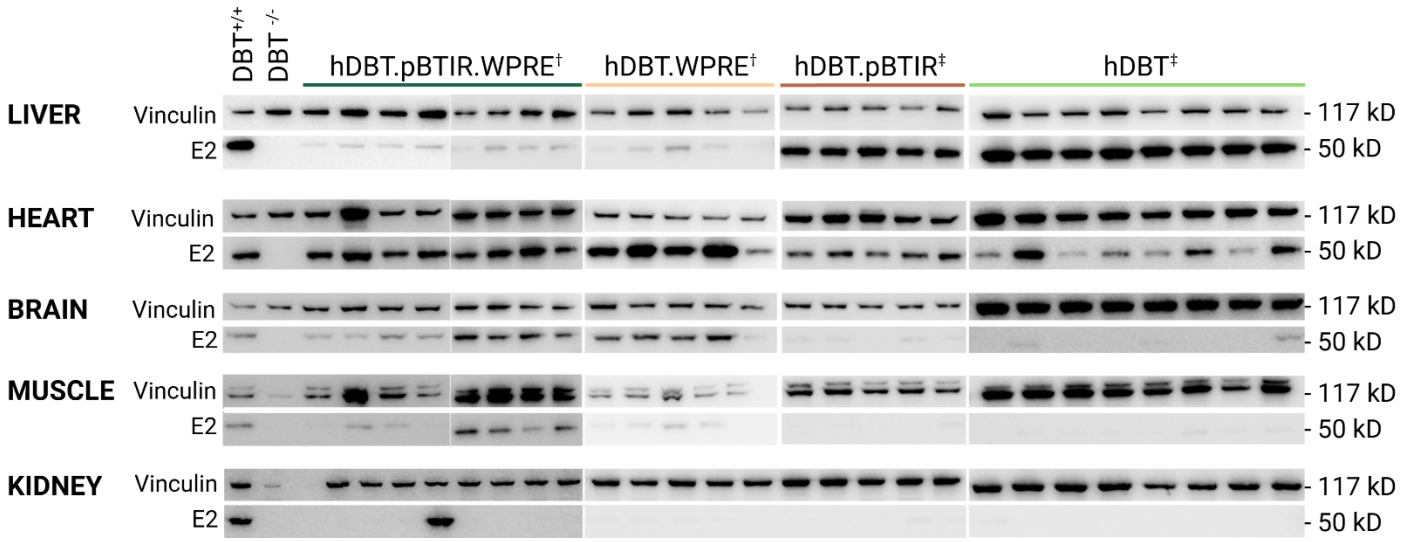
DBT+/+
DBT -/-
hDBT.pBTIR.WPRE†
hDBT.WPRE†
hDBT.pBTIR‡
hDBT‡
LIVER
Vinculin
E2
117 kD
50 kD
HEART
BRAIN
MUSCLE
KIDNEY

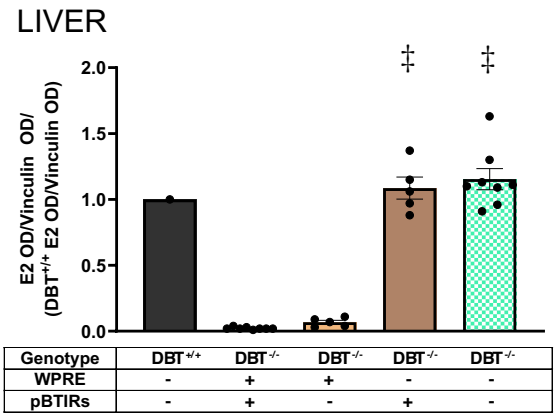
LIVER
E2 OD/Vinculin OD/
(DBT+/+ E2 OD/Vinculin OD)
2.0
1.5
1.0
0.5
0.0
‡
‡
Genotype DBT+/+ DBT-/- DBT-/- DBT-/- DBT-/-
WPRE - + + - -
pBTIRs - + - + -

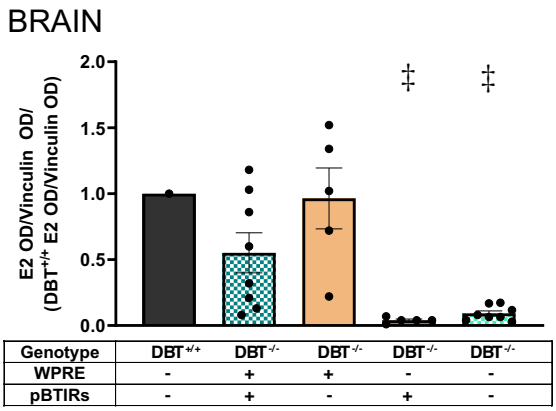
BRAIN
E2 OD/Vinculin OD/
(DBT+/+ E2 OD/Vinculin OD)
2.0
1.5
1.0
0.5
0.0
‡
‡
Genotype DBT+/+ DBT-/- DBT-/- DBT-/- DBT-/-
WPRE - + + - -
pBTIRs - + - + -

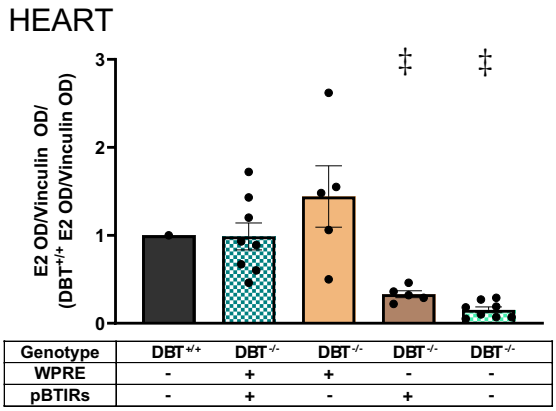
HEART
E2 OD/Vinculin OD/
(DBT+/+ E2 OD/Vinculin OD)
3
2
1
0
‡
‡
Genotype DBT+/+ DBT-/- DBT-/- DBT-/- DBT-/-
WPRE - + + - -
pBTIRs - + - + -

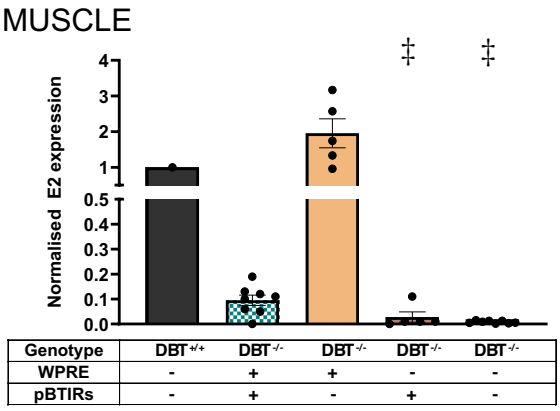
MUSCLE
Normalised E2 expression
4
3
2
1
0.5
0.4
0.3
0.2
0.1
0.0
‡
‡
Genotype DBT+/+ DBT-/- DBT-/- DBT-/- DBT-/-
WPRE - + + - -
pBTIRs - + - + -

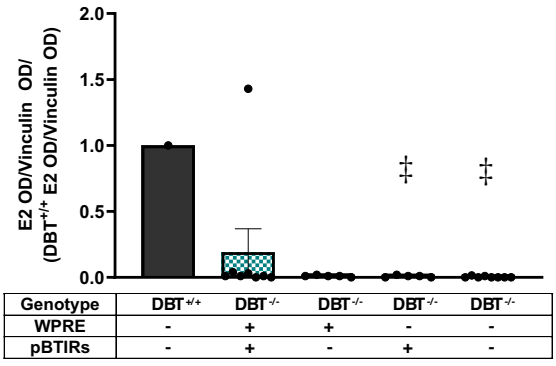
KIDNEY
E2 OD/Vinculin OD/
(DBT+/+ E2 OD/Vinculin OD)
2.0
1.5
1.0
0.5
0.0
‡
‡
Genotype DBT+/+ DBT-/- DBT-/- DBT-/- DBT-/-
WPRE - + + - -
pBTIRs - + - + -

Figure 5-22 (Previous page) E2 protein expression as determined by western blot for DBT$^{-/-}$ treated with AAV with different cis-regulatory elements. DBT$^{-/-}$ mice were treated at D_0 of life with 5×10^{11} VGC/pup of either the transposon vector rAAV2/8.APOe/hAAT.hDBT.WPRE.pBTIR (hDBT.**WPRE.pBTIR,** data from earlier in Chapter 5), rAAV2/8.APOe/hAAT.hDBT.WPRE (hDBT.**WPRE**), rAAV2/8.APOe/hAAT.hDBT.pBTIR (hDBT.**pBTIR**) or rAAV2/8.APOe/hAAT.hDBT (**hDBT**, data from Chapter 4). Each blot was cut and E2 and vinculin probed on respective sections using Anti-DBT (rabbit) and anti-vinculin (mouse) antibodies respectively. E2 and vinculin protein was quantified using Image J. Images are from multiple blots. Positive and negative controls were included in each blot. † Tissues harvested at 8 weeks; ‡ Tissues harvested when mice became unwell, as per Figure 5-18.

5.3.15 Biochemical phenotype of DBT$^{-/-}$ treated with hDBT transgene cassette improved with inclusion of WPRE in expression cassette

In keeping with the observed survival advantage seen in DBT$^{-/-}$ mice treated with rAAV vectors containing a WPRE in the expression cassette had a significantly better biochemical phenotype than mice treated with vectors without a WPRE (Figure 5-23). Mice treated with vector that did not have a WPRE in the expression cassette all became unwell, requiring human euthanasia and their biochemical phenotype was equivalent to that seen in untreated DBT$^{-/-}$ mice.

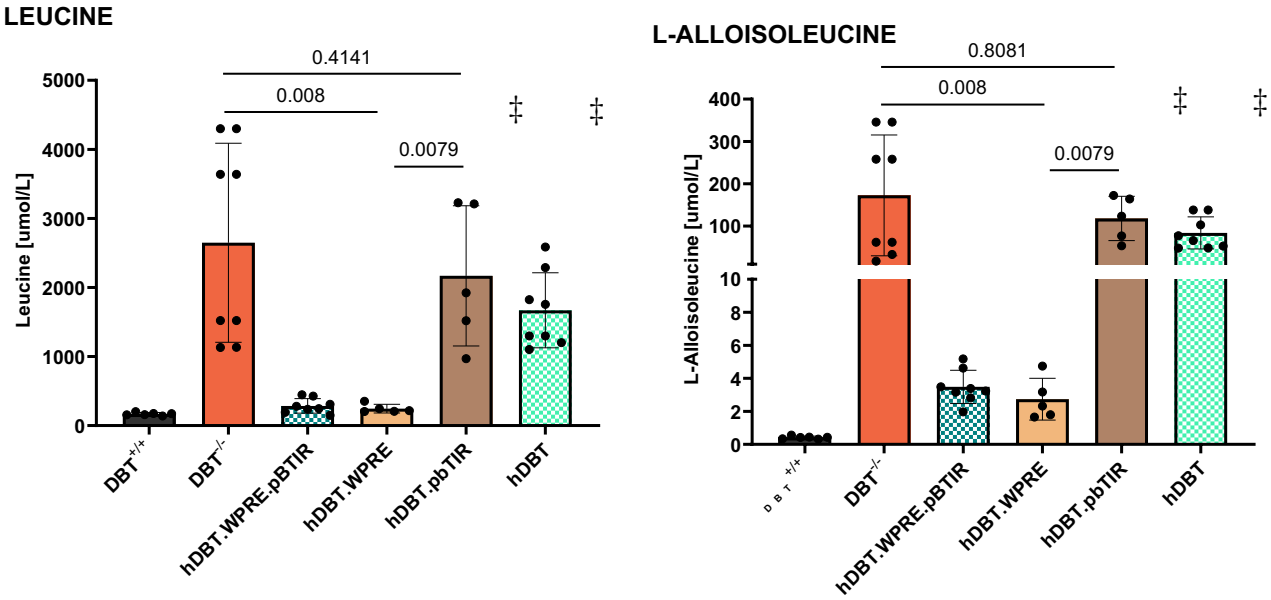

Figure 5-23 Biochemical phenotype in DBT-/- mic treated with AAV vectors with different cis-regulatory elements. DBT$^{-/-}$ mice were treated at D_0 of life with 5×10^{11} VGC/pup of either the transposon vector rAAV2/8.APOe/hAAT.hDBT.WPRE.pBTIR (hDBT.**WPRE.pBTIR,** data from earlier in Chapter 5), rAAV2/8.APOe/hAAT.hDBT.WPRE (hDBT.**WPRE**), rAAV2/8.APOe/hAAT.hDBT.pBTIR (hDBT.**pBTIR**) or rAAV2/8.APOe/hAAT.hDBT (**hDBT**, data from Chapter 4). Levels were determined by tandem mass spectrometry and *p* values determined using two tailed Mann Witney. † Sample collected at 8 weeks of life; ‡ Sample collected when mice became unwell, as per Figure 5-18.

5.3.16 Reproductive success in two male DBT$^{-/-}$ rescued with AAV *piggyBac* transposon system

Two DBT$^{-/-}$ males, #293 and #414 reached adulthood after administration of dual transposon and transposase vector at birth. They were paired with DBT heterozygous females and given the opportunity to breed. Male #293 (DBT$^{-/-}$) sired 6 litters and male #414 (DBT$^{-/-}$) sired 4 litters. There were no wildtype DBT$^{+/+}$ mice born in any litters with an example genogram below (Figure 5-24). Both males are alive as of January 2025 and are 10 months and 8 months old respectively.

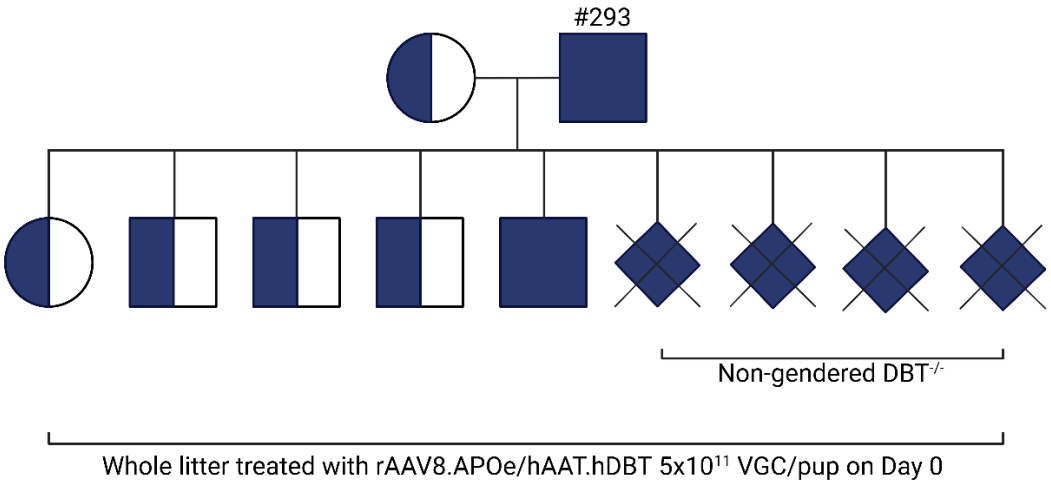

Figure 5-24 Example genogram from pairing a DBT$^{+/-}$ female with DBT$^{-/-}$ male rescued with neonatal administration of piggyBac transposase hybrid gene addition vectors. This litter was treated with rAAV8.APOe/hAAT.hDBT gene addition vector. One male DBT$^{-/-}$ survived to day 22 and the rest died within 48 hours of birth and were gendered not able to be determined.

5.4 Discussion

5.4.1 First report of AAV-mediated rescue of neonatal lethal DBT$^{-/-}$ MSUD model to adulthood

These experiments demonstrate the first successful AAV-mediated gene therapy rescue of a neonatal lethal DBT$^{-/-}$ murine model to adulthood. It is also the first instance of an adult DBT$^{-/-}$ mouse, rescued to adulthood by AAV-mediated gene transfer surviving 48 hours of severe metabolic stress. Whilst the vector configuration of the hybrid AAV/*piggyBac* vector rAAV2/8.APOe/hAAT.hDBT.WPRE.pBTIR was designed to enhance and restrict expression to hepatocytes, this was not observed, and the phenotypic rescue was observed to be equivalent in DBT$^{-/-}$ mice treated with high dose transposon vector independent of co-administration of high dose transposase encoding vector. Whilst an unexpected observation, this equivalent phenotypic correction highlighted the substantial contribution of extra-hepatic tissues transduced with a vector that was not optimised for expression in brain, muscle or cardiac tissue. Through exploring the effect of different *cis*-regulatory elements in AAV expression cassette *in vivo*, it was found that inclusion of a WPRE conferred improved functional transduction of an APOe/hAAT.hDBT expression cassette in the brain, heart and skeletal muscle of DBT$^{-/-}$ mice, independent to the presence of pBTIRs. Furthermore, this extra-hepatic expression in mice treated with the transposon encoding vector was critical to the durability of the vector effect as it was shown that the hepatic levels of E2 expression, even though higher and thus more stable in DBT$^{-/-}$ mice co-transduced with the transposase vectors, did not significantly influence the survival or biochemical correction.

5.4.2 Hybrid AAV/*piggyBac* System underperformed compared to other published studies

Durability of transgene expression with AAV-mediated gene transfer vectors is significantly influenced by the replicative state of the target cell population. For the neonatal murine liver, high mitotic rates of cell division result in rapid loss of AAV vector episomes which limit the durability of neonatally administrated liver targeting conventional AAV gene addition vectors, as demonstrated in Chapter 4 [341]. *PiggyBac* transposase encoding AAV vectors co-transduced with hybrid AAV/*piggyBac* transgene encoding transposons have been used effectively in other model systems to target neonatal livers generating upward of 70-fold increase in hepatic transgene expression persisting into adulthood [274, 275]. In this study, the use of an AAV/*piggyBac* transposon system did improve the stability of hepatic transgene expression, albeit not at clinically significant levels.

Whilst the higher levels of hepatic E2 expression were attributable to *piggyBac* transposase-mediated genomic integrations of the transposon hDBT expression cassette, these higher levels of hepatic E2 expression in $DBT^{-/-}$ mice co-transduced with high dose transposon and transposase encoding vectors did not confer a survival or phenotype correction advantage. Resultingly, in this study the levels of transposition and subsequent E2 protein produced in the liver of $DBT^{-/-}$ mice did not exceed the overall total body correction threshold for BCKDH activity. The E2 levels detected by western blot analysis in $DBT^{-/-}$ mice treated with both transposon and transposase encoding vectors were approximately a quarter of the levels detected for wildtype DBT mice. These expression levels are reflective of more modest levels of transposition than those achieved with the hybrid AAV/*piggyBac* transposase system in other murine models [274]. Given that $DBT^{-/-}$ mice transduced with the simple gene addition vector rAAV2/8.APOe.hAAT.hDBT in Chapter 4 did not survive into the third week of life, despite whole liver E2 protein levels as detected on western blot being supraphysiological, the levels of hepatic transposition and E2

protein expression achieved with the hybrid AAV/piggyBac vectors would be unlikely to support normal BCAA metabolism in the $DBT^{-/-}$ MSUD model or facilitate long term survival.

Despite achieving modest levels of hepatic transposition, the high dose transposon vector was the highest performing vector with regards to $DBT^{-/-}$ mouse survival and biochemical correction and this was independent of co-transduction with a *piggyBac* transposase encoding vector. The transposon vector outperformed the simple gene addition vector from Chapter 4, with mice treated with high dose hDBT transposon encoding vector ($dvDBT^{-/-}{}_{High}$ and $tDBT^{-/-}{}_{High}$) reaching adulthood with significantly improved growth and serum BCAA compared to untreated $DBT^{-/-}$ mice. The degree of biochemical correction in these mice approached wildtype levels when mice were in periods of metabolic stability, however a metabolic stress unmasked a persistent total body BCKDH deficiency.

5.4.3 Implications for extra-hepatic transgene expression under the putatively liver specific enhancer promoter APOe/hAAT

AAV-mediated phenotypic rescue of $DBT^{-/-}$ mice with high dose liver directed transposon encoding vector was demonstrated to be independent of co-administration of the transposase encoding vector. This finding was consistent with the possibility that the improved phenotype correction was secondary to extra-hepatic transgene expression in post mitotic tissues, rather than *piggyBac* transposase-mediated hepatic transgene expression at the high dose. Levels of transgene derived E2 protein detected in brain and heart of transposon-treated mice was equivalent to levels observed in wildtype mice on western blot analysis. Skeletal muscle E2 expression was assessed using the gastrocnemius muscle belly as a representative of transduced skeletal muscle in $DBT^{-/-}$ mice. The high dose transposon encoding vector was seen to increase E2 protein levels in treated $DBT^{-/-}$ mice to one tenth of the levels observed in wildtype gastrocnemius muscle. If skeletal muscle was transduced uniformly by the transposon vector and the same level of E2 was expressed

across all skeletal muscles, it is conceivable that this may have contributed substantially to the phenotypic correction given than skeletal muscle accounts for approximately 50% of total body BCKDH activity in wildtype mice [10]. These observations are consistent with the idea that there is value in further exploration of skeletal muscle as a target for an MSUD gene therapy.

5.3.4 WPRE improves expression of APOe/hAAT.hDBT AAV cassette in extra-hepatic tissues in the DBT$^{-/-}$ mouse model

The extra-hepatic E2 expression profile in DBT$^{-/-}$ mice treated with high dose transposon only, was notably different to that observed in DBT$^{-/-}$ mice treated with the simple gene addition in Chapter 4. This was highly relevant to explore given the significant differences in phenotypic rescue provided by these two vectors despite the vectors using the same AAV capsid serotype and the expression cassette containing identical APOe/hAAT enhancer-promoter, human *DBT* transgene and polyA-signal elements. Where these two vectors differed was in the inclusion of the pBTIRs and WPRE in the transposon encoding vector.

The configuration of vectors with or without the inclusion of the WPRE and pBTIR demonstrated that the inclusion of the WPRE element was crucial in effecting enhanced transgene expression in brain, cardiac and heart tissues, all more stable cell populations that the paediatric liver. This tissue expression profile conferred biologically significant phenotype improvements in the DBT$^{-/-}$ model with regards to overall survival and the leucine levels observed approached levels seen in wildtype mice during periods of metabolically stability. The inclusion of the pBTIR element did not meaningfully change the expression profile of the hDBT transgene or effect any clinically significant improvements in phenotype.

The mechanisms by which the WPRE may have exerted these heightened levels of transgene expression may be secondary to increasing the number of RNA transcripts generated in each

nucleus and may also be tissue dependant. Lentiviral studies have demonstrated that the number of RNA transcripts are increased when an WPRE is included in expression cassettes but that RNA half-life remains unchanged and it is possible that the WPRE may aid in functional export of RNA from the nucleus to aid in protein translation [232]. Clinical AAV vectors treating genetic retinal disorders have also included a WPRE which was demonstrated to improve transgene expression independent of the transgene itself in both *in vitro* and *in vivo* retinal models [423]. In these studies, which included assessment of extra-ocular tissues, WPRE-mediated transgene expression was most pronounced in the liver, brain and muscle tissues [424]. These tissues are highly relevant in MSUD, all three contributing substantially to total body BCKDH activity in humans and this study also demonstrated improved WPRE-mediated transgene tissue expression pattern in brain, heart and skeletal muscle.

These observed variations in the tissue expression profiles of the hDBT transgene are interesting considering the APOe/hAAT enhancer/promoter selected for use in these vectors. Also known as LP1, APOe/hAAT is a composite enhancer/promoter derived from the enhancer region of the apolipoprotein B gene locus of control region and the human alpha-1-antritrypsin promoter and includes the 5' untranslated region upstream of a modified SV40 small t antigen intron [402]. This enhancer/promoter was designed and has been used both preclinically and clinically in liver targeted AAV gene therapy for Haemophilia B. In pre-clinical studies with adult mice using AAV8 serotyped vectors, the vector biodistribution extended beyond hepatocytes, including transduction of testis, spleen, kidney, heart, brain, lung, and bowel, however RNA expression was strictly limited to the liver [402]. In these studies, adult mice were used, however due to the onset of metabolic intoxication in DBT-deficient mice, neonatal vector administration was mandated. During *ex utero* development, many paediatric organs and tissues continue to develop until adulthood. In tissues like the brain, there are significant differences in surface protein expression, cell recruitment and small molecule permeability all of which can influence AAV vector transduction [425]. Age related

transduction differences have been demonstrated with AAV9 serotypes and shown that liver is preferentially transduced in adult mice [426]. It is possible that neonatal vector administration may have increased the biodistribution of the AAV8 vectors used in this study and in conjunction with transgene expression effects exerted by the WPRE, culminated in the significant extra-hepatic rescue of the $DBT^{-/-}$ mouse. These results demonstrate the importance of screening tissues outside the intended target organ despite using a putatively organ restricted enhancer/promoter, in order to fully characterise mechanisms of vector-mediated phenotype correction.

5.4.5 Dose of AAV/*piggyBac* transposon encoding vector influences tissue biodistribution in organs relevant to BCKDH expression

In the low dose cohorts of these experiments, no $DBT^{-/-}$ mice treated with low dose vectors survived to adulthood, demonstrating that the minimally effective dose of transposon encoding vector was above 5×10^{10} vcg/pup. In these mice, the E2 protein expression was predominantly hepatic. Coupled with the observation that vector concentrations detected in the brain and heart of low dose cohorts was much lower than detected in the high dose cohorts, the lower vector doses used may have been insufficient to transduce these extra-hepatic tissues sufficiently. The low dose vector treated $DBT^{-/-}$ mice all required humane sacrifice around 3-4 weeks of age, which also provided insight into the levels of hepatic transgene with respect to vector copy number and E2 expression at this time point, too. At this time point, hepatic E2 expression was detected at 3-5 times higher than that observed in wildtype mice, further supporting the finding from Chapter 4 that physiological levels of a human DBT transgene derived E2 protein is insufficient to restore BCAA homeostasis in a murine MSUD model. It may also be possible that the translated E2 protein from the human DBT transgene interacts sub-optimally with the rest of the murine BCKDH subunits. This could be tested by using the murine DBT transgene in future experiments.

5.4.6 Translational lessons from hybrid AAV/*piggyBac* gene addition

These experiments attempted to answer if a hybrid AAV/*piggyBac* transposon system, rationally designed to target murine livers, could be used to improve the stability of gene transfer and expression of a hDBT transgene in murine hepatocytes. Whilst there were modest levels of hepatic transposition and corresponding increases in E2 protein with co-administration of high dose transposon and transposase encoding vectors, any positive contribution to the improved phenotype was superseded by extra-hepatic E2 expression. The implication of this observation is that even at the highest levels of hepatic transduction and integration achieved with the hybrid AAV/*piggyBac* system, the BCKDH enzyme level activity achieved in the $DBT^{-/-}$ murine livers did not exceed the total body therapeutic correction threshold. Coupled with the results from Chapter 4 and also with the reliance of extra-hepatic expression to provide enduring phenotypic correction, gene transfer to the paediatric liver regardless of the efficiency, may not be sufficient to provide clinically meaningful phenotype correction in a neonatal lethal murine $DBT^{-/-}$ model of MSUD. It is possible that a muscle targeting vector may further enhance the transgene expression observed with the liver directed transposon vector with the potential for even greater phenotypic correction.

In conclusion, these results from this Chapter demonstrate the rescue of $DBT^{-/-}$ mice to adulthood with a biochemical phenotype approaching wildtype using 5×10^{11} VCG of AAV APOE/hAAT.hDBT expression vectors containing a WPREs. Phenotypic rescue occurred independent of co-administration with a *piggyBac* transposase encoding vector and extra-hepatic tissue expression of the transgene protein E2 significantly contributed to the phenotypic rescue. The hDBT transgene was expressed in extra-hepatic tissues at therapeutic levels conferring significant phenotypic correction under a putative liver specific promoter enabled by inclusion of a WPRE. Optimising a therapeutic AAV vector for a post-mitotic tissue, such as striated myocytes, may represent a viable strategy to successfully target paediatric organs whilst overcome the inherent challenges in targeting paediatric livers with a predominantly episomal vector system.

Chapter 6

Muscle targeted AAV gene therapy rescues MUSD Murine Model to adulthood

6.1 Introduction

The challenges of achieving stable gene transfer in neonatal murine livers using AAV-mediated gene delivery were not able to be overcome with the liver-directed *piggyBac* hybrid vectors described in Chapter 5. An alternative approach to liver directed AAV gene therapy for MSUD may be to target muscle tissue. In humans, muscle tissue accounts for approximately 50% of total body BCKDH activity and represents a more stable cell population compared to the neonatal liver [10, 30]. These favourable tissue characteristics, in conjunction with contemporary advances in myotrophic AAV capsids and promoters/enhancer elements, may together overcome some of the limitations observed with a liver targeted AAV strategy and enable enduring, stable gene transfer following neonatal vector administration.

6.1.1 Muscle Trophic Capsids

The number of striated muscle trophic capsids has expanded since the discovery of AAV2, which itself has limited murine or human muscle transduction [427]. Vectors pseudoserotyped with the AAV8, AAV9, AAVrh74 and AAV6 capsids have demonstrated higher skeletal muscle transduction efficiencies and have been validated in clinical trials, but have been outperformed by more recent, highly efficient, bioengineered serotypes AAVMYO [368] and MyoAAV [369] in pre-clinical murine studies. AAVMYO was selected via a capsid shuffled library injected into CB57B/6J mice and shown to have superior transduction efficiency in murine cardiac, quadriceps

and diaphragmatic tissues compared to all other capsid variants tested. These novel synthetic capsids were engineered using directed evolution strategies and both AAVMYO and MyoAAV capsids contain an "RGD motif" of Arginine, Glycine and Aspartic Acid which allows interaction with muscle integrin surface receptors and may be the mechanism underlying superior transduction of striated myocytes in mice compared to AAV9 [428]. Furthermore, AAV vectors pseudoserotyped with AAVMYO have been demonstrated to preferentially transduce skeletal and cardiac muscle over liver and are highly effective at transducing across skeletal muscle fibre types, including type I (slow twitch) and types IIa and IIb (fast twitch).

The preferential transduction of striated myocyte cells by AAV vectors pseudoserotyped with new generation capsids AAVMYO and MyoAAV opens the possibility to other desirable effects when conceiving a muscle directed AAV gene therapy. Improved muscle transduction efficiencies may allow lower vector doses to be used which have important follow-on effects to reducing immunogenicity, reducing risk of systemic vector side effects and the eventual cost of the therapy. The preferential transduction of muscle cells also results in less vector entering non-target tissues, and subsequently reduces off target effects, thereby improving safety. The discovery of these new generation AAV capsids with highly efficient muscle transduction is an important development for generating a clinically viable AAV therapy for MSUD.

6.1.2 Engineering *cis*-regulatory elements of the rAAV cassette to improve muscle transgene expression

Whilst AAV capsid serotypes can influence transgene expression, engineering cis-regulatory elements such as enhancers, promoters, introns and microRNA (miRNA) mediated transgene post-transcriptional regulation can all be utilised to enhance transgene expression in myocyte cells. Non-tissue specific strategies include transgene codon optimisation, transgene CpG motif

reduction and using modified ITRs to generate self-complimentary dsDNA (rather than conventional ssDNA) with the aim to improve the efficiency of transcription and thus translation.

6.1.2.1 Selecting promoters for enhanced AAV vector transgene expression in muscle

In designing AAV expression cassettes to optimise muscle specific transgene expression a choice is often faced between selection of a ubiquitously expressing promoter or a more muscle restricted promoter. Ubiquitous promoters drive expression across multiple tissues, cell types and cell cycles. Widely used ubiquitous promoters include elongation factor 1α (E1-Fα), chicken beta-actin with CMV enhancer (CAG), ubiquitin C (UbC) and combination promoter/enhancers like the cytomegalovirus (CMV) promoter/enhancer. Widespread transgene expression can be desirable for certain gene transfer strategies, however certain promoters such as CMV and EF-1α are at risk of silencing over time through methylation of both CpG and non-CpG sites, resulting in decreased transgene transcription [429]. In conditions such as MSUD where there is an unmet need for an enduring gene therapy with stable, life-long transgene expression, promoter silencing is not desirable. Furthermore, expression in non-target tissues may induce increased immunogenicity and result in side effects such as antibody responses directed against transgene products attenuating the therapeutic benefit or driving more serious systemic inflammatory responses [430-433]. Many of these immune reactions have been demonstrated to be dose dependent, reinforcing the need for highly efficient transgene expression to allow for vector dose minimisation [433].

Several highly efficient muscle specific promoters have emerged over the past decade, mostly in relation to research for congenital muscular dystrophies. The size of the human dystrophin gene exceeds AAV viral vector packaging limitations and influenced research into promoters with robust muscle expression at increasingly small nucleotide lengths. Early muscle specific promoters were derived from promoter regions associated with the human skeletal actin (HAS) gene and desmin gene. These promoters, whilst highly muscle specific have largely been superseded by

shorter promoters with equal or better transcriptional efficiency [434]. Other muscle specific enhancer/promoters include synthetic promoters from myogenic transcription factors [435] and those derived from the muscle creatine kinase promoter, including CK6 [436], MHCK7 [437], dMCK and tMCK [438] and CK8 and CK8e [371, 439].

CK8e is of particular interest to this project. Recent canine studies in a Duchene muscular dystrophy disease model demonstrated robust skeletal muscle expression with near undetectable hepatic expression of a micro-dystrophin protein under the transcriptional regulation of the CK8e promoter following delivery using an AAV9/2 vector [440]. This protein expression pattern reflects the limited hepatic transcriptional activity of the CK8e promoter. Along with the advent of AAV capsids capable of highly efficient muscle transduction, the CK8e promoter could be utilised in the $DBT^{-/-}$ murine model to generate a single organ muscle directed approach for MSUD using AAV gene transfer.

6.1.2.2 MicroRNAs can be used to direct tissue specificity of transgene expression

MicroRNAs are gene regulatory molecules consisting of non-coding RNAs, approximately 18-24 bp in length with critical roles in tissue specific post-transcriptional gene regulation influencing cell proliferation, differentiation and apoptosis [441, 442]. Transcription of miRNAs is undertaken by polymerase II and once transcribed miRNAs form long hairpin precursor transcripts. These structures have a guide strand that can stably interact with mature RNA transcripts via complementary base pairing to silence translation by either inhibition of translation or mRNA degradation [443]. In this way, miRNAs influence the expression in over one third of human genes with conserved miRNA targeting sites and over 60% of mammalian protein coding genes are regulated by at least one miRNA [443-445].

MiRNAs have been found widely across animals, including humans, mice and plants with some homology between species [446]. Pre-clinical studies exploring miRNAs have demonstrated broad applications including decreasing viral pathogenicity and generating stable miRNA knockdown models to study cancer. The endogenous expression patterns of miRNAs have also been implicated in other conditions such as neurodegenerative diseases like Parkinson's, psychiatric diseases like schizophrenia and also after traumatic brain injury [447-449]. More recently, miRNA targeting sites have been used to influence tissue specific expression of transgenes delivered by AAV vectors [450-452].

Improving the tissue specificity, by way of de-targeting tissues where expression is not desirable, is highly relevant for many gene therapy strategies. De-targeting a particular tissue using miRNAs can be achieved through inclusion of one or more miRNA targeting sites (miRNA-TS) in vector transgene cassettes. In one study using AAV9 vectors in mice, a GFP encoding transgene cassette included three *mi*R-122-TS (miR-122 is the historical name for *mi*R-122-5p-TS) corresponding to the miRNA *mi*R-122, which is highly expressed in the human liver and has 100% homology in mice. The inclusion of these miRNA-TS resulted in absent expression of eGFP transgene cassette in murine hepatocytes without compromising target tissue expression [452].

This Chapter describes the rational design of a muscle optimised AAV gene addition vector using miRNA-TS to de-target liver and brain expression in order to determine if targeting a single organ system, straited muscle, in the DBT neonatal lethal murine MSUD model is a viable strategy for phenotypic rescue. The results in this chapter explore hypothesis 5 and aim 5 and 6 (see Chapter 1.6).

6.2 Chapter 6 specific methods

6.2.1 Identifying miRNA-TS sequences for liver and brain

The miRNA Tissue Atlas database [453] was used to identify ten candidate human miRNAs (hsa-miRNAs) with high activity in liver and brain, and low activity in skeletal muscle. Nucleotide sequences of the miRNAs were identified with the miRDB online database [454]. The miRNAs were then ranked based on level of activity in liver, brain, heart and skeletal muscle (Figure 6-1). The top liver miRNA was human- (hsa-) *mi*R-122-*5p* and the brain miRNA selected was hsa-*mi*R-124-*3p*. The homology between murine and hsa-*mi*R-124-*3p* is not well characterised, however murine studies have demonstrated neuronal activity of hsa-*mi*R-124-*3p* and so the human targeting site was used. As *mi*R-122-*5p* is 100% homologous between human and mouse no coding changes were required for the hsa-*mi*R-124-*5p*.

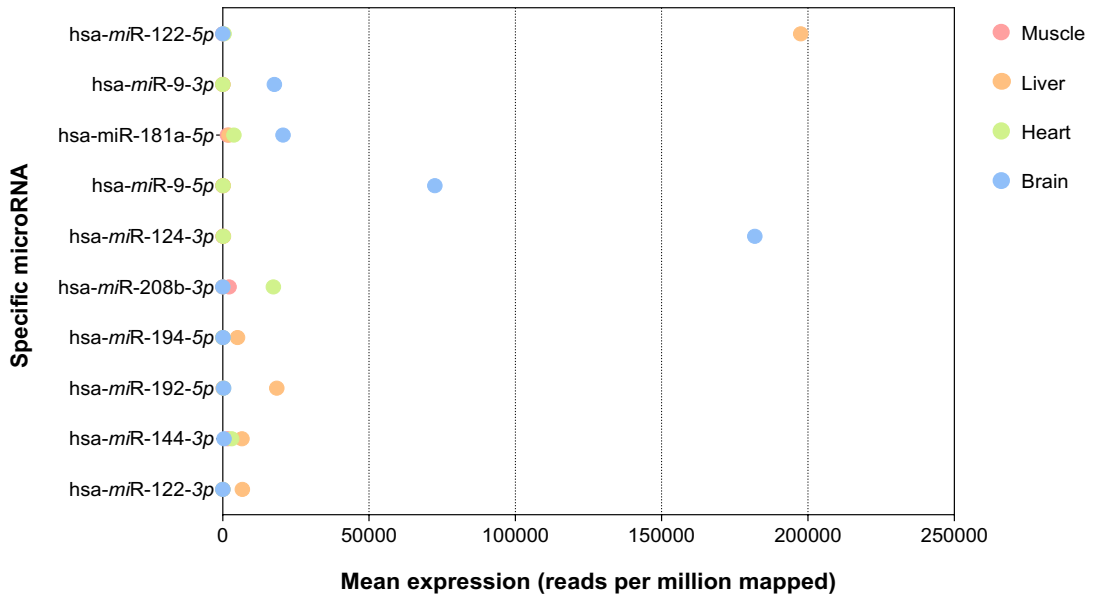

Figure 6-1 Candidate human miRNAs (hsa-*mi*R) and their relative expression in muscle, liver, heart and brain tissue. Candidate miRNAs were identified using an online database, miRNA TissueAtlas 2025 [453]. The highest expressing miRNA in liver and brain were then also ranked for lowest expression in muscle to generate the top ten candidate miRNAs displayed in the above graph.

6.2.2 Synthesis of muscle optimised AAV hDBT expression vector

A transgene expression plasmid was designed *in silico* with, from 5'-3', a CK8e promoter, SV40 intron, hDBT gene, WPRE, and triplicate repeats of the miRNA-TS for *miR*-122-*5p* (liver) and *miR*-124-*3p* (brain) and BGHpA. This plasmid, designated pCK8e.hDBT.WPRE.miRNA-TS was then synthesised by GenScript (Piscataway, U.S.A) and used to generate the pAAV2.CK8e.hDBT.WPRE.miRNA-TS plasmid (Figure 6-2) through restriction digest and T4 DNA ligation. DH5a cells were transformed with the ligation products and colonies selected and screened via restriction digest and sanger sequencing (AGRF, Westmead Institute of Medical Research, Australia). The muscle trophic AAV expression vector was then generated through triple transfection of HEK293 cells with pAAVMYO [368], plasmid donated by TVRU, CMRI, Australia), pAAV2.CK8e.hDBT.WPRE.miRNA-TS and pAd5 and purified via CsCl gradient as per Chapter 2.2.5 to generate the muscle trophic AAV vector designated rAAV2/AAVMYO.CK8e.hDBT.WPRE.miRNA-TS. Vector genome titre was determined using ddPCR as per Chapter 2.2.7.2.

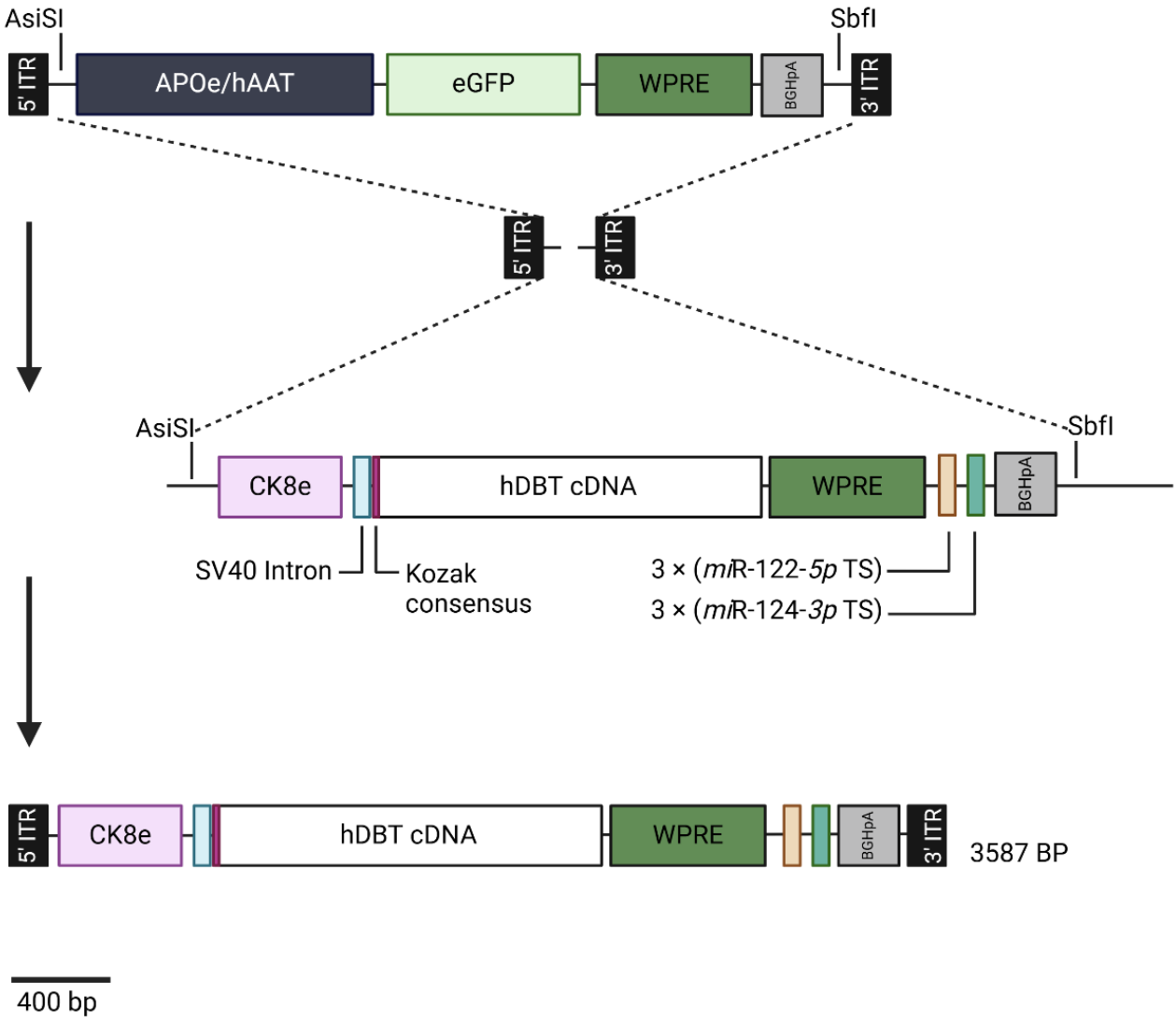

Figure 6-2 Flow diagram of molecular sub-cloning steps taken to generate pAAV2.CK8e.hDBT.WPRE.miRNA-TS. Detailed explanations of subcloning steps are described in Section 6.2.2. The expression cassettes are flanked by AAV ITRs (black boxes). Digest sites are marked with corresponding restriction enzymes. Other DNA components illustrated are the APOe/hAAT promoter enhancer, enhanced green fluorescent protein, eGFP, (light green box), woodchuck hepatitis post-transcriptional element, WPRE (dark green box), human *DBT* coding sequence preceded by Kozak consensus sequence (magenta), hDBT cDNA (white box) and bovine growth hormone polyadenylation signal, BGHpA (light grey boxes). miRNA targeting sites (3 × *mi*R-122-*5p* (tan box) and 3 × *mi*R-124-*3p* (teal box)) and the SV40 intron (light blue box) are marked on diagram. Scale bar = 400 bp. Figure created in BioRender.

6.2.3 Animal Experiments

$DBT^{-/-}$ pups were injected on post-natal day 0 (D_0) as close to birth as possible with IP $5x10^{11}$ VGC/pup of rAAV2/AAVMYO.CK8e.hDBT.WPRE.miRNA-TS in a volume of 10 μL. Pups were weighed daily until day 21, then weekly thereafter until reaching 56 days of life (D_{56}). Surviving $DBT^{-/-}$ pups were placed on a high protein diet at D_{56} for 48 hours, weighed every 24 hours and BCAA collected at 0 hours (h) and 48 h of high protein diet. The experiment was ended after the 48 h blood collection, animals humanely euthanised and biospecimens collected.

Individual muscle tissues for $DBT^{-/-}$ mice excepting the gastrocnemius muscle were difficult to harvest. Resultingly, $DBT^{-/-}$ gastrocnemius tissue was used as a negative loading control for all skeletal muscles in western blot analysis. Positive controls from $DBT^{+/+}$ mice were used from the corresponding muscle groups.

6.2.4 Statistical Analyses

Statistical analyses were undertaken using GraphPad Prism 10.4.1 using the nonparametric Mann-Whitney U test as normal distribution was not assumed due to small sample size. Log-Rank test was used to assess statistical significance of survival. Wilcoxon matched-pairs signed rank test use to assess changes in weight and BCAA levels between day 28 and day 56.

6.3 Results

6.3.1 Muscle optimised AAV vector provides enduring rescue of neonatally treated DBT$^{-/-}$ to adulthood

Neonatal administration of rAAV2/AAVMYO.CK8e.hDBT.WPRE.miRNA-TS at a dose of 5×10^{11} VGC via IP injection significantly improved survival of DBT$^{-/-}$ pups (n = 9) with 56% survival at 56 days compared to untreated DBT$^{-/-}$ (Figure 6-3). Growth of DBT$^{-/-}$ treated with the muscle optimised vector tracked in a similar manner to that seen in DBT$^{+/+}$ (Figure 6-4). The final average weight of DBT$^{-/-}$ (n = 5) treated with the muscle optimised AAV at 56 days was statistically similar to DBT$^{+/+}$.

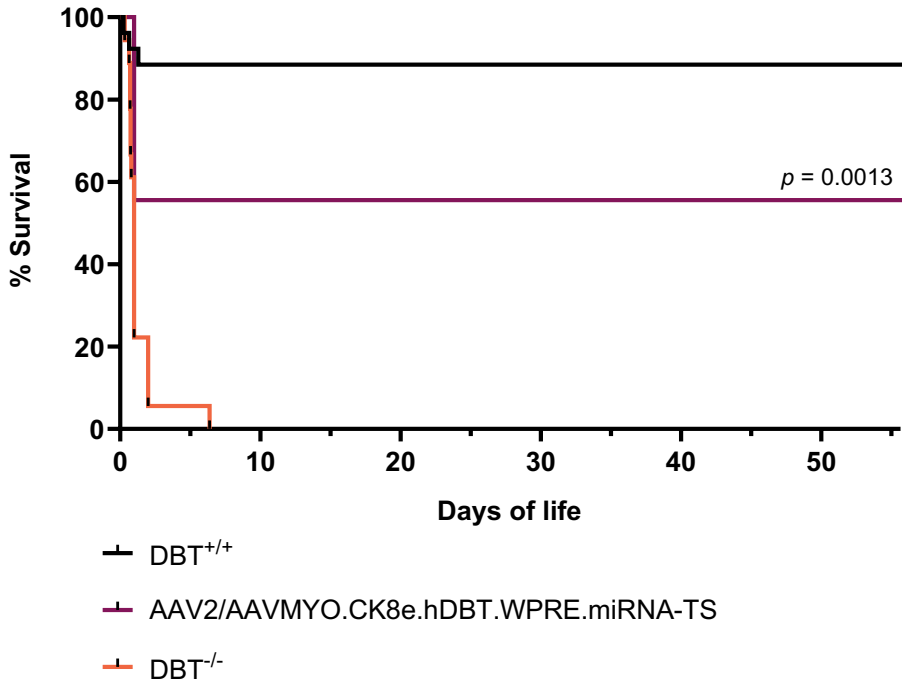

Figure 6-3 Survival of DBT$^{-/-}$ following neonatal delivery of muscle optimised AAV gene delivery vector. DBT$^{-/-}$ pups (n = 9) were injected via IP route with 5×10^{11} VGC per pup of rAAV2/AAVMYO.CK8e.hDBT.WPRE.miRNA-TS and had significantly improved survival compared to untreated DBT$^{-/-}$ pups ($p = 0.0013$, Log-rank (Mantel-Cox)).

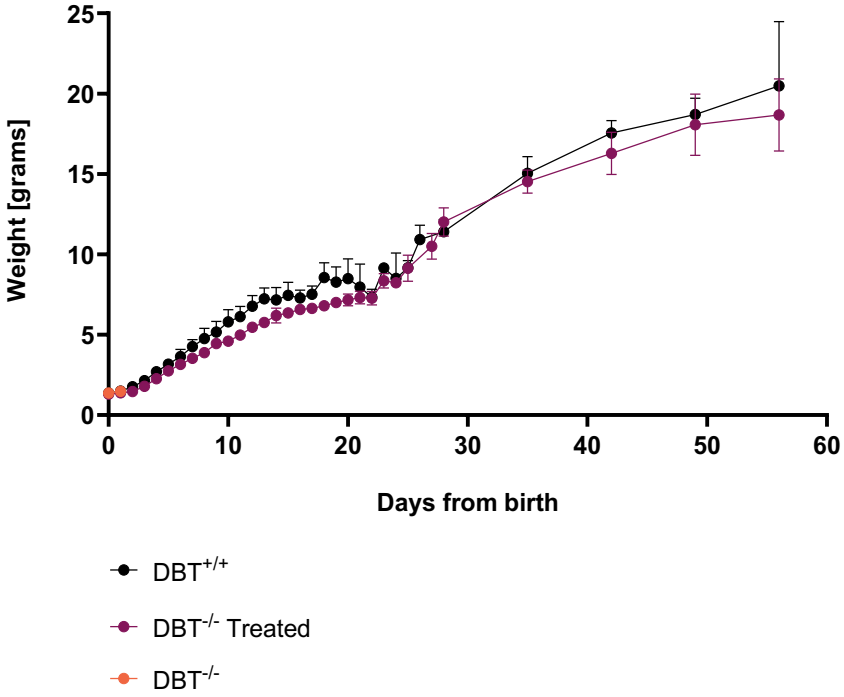

Figure 6-4 Growth of DBT$^{-/-}$ following neonatal delivery of muscle optimised AAV gene delivery vector. DBT$^{-/-}$ pups (n = 9) were treated at birth with IP 5 × 10^{11} VGC per pup of rAAV2/AAVMYO.CK8e.hDBT.WPRE.miRNA-TS. Dots represent mean weight (grams) ± standard deviation for each group.

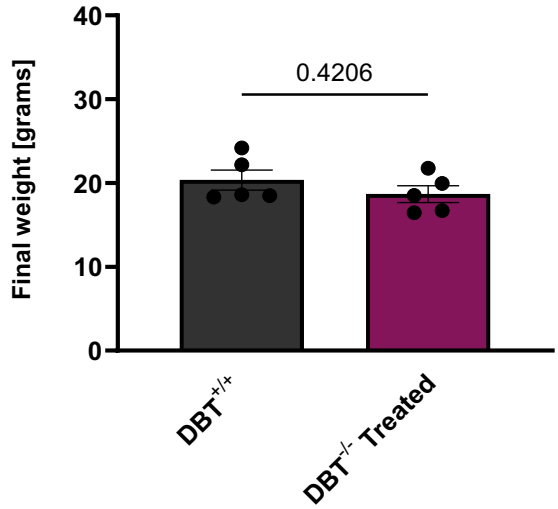

Figure 6-5 Comparison of weights at 8 weeks of age for wildtype and vector treated DBT$^{-/-}$. Muscle optimised vector treated mice that reached adulthood (n = 5, IP injection of 5 × 10^{11} VGC per pup rAAV2/AAVMYO.CK8e.hDBT.WPRE.miRNA-TS) had comparable weights at 8 weeks of age with wildtype DBT$^{+/+}$ (p = 0.4206). Previously shown data from DBT$^{-/-}$ treated with 5 × 10^{11} VGC per pup of rAAV2/8.APOe/hAAT.hDBT.WPRE (n = 8) is also displayed. Column height represent mean with bars ± standard error mean. Mann Witney test used to determine statistical significance.

6.3.2 Neonatally administered rAAV2/AAVMyo.Ck8e.hDBT.miRNA broadly transduces striated muscle groups

Vector transduction was assessed in liver, brain, kidney, cardiac muscle and skeletal muscles (gastrocnemius, hamstring, quadriceps, diaphragm, triceps and masseter). Vector copies were detected in all tissues tested, with the highest concentration in the liver and diaphragm, potentially a reflection of the intraperitoneal injection route and the physical proximity of these tissues in the abdominal cavity (Figure 6-6).

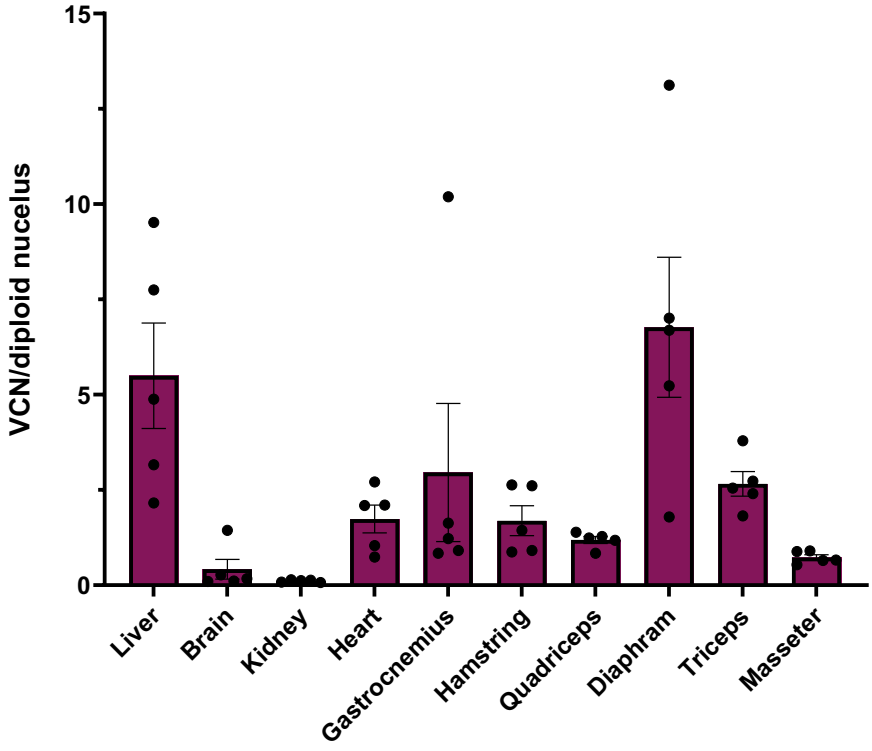

Figure 6-6 Vector biodistribution at in DBT$^{-/-}$ 8 weeks after neonatal IP injection with with rAAV2/AAVMYO. CK8e.hDBT.WPRE.miRNA-TS. Tissues were harvested from DBT$^{-/-}$ pups upon reaching adulthood. Genomic DNA was extracted from tissues and vector genome copies (VGC) per diploid nucleus quantified using ddPCR and signals normalised to murine albumin copies. Error bars represent mean and ± standard error mean.

6.3.3 CK8e promoter drives supraphysiological expression of hDBT transgene across whole skeletal muscles in DBT$^{-/-}$ mice

The RNA expression profile of the hDBT transgene observed in DBT$^{-/-}$ treated with the muscle optimised vector demonstrated predominance of expression in myocyte tissues (Figure 6-7). The gastrocnemius, quadriceps and triceps muscle groups had more than 1000-fold higher hDBT transgene RNA expression detected compared to liver tissue ($p = 0.0079$). The expression in cardiac tissue was more than 100-fold higher than the hDBT transgene RNA expression in liver tissue ($p = 0.0079$). Out of the non-myocyte tissues, liver had the highest RNA transgene expression.

E2 protein expression in DBT$^{-/-}$ mice treated with the muscle optimised vector was assessed with western blot (Figure 6-10). Across all sampled skeletal muscles, the E2 expression levels were 10 to 100-fold above that seen in wildtype adult mice at the same age (56 days). Cardiac muscle E2 expression in DBT$^{-/-}$ mice was approximately the same as wildtype levels. The E2 expression in liver, brain and kidney tissues of DBT$^{-/-}$ mice treated with the muscle optimised vector was between 10 to 100-fold lower than levels seen in wildtype mice, but still detectable. Immunofluorescence staining to detect E2 expression in hepatic tissues showed minimal E2 tissue expression (Figure 6-11) compared to sections from DBT$^{-/-}$ treated with liver directed vectors in Chapter 5.

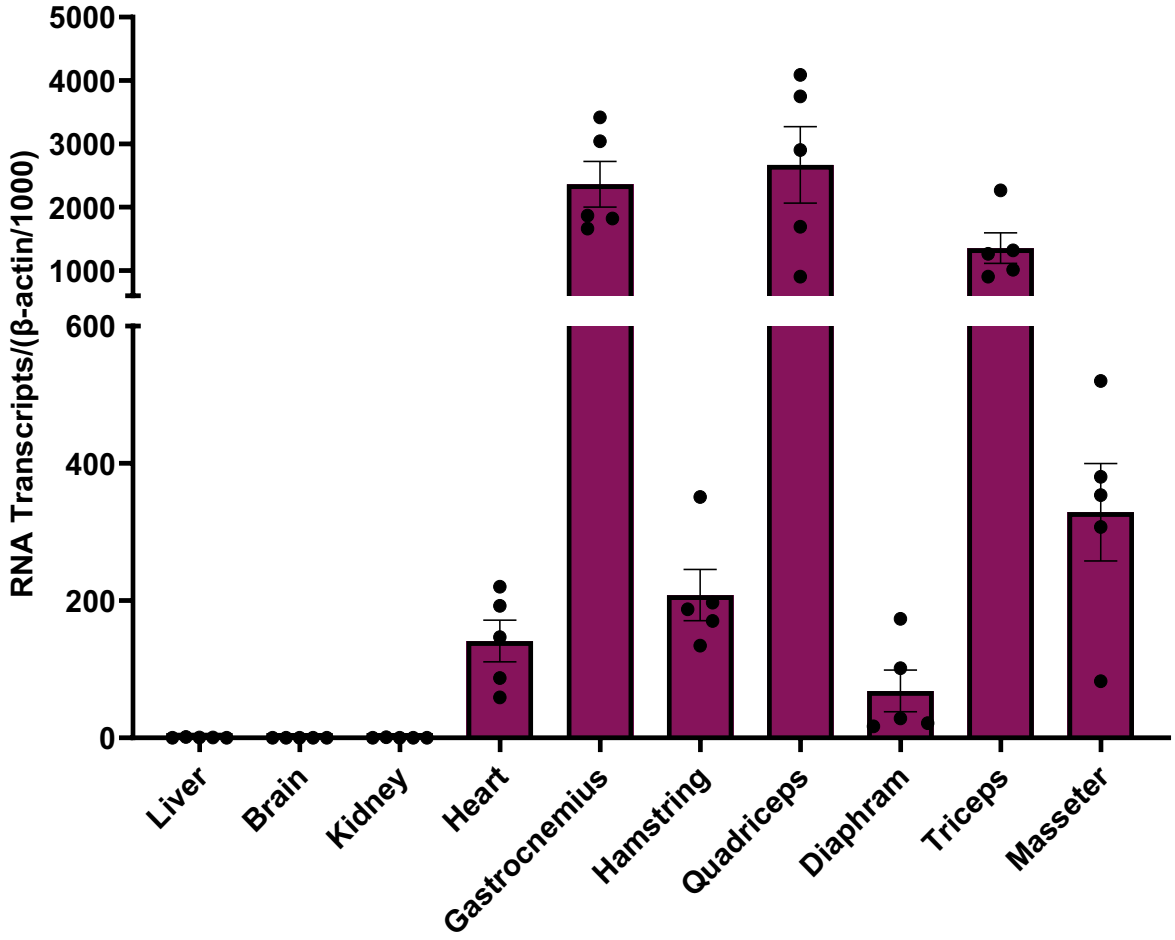

Figure 6-7 Relative transgene RNA transcripts detected in DBT$^{-/-}$ mice 8 weeks after treatment with rAAV2/AAVMYO.CKe.hDBT.WPRE.miRNA-TS. DBT$^{-/-}$ (n=5) were injected with 5×10^{11} VGC per pup at birth, tissues harvested and RNA extracted as and cDNA synthesised. Transcript reads are relative to the difference between RT+ and RT- PCR reactions for each sample, normalised to murine β-actin PCR signal for each sample. Error bars represent mean and ± standard error mean.

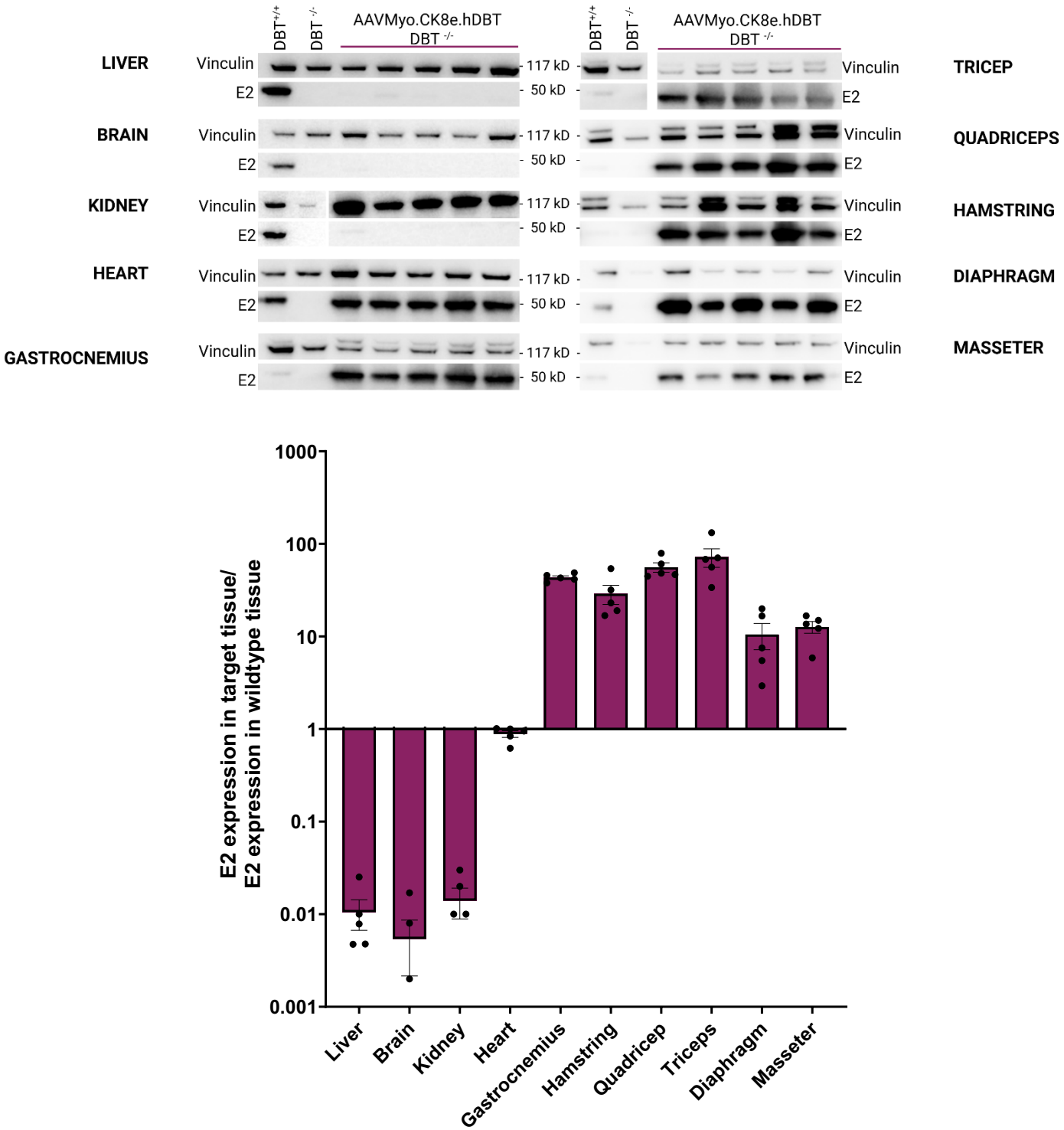

Figure 6-8 E2 protein detected in DBT$^{-/-}$ treated with muscle optimised AAV vector. Protein extracted from 8 week old DBT$^{-/-}$ (n=5) treated with neonatal IP injection on day 0 of life of rAAV2/AAVMYO.CK8e.hDBT.WPRE.miRNA-TS 5×10^{11} VGC per pup. Blots were cut at 75 kD after transfer to nitrocellulose and probed for vinculin and E2 protein. Relative E2 protein expression was determined by measuring the optical density (OD) of E2 for a certain tissue, (E2 OD/ vinculin OD) and then dividing by the wildtype E2 expression (WT tissues E2/Wildtype tissue vinculin OD). OD was determined in ImageJ. Error bars represent mean and ± standard error mean.

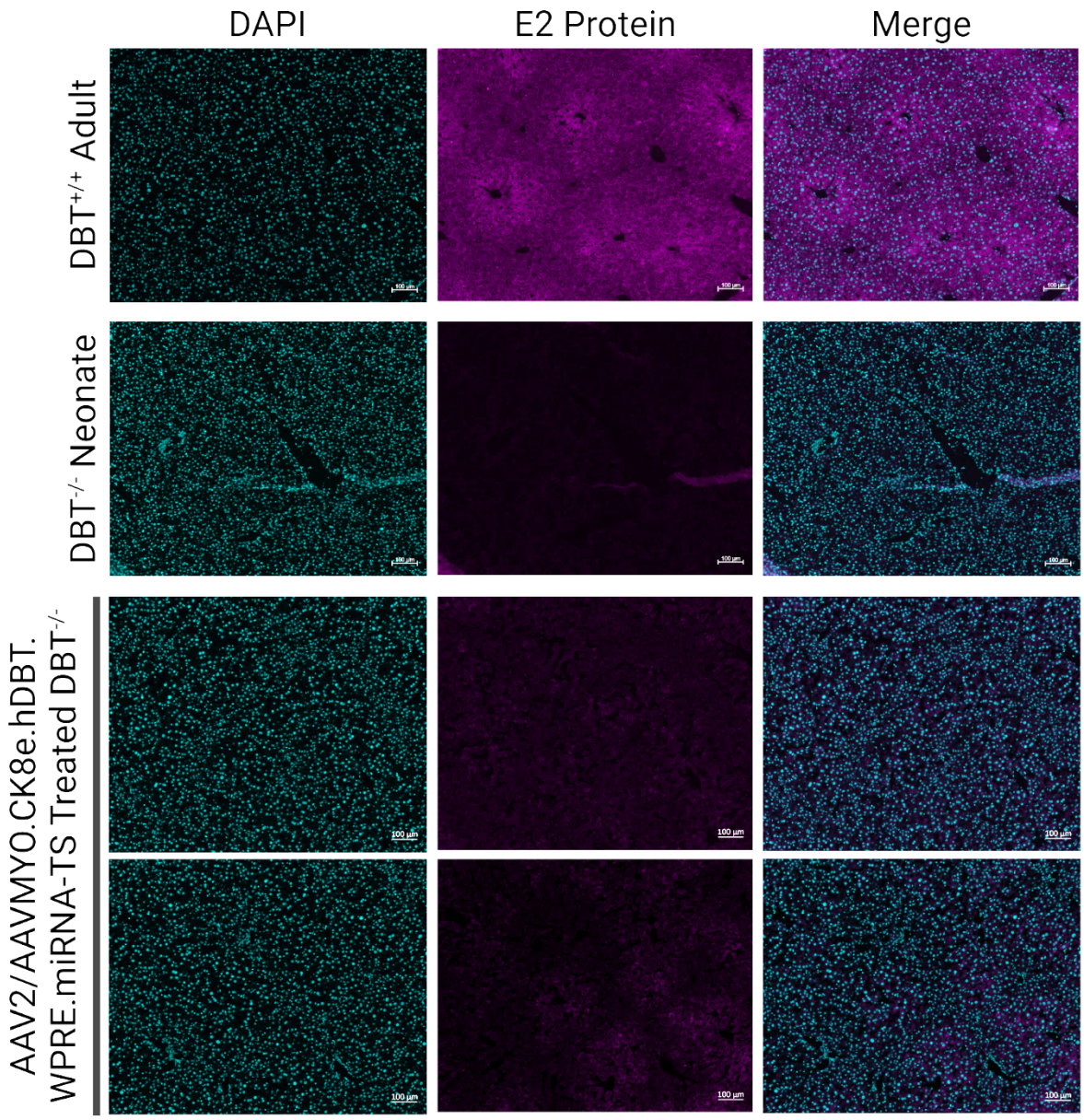

Figure 6-9 Representative liver immunofluorescence images from 8 week old DBT$^{-/-}$ mice treated with rAAV2/AAVMYO.CK8e.hDBT.WPRE.miRNA-TS. Liver sections were taken from 8 week old DBT$^{-/-}$ mice injected at birth with IP 5 × 10^{11} VGC per pup with rAAV2/AAVMYO.CK8e.hDBT.WPRE.miRNA-TS. Seven µm sections were probed for E2 protein with anti-DBT antibody (1:200, polyclonal Rabbit IgG, Invitrogen) and secondary Donkey anti-Rabbit antibody conjugated to Alexa Fluor® 594 and imaged under a light microscope. Scale bar equals 100 µm. Figure created in BioRender.

Analysing the amount of E2 protein per vector episome in tissues transduced with the muscle optimised vector demonstrated high expression across skeletal muscle compared to cardiac and non-myocyte tissues (Figure 6-10). This demonstrated that the CK8e promoter and multiple miRNA-TS conferred skeletal myocyte-restricted expression of the rAAV2/AAVMYO.CK8e.hDBT.WPRE.miRNA-TS vector.

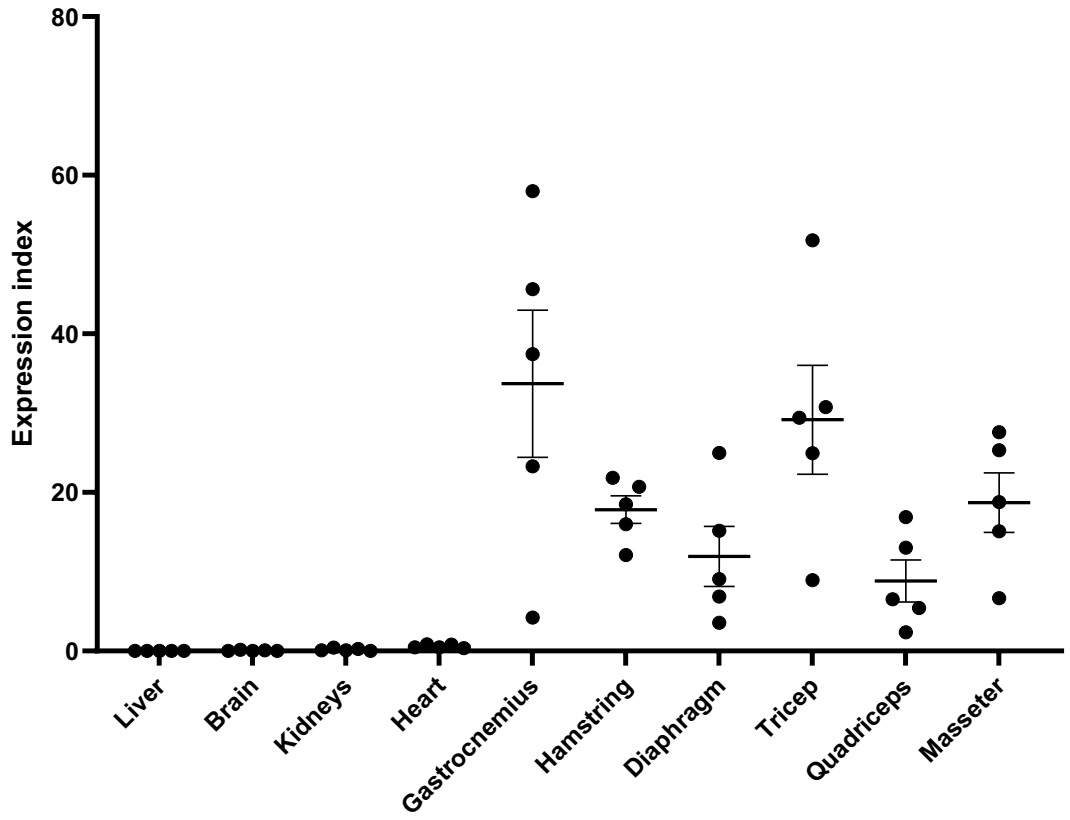

Figure 6-10 Expression Index of muscle optimised vector. DBT$^{-/-}$ (n=5) were injected with rAAV2/AAVMYO.CK8e.hDBT.WPRE.miRNA-TS 5 × 10^{11} VGC per pup at birth, tissues harvested 8 weeks later. Transduction efficiency was determined by dividing the E2 protein expression using western blot analysis for each tissue in each mouse by the corresponding vector copy number (VCN) per nucleated cell. Error bars represent standard error mean.

6.3.4 Biochemical phenotype of DBT$^{-/-}$ rescued with muscle optimised AAV vector equivalent to wildtype

The biochemical phenotype of DBT$^{-/-}$ mice at 56 days post injection with the muscle optimised vector was statistically equivalent to wildtype mice for the leucine, valine and isoleucine levels during periods of metabolic stability (Figure 6-11). L-alloisoleucine was significantly lower in muscle optimised vector treated DBT$^{-/-}$ at 56 days compared to untreated DBT$^{-/-}$ knockouts yet still significantly higher compared to wildtype (Figure 6-11). Leucine to valine ratios also normalised in rAAV2/AVVMYO.CK8e.hDBT.WPRE.miRNA-TS vector treated DBT$^{-/-}$ (Figure 6-12).

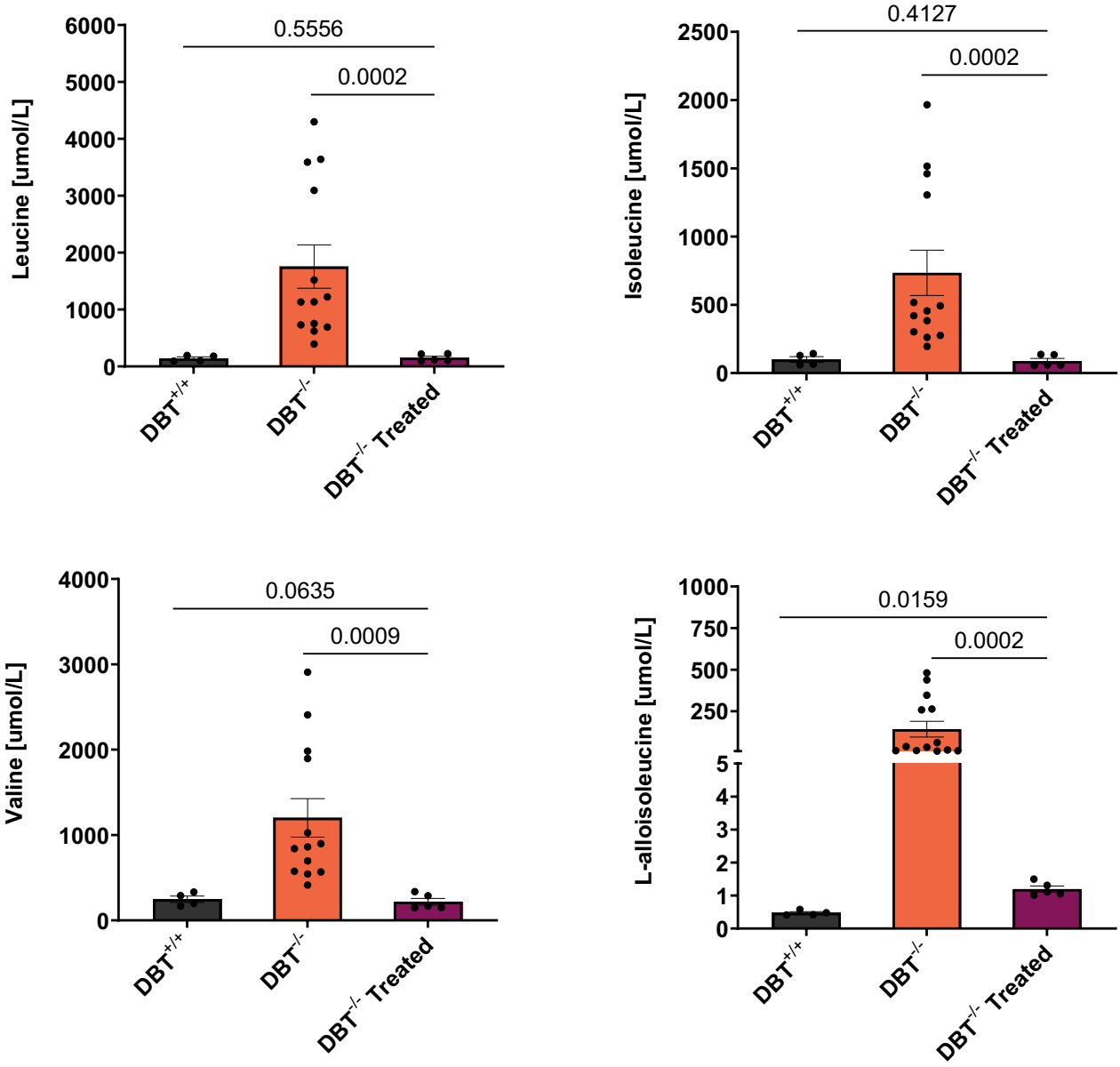

Figure 6-11 Branched chain amino acid levels and L-alloisoleucine levels in muscle optimised vector treated DBT$^{-/-}$. Blood levels (µmol/L) of BCAA Isoleucine, Leucine and Valine and L-alloisoleucine levels at 8 weeks of age in DBT$^{-/-}$ (n=5) treated with IP 5×10^{11} VGC per pup rAAV2/AAVMYO.CK8e.hDBT.WPRE.miRNA-TS. Whole blood was assayed with mass spectrometry. Error bars represent mean and ± standard error mean. Mann Witney test used to determine statistical significance.

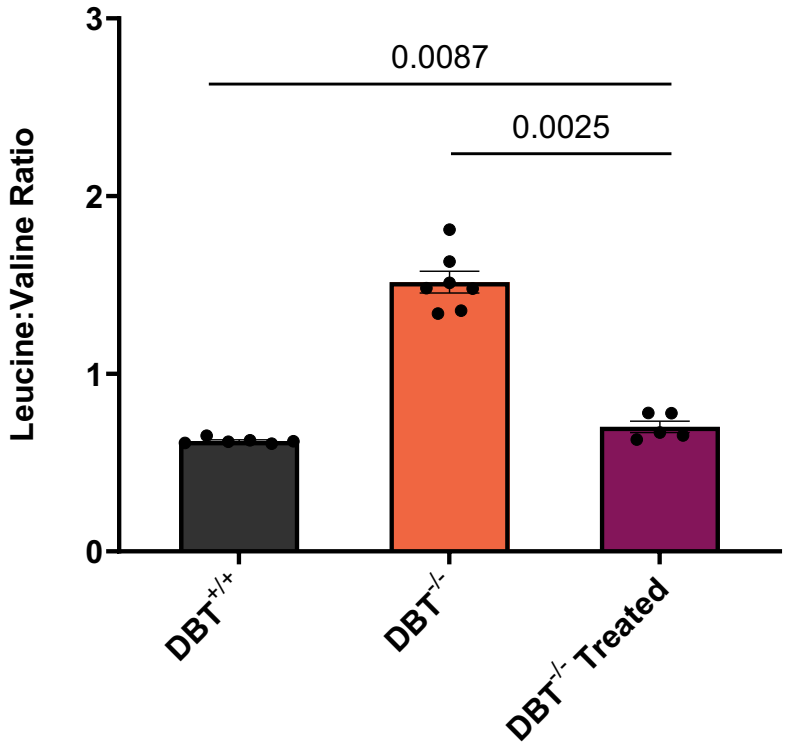

Figure 6-12 Leucine:Valine ratio of vector treated DBT$^{-/-}$. Leucine:Valine ratios were calculated from leucine and valine levels (µmol/L) obtained at 8 weeks of age using whole dried blood spots via mass spectrometry from DBT$^{-/-}$ treated with either 5 × 10^{11} VGC per pup rAAV2/AAVMYO.CK8e.hDBT.WPRE.miRNA-TS. Error bars represent mean and ± standard error mean. Mann Witney test used to determine statistical significance.

6.3.5 Physiological and induced metabolic challenges in DBT$^{-/-}$ rescued with rAAV2/AAVMYO.CK8e.hDBT.WPRE.miRNA-TS viral vector

BCAA levels were measured in rAAV2/AAVMYO.CK8e.hDBT.WPRE.miRNA-TS rescued DBT$^{-/-}$ pups at 28 days (D_{28}) and 56 days (D_{56}, 8 weeks measurements). The 8-week measurements were also used as 0 h for the high protein dietary challenge, as explained below. A non-significant trend of BCAA level reduction was observed between levels taken at D28 and at 56 days (Figure 6-13). DBT$^{-/-}$ mice are weaned from approximately the third week of life, and this time can be a relative metabolic stress compared with rapid growth compared to that experienced at 56 days of age. Relevant controls for wildtype mice at days 28 are being collected for comparison.

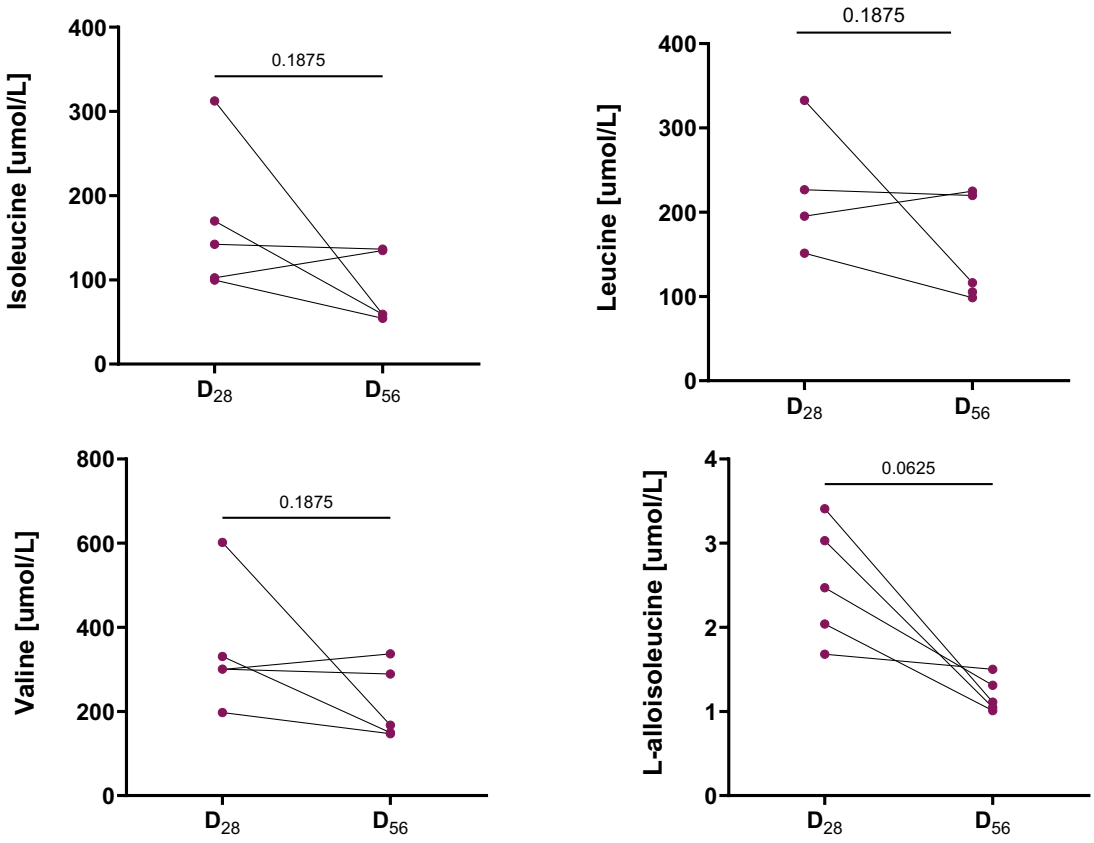

Figure 6-13 Branched chain amino acids and L-alloisoleucine trend downwards over first two months of life. Tandem mass spectrometry was used to determine BCAA from whole blood samples taken via submandibular bleed at day 28 and day 56 in DBT$^{-/-}$ mice treated with rAAV2/AAVMYO.CK8e.hDBT.WPRE.miRNA-TS. Wilcoxon matched-pairs signed rank test used to determine statistical significance, significant if p <0.05).

In DBT$^{-/-}$ treated with the muscle optimised vector that reached 56 days of age (n = 5) were placed on a high protein diet for 48 hours. Whilst the mice were seen to be eating the chow, the exact amount was not calculated, and it is possible that they may have also undergone relative starvation due to unpalatability of this chow. Furthermore, hydration status may have also affected this. All mice, independent of genotype, under these experimental conditions, lost a significant amount of weight during this time (Figure 6-14). However, whilst the wildtype mice maintained stable BCAAs, both leucine and L-alloisoleucine levels increased significantly for the muscle optimised vector treated DBT$^{-/-}$ (Figure 6-15).

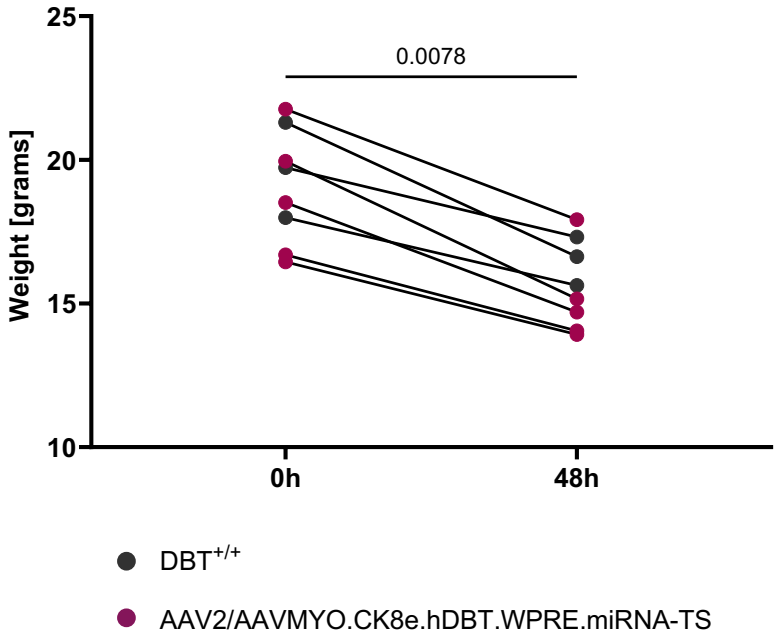

Figure 6-14 Weight loss during 48-hour high protein dietary challenge in all mice exposed to metabolic stress. Eight week old mice (DBT$^{+/+}$ n = 3, muscle vector treated DBT$^{-/-}$ n = 5) were weighed at hour zero and then at 48 hours after dietary restriction to high protein chow (61% protein). Statistical significance determined using Wilcoxon signed matched pairs rank test.

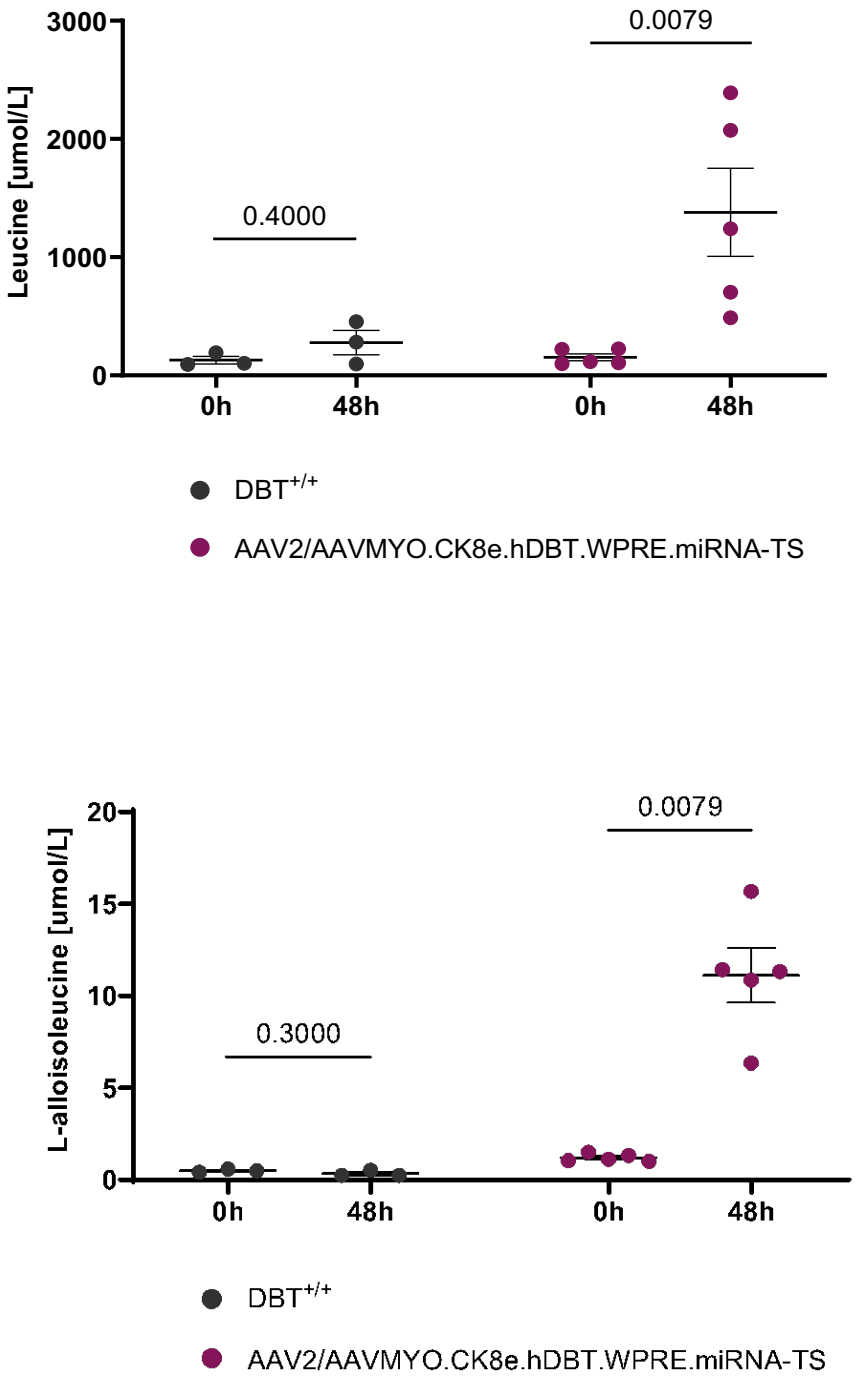

Figure 6-15 Leucine and L-Alloisoleucine levels increase during 48-hour high protein dietary challenge in vector treated DBT$^{-/-}$. Eight week old mice were bled via submandibular bleed at hour zero and then at 48 hours into a high protein (61% protein) dietary restriction and Leucine (top) and L-Alloisoleucine (bottom) levels measured. Error bars represent mean and ± standard error mean. Mann Witney test used to determine statistical significance.

6.4 Discussion

For genetic metabolic conditions like MSUD, paediatric patients arguably have the largest unmet therapeutic need and the most to gain from a stable gene transfer technology administered as early in life as possible. A muscle targeted AAV vector gene therapy may represent a viable, clinically translatable strategy to achieve this. These experiments demonstrated that single-dose neonatal administration of a muscle opimised AAV vector achieved systemic transductin of skeletal muscles and high expression levels of E2 protein as deteced on western blot analysis. Clinically signficiant therapeutic improvements were seen across all measured parameters of growth, biochemical phenotype in treated DBT$^{-/-}$ mice to a level statistically indistinguishable from wildtype mice during metabolic stability.

6.4.1 CK8e transcriptional regulation of hDBT main driver in phenotypic correction provided by rAAV2/AAVMYO.CK8e.hDBT.WPRE.miRNA-TS viral vector

The rAAV2/AAVMYO.CK8e.hDBT.WPRE.miRNA-TS viral vector was rationally designed to both optimise muscle transduction with the AAVMYO capsid and enhance myocyte transgene expression with the highly striated muscle specific CK8e promoter. Inclusion of miRNA-TS to detarget expression in the liver and brain, two highly relevant tissues to BCKDH activity, aimed to further tissue restrict the source of phenotypic correction to myocytes.

Neonatal administartion of rAAV2/AAVMYO.CK8e.hDBT.WPRE.miRNA-TS proved successful in rescuing DBT$^{-/-}$ pups to adulthood with growth and BCAA levels equivalent to those seen in adult wildtype mice. Evaluation of transgene expression profiles of RNA transcripts and E2 protein desmontrated a predominance of expression in myocytes with very minimal levels seen in liver, brain and kidney. In addition, comparing the vector biodistribution with the expression

profile showed the liver and diaphragm as the most highly transduced organs, however the vector expression was restricted to muscle tissue. This expression profile is demonstrative of the promoter and miRNA-TS conferring tissue specificity. From this it can be concluded that the majority of E2 expression, subsequent BCKDH activity and phenotypic correction was due to transgene expression in muscle. This study represents the first reported phenotype rescue of the neonatal lethal MSUD DBT$^{-/-}$ murine model exclusively through a single tissue type.

Whilst this study is the first to demonstrate phenotypic correction in DBT$^{-/-}$ mice predominantly from gene transfer in muscle tissue, it is not possible to define the relative contributions from either the muscle restricted CK8e promoter or the miRNA-TS. Future studies should interrogate relative contributions of the CK8e promoter and miRNA-TS to the tissue specificity through testing vectors configured with/without these elements.

6.4.2 Insights into disease correction threshold in DBT$^{-/-}$ mice treated with muscle optimised AAV vector

E2 expression as detected on western blot analaysis across sampled skeletal muscles (gastrocnemius, hamstring, quadriceps, diaphram, masseter and triceps) of DBT$^{-/-}$ mice treated with rAAV2/AAVMYO.CK8e.hDBT.WPRE.miRNA-TS, occurred at levels 10 to 100 fold higher than wildtype DBT mice. Cardiac tissue in vector treated DBT$^{-/-}$ mice had E2 protein levels which approximated the same level seen in wildtype cardiac tissue as detected on western blot analysis. These levels of E2 protein expression were associated with a biochemical phenotype that was statistically equivalent to wildtype for blood isoleucine, leucine and valine levels at 56 days, in the absence of a physiological stress. Levels of L-alloisoleucine, the most sensitive biomarker of total body BCKDH activity and distrubed BCAA metabolism, were still significantly higher in DBT$^{-/-}$ treated with muscle optimised vector comapred to wildtype, though lower than those measured for DBT$^{-/-}$ treated with AAV2/8.APOe/hAAT.hDBT.WPRE. This suggets that despite BCAA

correction, an underlying total body BCKDH deficiency remains in $DBT^{-/-}$ treated with the muscle optimised vector.

The clinical significance of persisent L-alloisoleucine elevation with otherwise normalised BCAA levels acheived with rAAV2/AAVMYO.CK8e.hDBT.WPRE.miRNA-TS is uncertain but does point to persistently disturbed total body BCAA metabolism. This residual deficiency was further unmasked by deliberately inducing a period of physiological stress with a 48 hour high protein diet in vector rescued $DBT^{-/-}$. Whilst mice were seen to be ingesting the high protein diet, it is suspected that the high level of protein rendered the chow unpalatable, and it is possible that there was a negative calorie balance due to inadequate food intake during this time frame. Regardless of the underlying mechanism, the high protein diet exposure proved a physiological stress to all mice, as evidenced by the weight lost across wildtype and treated $DBT^{-/-}$ groups. Leucine and L-alloisoleucine levels increased signifincatly for $DBT^{-/-}$ treated with rAAV2/AAVMYO.CK8e.hDBT.WPRE.miRNA-TS. Despite the significant elevations in leucine and L-alloisoleucine and accompanying weight loss, no vector rescued $DBT^{-/-}$ displayed any other phsyical signs of metabolic intoxication during this high protein dietary challenge. This was also in the context of very low CNS transduction and E2 expression. It may be that the duration of physiological stress was not sufficiently long to cause features of meatbolic intoxication other than weight loss and/or that the threshold of BCAA at which features such as ataxis, seizures or weakness appear, was not reached.

Metabolic demands on BCKDH acvitiy may also be dynamic as mice grow from neonates to adulthood. Whilst not statistically significant, blood leucine and L-Alloisoleucine levels between D_{28} and D_{56} days for $DBT^{-/-}$ treated with the muscle optimised vector trended lower, though this was not observed in every mouse. Assuming that the degree of vector mediated correction is stable, the higher leucine and L-alloisleucine levels at D_{28} may be reflective of heighted metabolic demands

associated with weaning and higher growth velocity in the juvenile $DBT^{-/-}$ mouse. Relevant controls in wildtype mice at D_{28} are being collected for comparison.

Eliminating the risk of leucinosis in MSUD patients and thus encephalopathy during periods of metabolic stress is an important therapeutic goal for MSUD. Current therapies, diet or liver transplantation, do not universally protect against this risk. In MSUD patients treated with liver transplantion, post-transplant leucine and L-alloisoleucine levels universally fall post transplant, but do not always completely normalise. Elevations in L-alloisoleucine up to 20 μmol/L post transplant have been reported (normal <2 μmol/L) [455] and have occurred despite otherwise normalised leucine levels and unrestricted dietary protien intake.

Whilst liver transplant protects most patients from severe metabolic decompensation during periods of heightened physiological stress, there are case reports of leucinosis and/or encephalopathy precipitated by intercurrent illness in MSUD patients post-transplantation [456]. These episodes of leucinosis have occurred in recipients from heterozygous-affected living related donors as well as in homozygous-unaffected donors. In humans, the liver contributes up to 13% of total body BCKDH activity and for MSUD transplant recipients in whom leucinosis occurs during episodes of metabolic stress, a relative deficiency must exist between the enzyme replacement provided by transplant and their maximal body BCKDH requirements during catabolic states. It is possible that in the $DBT^{-/-}$ murine model, the level of correction provided by the rAAV2/AAVMYO.CK8e.hDBT.WPRE.miRNA-TS vector was such that BCAA normalised during baseline levels of metabolism, however was not sufficient to completely protect against leucinosis during a catabolic stress.

The correction thresholds required to liberalise dietary protein, maintain BCAA homeostasis and protect against leucinosis and encephalopathy during times of metabolic stress are an important

consideration for any novel therapeutic intervention, such an an AAV gene therapy. The muscle optimised vector in this study provided enduring rescue to adulthood with normal BCAA levels during a period of metabolic homeostasis, but during episodes of metabolic stress, such as weaning and a high protein dietary challenge, the correction level attained with AAV mediated gene therapy was not sufficient to maintain normal leucine or L-alloisoleucine levels.

The exact percentage contribution of individual organs to total body BCKDH in mice and humans has only been reported in a handful of published studies. In mice, skeletal muscle contributes appromiately 57% and the liver contributes 8% of total body BCAA oxidation by BCKDH. In humans, skeletal muscle contributes approximately 50%-66% of total body BCKDH activity compared to 13% in the liver [12, 30]. Given the higher contribution of skeletal muscle in humans to total body BCKDH activity compare to that seen in mice it is possible that a muscle optimised vector may have even greater phenoyptic correction potential in humans, however further studies would be required to determine maximal correction thresholds in humans with MSUD. The success in this murine model suggests muscle as a viable target organ for MSUD and warrants further investiagtion in the search for novel therapies for MSUD.

6.4.3 Future directions in pre-clinical muscle directed AAV gene therapy for MSUD

The superior phenotypic correction observed with neonatal adminstration of rAAV2/AAVMYO.hDBT.WPRE.miRNA-TS vector to $DBT^{-/-}$ pups compared to liver directed vectors is promising with regards to developing a novel therapy for MSUD, however requires additional pre-clinical investigations. Dose tirtation experiments are necessary, at doses below and above the 5×10^{11} VGC/pup used in this study, to assess minimum and maximal effective doses. Long-term studies in the $DBT^{-/-}$ murine model with the muscle optimised vector to assess durability are currently underway. Where possible, maintaining gender parity in future experiments

is also necessary to further validate this strategy as there is potentially some sexual dimorphism in BCKDH expression and activity and MSUD affects both genders equally [53]. Widening the vector biodistribution studies to include reproductive tissues as well as other intra-abdominal organs, eyes and skin is also necessary to further interrogate the safety profile of the therapy. Other biometric testing, such as muscle strength and cognitive testing may also be useful to further interrogate the murine phenotype and help improve the sensitivity of our overall phenotype correction assessments [457].

6.4.4 Clinical translation considerations of muscle directed AAV therapy for MSUD

Optimising an rAAV gene transfer vector for muscle transduction and expression has demonstrated that targeting a single tissue system, striated muscle, provides significant phenotypic rescue to a murine neonatal lethal model of MSUD. In humans, muscle cells are a more stable cell population compared to paediatric livers and a muscle optimised AAV viral vector may represent a viable therapeutic strategy for MSUD in humans. Given the more stable cell populations, vector administration could conceivably be utilised in paediatric patients who would benefit from vector conferred metabolic stability during their most vulnerable and critical time development and growth. Furthermore, the biochemical correction possible in humans may be further enhanced compared to the chimeric BCKDH generated with human E2 in the murine model.

Whilst AAVMYO is yet to be clinically validated, there are other muscle directed validated AAV vectors used in clinical trials for Duchenne Muscular Dystrophy (DMD) and include AAV2/5, AAV9 and AAVrh74. The newest FDA registered DMD gene therapy viral vector, delandistrogene moxeparvovec-rokl (Elevydis, Sarepta, USA) [458], is approved for use in Australia and contains a micro-dystrophin under the transcriptional regulation of MHCK [437] promoter carried in the AAVrh74 capsid. A phase 2 clinical trial, IGNITE, investigating an AAV9

encapsulated micro-dystrophin under the CK8e promoter (Solid Biosciences) is currently undergoing clinical validation and with interim updates reporting meaningful clinical benefit to the study participants [459].

Muscle-directed AAV therapies have encountered difficulties with regards to dose related adverse effects in the past, often needing high systemic doses to achieve adequate transduction to confer clinical benefit. Serious adverse events, including death of trial patients, have been associated with higher doses of systemic AAV gene replacement therapies [303]. The increasing efficiency and muscle restricted expression of promoter/enhancers such as CK8e may aid in balancing vector dose reduction whilst maintaining adequate tissue expression. Furthermore, the continual quest for optimisation of myotrophic capsids and promoters will no doubt increase the selection and improve the clinical translatability of gene therapy strategies in the future [370].

In summary, single dose neonatal administration of rAAV2/AAVMYO.hDBT.WPRE.miRNA-TS to $DBT^{-/-}$ pups acheived stable gene transfer of a human DBT transgene to striated muslces and achieved supraphysiological levels of E2 protein expression across whole skeletal muscles and physiological E2 expression in across whole cardiac tissue. Overall, this provided a level of phenotypic correction characterised by significantly improvments in growth, survival and BCAA homeostasis in adult $DBT^{-/-}$ mice was observed. These experiments demonstrate the viability of striated muscle as a target tissue for an AAV mediated gene therapy for MSUD.

Chapter 7
General discussion & final conclusions

The unmet clinical need for definitive cures of genetic metabolic conditions like MSUD has fuelled the pursuit of novel, advanced therapeutic options such as gene therapy. This thesis focussed on the exploration of both liver-directed and muscle-directed gene addition strategies using conventional recombinant AAV gene transfer and a hybrid AAV/*piggyBac* transposase system in a neonatal lethal murine disease model of MSUD. Through established molecular analysis techniques, vector-specific and target tissue-specific considerations unique to MSUD were evaluated. This thesis provides new insights into optimal AAV vector configurations for a single tissue gene therapy strategy for MSUD targeting skeletal muscle which has the potential to provide enduring therapeutic benefit in both paediatric and adult MSUD patients.

Prior to this research project, partial phenotype correction of murine MSUD models using AAV-mediated gene transfer had been achieved through either the deliberate or inadvertent targeting of more than one target tissue [323, 324, 326]. Whilst precise relative contributions of different tissues to BCAA homeostasis in the context of gene therapy has not been fully understood, these studies have provided some insight into likely therapeutic thresholds in murine models. Liver directed approaches did not achieve complete phenotype correction during periods of metabolic stability without the co-transduction of muscle in the DBT intermediate murine model iMSUD [326]. The use expression cassettes employing ubiquitous enhancer/promoter elements in recombinant AAV vector genomes packaged in an AAV8 capsid allowed for rescue of the BCKDHA and BCKDHB neonatal lethal murine MSUD models with extrahepatic expression across brain, heart and skeletal muscle potentially the main source of rescue for these models. Given that the murine liver

contributes to approximately 8% of total body BCKDH activity [12], it is not unexpected that targeting the liver alone is insufficient for phenotypic correction in the iMSUD murine disease model. Contrasting the significant stabilisation of BCAA levels that occur in children with MSUD post-transplantation, it is plausible that the higher proportion of total body BCKDH activity the human liver, approximately 9-12%, is enough to tip the balance in favour of improved BCAA homeostasis during periods of metabolic stability [10, 30].

In contrast, the handful of reported cases of leucinosis occurring in MSUD patients post-transplant during metabolic stress imply that even a BCKDH liver graft with physiologically normal levels of BCKDH activity can be insufficient to maintain BCAA homeostasis during times of catabolic stress in certain MSUD patients. Whilst the underlying mechanism of this phenomenon has not been fully characterised, it is conceivable that there the level of metabolic stress able to be tolerated by a MSUD patient post-liver transplant would be inversely proportional to their levels of residual extra-hepatic BCKDH enzyme activity. Should this tolerance threshold be exceeded, leucinosis would occur. This has important implications in predicting clinical benefit of an AAV gene therapy as the residual BCKDH enzyme activity is dependent upon the pathogenicity of individuals underlying mutations. Characterising the residual BCKDH enzyme activity in MSUD affected individuals may prove an important and critical component to determining suitability for any future MSUD gene therapy clinical trials and may allow for better prognostication of expected therapeutic benefit.

The liver-directed rAAV-mediated gene transfer strategies described in this study explored both simple gene addition and a hybrid AAV-*piggyBac* transposase mediated gene addition. The gene addition experiments highlighted the difficulty in achieving stable long-term gene transfer to $DBT^{-/-}$ hepatocytes after neonatal vector administration with a predominantly episomal gene transfer system. Compared to untreated DBT-deficient mice, vector treated $DBT^{-/-}$ displayed

significantly improved survival, growth and biochemistry after intraperitoneal injection of an AAV8 pseudoserotyped vector encoding a human DBT expression cassette (rAAV2/8.APOe/hAAT.hDBT). At one week post vector administration, APOe/hAAT transcriptional regulation of the hDBT transgene conferred levels of hepatic E2 expression that were higher across the whole liver compared to levels seen in wildtype mice on western blot analysis. However, L-alloisoleucine levels and leucine levels remained significantly higher than levels observed in wildtype mice and indicated an ongoing deficiency of total body BCKDH activity, despite these high levels of transgene expression. The phenotypic improvements were also transient, and all rescued mice developed metabolic intoxication just before reaching 3 weeks of life where upon hepatic expression of E2 protein approximated that detected in wildtype mice. Together, these observations support the critical role that extra-hepatic BCKDH activity has in maintaining BCAA homeostasis in the $DBT^{-/-}$ murine model. The timing of this vector loss has been seen with other models of liver-directed AAV gene transfer for metabolic conditions [346]. This timing is almost certainly a reflection of the loss of AAV episomes secondary to hepatocyte proliferation in the growing juvenile liver below the hepatocyte therapeutic correction threshold coinciding with increasing metabolic demands associated with weaning, increasing physical activity and ongoing growth, all of which coincide between the 2^{nd} and 3^{rd} week of life in mice.

In an attempt to circumvent the episomal loss of AAV in transduced neonatal hepatocytes, the hybrid AAV/*piggyBac* transposase system was utilised [417]. Whilst neonatal administration of transposon vector configured for hepatic expression in $DBT^{-/-}$ mice conferred significant improvements in survival and biochemical phenotype, this was shown to be independent of transposase vector co-transduction and thus independent of the levels of transgene transposition in hepatocytes. This result illuminated two things, firstly, that in this study *piggyBac* transposase did not achieve for technical reasons the durable hepatic gene transfer seen in other studies [274, 275] and secondly, that there was a significant contribution from extrahepatic tissues to the observed

levels of phenotypic correction. This was interesting given that the APOe/hAAT enhancer/promoter is putatively described as liver specific in the literature [341, 402, 460].

The observation of extra-hepatic transgene expression prompted an exploration of how *cis* regulatory elements included in the transposon vector, but not in the gene addition vector used in Chapter 4, changed the expression pattern and conferred more stable transgene expression in the $DBT^{-/-}$ neonatal lethal model. We hypothesised that the inclusion of the WPRE and/or pBTIR sequence elements contributed to the broader tissue expression profile and configured *in vivo* experiments to test this. From these experiments, it can be concluded that the presence of a WPRE in the transposon vector resulted in enhanced extrahepatic expression in post mitotic tissues, thus conferring the improved vector durability and phenotypic rescue. The presence of pBTIRs did not significantly change the tissue expression pattern of the hDBT transgene from the simple gene addition vector described in Chapter 3. The wider tissue expression and improved durability of the hDBT transgene expression associated with WPRE enhanced post-transcriptional regulation has important considerations for clinical vector design and development.

Widely used pre-clinically to enhance transgene expression [423], the WPRE was the subject of intense scrutiny secondary to reported heightened oncogenic risk reported in murine studies [461, 462]. This risk was negated through removal of the oncogenic sequence from the original WPRE, generating a reportedly safer ΔWPRE [462]. Whilst the ΔWPRE sequence was used throughout this research project, pre-clinical studies without this element may be useful to assess the degree to which the expression profiles are reliant upon the ΔWPRE regulatory element with regards to tissue functional transduction and oncogenic risk and thus improve the rigour of pre-clinical vector testing with respect to safety.

The studies described in this thesis also offer insights into potentially unachievable hepatic correction thresholds required in MSUD. Ultimately, this study was not able to demonstrate that single organ gene transfer to the liver is sufficient to completely correct the MSUD phenotype of $DBT^{-/-}$ mice. Despite the anticipated phenomenon of episome loss from transduced neonatal hepatocytes as the liver grew, there were still high levels of hepatic transgene expression with the liver directed AAV gene addition vector 1 week after vector administration with the gene addition vector rAAV2/8.APOe/hAAT.hDBT. Across the whole liver, hepatic E2 expression levels in treated $DBT^{-/-}$ mice were supraphysiological as detected on western blot analysis. Despite the high levels of E2 expression, the $DBT^{-/-}$ biochemical phenotype was not fully corrected and residual elevations in leucine and L-alloisoleucine were still present.

That this residual $DBT^{-/-}$ biochemical phenotype persisted despite the high E2 protein levels detected across the whole liver is interesting, offering some insights into the required biodistribution of E2 in each hepatocyte. The high tissue levels of E2 protein may reflect multiple vector copies in one $DBT^{-/-}$ transduced hepatocyte cell with corresponding high levels of E2 expression and minimal transduction in another cell with relatively less expression. However, across the whole organ, this would reflect supraphysiological expression, even though some cells may not be expressing any protein. For MSUD, it is not known if there is more benefit to having a higher number of cells corrected to a minor degree, or fewer cells with a higher degree of BCKDH enzyme activity. Furthermore, it is not known if all expressed E2 protein is incorporated into functional BCKDH, and thus further studies looking at BCKDH enzyme activity would be helpful to further assess the phenotypic correction and if expressed E2 protein levels correlate with BCKDH activity.

Further insights into the hepatic correction threshold were gained through observing the loss of therapeutic effect with the simple gene addition vector AAV2/8.APOe/hAAT.hDBT. Whilst this

vector initially improved the phenotype of DBT$^{-/-}$ mice, episome loss in transduced hepatocytes led to a delayed onset of metabolic intoxication occurring at 2 and 3 weeks of age, necessitating euthanasia. At this time point the transgene derived E2 protein levels detected via western blot analysis reconstituted the levels seen in wildtype mice with around 50% of hepatocytes positive for E2 protein on immunofluorescence. This suggests that in mice, where the liver contributes around 8% of total body BCKDH [12], wildtype levels of the deficient E2 subunit provided by the human DBT transgene were also not sufficient to restore the biochemical phenotype. Although the fraction of total body BCKDH activity attributable to liver is lower in mice than in men, coupled with the knowledge that liver transplantation in humans does not fully correct the biochemical phenotype in MSUD patients, this residual murine MSUD phenotype is demonstrative of the inability to achieve phenotype correction with liver directed gene transfer using current technologies and that targeting extrahepatic tissues will be necessary.

Whilst the exact hepatic therapeutic threshold for complete BCKDH activity restoration has not been identified by this study, some conclusions can still be drawn. Given the above limitations of AAV gene transfer to murine livers and that complete phenotype restoration is not always possible with liver transplantation in humans, it follows that for an AAV therapy in humans to achieve the equivalent therapeutic benefit of a liver transplant, vector transduction efficiency would need to approach 100% of hepatocytes and confer transgene protein levels equal to or above wildtype levels with no attenuation of vector effect. As these mandates are currently unachievable with current AAV technologies, presently any liver-directed AAV gene therapy for MSUD is likely to be inferior to transplantation, pointing towards a possible requirement for multi-organ delivery. Ultimately, the liver directed gene transfer experiments in this study were not sufficient to completely rescue the DBT$^{-/-}$ phenotype and neonatal administration of a muscle optimised vector provided superior, albeit still incomplete, biochemical rescue of the DBT$^{-/-}$ MSUD murine model.

The challenges in achieving durable gene transfer in murine hepatocytes and the suboptimal hepatic integration achieved with *piggyBac* transposase in the current studies prompted an exploration of an alternative target tissue: striated muscle. Skeletal muscle represented the organ with the highest contribution to total body BCKDH activity and prior to this study, not published attempts had demonstrated complete phenotypic rescue of a murine model with muscle gene transfer alone. This study sought to evaluate if expression of a hDBT transgene in a muscle optimised vector could be restricted to muscle tissue alone and if so, would phenotypic rescue have superior efficacy and durability compared with liver directed transgene expression in the $DBT^{-/-}$ neonatal lethal murine model. The muscle optimised AAV vector and expression cassette was rationally designed to test this with a promoter/enhancer that was muscle specific and miRNA targeting sites for liver and brain tissues intended as a further safeguard to restrict transgene expression to the muscle. Neonatal administration of this muscle optimised vector at dose of 5×10^{11} vgc per mouse conferred significant improvements in survival compared to untreated $DBT^{-/-}$. Furthermore, at 8 weeks post vector administration growth and blood levels of leucine, isoleucine and valine in the $DBT^{-/-}$ treated mice with the muscle optimised vector were statistically equivalent to those seen in wildtype mice at the same age in the absence of metabolic stress.

The efficacy of phenotype correction conferred by this muscle optimised vector was superior to that seen with any of the liver directed vectors and was achieved by the functional transduction of a sole target tissue, straited muscle. Whilst the muscle optimised vectors biodistribution extended to tissues outside straited muscle, the functional transduction in tissues relevant to total body BCKDH expression such as the liver, brain kidney was minimal. In the muscle optimised vector, the functional transduction of the hDBT transgene was heavily constrained to straited muscle through the deliberate inclusion of the CK8e promoter/enhancer and liver and brain miRNA-TS. This vector configuration conferred higher levels of E2 expression compared to wildtype as detected on western blot analysis across all sampled skeletal muscles. From this it can be concluded

that the inclusion of the *cis* transcriptional elements of the CK8e promoter/enhancer and miRNA-TSs highly restricted transgene expression to striated muscle. Whilst the experimental configuration did not distinguish between the transcriptional restriction derived from CK8e or the miRNA-TS, it did allow for interrogation of the phenotypic correction potential of striated myocytes as a single target organ. Thus, the superior phenotypic correction seen with the muscle optimised vector can be attributed to the stable transduction of striated myocytes alone. The post mitotic nature of striated myocytes likely contributed significantly to the durability of phenotypic correction conferred by a non-integrating AAV-mediated gene transfer strategy, in direct contrast with the loss of vector episomes and accompanying loss of phenotypic correction observed in $DBT^{-/-}$ treated with liver-directed AAV vectors without WPRE.

Although the muscle optimised vector in this study demonstrated superior target tissue durability and treated $DBT^{-/-}$ demonstrated blood leucine levels equivalent to wildtype in the absence of metabolic stress at 8 weeks of life, they still displayed subtle, significant elevations in L-alloisoleucine levels at this time. Elevated L-alloisoleucine levels were also seen in $DBT^{-/-}$ treated mice with the liver directed vectors and were even more pronounced. This suggests that for treated $DBT^{-/-}$ mice reaching adulthood and with it a period of metabolic stability, there still persisted a deficiency in total body BCKDH activity. Whilst L-alloisoleucine itself is not pathological in manner of leucine and levels in humans post-transplant have been seen up to 20 μmol/L with normal leucine levels, L-alloisoleucine elevations do reflect an underlying total body BCKDH deficiency. The degree of phenotype rescue was thus further interrogated for $DBT^{-/-}$ mice surviving to adulthood treated with the liver-directed and muscle-directed vectors. The degree of phenotype rescue was tested with a severe metabolic stress, nominally 48 hours of high protein diet exposure which caused significant weight loss of between 10-20% of body weight over this time frame. This challenge might also inadvertently expose the mice to starvation due to the unpalatability of the high protein diet. Regardless of the mechanism, this challenge represented a

significant catabolic stress. Whilst no treated DBT$^{-/-}$ mice were able to maintain BCAA homeostasis during this catabolic challenge, no physical signs of metabolic intoxication were observed, such as ataxia or seizures reflective of encephalopathy which are more advanced signs of metabolic intoxication. The maximal leucine levels observed in the treated DBT$^{-/-}$ mice were of clinical significance, however and equivalent elevations in humans during periods of metabolic stress would likely necessitate hospitalisation and supportive management to reverse the catabolism.

From here, it can be concluded that the muscle optimised vector was not able to completely reverse the phenotype in the DBT$^{-/-}$ mice, though the durability and degree of phenotypic correction provided during periods of metabolic stability on a standard chow diet is encouraging. If translated to humans with similar efficacy it may represent a strategy with equivalent therapeutic benefit to liver transplantation without need for life-long immunosuppression. However, in these experiments the exact degree of catabolic stress experienced by the mice during the high protein diet exposure was not quantified. Further assessment of phenotypic correction in vector treated DBT$^{-/-}$ mice across degrees of physiological stress will be required. For example, replicating in mice the levels of catabolic stress experienced by humans with a mild respiratory viral infection or severe dehydration or excessive exercise. Quantitating these levels of murine stress and subsequent BCAA perturbations in vector treated DBT$^{-/-}$ mice across levels of physiological stress likely to be experienced in MSUD patients may be more meaningful in predicting the likely levels of phenotypic correction attainable in humans treated with an equivalent AAV gene therapy. Ways to undertake this would be to house mice undergoing the metabolic stress in respiration chambers with strict measurements of water and caloric intake and composition in order to determine respiratory quotients and thus better quantify overall anabolism and catabolism [463].

Overall, results described in this thesis contribute important novel discoveries with regards to developing AAV-mediated gene therapy for MSUD. This study represents the first successful rescue of a DBT neonatal lethal mouse model with AAV-mediated gene transfer. This is also the first study using a neonatal lethal model of MSUD that attempted to restrict transgene expression to myocytes as single target organ and demonstrate near complete phenotypic correction during metabolic stability. Attempts to similarly target the liver with AAV-mediated gene transfer in the DBT neonatal lethal model of MSUD demonstrated that expression of E2 protein in DBT-deficient mice at levels higher than detected in wildtype mice on western blot is insufficient to completely restore the biochemical phenotype. In conjunction with episomal loss known to occur with the cellular replication in juvenile organs like neonatal livers, it can be concluded that at least for $DBT^{-/-}$ mice, the paediatric liver is not viable a target for single organ AAV-mediated gene transfer.

Demonstrably, at current rates of AAV gene transfer efficiencies phenotypic correction via liver targeted AAV-mediated gene transfer alone is not likely to translate to success in a clinical setting. However, transgene expression by hepatocytes may still have an important role in any future gene therapy for MSUD. Grieg *et al.* explored the potential of a dual organ AAV strategy, where muscle and liver of iMSUD affected mice were transduced with an AAV9 pseudo-serotyped gene addition vector, however there was still incomplete phenotypic rescue with their vector configurations. Furthermore, should the rate of episome loss seen with neonatal murine hepatocytes be recapitulated in MSUD infants, using the liver as reservoir for gene transfer may be unsuccessful due to predicted episomal loss in mitotic tissues.

Dual transduction of the liver alongside another organ such as muscle however, may have a role in conferring immunotolerance towards the transgene and protein products. As seen in muti-visceral transplants, transplanting a liver allograft alongside another organ can positively influence

allograft survival and reduce immune rejection [464, 465]. This phenomenon, has also been noted in gene therapy studies whereby liver gene transfer can drive immune tolerance [466-468]. The mechanism of this is still under investigation, however it hypothesised to be secondary to the multiple types of antigen presenting cells in the liver, including the Kupffer cells and hepatic dendritic cells which have a less mature phenotype compared to peripheral antigen presenting cells [469]. In this way, hepatic expression of the transgene has been demonstrated to reduce the immunogenicity of transgene products in pre-clinical studies and may be an important consideration in clinical vector design for conditions like MSUD.

In the pursuit of a clinically translatable AAV therapy for MSUD, future pre-clinical studies are necessary. Whilst this thesis has demonstrated the potential of a muscle targeted vector in mice, further interrogation of this strategy is required to bridge the gap from mouse to man. Additional areas of inquiry could include formal quantitation of the degree of vector driven tissue correction with an BCKDH enzyme activity assay. There are two published methods of assessing BCKDH enzyme activity, via spectrophotometry or liquid scintillography [41, 470]. Attempts were made by the candidate to establish the spectrophotometric assay for this project, however were ultimately unsuccessful. More extensive biodistribution studies in mice and non-human primates would also be useful, as would dose titration studies. Whilst the dose used for the muscle optimised is at the limit of vector copies per kg used in the clinical setting [13, 395], understanding transduction efficiencies across a range of doses pre-clinically would aid in balancing the degree of therapeutic correction with potential undesirable dose related side effects for MSUD patients. Another area of inquiry could explore the efficacy of muscle targeted AAV-mediated gene transfer in the *BCKDHA* and *BCKDHB* murine MSUD models. Furthermore, an interrogation of myocyte cells with regards to fibre type would also be of use to better understand any difference in tissue transduction or vector expression based on inter-fascicle fibre type variability and possible implications for vector efficacy. Additional important pre-clinical assessments would also include

toxicology studies in wild-type controls, increasing the range of doses studied to define therapeutic ranges. Furthermore, expanding the phenotype correction assessments to include motor and neuropsychometirc testing as well as assessing histological changes in the liver and muscle would further strengthen the depth of pre-clinical knowledge to aid in the clinical translation of these findings.

It is also possible that BCKDH requirements across childhood to adulthood may be dynamic. In BCKDH sufficient humans, the enzyme is expressed broadly across many tissue types. Furthermore, there is a large redundancy of enzyme expression with mild types of MSUD only manifest clinically when BCKDH enzyme activity is ≤ 30% and severe when ≤ 4% of normal [5]. Teleologically, this suggests that the physiological redundancy in the amount of BCKDH produced means that a human body is requisitely equipped to manage large influxes of BCAA and catabolic stresses. Given that childhood represents a heightened period of growth and intercurrent illness compared to adulthood, it is possible that the relative requirements of BCKDH may be higher in childhood than adulthood. Assuming vector efficacy conferred by the muscle optimised vector is stable in conjunction with that observation that leucine levels decreased from day 28 to day 56 in $DBT^{-/-}$ treated mice with the muscle optimised vector, this may reflect decreasing BCKDH demands with advancing age in the DBT murine model and potentially also may be the case in humans. Further assessment of the potential dynamic requirements of BCKDH activity would be useful to inform translational studies with regards to optimising the timing of vector delivery and determining if therapeutic thresholds are also dynamic in humans.

Striated muscle has been a target of gene therapy research in degenerative myocyte diseases such as DMD and other muscular dystrophies [204, 366, 459]. Given that skeletal muscle is the organ that contributes the highest percentage of total body BCKDH activity in humans and two highly relevant pre-clinical species mice and monkey, it follows both teleologically and practically that

future gene therapy research for MSUD explore this tissue as a target for AAV-mediated gene transfer. This thesis has demonstrated the potential for muscle to be a therapeutic target for AAV-mediated gene transfer for MSUD. The post-mitotic nature of striated muscles confers inherent advantages in this tissue type over hepatocytes for MSUD and this study has demonstrated the superior viability of striated muscle and in particular skeletal muscle, over the liver, as a target tissue for a neonatal, single dose, AAV-mediated gene transfer in MSUD.

In the clinical setting, targeting striated muscle also has other practical advantages. Clearly the difference in miotic rates between liver and muscle seen in juvenile mice, similar to humans, mean that the durability of a single dose of muscle expressing vector would outperform any liver targeted vector. Thus, a striated muscle targeted AAV-mediated gene therapy has the potential be able to be delivered once with durable, stable gene transfer and subsequent phenotypic correction afforded by virtue of the AAV vector episomes stably present in non-dividing myocytes. This has important implications with regards to clinical and financial efficiency. Repeat dosing with AAV vectors is fraught with immune mediated vector neutralisation and loss of efficacy. Furthermore, administration of a single vector dose represents a significant financial cost saving compared to multiple dosing strategies. For example, a single dose of the PBS approved SMA AAV9 gene therapy Zolgensma in 2025 comes with a price tag of $AUD2,527,773.87. Thus, there is significant motivation in improving accessibility by way of cost reduction in the development of gene therapies that are efficacious, durable and ideally limited to single dosing regimens.

In summary, this thesis has described the first instance of AAV-mediated gene transfer in a $DBT^{-/-}$ neonatal lethal mouse model of MSUD. It is also the first to demonstrate significant phenotypic correction attained with AAV-gene transfer that is attributable to a single target tissue, striated myocytes. This thesis also explored the liver as a single organ target for MSUD and highlights the currently insurmountable barriers preventing durable AAV gene transfer at

therapeutic levels exceeding that currently conferred with liver transplantation. The biochemical correction of leucine levels achieved by AAV-gene transfer to a post-mitotic tissue in an MSUD murine model were equivalent to wildtype mice during periods of metabolic stability. A persisting disease biochemical phenotype was unmasked however with a severe catabolic challenge, similar to that observed in some MSUD patients post liver transplantation during catabolic crisis. The degree of phenotypic correction achieved by the muscle optimised AAV-mediated gene addition in post mitotic murine skeletal muscle, which corresponds to the largest endogenous reservoir of BCKDH enzyme in both mice and humans, has enormous clinical potential. Whilst further, rigorous pre-clinical testing is required before an equivalent muscle optimised vector would be safe for human clinical trials, these experiments have demonstrated the viability of AAV-mediated gene transfer to striated myocytes in a neonatal lethal MSUD murine model and are an encouraging step in the search for a cure for MSUD patients and their families.

Appendix

Appendix A

Generation of DBT maple syrup urine disease model from the CB57B/6J mouse [325, 376].

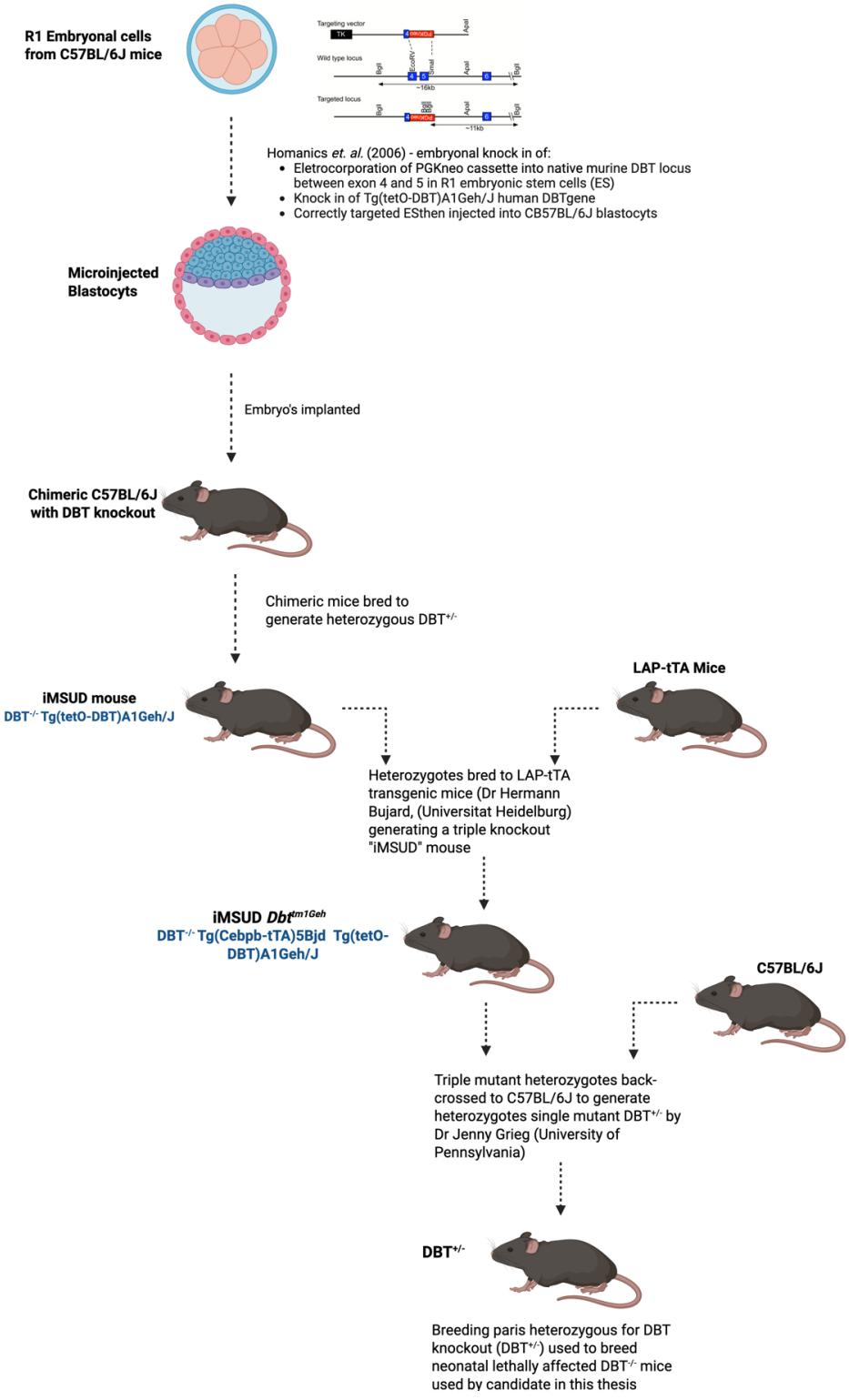

Figure A-1 Development of DBT Murine Mouse Model of Maple Syrup Urine Disease

Appendix B

Sequence of DBT mouse knockout allele as confirmed through sanger sequencing transcripts generated through overlapping sequential PCR reactions is displayed in figure A-1.

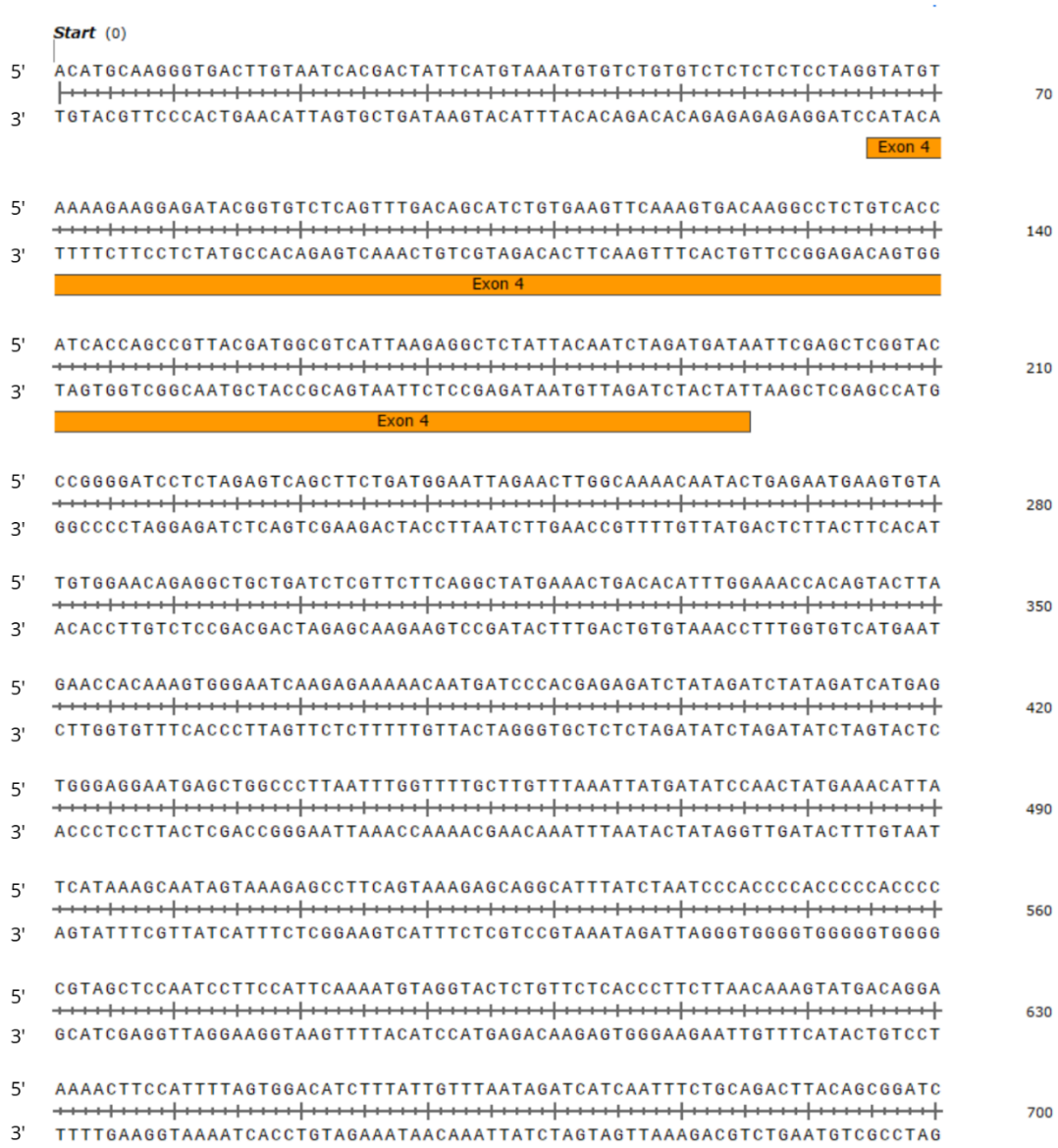

(Sequence continues over page)

(Continued from previous page)

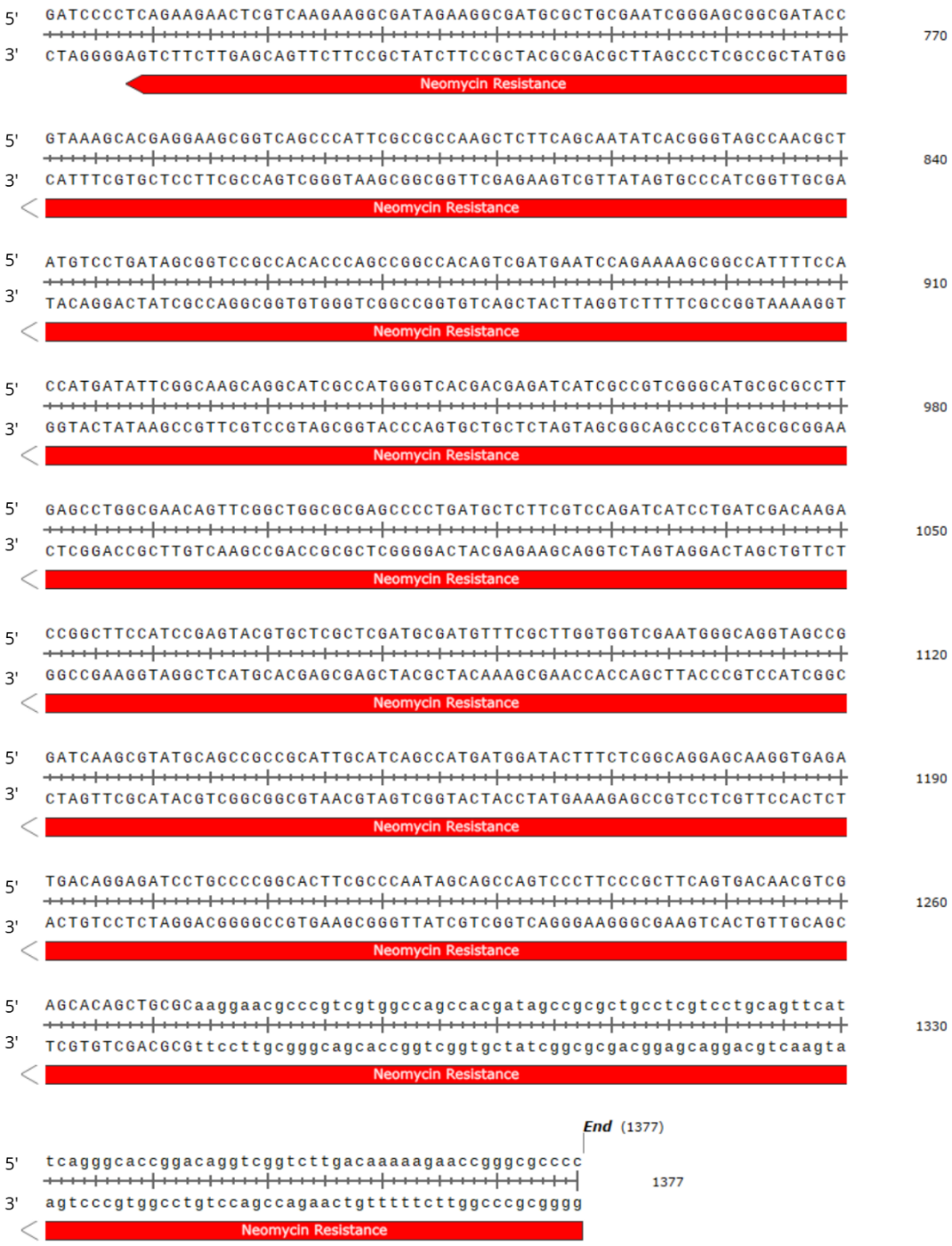

Figure A-1 Sequence of DBT gene knockout allele in the DBT$^{-/-}$ mouse model of MSUD. Sequence determined through sequential overlapping PCR of DNA extracted from DBT heterozygote mice as per Chapter 3.2.1.

Appendix C

Table A-1 Components of each vector used to explore the effect of cis regulatory elements

Vector Name	Capsid	Enhancer/Promoter	Transgene	PolyA	Cassette* (bp)	pBTIR	WPRE
rAAV8.APOe/hAAT.**WPRE.pBTIR**	rAAV8	APOe/hAAT	hDBT	BGHpA	4315	+	+
rAAV8.APOe/hAAT.hDBT.**WPRE**	rAAV8	APOe/hAAT	hDBT	BGHpA	3965	-	+
rAAV8/APOe/hAAT.hDBT.**pBTIR**	rAAV8	APOe/hAAT	hDBT	BGHpA	3924	+	-
rAAV8.APOe/hAAT.hDBT	rAAV8	APOe/hAAT	hDBT	BGHpA	3284	-	-

Abbreviations: bp (Base pairs)
*Cassette length measures from start of AAV 5' ITR to end of AAV 3' ITR

References

1. Fox, T.A. and C. Booth, *Improving access to gene therapy for rare diseases.* Dis Model Mech, 2024. **17**(6).
2. Lord Bethell of Romford, R.S., Vaughan Gething, Mairi Gougeon, *The UK Rare Diseases Framework*. 2021, United Kingdom Government.
3. US National Library of Medicine. *Maple Syrup Urine Disease*. Genetic Home Reference 2020; Available from: https://ghr.nlm.nih.gov/condition/maple-syrup-urine-disease#statistics.
4. Harper, A.E., R.H. Miller, and K.P. Block, *Branched-Chain Amino Acid Metabolism.* Annual Review of Nutrition, 1984. **4**(1): p. 409-454.
5. Nellis, M.M. and D.J. Danner, *Gene preference in maple syrup urine disease.* American journal of human genetics, 2001. **68**(1): p. 232-237.
6. Yang, N., et al., *Analysis of gene mutations in Chinese patients with maple syrup urine disease.* Molecular Genetics and Metabolism, 2012. **106**(4): p. 412-418.
7. Zeynalzadeh, M., et al., *Four novel mutations of the BCKDHA, BCKDHB and DBT genes in Iranian patients with maple syrup urine disease.* J Pediatr Endocrinol Metab, 2018. **31**(2): p. 205-212.
8. Zabaleta, N., et al., *Genetic-Based Approaches to Inherited Metabolic Liver Diseases.* Human Gene Therapy, 2019. **30**(10): p. 1190-1203.
9. Wei-Hua Sun, B.-B.W., Ya-Qiong Wang, Meng-Yuan Wu, Xin-Ran Dong, Yue-Ping Zhang, Wei Lu, Ping Zhang, Bin Yang, Min Zhang, Hong-Jiang Wu & Wen-Hao Zhou, *Identification of eight novel mutations in 11 Chinese patients with maple syrup urine disease.* World Journal Of Pediatrics: WJP, 2020. **16**.
10. Brosnan, J.T. and M.E. Brosnan, *Branched-chain amino acids: enzyme and substrate regulation.* J Nutr, 2006. **136**(1 Suppl): p. 207S-11S.
11. Shimomura, Y., et al., *Branched-chain alpha-keto acid dehydrogenase complex in rat skeletal muscle: regulation of the activity and gene expression by nutrition and physical exercise.* J Nutr, 1995. **125**(6 Suppl): p. 1762s-1765s.
12. Neinast, M.D., et al., *Quantitative Analysis of the Whole-Body Metabolic Fate of Branched-Chain Amino Acids.* Cell Metab, 2019. **29**(2): p. 417-429.e4.
13. Ginn, S.L., et al., *Gene therapy clinical trials worldwide to 2023-an update.* J Gene Med, 2024. **26**(8): p. e3721.
14. Administration, U.S.F.a.D., *FDA Expands Approval of Gene Therapy for Patients with Duchenne Muscular Dystrophy*. 2024.
15. Hinton, C.F., et al., *Developing a public health-tracking system for follow-up of newborn screening metabolic conditions: a four-state pilot project structure and initial findings.* Genetics in Medicine, 2014. **16**(6): p. 484-490.
16. Therrell, B.L., et al., *Inborn errors of metabolism identified via newborn screening: Ten-year incidence data and costs of nutritional interventions for research agenda planning.* Molecular Genetics and Metabolism, 2014. **113**(1): p. 14-26.
17. Metabolic Dietary Disorders Association. *Amino Acid Disorders - Maple Syrup Urine Disease*. 2017 [cited 2020 April 1 2020]; Available from: https://www.mdda.org.au/diagnosis/msud/.
18. Puffenberger, E.G., *Genetic heritage of the Old Order Mennonites of southeastern Pennsylvania.* American Journal of Medical Genetics Part C: Seminars in Medical Genetics, 2003. **121C**(1): p. 18-31.

19. Love-Gregory, L.D., et al., *Evidence of Common Ancestry for the Maple Syrup Urine Disease (MSUD) Y438N Allele in Non-Mennonite MSUD Patients.* Molecular Genetics and Metabolism, 2002. **75**(1): p. 79-90.
20. Strauss, K.A., et al., *Branched-chain α-ketoacid dehydrogenase deficiency (maple syrup urine disease): Treatment, biomarkers, and outcomes.* Molecular Genetics and Metabolism, 2020. **129**(3): p. 193-206.
21. Chapman, K.A., et al., *Incidence of maple syrup urine disease, propionic acidemia, and methylmalonic aciduria from newborn screening data.* Molecular genetics and metabolism reports, 2018. **15**: p. 106-109.
22. Edelmann, L., et al., *Maple syrup urine disease: identification and carrier-frequency determination of a novel founder mutation in the Ashkenazi Jewish population.* American journal of human genetics, 2001. **69**(4): p. 863-868.
23. Quental, S., et al., *Revisiting MSUD in Portuguese Gypsies: Evidence for a Founder Mutation and for a Mutational Hotspot within the BCKDHA Gene.* Annals of Human Genetics, 2009. **73**(3): p. 298-303.
24. Menkes, J.H., P.L. Hurst, and J.M. Craig, *A NEW SYNDROME: PROGRESSIVE FAMILIAL INFANTILE CEREBRAL DYSFUNCTION ASSOCIATED WITH AN UNUSUAL URINARY SUBSTANCE.* Pediatrics, 1954. **14**(5): p. 462-467.
25. Mazariegos, G.V., et al., *Liver Transplantation for Classical Maple Syrup Urine Disease: Long-Term Follow-Up in 37 Patients and Comparative United Network for Organ Sharing Experience.* The Journal of Pediatrics, 2012. **160**(1): p. 116-121.e1.
26. Brosnan, J.T. and M.E. Brosnan, *Branched-Chain Amino Acids: Enzyme and Substrate Regulation.* The Journal of Nutrition, 2006. **136**(1): p. 207S-211S.
27. Ananieva, E.A., et al., *Liver BCATm transgenic mouse model reveals the important role of the liver in maintaining BCAA homeostasis.* The Journal of nutritional biochemistry, 2017. **40**: p. 132-140.
28. Hall, T.R., et al., *Branched chain aminotransferase isoenzymes. Purification and characterization of the rat brain isoenzyme.* Journal of Biological Chemistry, 1993. **268**(5): p. 3092-3098.
29. Ichihara, A. and E. Koyama, *Transaminase of Branched Chain Amino Acids: I. Branched Chain Amino Acids-α-Ketoglutarate Transaminase.* The Journal of Biochemistry, 1966. **59**(2): p. 160-169.
30. Suryawan, A., et al., *A molecular model of human branched-chain amino acid metabolism.* The American Journal of Clinical Nutrition, 1998. **68**(1): p. 72-81.
31. Ævarsson, A., et al., *Crystal structure of human branched-chain α-ketoacid dehydrogenase and the molecular basis of multienzyme complex deficiency in maple syrup urine disease.* Structure, 2000. **8**(3): p. 277-291.
32. Wynn R.M., D.J.R., Meng M., Chuang D.T. , *Structure, function and assembly of mammalian branched-chain α-ketoacid dehydrogenase complex. I.* Alpha-Keto Acid Dehydrogenase Complexes. MCBU Molecular and Cell Biology Updates., ed. R.T.E. Patel M.S., Harris R.A. . 1996, Alpha-Keto Acid Dehydrogenase Complexes. MCBU Molecular and Cell Biology Updates.: Birkhäuser Basel.
33. Yeaman, S.J., *The 2-oxo acid dehydrogenase complexes: recent advances.* The Biochemical journal, 1989. **257**(3): p. 625-632.
34. Wynn, R.M., et al., *Chaperonins groEL and groES promote assembly of heterotetramers (alpha 2 beta 2) of mammalian mitochondrial branched-chain alpha-keto acid decarboxylase in Escherichia coli.* Journal of Biological Chemistry, 1992. **267**(18): p. 12400-3.

35. Kato, M., et al., *A synchronized substrate-gating mechanism revealed by cubic-core structure of the bovine branched-chain α-ketoacid dehydrogenase complex.* The EMBO Journal, 2006. **25**(24): p. 5983-5994.
36. Harper, A.E., R.H. Miller, and K.P. Block, *Branched-chain amino acid metabolism.* Annu Rev Nutr, 1984. **4**: p. 409-54.
37. Reed, L.J., *Multienzyme complexes.* Accounts of Chemical Research, 1974. **7**(2): p. 40-46.
38. Parker, P.J. and P.J. Randle, *Inactivation of rat heart branched-chain 2-oxoacid dehydrogenase complex by adenosine triphosphate.* FEBS Lett, 1978. **95**(1): p. 153-6.
39. Parker, P.J. and P.J. Randle, *Active and inactive forms of branched-chain 2-oxoacid dehydrogenase complex in rat heart and skeletal muscle.* FEBS Lett, 1980. **112**(2): p. 186-90.
40. Harris, R.A., R. Paxton, and R.A. Parker, *Activation of the branched-chain α-ketoacid dehydrogenase complex by a broad specificity protein phosphatase.* Biochemical and Biophysical Research Communications, 1982. **107**(4): p. 1497-1503.
41. Popov, K.M., Y. Shimomura, and R.A. Harris, *Purification and comparative study of the kinases specific for branched chain α-ketoacid dehydrogenase and pyruvate dehydrogenase.* Protein Expression and Purification, 1991. **2**(4): p. 278-286.
42. Harris, R.A., et al., *Regulation of Branched-Chain α-Keto Acid Dehydrogenase Kinase Expression in Rat Liver.* The Journal of Nutrition, 2001. **131**(3): p. 841S-845S.
43. Danner, D.J., S.K. Lemmon, and L.J. Elsas, *Substrate specificity and stabilization by thiamine pyrophosphate of rat liver branched chain α-ketoacid dehydrogenase.* Biochemical Medicine, 1978. **19**(1): p. 27-38.
44. Indo, Y., et al., *Altered kinetic properties of the branched-chain alpha-keto acid dehydrogenase complex due to mutation of the beta-subunit of the branched-chain alpha-keto acid decarboxylase (E1) component in lymphoblastoid cells derived from patients with maple syrup urine disease.* J Clin Invest, 1987. **80**(1): p. 63-70.
45. Mueller, G.M., et al., *Complementation of defective leucine decarboxylation in fibroblasts from a maple syrup urine disease patient by retrovirus-mediated gene transfer.* Gene Ther, 1995. **2**(7): p. 461-8.
46. Goodwin, G.W., et al., *[23] Determination of activity and activity state of branched-chain α-keto acid dehydrogenase in rat tissues*, in *Methods in Enzymology*. 1988, Academic Press. p. 189-201.
47. Paxton, R. and R.A. Harris, *Isolation of rabbit liver branched chain alpha-ketoacid dehydrogenase and regulation by phosphorylation.* J Biol Chem, 1982. **257**(23): p. 14433-9.
48. Paul, H.S. and S.A. Adibi, *Role of ATP in the regulation of branched-chain alpha-keto acid dehydrogenase activity in liver and muscle mitochondria of fed, fasted, and diabetic rats.* J Biol Chem, 1982. **257**(9): p. 4875-81.
49. Popov, K.M., et al., *Dietary control and tissue specific expression of branched-chain alpha-ketoacid dehydrogenase kinase.* Arch Biochem Biophys, 1995. **316**(1): p. 148-54.
50. Fujii, H., et al., *Branched-chain alpha-keto acid dehydrogenase kinase content in rat skeletal muscle is decreased by endurance training.* Biochem Mol Biol Int, 1998. **44**(6): p. 1211-6.
51. Rodríguez, T., et al., *The increased skeletal muscle protein turnover of the streptozotocin diabetic rat is associated with high concentrations of branched-chain amino acids.* Biochem Mol Med, 1997. **61**(1): p. 87-94.
52. Shimomura, Y., et al., *Regulation of branched-chain amino acid catabolism: nutritional and hormonal regulation of activity and expression of the branched-chain*

alpha-keto acid dehydrogenase kinase. Curr Opin Clin Nutr Metab Care, 2001. **4**(5): p. 419-23.
53. Kobayashi, R., et al., *Gender difference in regulation of branched-chain amino acid catabolism.* Biochem J, 1997. **327 (Pt 2)**(Pt 2): p. 449-53.
54. Xu, M., et al., *Mechanism of Activation of Branched-Chain α-Keto Acid Dehydrogenase Complex by Exercise.* Biochemical and Biophysical Research Communications, 2001. **287**(3): p. 752-756.
55. Huang, Y.S. and D.T. Chuang, *Down-regulation of rat mitochondrial branched-chain 2-oxoacid dehydrogenase kinase gene expression by glucocorticoids.* Biochem J, 1999. **339 (Pt 3)**(Pt 3): p. 503-10.
56. Kobayashi, R., et al., *Experimental Hyperthyroidism Causes Inactivation of the Branched-Chain α-Ketoacid Dehydrogenase Complex in Rat Liver.* Archives of Biochemistry and Biophysics, 2000. **375**(1): p. 55-61.
57. May, M.E., R.P. Aftring, and M.G. Buse, *Mechanism of the stimulation of branched chain oxoacid oxidation in liver by carnitine.* J Biol Chem, 1980. **255**(18): p. 8394-7.
58. Yue, S.J., et al., *Berberine alleviates insulin resistance by reducing peripheral branched-chain amino acids.* Am J Physiol Endocrinol Metab, 2019. **316**(1): p. E73-e85.
59. Kobayashi, R., et al., *Clofibric acid stimulates branched-chain amino acid catabolism by three mechanisms.* Arch Biochem Biophys, 2002. **407**(2): p. 231-40.
60. Van Koevering, M. and S. Nissen, *Oxidation of leucine and alpha-ketoisocaproate to beta-hydroxy-beta-methylbutyrate in vivo.* Am J Physiol, 1992. **262**(1 Pt 1): p. E27-31.
61. Muelly, E.R., et al., *Biochemical correlates of neuropsychiatric illness in maple syrup urine disease.* The Journal of Clinical Investigation, 2013. **123**(4): p. 1809-1820.
62. Smith, Q.R., et al., *Kinetics of Neutral Amino Acid Transport Across the Blood-Brain Barrier.* Journal of Neurochemistry, 1987. **49**(5): p. 1651-1658.
63. Strauss KA, P.E., Carson VJ. , *Maple Syrup Urine Disease*. Gene Reviews, ed. A.H. Adam MP, Pagon RA, et al., editors. 2006, Seattle: University of Washington.
64. Simon, E., U. Wendel, and P. Schadewaldt, *Maple syrup urine disease-treatment and outcome in patients of Turkish descent in Germany.* Turk J Pediatr, 2005. **47**(1): p. 8-13.
65. Hoffmann, B., et al., *Impact of longitudinal plasma leucine levels on the intellectual outcome in patients with classic MSUD.* Pediatr Res, 2006. **59**(1): p. 17-20.
66. Schulman, J.D., et al., *A new variant of maple syrup urine disease (branched chain ketoaciduria): Clinical and biochemical evaluation.* The American Journal of Medicine, 1970. **49**(1): p. 118-124.
67. Simon, E., et al., *Variant maple syrup urine disease (MSUD)--the entire spectrum.* J Inherit Metab Dis, 2006. **29**(6): p. 716-24.
68. Dancis, J., J. Hutzler, and T. Rokkones, *Intermittent branched-chain ketonuria. Variant of maple-syrup-urine disease.* N Engl J Med, 1967. **276**(2): p. 84-9.
69. Zhang, B., et al., *Evidence for both a regulatory mutation and a structural mutation in a family with maple syrup urine disease.* The Journal of clinical investigation, 1989. **83**(4): p. 1425-1429.
70. Scriver, C.R., et al., *Thiamine-responsive maple-syrup-urine disease.* Lancet, 1971. **1**(7694): p. 310-2.
71. Shaag, A., et al., *Molecular basis of lipoamide dehydrogenase deficiency in Ashkenazi Jews.* Am J Med Genet, 1999. **82**(2): p. 177-82.
72. TOKITOMO, Y.K., A; YAMANISHI, T ; MURAKI, S, *STUDIES ON THE SUGARY FLAVOR OF RAW CANE SUGAR .3. KEY COMPOUND OF THE SUGARY FLAVOR.*

Proceedings of the Japan Academy Series B-Physical and Biological Sciences, 1980. **56**(7): p. 457-462.
73. Korman, S.H., E. Cohen, and A. Preminger, *Pseudo-maple syrup urine disease due to maternal prenatal ingestion of fenugreek.* Journal of Paediatrics and Child Health, 2001. **37**(4): p. 403-404.
74. Bartley, G.B., et al., *"Maple-syrup" urine odor due to fenugreek ingestion.* N Engl J Med, 1981. **305**(8): p. 467.
75. Sewell, A.C., A. Mosandl, and H. Böhles, *False diagnosis of maple syrup urine disease owing to ingestion of herbal tea.* N Engl J Med, 1999. **341**(10): p. 769.
76. Mamer, O.A. and M.L.J. Reimer, *On the mechanisms of the formation of L-alloisoleucine and the 2-hydroxy- 3-methylvaleric acid stereoisomers from L-isoleucine in maple syrup urine disease patients and in normal humans.* Journal of Biological Chemistry, 1992. **267**(31): p. 22141-22147.
77. Schadewaldt, P., et al., *Significance of L-alloisoleucine in plasma for diagnosis of maple syrup urine disease.* Clin Chem, 1999. **45**(10): p. 1734-40.
78. Simon, E., et al., *Maple syrup urine disease: favourable effect of early diagnosis by newborn screening on the neonatal course of the disease.* J Inherit Metab Dis, 2006. **29**(4): p. 532-7.
79. Lu, G., et al., *A novel mitochondrial matrix serine/threonine protein phosphatase regulates the mitochondria permeability transition pore and is essential for cellular survival and development.* Genes Dev, 2007. **21**(7): p. 784-96.
80. Imre, G., et al., *Prolonged activity of the transposase helper may raise safety concerns during DNA transposon-based gene therapy.* Molecular Therapy Methods & Clinical Development, 2023. **29**: p. 145-159.
81. Khalifa, O.A., et al., *Genotype-phenotype correlation of 33 patients with maple syrup urine disease.* Am J Med Genet A, 2020. **182**(11): p. 2486-2500.
82. Ambrus, A. and V. Adam-Vizi, *Human dihydrolipoamide dehydrogenase (E3) deficiency: Novel insights into the structural basis and molecular pathomechanism.* Neurochemistry International, 2018. **117**: p. 5-14.
83. Chuang, J.L., et al., *Molecular basis of maple syrup urine disease: novel mutations at the E1 alpha locus that impair E1(alpha 2 beta 2) assembly or decrease steady-state E1 alpha mRNA levels of branched-chain alpha-keto acid dehydrogenase complex.* American journal of human genetics, 1994. **55**(2): p. 297-304.
84. Oyarzabal, A., et al., *A Novel Regulatory Defect in the Branched-Chain α-Keto Acid Dehydrogenase Complex Due to a Mutation in the PPM1K Gene Causes a Mild Variant Phenotype of Maple Syrup Urine Disease.* Human Mutation, 2013. **34**(2): p. 355-362.
85. Stenson, P.D., et al., *The Human Gene Mutation Database (HGMD(®)): optimizing its use in a clinical diagnostic or research setting.* Hum Genet, 2020. **139**(10): p. 1197-1207.
86. Abiri, M., et al., *Maple syrup urine disease mutation spectrum in a cohort of 40 consanguineous patients and insilico analysis of novel mutations.* Metabolic Brain Disease, 2019. **34**(4): p. 1145-1156.
87. Abiri, M., et al., *In silico analysis of novel mutations in maple syrup urine disease patients from Iran.* Metab Brain Dis, 2017. **32**(1): p. 105-113.
88. Abiri, M., et al., *Identification of six novel mutations in Iranian patients with maple syrup urine disease and their in silico analysis.* Mutat Res, 2016. **786**: p. 34-40.
89. Ali, E.Z. and L.-H. Ngu, *Fourteen new mutations of BCKDHA, BCKDHB and DBT genes associated with maple syrup urine disease (MSUD) in Malaysian population.* Molecular genetics and metabolism reports, 2018. **17**: p. 22-30.

90. Bashyam, M.D., et al., *Molecular genetic analysis of MSUD from India reveals mutations causing altered protein truncation affecting the C-termini of E1α and E1β.* Journal of Cellular Biochemistry, 2012. **113**(10): p. 3122-3132.
91. Brodtkorb, E., et al., *Four novel mutations identified in Norwegian patients result in intermittent maple syrup urine disease when combined with the R301C mutation.* Molecular Genetics and Metabolism, 2010. **100**(4): p. 324-332.
92. Chinsky, J., et al., *A nonsense mutation (R242X) in the branched-chain alpha-keto acid dehydrogenase E1alpha subunit gene (BCKDHA) as a cause of maple syrup urine disease. Mutations in brief no. 160. Online.* Hum Mutat, 1998. **12**(2): p. 136.
93. Chuang, J.L., R.P. Cox, and D.T. Chuang, *Maple syrup urine disease: the E1beta gene of human branched-chain alpha-ketoacid dehydrogenase complex has 11 rather than 10 exons, and the 3' UTR in one of the two E1beta mRNAs arises from intronic sequences.* American journal of human genetics, 1996. **58**(6): p. 1373-1377.
94. Chuang, J.L., et al., *Molecular and biochemical basis of intermediate maple syrup urine disease. Occurrence of homozygous G245R and F364C mutations at the E1 alpha locus of Hispanic-Mexican patients.* The Journal of clinical investigation, 1995. **95**(3): p. 954-963.
95. Dursun, A., et al., *Maple syrup urine disease: Mutation analysis in Turkish patients.* Journal of Inherited Metabolic Disease, 2002. **25**(2): p. 89-97.
96. Fernández-Lainez, C., et al., *In silico prediction of the pathogenic effect of a novel variant of BCKDHA leading to classical maple syrup urine disease identified using clinical exome sequencing.* Clin Chim Acta, 2018. **483**: p. 33-38.
97. Gorzelany, K., et al., *Molecular genetics of maple syrup urine disease in the Turkish population.* The Turkish Journal of Pediatrics, 2009. **51**(2): p. 97-102.
98. Han, B., et al., *Two novel mutations in the BCKDHB gene that cause maple syrup urine disease.* Pediatrics & Neonatology, 2018. **59**(5): p. 515-519.
99. Henneke, M., et al., *Identification of twelve novel mutations in patients with classic and variant forms of maple syrup urine disease.* Human Mutation, 2003. **22**(5): p. 417-417.
100. Hou, J.-W. and T.-L. Hwang, *Different Gene Preferences of Maple Syrup Urine Disease in the Aboriginal Tribes of Taiwan.* Pediatrics & Neonatology, 2014. **55**(3): p. 213-217.
101. Imtiaz, F., et al., *Twenty novel mutations in BCKDHA, BCKDHB and DBT genes in a cohort of 52 Saudi Arabian patients with maple syrup urine disease.* Molecular genetics and metabolism reports, 2017. **11**: p. 17-23.
102. Jaafar, N., et al., *Molecular characterization of maple syrup urine disease patients from Tunisia.* Gene, 2013. **517**(1): p. 116-119.
103. Li T, W.Y., Li C, Xu WW, Niu FH, Zhang D, *Maple syrup urine disease and gene mutations in twin neonates.* Zhongguo Dang Dai Er Ke Za Zhi, 2016. **18**(12): p. 1242-1246.
104. Li, X., et al., *Clinical characteristics and mutation analysis of five Chinese patients with maple syrup urine disease.* Metabolic Brain Disease, 2018. **33**(3): p. 741-751.
105. Mei S, B.N., Hu S, Liu N, Zhao Z, Kong X., *Mutation analysis and prenatal diagnosis for a pedigree affected with maple syrup urine disease.* Chuan Hsueh Tsa Chih, 2018. **35**(5): p. 679-682.
106. Nellis, M.M., et al., *Relationship of causative genetic mutations in maple syrup urine disease with their clinical expression.* Molecular Genetics and Metabolism, 2003. **80**(1): p. 189-195.
107. Park, H.-D., et al., *Three Korean Patients with Maple Syrup Urine Disease: Four Novel Mutations in the BCKDHA Gene.* Annals of Clinical & Laboratory Science, 2011. **41**(2): p. 167-173.

108. Rodríguez-Pombo, P., et al., *Mutational spectrum of maple syrup urine disease in Spain.* Human Mutation, 2006. **27**(7): p. 715-715.
109. Sedaghat, A., et al., *Frequent novel mutations are causative for maple syrup urine disease from Southwest Iran.* Meta Gene, 2018. **16**: p. 96-104.
110. Song, D., et al., *A classic case with maple syrup urine disease caused by compound heterozygous mutations of BCKDHB gene.* Chinese Journal of Medical Genetics, 2018. **35**(5): p. 699-702.
111. Stojiljkovic, M., et al., *Molecular and phenotypic characteristics of seven novel mutations causing branched-chain organic acidurias.* Clinical Genetics, 2016. **90**(3): p. 252-257.
112. Sun, W.-H., et al., *Identification of eight novel mutations in 11 Chinese patients with maple syrup urine disease.* World Journal Of Pediatrics: WJP, 2020.
113. Wynn, R.M., et al., *Impaired Assembly of E1 Decarboxylase of the Branched-chain α-Ketoacid Dehydrogenase Complex in Type IA Maple Syrup Urine Disease.* Journal of Biological Chemistry, 1998. **273**(21): p. 13110-13118.
114. Li, X., et al., *Eleven novel mutations of the BCKDHA, BCKDHB and DBT genes associated with maple syrup urine disease in the Chinese population: Report on eight cases.* European Journal of Medical Genetics, 2015. **58**(11): p. 617-623.
115. Russell, G.C. and J.R. Guest, *Sequence similarities within the family of dihydrolipoamide acyltransferases and discovery of a previously unidentified fungal enzyme.* Biochimica et Biophysica Acta (BBA)/Protein Structure and Molecular, 1991. **1076**(2): p. 225-232.
116. Wexler, I.D., S.G. Hemalatha, and M.S. Patel, *Sequence conservation in the α and β subunits of pyruvate dehydrogenase and its similarity to branched-chain α-keto acid dehydrogenase.* FEBS Letters, 1991. **282**(1): p. 209-213.
117. Eisenstein, R.S., et al., *Altered phosphorylation state of branched-chain 2-oxo acid dehydrogenase in a branched-chain acyltransferase deficient human fibroblast cell line.* J Inherit Metab Dis, 1991. **14**(1): p. 37-44.
118. Chuang, J.L., R.P. Cox, and D.T. Chuang, *Molecular cloning of the mature E1b-beta subunit of human branched-chain alpha-keto acid dehydrogenase complex.* FEBS Lett, 1990. **262**(2): p. 305-9.
119. Dyson, N., et al., *Homologous sequences in adenovirus E1A and human papillomavirus E7 proteins mediate interaction with the same set of cellular proteins.* J Virol, 1992. **66**(12): p. 6893-902.
120. Frazier, D.M., et al., *Nutrition management guideline for maple syrup urine disease: An evidence- and consensus-based approach.* Molecular Genetics and Metabolism, 2014. **112**(3): p. 210-217.
121. Zheng, Y., et al., *Cumulative consumption of branched-chain amino acids and incidence of type 2 diabetes.* Int J Epidemiol, 2016. **45**(5): p. 1482-1492.
122. Jennings, A., et al., *Associations between branched chain amino acid intake and biomarkers of adiposity and cardiometabolic health independent of genetic factors: A twin study.* Int J Cardiol, 2016. **223**: p. 992-998.
123. Strauss, K.A., et al., *Classical maple syrup urine disease and brain development: principles of management and formula design.* Molecular genetics and metabolism, 2010. **99**(4): p. 333-345.
124. de Lonlay, P., et al., *Real-world management of maple syrup urine disease (MSUD) metabolic decompensations with branched chain amino acid-free formulas in France and Germany: A retrospective observational study.* JIMD Rep, 2021. **59**(1): p. 110-119.

125. Elserafy, N., et al., *Liver transplantation in children with inborn errors of metabolism: 30 years experience in NSW, Australia.* JIMD Rep, 2021. **60**(1): p. 88-95.
126. Oishi, K., et al., *Liver transplantation for pediatric inherited metabolic disorders: Considerations for indications, complications, and perioperative management.* Pediatr Transplant, 2016. **20**(6): p. 756-69.
127. Shneider, B.L., J. Vockley, and G.V. Mazariegos, *Trading places: Liver transplantation as a treatment, not a cure, for metabolic liver disease.* Liver Transplantation, 2011. **17**(6): p. 628-630.
128. McCaughan, G.W. and S.R. Munn, *Liver transplantation in Australia and New Zealand.* Liver Transpl, 2016. **22**(6): p. 830-8.
129. Spada, M., et al., *Pediatric liver transplantation.* World J Gastroenterol, 2009. **15**(6): p. 648-74.
130. Aras, A., et al., *Long-term results of liver transplantation for maple syrup urine disease: A single-center experience in Turkey.* Pediatr Transplant, 2023. **27**(3): p. e14464.
131. Herden, U., et al., *Surgical Aspects of Liver Transplantation and Domino Liver Transplantation in Maple Syrup Urine Disease: Analysis of 15 Donor-Recipient Pairs.* Liver Transplantation, 2019. **25**(6): p. 889-900.
132. McCaughan, G.W. and S.R. Munn, *Liver transplantation in Australia and New Zealand.* Liver Transplantation, 2016. **22**(6): p. 830-838.
133. le Roux, C., et al., *The longest-surviving patient with classical maple syrup urine disease.* Journal of Inherited Metabolic Disease, 2006. **29**(1): p. 190-194.
134. Mütze, U., et al., *Long-term Outcomes of Individuals With Metabolic Diseases Identified Through Newborn Screening.* Pediatrics, 2020. **146**(5): p. e20200444.
135. Lee, J.Y., et al., *Maple syrup urine disease (MSUD)--clinical profile of 47 Filipino patients.* J Inherit Metab Dis, 2008. **31 Suppl 2**: p. S281-5.
136. Avila, C.M.S. and M.A.R. Abacan, *Factors associated with poor outcomes in patients with maple syrup urine disease in a tertiary government hospital: A retrospective cohort study.* JIMD Reports, 2024. **n/a**(n/a).
137. Ti, W.J., *Maple syrup urine disease in mainland China.* J Pediatr Endocrinol Metab, 2011. **24**(9-10): p. 857.
138. Chiong, M.A.D., et al., *Plasma amino acid and urine organic acid profiles of Filipino patients with maple syrup urine disease (MSUD) and correlation with their neurologic features.* Molecular genetics and metabolism reports, 2016. **9**: p. 46-53.
139. De Castro-Hamoy, L.G., et al., *Challenges in the management of patients with maple syrup urine disease diagnosed by newborn screening in a developing country.* Journal of community genetics, 2017. **8**(1): p. 9-15.
140. Packman, W., et al., *Psychosocial issues in families affected by maple syrup urine disease.* J Genet Couns, 2007. **16**(6): p. 799-809.
141. Tchan, M., et al., *The management of pregnancy in maple syrup urine disease: experience with two patients.* JIMD Rep, 2013. **10**: p. 113-7.
142. Skvorak, K.J., et al., *Hepatocyte transplantation improves phenotype and extends survival in a murine model of intermediate maple syrup urine disease.* Mol Ther, 2009. **17**(7): p. 1266-73.
143. Sonnet, D.S., et al., *Metformin inhibits Branched Chain Amino Acid (BCAA) derived ketoacidosis and promotes metabolic homeostasis in MSUD.* Scientific Reports, 2016. **6**(1): p. 28775.
144. Yue, S.-J., et al., *Berberine alleviates insulin resistance by reducing peripheral branched-chain amino acids.* American Journal of Physiology-Endocrinology and Metabolism, 2018. **316**(1): p. E73-E85.

145. F, M., *Die Histochemischen und Physiologischen Arbeiten von Friedrich Miescher - Aus dem wissenschaftlichen Briefwechsel* Leipzig, pp 33–38, 1869.
146. Avery, O.T., C.M. Macleod, and M. McCarty, *STUDIES ON THE CHEMICAL NATURE OF THE SUBSTANCE INDUCING TRANSFORMATION OF PNEUMOCOCCAL TYPES : INDUCTION OF TRANSFORMATION BY A DESOXYRIBONUCLEIC ACID FRACTION ISOLATED FROM PNEUMOCOCCUS TYPE III.* J Exp Med, 1944. **79**(2): p. 137-58.
147. Levene, P.A. and J.A. Mandel, *Über die Konstitution der Thymo-nucleinsäure.* Berichte der deutschen chemischen Gesellschaft, 1908. **41**(2): p. 1905-1909.
148. Vischer, E. and E. Chargaff, *THE SEPARATION AND QUANTITATIVE ESTIMATION OF PURINES AND PYRIMIDINES IN MINUTE AMOUNTS.* Journal of Biological Chemistry, 1948. **176**(2): p. 703-714.
149. Franklin, R.E. and R.G. Gosling, *Molecular configuration in sodium thymonucleate.* Nature, 1953. **171**(4356): p. 740-1.
150. Watson, J.D. and F.H. Crick, *Molecular structure of nucleic acids; a structure for deoxyribose nucleic acid.* Nature, 1953. **171**(4356): p. 737-8.
151. Goswami, R., et al., *Gene Therapy Leaves a Vicious Cycle.* Frontiers in Oncology, 2019. **9**: p. 297.
152. Lander, E.S., et al., *Initial sequencing and analysis of the human genome.* Nature, 2001. **409**(6822): p. 860-921.
153. Griffith, F., *The Significance of Pneumococcal Types.* J Hyg (Lond), 1928. **27**(2): p. 113-59.
154. Zinder, N.D. and J. Lederberg, *Genetic exchange in Salmonella.* J Bacteriol, 1952. **64**(5): p. 679-99.
155. Rogers, S., et al., *Induction of arginase activity with the Shope papilloma virus in tissue culture cells from an argininemic patient.* J Exp Med, 1973. **137**(4): p. 1091-6.
156. Rosenberg, S.A., et al., *Gene transfer into humans--immunotherapy of patients with advanced melanoma, using tumor-infiltrating lymphocytes modified by retroviral gene transduction.* N Engl J Med, 1990. **323**(9): p. 570-8.
157. Orkin SH, M.A., *Report and Recommendations of the Panel to Assess the NIH Investment in Research on Gene Therapy*. 1995, National Institutes of Health: Bethesda, MD.
158. Savulescu, J., *Harm, ethics committees and the gene therapy death.* Journal of Medical Ethics, 2001. **27**(3): p. 148.
159. Marshall, E., *Gene Therapy Death Prompts Review of Adenovirus Vector.* Science, 1999. **286**(5448): p. 2244-2245.
160. Check, E., *Gene therapy put on hold as third child develops cancer.* Nature, 2005. **433**(7026): p. 561.
161. Hacein-Bey-Abina, S., et al., *LMO2-associated clonal T cell proliferation in two patients after gene therapy for SCID-X1.* Science, 2003. **302**(5644): p. 415-9.
162. Hacein-Bey-Abina, S., et al., *Insertional oncogenesis in 4 patients after retrovirus-mediated gene therapy of SCID-X1.* J Clin Invest, 2008. **118**(9): p. 3132-42.
163. Dunbar, C.E., et al., *Gene therapy comes of age.* Science, 2018. **359**(6372): p. eaan4672.
164. Ginn, S.L., et al., *Gene therapy clinical trials worldwide to 2017: An update.* J Gene Med, 2018. **20**(5): p. e3015.
165. Wang, D., P.W.L. Tai, and G. Gao, *Adeno-associated virus vector as a platform for gene therapy delivery.* Nature reviews. Drug discovery, 2019. **18**(5): p. 358-378.

166. Kay, M.A., J.C. Glorioso, and L. Naldini, *Viral vectors for gene therapy: the art of turning infectious agents into vehicles of therapeutics.* Nature Medicine, 2001. **7**(1): p. 33-40.
167. Servellita, V., et al., *Adeno-associated virus type 2 in US children with acute severe hepatitis.* Nature, 2023. **617**(7961): p. 574-580.
168. Ehrhardt, A., H. Xu, and M.A. Kay, *Episomal persistence of recombinant adenoviral vector genomes during the cell cycle in vivo.* J Virol, 2003. **77**(13): p. 7689-95.
169. Escors, D. and K. Breckpot, *Lentiviral Vectors in Gene Therapy: Their Current Status and Future Potential.* Archivum Immunologiae et Therapiae Experimentalis, 2010. **58**(2): p. 107-119.
170. Zhao, Y. and L. Huang, *Lipid nanoparticles for gene delivery.* Advances in genetics, 2014. **88**: p. 13-36.
171. Jayant, R.D., et al., *Current status of non-viral gene therapy for CNS disorders.* Expert opinion on drug delivery, 2016. **13**(10): p. 1433-1445.
172. Li, S.D., S. Chono, and L. Huang, *Efficient oncogene silencing and metastasis inhibition via systemic delivery of siRNA.* Mol Ther, 2008. **16**(5): p. 942-6.
173. Xiang, B., et al., *PSA-responsive and PSMA-mediated multifunctional liposomes for targeted therapy of prostate cancer.* Biomaterials, 2013. **34**(28): p. 6976-91.
174. Huang, X., et al., *Targeted delivery of microRNA-29b by transferrin-conjugated anionic lipopolyplex nanoparticles: a novel therapeutic strategy in acute myeloid leukemia.* Clin Cancer Res, 2013. **19**(9): p. 2355-67.
175. Majzoub, R.N., et al., *Uptake and transfection efficiency of PEGylated cationic liposome-DNA complexes with and without RGD-tagging.* Biomaterials, 2014. **35**(18): p. 4996-5005.
176. Gomes-da-Silva, L.C., et al., *Lipid-based nanoparticles for siRNA delivery in cancer therapy: paradigms and challenges.* Acc Chem Res, 2012. **45**(7): p. 1163-71.
177. Nathwani, A.C., et al., *Long-Term Safety and Efficacy of Factor IX Gene Therapy in Hemophilia B.* New England Journal of Medicine, 2014. **371**(21): p. 1994-2004.
178. Moore, A.R., et al., *Vaccinia virus as a subhelper for AAV replication and packaging.* Molecular Therapy - Methods & Clinical Development, 2015. **2**: p. 15044.
179. Buller, R.M.L., et al., *Herpes Simplex Virus Types 1 and 2 Completely Help Adenovirus-Associated Virus Replication.* Journal of Virology, 1981. **40**(1): p. 241.
180. Ogston, P., K. Raj, and P. Beard, *Productive Replication of Adeno-Associated Virus Can Occur in Human Papillomavirus Type 16 (HPV-16) Episome-Containing Keratinocytes and Is Augmented by the HPV-16 E2 Protein.* Journal of Virology, 2000. **74**(8): p. 3494.
181. Atchison, R.W., B.C. Casto, and D.H. William Mc, *Adenovirus-Associated Defective Virus Particles.* Science, 1965. **149**(3685): p. 754-756.
182. Flotte, T.R. and K.I. Berns, *Adeno-Associated Virus: A Ubiquitous Commensal of Mammals.* Human Gene Therapy, 2005. **16**(4): p. 401-407.
183. Srivastava, A., E.W. Lusby, and K.I. Berns, *Nucleotide sequence and organization of the adeno-associated virus 2 genome.* J Virol, 1983. **45**(2): p. 555-64.
184. Kotin, R.M. and K.I. Berns, *Organization of adeno-associated virus DNA in latently infected detroit 6 cells.* Virology, 1989. **170**(2): p. 460-467.
185. Kotin, R.M., et al., *Mapping and direct visualization of a region-specific viral DNA integration site on chromosome 19q13-qter.* Genomics, 1991. **10**(3): p. 831-834.
186. Philpott, N.J., et al., *A p5 integration efficiency element mediates Rep-dependent integration into AAVS1 at chromosome 19.* Proc Natl Acad Sci U S A, 2002. **99**(19): p. 12381-5.

187. Pereira, D.J., D.M. McCarty, and N. Muzyczka, *The adeno-associated virus (AAV) Rep protein acts as both a repressor and an activator to regulate AAV transcription during a productive infection.* J Virol, 1997. **71**(2): p. 1079-88.
188. Daya, S. and K.I. Berns, *Gene therapy using adeno-associated virus vectors.* Clinical microbiology reviews, 2008. **21**(4): p. 583-593.
189. Kozak, M., *Compilation and analysis of sequences upstream from the translational start site in eukaryotic mRNAs.* Nucleic Acids Res, 1984. **12**(2): p. 857-72.
190. Earley, L.F., et al., *Adeno-Associated Virus Serotype-Specific Inverted Terminal Repeat Sequence Role in Vector Transgene Expression.* Hum Gene Ther, 2020. **31**(3-4): p. 151-162.
191. Gao, G., et al., *Clades of Adeno-associated viruses are widely disseminated in human tissues.* Journal of virology, 2004. **78**(12): p. 6381-6388.
192. Hüser, D., et al., *High Prevalence of Infectious Adeno-associated Virus (AAV) in Human Peripheral Blood Mononuclear Cells Indicative of T Lymphocytes as Sites of AAV Persistence.* Journal of Virology, 2017. **91**(4): p. e02137-16.
193. Chen, C.L., et al., *Molecular characterization of adeno-associated viruses infecting children.* J Virol, 2005. **79**(23): p. 14781-92.
194. Calcedo, R., et al., *Worldwide epidemiology of neutralizing antibodies to adeno-associated viruses.* J Infect Dis, 2009. **199**(3): p. 381-90.
195. Boutin, S., et al., *Prevalence of serum IgG and neutralizing factors against adeno-associated virus (AAV) types 1, 2, 5, 6, 8, and 9 in the healthy population: implications for gene therapy using AAV vectors.* Hum Gene Ther, 2010. **21**(6): p. 704-12.
196. Yates, V.J., et al., *Isolation and Characterization of an Avian Adenovirus-Associated Virus.* Infection and Immunity, 1973. **7**(6): p. 973.
197. Lochrie, M.A., et al., *Adeno-associated virus (AAV) capsid genes isolated from rat and mouse liver genomic DNA define two new AAV species distantly related to AAV-5.* Virology, 2006. **353**(1): p. 68-82.
198. Arbetman, A.E., et al., *Novel caprine adeno-associated virus (AAV) capsid (AAV-Go.1) is closely related to the primate AAV-5 and has unique tropism and neutralization properties.* Journal of virology, 2005. **79**(24): p. 15238-15245.
199. Li, Y., et al., *Bat adeno-associated viruses as gene therapy vectors with the potential to evade human neutralizing antibodies.* Gene Therapy, 2019. **26**(6): p. 264-276.
200. Raupp, C., et al., *The threefold protrusions of adeno-associated virus type 8 are involved in cell surface targeting as well as postattachment processing.* J Virol, 2012. **86**(17): p. 9396-408.
201. Girod, A., et al., *Genetic capsid modifications allow efficient re-targeting of adeno-associated virus type 2.* Nat Med, 1999. **5**(9): p. 1052-6.
202. Münch, R.C., et al., *Off-target-free gene delivery by affinity-purified receptor-targeted viral vectors.* Nat Commun, 2015. **6**: p. 6246.
203. Yang, Q., et al., *Development of Novel Cell Surface CD34-Targeted Recombinant Adenoassociated Virus Vectors for Gene Therapy.* Human Gene Therapy, 1998. **9**(13): p. 1929-1937.
204. Bowles, D.E., et al., *Phase 1 gene therapy for Duchenne muscular dystrophy using a translational optimized AAV vector.* Mol Ther, 2012. **20**(2): p. 443-55.
205. Hordeaux, J., et al., *The Neurotropic Properties of AAV-PHP.B Are Limited to C57BL/6J Mice.* Mol Ther, 2018. **26**(3): p. 664-668.
206. Dayton, R.D., M.S. Grames, and R.L. Klein, *More expansive gene transfer to the rat CNS: AAV PHP.EB vector dose-response and comparison to AAV PHP.B.* Gene Ther, 2018. **25**(5): p. 392-400.

207. Matsuzaki, Y., et al., *Intravenous administration of the adeno-associated virus-PHP.B capsid fails to upregulate transduction efficiency in the marmoset brain.* Neurosci Lett, 2018. **665**: p. 182-188.
208. Srivastava, A., *In vivo tissue-tropism of adeno-associated viral vectors.* Current opinion in virology, 2016. **21**: p. 75-80.
209. Pillay, S., et al., *An essential receptor for adeno-associated virus infection.* Nature, 2016. **530**(7588): p. 108-112.
210. Summerford, C. and R.J. Samulski, *Membrane-associated heparan sulfate proteoglycan is a receptor for adeno-associated virus type 2 virions.* J Virol, 1998. **72**(2): p. 1438-45.
211. Qing, K., et al., *Human fibroblast growth factor receptor 1 is a co-receptor for infection by adeno-associated virus 2.* Nat Med, 1999. **5**(1): p. 71-7.
212. Summerford, C., J.S. Bartlett, and R.J. Samulski, *AlphaVbeta5 integrin: a co-receptor for adeno-associated virus type 2 infection.* Nat Med, 1999. **5**(1): p. 78-82.
213. Kashiwakura, Y., et al., *Hepatocyte growth factor receptor is a coreceptor for adeno-associated virus type 2 infection.* J Virol, 2005. **79**(1): p. 609-14.
214. Gao, G.-P., et al., *Novel adeno-associated viruses from rhesus monkeys as vectors for human gene therapy.* Proceedings of the National Academy of Sciences, 2002. **99**(18): p. 11854.
215. Vandenberghe, L.H., et al., *Efficient serotype-dependent release of functional vector into the culture medium during adeno-associated virus manufacturing.* Human gene therapy, 2010. **21**(10): p. 1251-1257.
216. Grimm, D., et al., *In vitro and in vivo gene therapy vector evolution via multispecies interbreeding and retargeting of adeno-associated viruses.* Journal of virology, 2008. **82**(12): p. 5887-5911.
217. Lisowski, L., et al., *Selection and evaluation of clinically relevant AAV variants in a xenograft liver model.* Nature, 2014. **506**(7488): p. 382-6.
218. Nathwani, A.C., et al., *Adenovirus-Associated Virus Vector–Mediated Gene Transfer in Hemophilia B.* New England Journal of Medicine, 2011. **365**(25): p. 2357-2365.
219. Yan, Z., H. Yan, and H. Ou, *Human thyroxine binding globulin (TBG) promoter directs efficient and sustaining transgene expression in liver-specific pattern.* Gene, 2012. **506**(2): p. 289-94.
220. Foecking, M.K. and H. Hofstetter, *Powerful and versatile enhancer-promoter unit for mammalian expression vectors.* Gene, 1986. **45**(1): p. 101-105.
221. Thomsen, D.R., et al., *Promoter-regulatory region of the major immediate early gene of human cytomegalovirus.* Proceedings of the National Academy of Sciences, 1984. **81**(3): p. 659-663.
222. Kim, D.W., et al., *Use of the human elongation factor 1 alpha promoter as a versatile and efficient expression system.* Gene, 1990. **91**(2): p. 217-23.
223. Okabe, M., et al., *'Green mice' as a source of ubiquitous green cells.* FEBS Letters, 1997. **407**(3): p. 313-319.
224. Crinelli, R., et al., *Molecular Dissection of the Human Ubiquitin C Promoter Reveals Heat Shock Element Architectures with Activating and Repressive Functions.* PLoS One, 2015. **10**(8): p. e0136882.
225. Hannan, G.N., et al., *An engineered PGK promoter and lac operator-repressor system for the regulation of gene expression in mammalian cells.* Gene, 1993. **130**(2): p. 233-9.
226. Angov, E., et al., *Heterologous protein expression is enhanced by harmonizing the codon usage frequencies of the target gene with those of the expression host.* PLoS One, 2008. **3**(5): p. e2189.

227. Fu, H., et al., *Codon optimization with deep learning to enhance protein expression.* Scientific Reports, 2020. **10**(1): p. 17617.
228. Xu, D.H., et al., *SV40 intron, a potent strong intron element that effectively increases transgene expression in transfected Chinese hamster ovary cells.* J Cell Mol Med, 2018. **22**(4): p. 2231-2239.
229. Wakabayashi-Ito, N. and S. Nagata, *Characterization of the regulatory elements in the promoter of the human elongation factor-1 alpha gene.* J Biol Chem, 1994. **269**(47): p. 29831-7.
230. Quilici, L.S., et al., *A minimal cytomegalovirus intron A variant can improve transgene expression in different mammalian cell lines.* Biotechnol Lett, 2013. **35**(1): p. 21-7.
231. Haddad-Mashadrizeh, A., et al., *A systematic study of the function of the human beta-globin introns on the expression of the human coagulation factor IX in cultured Chinese hamster ovary cells.* J Gene Med, 2009. **11**(10): p. 941-50.
232. Zufferey, R., et al., *Woodchuck hepatitis virus posttranscriptional regulatory element enhances expression of transgenes delivered by retroviral vectors.* J Virol, 1999. **73**(4): p. 2886-92.
233. Higashimoto, T., et al., *The woodchuck hepatitis virus post-transcriptional regulatory element reduces readthrough transcription from retroviral vectors.* Gene Therapy, 2007. **14**(17): p. 1298-1304.
234. Pillai, R.S., et al., *Inhibition of translational initiation by Let-7 MicroRNA in human cells.* Science, 2005. **309**(5740): p. 1573-6.
235. Lim, L. and E.S. Canellakis, *Adenine-rich polymer associated with rabbit reticulocyte messenger RNA.* Nature, 1970. **227**(5259): p. 710-2.
236. Goodwin, E.C. and F.M. Rottman, *The 3'-flanking sequence of the bovine growth hormone gene contains novel elements required for efficient and accurate polyadenylation.* J Biol Chem, 1992. **267**(23): p. 16330-4.
237. Salem, T.Z., et al., *The Influence of SV40 polyA on Gene Expression of Baculovirus Expression Vector Systems.* PLoS One, 2015. **10**(12): p. e0145019.
238. Hagedorn, C., et al., *S/MAR Element Facilitates Episomal Long-Term Persistence of Adeno-Associated Virus Vector Genomes in Proliferating Cells.* Hum Gene Ther, 2017. **28**(12): p. 1169-1179.
239. Piechaczek, C., et al., *A vector based on the SV40 origin of replication and chromosomal S/MARs replicates episomally in CHO cells.* Nucleic acids research, 1999. **27**(2): p. 426-428.
240. Yang, Y., et al., *A dual AAV system enables the Cas9-mediated correction of a metabolic liver disease in newborn mice.* Nat Biotechnol, 2016. **34**(3): p. 334-8.
241. Cary, L.C., et al., *Transposon mutagenesis of baculoviruses: analysis of Trichoplusia ni transposon IFP2 insertions within the FP-locus of nuclear polyhedrosis viruses.* Virology, 1989. **172**(1): p. 156-69.
242. Mojica, F.J.M., et al., *Biological significance of a family of regularly spaced repeats in the genomes of Archaea, Bacteria and mitochondria.* Molecular Microbiology, 2000. **36**(1): p. 244-246.
243. van der Oost, J., et al., *CRISPR-based adaptive and heritable immunity in prokaryotes.* Trends Biochem Sci, 2009. **34**(8): p. 401-7.
244. Sorek, R., V. Kunin, and P. Hugenholtz, *CRISPR--a widespread system that provides acquired resistance against phages in bacteria and archaea.* Nat Rev Microbiol, 2008. **6**(3): p. 181-6.
245. Li, H., et al., *In vivo genome editing restores haemostasis in a mouse model of haemophilia.* Nature, 2011. **475**(7355): p. 217-21.

246. Yin, H., et al., *Therapeutic genome editing by combined viral and non-viral delivery of CRISPR system components in vivo.* Nat Biotechnol, 2016. **34**(3): p. 328-33.
247. Cox, D.B., R.J. Platt, and F. Zhang, *Therapeutic genome editing: prospects and challenges.* Nat Med, 2015. **21**(2): p. 121-31.
248. Suzuki, K., et al., *In vivo genome editing via CRISPR/Cas9 mediated homology-independent targeted integration.* Nature, 2016. **540**(7631): p. 144-149.
249. Maresca, M., et al., *Obligate ligation-gated recombination (ObLiGaRe): custom-designed nuclease-mediated targeted integration through nonhomologous end joining.* Genome Res, 2013. **23**(3): p. 539-46.
250. Auer, T.O., et al., *Highly efficient CRISPR/Cas9-mediated knock-in in zebrafish by homology-independent DNA repair.* Genome Res, 2014. **24**(1): p. 142-53.
251. Amoasii, L., et al., *Gene editing restores dystrophin expression in a canine model of Duchenne muscular dystrophy.* Science, 2018. **362**(6410): p. 86-91.
252. Long, C., et al., *Postnatal genome editing partially restores dystrophin expression in a mouse model of muscular dystrophy.* Science, 2016. **351**(6271): p. 400.
253. Wang, D., et al., *Cas9-mediated allelic exchange repairs compound heterozygous recessive mutations in mice.* Nature Biotechnology, 2018. **36**(9): p. 839-842.
254. Suzuki, K. and J.C. Izpisua Belmonte, *In vivo genome editing via the HITI method as a tool for gene therapy.* J Hum Genet, 2018. **63**(2): p. 157-164.
255. Suchy, F.P., et al., *Genome engineering with Cas9 and AAV repair templates generates frequent concatemeric insertions of viral vectors.* Nature Biotechnology, 2024.
256. Bourque, G., et al., *Ten things you should know about transposable elements.* Genome Biol, 2018. **19**(1): p. 199.
257. Aziz, R.K., M. Breitbart, and R.A. Edwards, *Transposases are the most abundant, most ubiquitous genes in nature.* Nucleic Acids Res, 2010. **38**(13): p. 4207-17.
258. Senft, A.D. and T.S. Macfarlan, *Transposable elements shape the evolution of mammalian development.* Nature Reviews Genetics, 2021. **22**(11): p. 691-711.
259. Feschotte, C. and E.J. Pritham, *DNA transposons and the evolution of eukaryotic genomes.* Annu Rev Genet, 2007. **41**: p. 331-68.
260. Payer, L.M. and K.H. Burns, *Transposable elements in human genetic disease.* Nature Reviews Genetics, 2019. **20**(12): p. 760-772.
261. Tipanee, J., et al., *Preclinical and clinical advances in transposon-based gene therapy.* Biosci Rep, 2017. **37**(6).
262. Ivics, Z., et al., *Molecular Reconstruction of Sleeping Beauty, a Tc1-like Transposon from Fish, and Its Transposition in Human Cells.* Cell, 1997. **91**(4): p. 501-510.
263. Yusa, K., *piggyBac Transposon.* Microbiol Spectr, 2015. **3**(2): p. Mdna3-0028-2014.
264. Mitra, R., J. Fain-Thornton, and N.L. Craig, *piggyBac can bypass DNA synthesis during cut and paste transposition.* Embo j, 2008. **27**(7): p. 1097-109.
265. Chen, Q., et al., *Structural basis of seamless excision and specific targeting by piggyBac transposase.* Nature Communications, 2020. **11**(1): p. 3446.
266. Katter, K., et al., *Transposon-mediated transgenesis, transgenic rescue, and tissue-specific gene expression in rodents and rabbits.* Faseb j, 2013. **27**(3): p. 930-41.
267. Bai, J., et al., *A high-throughput screen for genes essential for PRRSV infection using a piggyBac-based system.* Virology, 2019. **531**: p. 19-30.
268. Yusa, K., et al., *A hyperactive piggyBac transposase for mammalian applications.* Proc Natl Acad Sci U S A, 2011. **108**(4): p. 1531-6.
269. Li, X., et al., *piggyBac transposase tools for genome engineering.* Proc Natl Acad Sci U S A, 2013. **110**(25): p. E2279-87.

270. Ivics, Z. and Z. Izsvák, *Sleeping Beauty Transposition.* Microbiology Spectrum, 2015. **3**(2): p. 10.1128/microbiolspec.mdna3-0042-2014.
271. Plasterk, R.H., Z. Izsvák, and Z. Ivics, *Resident aliens: the Tc1/mariner superfamily of transposable elements.* Trends Genet, 1999. **15**(8): p. 326-32.
272. Ding, S., et al., *Efficient transposition of the piggyBac (PB) transposon in mammalian cells and mice.* Cell, 2005. **122**(3): p. 473-83.
273. Jung, C.J., et al., *Comparative Analysis of piggyBac, CRISPR/Cas9 and TALEN Mediated BAC Transgenesis in the Zygote for the Generation of Humanized SIRPA Rats.* Sci Rep, 2016. **6**: p. 31455.
274. Cunningham, S.C., et al., *Modeling correction of severe urea cycle defects in the growing murine liver using a hybrid recombinant adeno-associated virus/piggyBac transposase gene delivery system.* Hepatology, 2015. **62**(2): p. 417-28.
275. Siew, S.M., et al., *Prevention of Cholestatic Liver Disease and Reduced Tumorigenicity in a Murine Model of PFIC Type 3 Using Hybrid AAV-piggyBac Gene Therapy.* Hepatology, 2019. **70**(6): p. 2047-2061.
276. Nakanishi, H., et al., *piggyBac transposon-mediated long-term gene expression in mice.* Mol Ther, 2010. **18**(4): p. 707-14.
277. Matsui, H., et al., *Delivery of full-length factor VIII using a piggyBac transposon vector to correct a mouse model of hemophilia A.* PLoS One, 2014. **9**(8): p. e104957.
278. Cooney, A.L., B.K. Singh, and P.L. Sinn, *Hybrid nonviral/viral vector systems for improved piggyBac DNA transposon in vivo delivery.* Mol Ther, 2015. **23**(4): p. 667-74.
279. Micklethwaite, K.P., et al., *Investigation of product-derived lymphoma following infusion of piggyBac-modified CD19 chimeric antigen receptor T cells.* Blood, 2021. **138**(16): p. 1391-1405.
280. Bishop, D.C., et al., *Development of CAR T-cell lymphoma in 2 of 10 patients effectively treated with piggyBac-modified CD19 CAR T cells.* Blood, 2021. **138**(16): p. 1504-1509.
281. Chen, J., et al., *Peptide-Based and Polypeptide-Based Gene Delivery Systems.* Topics in Current Chemistry, 2017. **375**(2): p. 32.
282. Mark, H.F., *ENCYCLOPEDIA OF POLYMER SCIENCE AND TECHNOLOGY, 15 VOLUME SET, 4TH EDITION*. 4th ed, ed. H.F. Mark. 2014, Hoboken, NJ: John Wiley and Sons. 344.
283. Xu, Y. and F.C. Szoka, Jr., *Mechanism of DNA release from cationic liposome/DNA complexes used in cell transfection.* Biochemistry, 1996. **35**(18): p. 5616-23.
284. Zelphati, O. and F.C. Szoka, Jr., *Mechanism of oligonucleotide release from cationic liposomes.* Proc Natl Acad Sci U S A, 1996. **93**(21): p. 11493-8.
285. Dell'Antone, P., *Evidence for an ATP-driven "proton pump" in rat liver lysosomes by basic dyes uptake.* Biochem Biophys Res Commun, 1979. **86**(1): p. 180-9.
286. Ishida, Y., et al., *A model of lysosomal pH regulation.* The Journal of general physiology, 2013. **141**(6): p. 705-720.
287. De Duve, C. and R. Wattiaux, *Functions of lysosomes.* Annu Rev Physiol, 1966. **28**: p. 435-92.
288. Brunner, S., et al., *Cell cycle dependence of gene transfer by lipoplex, polyplex and recombinant adenovirus.* Gene Ther, 2000. **7**(5): p. 401-7.
289. Dean, D.A., D.D. Strong, and W.E. Zimmer, *Nuclear entry of nonviral vectors.* Gene Ther, 2005. **12**(11): p. 881-90.
290. Kawabata, K., Y. Takakura, and M. Hashida, *The fate of plasmid DNA after intravenous injection in mice: involvement of scavenger receptors in its hepatic uptake.* Pharm Res, 1995. **12**(6): p. 825-30.

291. Boutin, S., et al., *Prevalence of serum IgG and neutralizing factors against adeno-associated virus (AAV) types 1, 2, 5, 6, 8, and 9 in the healthy population: implications for gene therapy using AAV vectors.* Human gene therapy, 2010. **21**(6): p. 704-712.
292. Calcedo, R., et al., *Worldwide epidemiology of neutralizing antibodies to adeno-associated viruses.* The Journal of infectious diseases, 2009. **199**(3): p. 381-390.
293. Fu, H., et al., *Differential prevalence of antibodies against adeno-associated virus in healthy children and patients with mucopolysaccharidosis III: perspective for AAV-mediated gene therapy.* Human gene therapy Clinical development, 2017. **28**(4): p. 187-196.
294. Kruzik, A., et al., *Prevalence of anti-adeno-associated virus immune responses in international cohorts of healthy donors.* Molecular therapy Methods & clinical development, 2019. **14**: p. 126-133.
295. Jiang, H., et al., *Effects of transient immunosuppression on adenoassociated, virus-mediated, liver-directed gene transfer in rhesus macaques and implications for human gene therapy.* Blood, 2006. **108**(10): p. 3321-3328.
296. Earley, J., et al., *Evading and overcoming AAV neutralization in gene therapy.* Trends in Biotechnology, 2023. **41**(6): p. 836-845.
297. Greig, J.A., et al., *Integrated vector genomes may contribute to long-term expression in primate liver after AAV administration.* Nature Biotechnology, 2024. **42**(8): p. 1232-1242.
298. Hacein-Bey-Abina, S., et al., *LMO2-Associated Clonal T Cell Proliferation in Two Patients after Gene Therapy for SCID-X1.* Science, 2003. **302**(5644): p. 415-419.
299. Büning, H. and M. Schmidt, *Adeno-associated Vector Toxicity-To Be or Not to Be?* Molecular therapy : the journal of the American Society of Gene Therapy, 2015. **23**(11): p. 1673-1675.
300. Srivastava, A. and B.J. Carter, *AAV Infection: Protection from Cancer.* Human gene therapy, 2017. **28**(4): p. 323-327.
301. Donsante, A., et al., *AAV vector integration sites in mouse hepatocellular carcinoma.* Science, 2007. **317**(5837): p. 477.
302. Gil-Farina, I., et al., *Recombinant AAV Integration Is Not Associated With Hepatic Genotoxicity in Nonhuman Primates and Patients.* Molecular therapy : the journal of the American Society of Gene Therapy, 2016. **24**(6): p. 1100-1105.
303. Lehrman, S., *Virus treatment questioned after gene therapy death.* Nature, 1999. **401**(6753): p. 517-518.
304. Soenen, S.J., A.R. Brisson, and M. De Cuyper, *Addressing the problem of cationic lipid-mediated toxicity: the magnetoliposome model.* Biomaterials, 2009. **30**(22): p. 3691-701.
305. Yew, N.S. and R.K. Scheule, *Toxicity of Cationic Lipid-DNA Complexes.* Adv Genet, 2005. **53pa**: p. 189-214.
306. Ruiz, F.E., et al., *A clinical inflammatory syndrome attributable to aerosolized lipid-DNA administration in cystic fibrosis.* Human Gene Therapy, 2001. **12**(7): p. 751-761.
307. Omidi, Y., et al., *Microarray analysis of the toxicogenomics and the genotoxic potential of a cationic lipid-based gene delivery nanosystem in human alveolar epithelial a549 cells.* Toxicol Mech Methods, 2008. **18**(4): p. 369-78.
308. Ho, A., et al., *Adeno-associated virus 2 infection in children with non-A–E hepatitis.* Nature, 2023. **617**(7961): p. 555-563.
309. Vandamme, C., O. Adjali, and F. Mingozzi, *Unraveling the Complex Story of Immune Responses to AAV Vectors Trial After Trial.* Hum Gene Ther, 2017. **28**(11): p. 1061-1074.

310. Mingozzi, F. and K.A. High, *Overcoming the Host Immune Response to Adeno-Associated Virus Gene Delivery Vectors: The Race Between Clearance, Tolerance, Neutralization, and Escape.* Annual Review of Virology, 2017. **4**(1): p. 511-534.
311. Wang, L., et al., *The pleiotropic effects of natural AAV infections on liver-directed gene transfer in macaques.* Molecular therapy : the journal of the American Society of Gene Therapy, 2010. **18**(1): p. 126-134.
312. Perocheau, D.P., et al., *Age-Related Seroprevalence of Antibodies Against AAV-LK03 in a UK Population Cohort.* Hum Gene Ther, 2019. **30**(1): p. 79-87.
313. Colella, P., G. Ronzitti, and F. Mingozzi, *Emerging Issues in AAV-Mediated In Vivo Gene Therapy.* Molecular Therapy Methods & Clinical Development, 2018. **8**: p. 87-104.
314. Burnett, J.R. and A.J. Hooper, *Alipogene tiparvovec, an adeno-associated virus encoding the Ser(447)X variant of the human lipoprotein lipase gene for the treatment of patients with lipoprotein lipase deficiency.* Curr Opin Mol Ther, 2009. **11**(6): p. 681-91.
315. Flemming, A., *Pioneering gene therapy on brink of approval.* Nature Reviews Drug Discovery, 2012. **11**(9): p. 664-664.
316. Senior, M., *After Glybera's withdrawal, what's next for gene therapy?* Nature Biotechnology, 2017. **35**(6): p. 491-492.
317. Koyata, H., R.P. Cox, and D.T. Chuang, *Stable correction of maple syrup urine disease in cells from a Mennonite patient by retroviral-mediated gene transfer.* Biochemical Journal, 1993. **295**(3): p. 635-639.
318. Healy, P.J. and J.A. Dennis, *Heterozygote detection for maple syrup urine disease in cattle.* Australian Veterinary Journal, 1995. **72**(9): p. 346-348.
319. Healy, P.J., et al., *Maple syrup urine disease in Poll Shorthorn calves.* Aust Vet J, 1992. **69**(6): p. 143-4.
320. Robarge, M.E., et al., *Maple Syrup Urine Disease in a Central Indiana Hereford Herd.* Case Reports in Veterinary Medicine, 2015. **2015**(1): p. 204037.
321. Azuma, H., et al., *Robust expansion of human hepatocytes in Fah-/-/Rag2-/-/Il2rg-/- mice.* Nature biotechnology, 2007. **25**(8): p. 903-910.
322. Gramignoli, R., et al., *New potential cell source for hepatocyte transplantation: Discarded livers from metabolic disease liver transplants.* Stem Cell Research, 2013. **11**(1): p. 563-573.
323. Pontoizeau, C., et al., *Neonatal gene therapy achieves sustained disease rescue of maple syrup urine disease in mice.* Nat Commun, 2022. **13**(1): p. 3278.
324. Pontoizeau, C., et al., *Successful treatment of severe MSUD in Bckdhb mice with neonatal AAV gene therapy.* Journal of Inherited Metabolic Disease, 2024. **47**(1): p. 41-49.
325. Greig, J.A., et al., *Lipid Nanoparticle mRNA Therapy Improves Survival and Reduces Serum Branched-Chain Amino Acids in Mouse Models of Maple Syrup Urine Disease.* Human Gene Therapy, 2024. **35**(17-18): p. 726-733.
326. Greig, J.A., et al., *Muscle-directed AAV gene therapy rescues the maple syrup urine disease phenotype in a mouse model.* Mol Genet Metab, 2021. **134**(1-2): p. 139-146.
327. Westhaus, A., et al., *High-Throughput In Vitro, Ex Vivo, and In Vivo Screen of Adeno-Associated Virus Vectors Based on Physical and Functional Transduction.* Human Gene Therapy, 2020. **31**(9-10): p. 575-589.
328. Di, J., et al., *Biodistribution and Non-linear Gene Expression of mRNA LNPs Affected by Delivery Route and Particle Size.* Pharm Res, 2022. **39**(1): p. 105-114.
329. Chuecos, M.A. and W.R. Lagor, *Liver directed adeno-associated viral vectors to treat metabolic disease.* Journal of Inherited Metabolic Disease, 2024. **47**(1): p. 22-40.

330. Uhlén, M., et al., *Tissue-based map of the human proteome.* Science, 2015. **347**(6220): p. 1260419.
331. Myers, J.D. and J.B. Hickam, *AN ESTIMATION OF THE HEPATIC BLOOD FLOW AND SPLANCHNIC OXYGEN CONSUMPTION IN HEART FAILURE.* J Clin Invest, 1948. **27**(5): p. 620-7.
332. Lautt, W.W. and C.V. Greenway, *Conceptual review of the hepatic vascular bed.* Hepatology, 1987. **7**(5): p. 952-63.
333. Si-Tayeb, K., F.P. Lemaigre, and S.A. Duncan, *Organogenesis and development of the liver.* Dev Cell, 2010. **18**(2): p. 175-89.
334. Kietzmann, T., *Metabolic zonation of the liver: The oxygen gradient revisited.* Redox Biology, 2017. **11**: p. 622-630.
335. Schleicher, J., et al., *Zonation of hepatic fatty acid metabolism - The diversity of its regulation and the benefit of modeling.* Biochimica et Biophysica Acta - Molecular and Cell Biology of Lipids, 2015. **1851**(5): p. 641-656.
336. Gebhardt, R., *Metabolic zonation of the liver: Regulation and implications for liver function.* Pharmacology and Therapeutics, 1992. **53**(3): p. 275-354.
337. Jungermann, K. and T. Kietzmann, *Zonation of parenchymal and nonparenchymal metabolism in liver*, in *Annual Review of Nutrition*. 1996. p. 179-203.
338. Jungermann, K., *Zonation of metabolism and gene expression in liver.* Histochemistry and Cell Biology, 1995. **103**(2): p. 81-91.
339. Häussinger, D., W.H. Lamers, and A.F. Moorman, *Hepatocyte heterogeneity in the metabolism of amino acids and ammonia.* Enzyme, 1992. **46**(1-3): p. 72-93.
340. Bell, P., et al., *Inverse zonation of hepatocyte transduction with AAV vectors between mice and non-human primates.* Molecular genetics and metabolism, 2011. **104**(3): p. 395-403.
341. Cunningham, S.C., et al., *Gene delivery to the juvenile mouse liver using AAV2/8 vectors.* Mol Ther, 2008. **16**(6): p. 1081-8.
342. Cunningham, S.C., et al., *AAV2/8-mediated correction of OTC deficiency is robust in adult but not neonatal Spf(ash) mice.* Mol Ther, 2009. **17**(8): p. 1340-6.
343. Dane, A.P., et al., *Sexually dimorphic patterns of episomal rAAV genome persistence in the adult mouse liver and correlation with hepatocellular proliferation.* Mol Ther, 2009. **17**(9): p. 1548-54.
344. Zajicek, G., R. Oren, and M. Weinreb, Jr., *The streaming liver.* Liver, 1985. **5**(6): p. 293-300.
345. Furuyama, K., et al., *Continuous cell supply from a Sox9-expressing progenitor zone in adult liver, exocrine pancreas and intestine.* Nat Genet, 2011. **43**(1): p. 34-41.
346. Kok, C.Y., et al., *Adeno-associated Virus-mediated Rescue of Neonatal Lethality in Argininosuccinate Synthetase-deficient Mice.* Molecular Therapy, 2013. **21**(10): p. 1823-1831.
347. Bucher NLR, M.R., *Regeneration of liver and kidney*. 1971, Boston, MA: Little. Brown.
348. Duncan, A.W., C. Dorrell, and M. Grompe, *Stem cells and liver regeneration.* Gastroenterology, 2009. **137**(2): p. 466-481.
349. Lalwani, N.D., et al., *Development of hepatocellular carcinomas and increased peroxisomal fatty acid beta-oxidation in rats fed [4-chloro-6-(2,3-xylidino)-2-pyrimidinylthio] acetic acid (Wy-14,643) in the semipurified diet.* Carcinogenesis, 1981. **2**(7): p. 645-50.
350. Lindroos, P.M., R. Zarnegar, and G.K. Michalopoulos, *Hepatocyte growth factor (hepatopoietin A) rapidly increases in plasma before DNA synthesis and liver*

regeneration stimulated by partial hepatectomy and carbon tetrachloride administration. Hepatology, 1991. **13**(4): p. 743-50.
351. Wisse, E., et al., *The size of endothelial fenestrae in human liver sinusoids: implications for hepatocyte-directed gene transfer.* Gene Therapy, 2008. **15**(17): p. 1193-1199.
352. Lievens, J., et al., *The size of sinusoidal fenestrae is a critical determinant of hepatocyte transduction after adenoviral gene transfer.* Gene Therapy, 2004. **11**(20): p. 1523-1531.
353. Snoeys, J., et al., *Species differences in transgene DNA uptake in hepatocytes after adenoviral transfer correlate with the size of endothelial fenestrae.* Gene Therapy, 2007. **14**(7): p. 604-612.
354. Schaffner, F. and H. Popper, *Capillarization of Hepatic Sinusoids in Man.* Gastroenterology, 1963. **44**(3): p. 239-242.
355. Alberts, B., et al., *Molecular biology of the cell: seventh international student edition with registration card*. 2022: WW Norton & Company.
356. Frontera, W.R. and J. Ochala, *Skeletal Muscle: A Brief Review of Structure and Function.* Calcified Tissue International, 2015. **96**(3): p. 183-195.
357. Alberts B, J.A., Lewis J, et al. , *Genesis, Modulation, and Regeneration of Skeletal Muscle.* 4th edition ed. Molecular Biology of the Cell, ed. G. Science. Vol. 2002. . 2002, New York: .
358. Frontera, W.R., et al., *Aging of skeletal muscle: a 12-yr longitudinal study.* J Appl Physiol (1985), 2000. **88**(4): p. 1321-6.
359. Tracy, R.E., *Cardiac myocyte sizes in right compared with left ventricle during overweight and hypertension.* Journal of the American Society of Hypertension, 2014. **8**(7): p. 457-463.
360. Topol, E.J. and R.M. Califf, *Textbook of cardiovascular medicine*. 2007: Lippincott Williams & Wilkins.
361. Shefer, G., et al., *Satellite-cell pool size does matter: defining the myogenic potency of aging skeletal muscle.* Dev Biol, 2006. **294**(1): p. 50-66.
362. Smith, C., et al., *The inflammatory response to skeletal muscle injury: illuminating complexities.* Sports Med, 2008. **38**(11): p. 947-69.
363. Larsson, L. and R.L. Moss, *Maximum velocity of shortening in relation to myosin isoform composition in single fibres from human skeletal muscles.* J Physiol, 1993. **472**: p. 595-614.
364. Schiaffino, S. and C. Reggiani, *Fiber types in mammalian skeletal muscles.* Physiol Rev, 2011. **91**(4): p. 1447-531.
365. Ferrière, G., M. de Castro, and J. Rodriguez, *Abnormalities of muscle fibers in maple syrup urine disease.* Acta Neuropathol, 1984. **63**(3): p. 249-54.
366. Chamberlain, J.R. and J.S. Chamberlain, *Progress toward Gene Therapy for Duchenne Muscular Dystrophy.* Mol Ther, 2017. **25**(5): p. 1125-1131.
367. Horowitz, E.D., M.S. Weinberg, and A. Asokan, *Glycated AAV vectors: chemical redirection of viral tissue tropism.* Bioconjug Chem, 2011. **22**(4): p. 529-32.
368. Weinmann, J., et al., *Identification of a myotropic AAV by massively parallel in vivo evaluation of barcoded capsid variants.* Nature Communications, 2020. **11**(1): p. 5432.
369. Tabebordbar, M., et al., *Directed evolution of a family of AAV capsid variants enabling potent muscle-directed gene delivery across species.* Cell, 2021. **184**(19): p. 4919-4938.e22.
370. El Andari, J., et al., *Semirational bioengineering of AAV vectors with increased potency and specificity for systemic gene therapy of muscle disorders.* Science Advances. **8**(38): p. eabn4704.

371. Ramos, J.N., et al., *Development of Novel Micro-dystrophins with Enhanced Functionality.* Mol Ther, 2019. **27**(3): p. 623-635.
372. Miciak, J.J., J. Hirshberg, and F. Bunz, *Seamless assembly of recombinant adenoviral genomes from high-copy plasmids.* PLoS One, 2018. **13**(6): p. e0199563.
373. Gao, G.P., et al., *Novel adeno-associated viruses from rhesus monkeys as vectors for human gene therapy.* Proc Natl Acad Sci U S A, 2002. **99**(18): p. 11854-9.
374. Snyder, R., Xiao, X and Samulski, RJ *Production of recombinant adenoassociated viral vectors.* . Current Protocols in Human Genetics. , ed. N. Dracopoli, Haines, J, Krof, B, Moir, C, Morton, C, Seidman, C et al. (eds). 1996 Chichester, UK John Wiley & Sons, Inc.
375. Truett, G.E., et al., *Preparation of PCR-Quality Mouse Genomic DNA with Hot Sodium Hydroxide and Tris (HotSHOT).* BioTechniques, 2000. **29**(1): p. 52-54.
376. Homanics, G.E., et al., *Production and characterization of murine models of classic and intermediate maple syrup urine disease.* BMC medical genetics, 2006. **7**: p. 33-33.
377. Kistner, A., et al., *Doxycycline-mediated quantitative and tissue-specific control of gene expression in transgenic mice.* Proc Natl Acad Sci U S A, 1996. **93**(20): p. 10933-8.
378. Ye, X., et al., *Differences in the human and mouse amino-terminal leader peptides of ornithine transcarbamylase affect mitochondrial import and efficacy of adenoviral vectors.* Hum Gene Ther, 2001. **12**(9): p. 1035-46.
379. Shimomura, Y., et al., *Branched-chain amino acid catabolism in exercise and liver disease.* J Nutr, 2006. **136**(1 Suppl): p. 250s-3s.
380. She, P., et al., *Obesity-related elevations in plasma leucine are associated with alterations in enzymes involved in branched-chain amino acid metabolism.* Am J Physiol Endocrinol Metab, 2007. **293**(6): p. E1552-63.
381. Gumus Balikcioglu, P., et al., *Branched-chain α-keto acids and glutamate/glutamine: Biomarkers of insulin resistance in childhood obesity.* Endocrinol Diabetes Metab, 2023. **6**(1): p. e388.
382. Schneider, M.R., R. Mangels, and M.D. Dean, *The molecular basis and reproductive function(s) of copulatory plugs.* Molecular Reproduction and Development, 2016. **83**(9): p. 755-767.
383. Gao, S. and D.P. Calderon, *Robust alternative to the righting reflex to assess arousal in rodents.* Scientific Reports, 2020. **10**(1): p. 20280.
384. Eltokhi, A., B. Kurpiers, and C. Pitzer, *Behavioral tests assessing neuropsychiatric phenotypes in adolescent mice reveal strain- and sex-specific effects.* Scientific Reports, 2020. **10**(1): p. 11263.
385. Hwang, D., et al., *Micro-Current Stimulation Has Potential Effects of Hair Growth-Promotion on Human Hair Follicle-Derived Papilla Cells and Animal Model.* Int J Mol Sci, 2021. **22**(9).
386. Mitsubuchi, H., M. Owada, and F. Endo, *Markers Associated with Inborn Errors of Metabolism of Branched-Chain Amino Acids and Their Relevance to Upper Levels of Intake in Healthy People: An Implication from Clinical and Molecular Investigations on Maple Syrup Urine Disease12.* The Journal of Nutrition, 2005. **135**(6): p. 1565S-1570S.
387. Paul, H.S. and S.A. Adibi, *Mechanism of activation of hepatic branched-chain alpha-ketoacid dehydrogenase by a muscle factor.* Journal of Biological Chemistry, 1983. **258**(19): p. 11471-11475.
388. Ishikawa, H., et al., *Relationship between fetal weight, placental growth and litter size in mice from mid- to late-gestation.* Reprod Toxicol, 2006. **21**(3): p. 267-70.

389. Turgeon, B. and S. Meloche, *Interpreting neonatal lethal phenotypes in mouse mutants: insights into gene function and human diseases.* Physiol Rev, 2009. **89**(1): p. 1-26.
390. Weber, E.M., A.S. Olsson, and B. Algers, *High mortality rates among newborn laboratory mice – is it natural and which are the causes?* Acta Veterinaria Scandinavica, 2007. **49**(1): p. S8.
391. Kok, C.Y., et al., *Adeno-associated virus-mediated rescue of neonatal lethality in argininosuccinate synthetase-deficient mice.* Mol Ther, 2013. **21**(10): p. 1823-31.
392. Murray, S.A., et al., *Mouse gestation length is genetically determined.* PLoS One, 2010. **5**(8): p. e12418.
393. Bryant, C.D., *The blessings and curses of C57BL/6 substrains in mouse genetic studies.* Ann N Y Acad Sci, 2011. **1245**: p. 31-3.
394. Mekada, K. and A. Yoshiki, *Substrains matter in phenotyping of C57BL/6 mice.* Exp Anim, 2021. **70**(2): p. 145-160.
395. Wang, J.-H., et al., *Adeno-associated virus as a delivery vector for gene therapy of human diseases.* Signal Transduction and Targeted Therapy, 2024. **9**(1): p. 78.
396. Wang, L., et al., *Hepatic gene transfer in neonatal mice by adeno-associated virus serotype 8 vector.* Hum Gene Ther, 2012. **23**(5): p. 533-9.
397. Baruteau, J., et al., *Delivering efficient liver-directed AAV-mediated gene therapy.* Gene Therapy, 2017. **24**(5): p. 263-264.
398. Melchiorri, C., et al., *Ploidy and nuclearity of rat hepatocytes after compensatory regeneration or mitogen-induced liver growth.* Carcinogenesis, 1993. **14**(9): p. 1825-30.
399. Rollins, M.F., et al., *Hepatocytes lacking thioredoxin reductase 1 have normal replicative potential during development and regeneration.* J Cell Sci, 2010. **123**(Pt 14): p. 2402-12.
400. Baruteau, J., N. Brunetti-Pierri, and P. Gissen, *Liver-directed gene therapy for inherited metabolic diseases.* Journal of Inherited Metabolic Disease, 2024. **47**(1): p. 9-21.
401. Wang, Z., et al., *Adeno-associated virus serotype 8 efficiently delivers genes to muscle and heart.* Nat Biotechnol, 2005. **23**(3): p. 321-8.
402. Nathwani, A.C., et al., *Self-complementary adeno-associated virus vectors containing a novel liver-specific human factor IX expression cassette enable highly efficient transduction of murine and nonhuman primate liver.* Blood, 2006. **107**(7): p. 2653-61.
403. Grzegorski, S.J., et al., *Natural variability of Kozak sequences correlates with function in a zebrafish model.* PLoS One, 2014. **9**(9): p. e108475.
404. Benson, D.A., et al., *GenBank.* Nucleic Acids Res, 2013. **41**(Database issue): p. D36-42.
405. Piletz, J.E. and R.E. Ganschow, *Genetic variation of milk proteins in mice.* Biochemical Genetics, 1981. **19**(9): p. 1023-1030.
406. Boumahrou, N., et al., *Evolution of major milk proteins in Mus musculus and Mus spretus mouse species: a genoproteomic analysis.* BMC Genomics, 2011. **12**: p. 80.
407. Chandler, R.J., et al., *Systemic gene therapy for methylmalonic acidemia using the novel adeno-associated viral vector 44.9.* Mol Ther Methods Clin Dev, 2022. **27**: p. 61-72.
408. Wang, G., et al., *Assessment of toxicity and biodistribution of recombinant AAV8 vector–mediated immunomodulatory gene therapy in mice with Pompe disease.* Molecular Therapy - Methods & Clinical Development, 2014. **1**: p. 14018.
409. Pan, X., et al., *Long-Term Robust Myocardial Transduction of the Dog Heart from a Peripheral Vein by Adeno-Associated Virus Serotype-8.* Human Gene Therapy, 2013. **24**(6): p. 584-594.

410. Aranda-Anzaldo, A., *The post-mitotic state in neurons correlates with a stable nuclear higher-order structure.* Commun Integr Biol, 2012. **5**(2): p. 134-9.
411. Radonić, A., et al., *Guideline to reference gene selection for quantitative real-time PCR.* Biochem Biophys Res Commun, 2004. **313**(4): p. 856-62.
412. Mingozzi, F. and K.A. High, *Immune responses to AAV vectors: overcoming barriers to successful gene therapy.* Blood, 2013. **122**(1): p. 23-36.
413. Jinek, M., et al., *A programmable dual-RNA-guided DNA endonuclease in adaptive bacterial immunity.* Science, 2012. **337**(6096): p. 816-21.
414. Anzalone, A.V., et al., *Search-and-replace genome editing without double-strand breaks or donor DNA.* Nature, 2019. **576**(7785): p. 149-157.
415. Komor, A.C., et al., *Programmable editing of a target base in genomic DNA without double-stranded DNA cleavage.* Nature, 2016. **533**(7603): p. 420-424.
416. Troyanovsky, B., et al., *The Functionality of Minimal PiggyBac Transposons in Mammalian Cells.* Molecular Therapy - Nucleic Acids, 2016. **5**: p. e369.
417. Wilson, M.H., C.J. Coates, and A.L. George, *PiggyBac Transposon-mediated Gene Transfer in Human Cells.* Molecular Therapy, 2007. **15**(1): p. 139-145.
418. Sander, J.D. and J.K. Joung, *CRISPR-Cas systems for editing, regulating and targeting genomes.* Nat Biotechnol, 2014. **32**(4): p. 347-55.
419. Zhang, Q.S., et al., *Induced Liver Regeneration Enhances CRISPR/Cas9-Mediated Gene Repair in Tyrosinemia Type 1.* Hum Gene Ther, 2021. **32**(5-6): p. 294-301.
420. Ginn, S.L., et al., *Efficient in vivo editing of OTC-deficient patient-derived primary human hepatocytes.* JHEP Rep, 2020. **2**(1): p. 100065.
421. Crudele, J.M. and J.S. Chamberlain, *Cas9 immunity creates challenges for CRISPR gene editing therapies.* Nat Commun, 2018. **9**(1): p. 3497.
422. Park, S.H.J.P., et al., *CRISPR/Cas9 Editing Induces High Rates of Unintended Large Gene Modifications in HSPCs from Patients with Sickle Cell Disease.* Blood, 2021. **138**(Supplement 1): p. 3969-3969.
423. Patrício, M.I., et al., *Inclusion of the Woodchuck Hepatitis Virus Posttranscriptional Regulatory Element Enhances AAV2-Driven Transduction of Mouse and Human Retina.* Mol Ther Nucleic Acids, 2017. **6**: p. 198-208.
424. Wang, L., et al., *Enhancing Transgene Expression from Recombinant AAV8 Vectors in Different Tissues Using Woodchuck Hepatitis Virus Post-Transcriptional Regulatory Element.* Int J Med Sci, 2016. **13**(4): p. 286-91.
425. Fernández-López, D., et al., *Blood-brain barrier permeability is increased after acute adult stroke but not neonatal stroke in the rat.* J Neurosci, 2012. **32**(28): p. 9588-600.
426. Bostick, B., et al., *Systemic AAV-9 transduction in mice is influenced by animal age but not by the route of administration.* Gene Ther, 2007. **14**(22): p. 1605-9.
427. Muraine, L., et al., *Transduction Efficiency of Adeno-Associated Virus Serotypes After Local Injection in Mouse and Human Skeletal Muscle.* Hum Gene Ther, 2020. **31**(3-4): p. 233-240.
428. Yamada, Y., et al., *Structure-Activity Relationships of RGD-Containing Peptides in Integrin αvβ5-Mediated Cell Adhesion.* ACS Omega, 2023. **8**(5): p. 4687-4693.
429. Brooks, A.R., et al., *Transcriptional silencing is associated with extensive methylation of the CMV promoter following adenoviral gene delivery to muscle.* The Journal of Gene Medicine, 2004. **6**(4): p. 395-404.
430. Costa Verdera, H., K. Kuranda, and F. Mingozzi, *AAV Vector Immunogenicity in Humans: A Long Journey to Successful Gene Transfer.* Molecular Therapy, 2020. **28**(3): p. 723-746.

431. Herzog, R.W., et al., *Regulatory T cells and TLR9 activation shape antibody formation to a secreted transgene product in AAV muscle gene transfer.* Cellular Immunology, 2019. **342**: p. 103682.
432. Butterfield, J.S.S., et al., *TLR9-Activating CpG-B ODN but Not TLR7 Agonists Triggers Antibody Formation to Factor IX in Muscle Gene Transfer.* Human Gene Therapy Methods, 2019. **30**(3): p. 81-92.
433. Hoffman, B.E., et al., *Nonredundant Roles of IL-10 and TGF-β in Suppression of Immune Responses to Hepatic AAV-Factor IX Gene Transfer.* Molecular Therapy, 2011. **19**(7): p. 1263-1272.
434. Skopenkova, V.V., T.V. Egorova, and M.V. Bardina, *Muscle-Specific Promoters for Gene Therapy.* Acta Naturae, 2021. **13**(1): p. 47-58.
435. Aysha, J., et al., *Synthetic Promoters: Designing the cis Regulatory Modules for Controlled Gene Expression.* Mol Biotechnol, 2018. **60**(8): p. 608-620.
436. Hauser, M.A., et al., *Analysis of muscle creatine kinase regulatory elements in recombinant adenoviral vectors.* Mol Ther, 2000. **2**(1): p. 16-25.
437. Salva, M.Z., et al., *Design of tissue-specific regulatory cassettes for high-level rAAV-mediated expression in skeletal and cardiac muscle.* Mol Ther, 2007. **15**(2): p. 320-9.
438. Wang, B., et al., *Construction and analysis of compact muscle-specific promoters for AAV vectors.* Gene Therapy, 2008. **15**(22): p. 1489-1499.
439. Gonçalves, M.A., et al., *Transcription factor rational design improves directed differentiation of human mesenchymal stem cells into skeletal myocytes.* Mol Ther, 2011. **19**(7): p. 1331-41.
440. Birch, S.M., et al., *Assessment of systemic AAV-microdystrophin gene therapy in the GRMD model of Duchenne muscular dystrophy.* Science Translational Medicine. **15**(677): p. eabo1815.
441. Lee, R.C., R.L. Feinbaum, and V. Ambros, *The C. elegans heterochronic gene lin-4 encodes small RNAs with antisense complementarity to lin-14.* Cell, 1993. **75**(5): p. 843-854.
442. Bartel, D.P., *MicroRNAs: genomics, biogenesis, mechanism, and function.* Cell, 2004. **116**(2): p. 281-97.
443. Lewis, B.P., C.B. Burge, and D.P. Bartel, *Conserved seed pairing, often flanked by adenosines, indicates that thousands of human genes are microRNA targets.* Cell, 2005. **120**(1): p. 15-20.
444. Bartel, D.P., *MicroRNAs: target recognition and regulatory functions.* Cell, 2009. **136**(2): p. 215-33.
445. O'Connor, R.M., et al., *All Roads Lead to the miRNome: miRNAs Have a Central Role in the Molecular Pathophysiology of Psychiatric Disorders.* Trends Pharmacol Sci, 2016. **37**(12): p. 1029-1044.
446. Axtell, M.J., J.O. Westholm, and E.C. Lai, *Vive la différence: biogenesis and evolution of microRNAs in plants and animals.* Genome Biol, 2011. **12**(4): p. 221.
447. Vuokila, N., et al., *Chronic Regulation of miR-124-3p in the Perilesional Cortex after Experimental and Human TBI.* Int J Mol Sci, 2020. **21**(7).
448. Żurawek, D. and G. Turecki, *miR-124-3p mediates polygenic risk shared between schizophrenia and bipolar disorder.* Neuron, 2023. **111**(2): p. 144-146.
449. Ghafouri-Fard, S., et al., *An update on the role of miR-124 in the pathogenesis of human disorders.* Biomedicine & Pharmacotherapy, 2021. **135**: p. 111198.
450. Kelly, E.J., et al., *Engineering microRNA responsiveness to decrease virus pathogenicity.* Nature Medicine, 2008. **14**(11): p. 1278-1283.
451. Gentner, B., et al., *Stable knockdown of microRNA in vivo by lentiviral vectors.* Nat Methods, 2009. **6**(1): p. 63-6.

452. Geisler, A., et al., *microRNA122-regulated transgene expression increases specificity of cardiac gene transfer upon intravenous delivery of AAV9 vectors.* Gene Ther, 2011. **18**(2): p. 199-209.
453. Rishik, S., et al., *miRNATissueAtlas 2025: an update to the uniformly processed and annotated human and mouse non-coding RNA tissue atlas.* Nucleic Acids Research, 2025. **53**(D1): p. D129-D137.
454. Chen, Y. and X. Wang, *miRDB: an online database for prediction of functional microRNA targets.* Nucleic Acids Res, 2020. **48**(D1): p. D127-d131.
455. Díaz, V.M., et al., *Liver transplantation for classical maple syrup urine disease: long-term follow-up.* J Pediatr Gastroenterol Nutr, 2014. **59**(5): p. 636-9.
456. Guilder, L., et al., *Hyperleucinosis during infections in maple syrup urine disease post liver transplantation.* Mol Genet Metab Rep, 2021. **27**: p. 100763.
457. Ghafarimoghadam, M., et al., *A review of behavioral methods for the evaluation of cognitive performance in animal models: Current techniques and links to human cognition.* Physiology & Behavior, 2022. **244**: p. 113652.
458. Mendell, J.R., et al., *Long-term safety and functional outcomes of delandistrogene moxeparvovec gene therapy in patients with Duchenne muscular dystrophy: A phase 1/2a nonrandomized trial.* Muscle Nerve, 2024. **69**(1): p. 93-98.
459. Dreghici, R.D., et al., *FP.28 IGNITE DMD phase I/II study of SGT-001 microdystrophin gene therapy for DMD: Long-term outcomes and expression update.* Neuromuscular Disorders, 2022. **32**: p. S98.
460. Mensenkamp, A.R., et al., *Mice expressing only the mutant APOE3Leiden gene show impaired VLDL secretion.* Arteriosclerosis, thrombosis, and vascular biology, 2001. **21**(8): p. 1366-1372.
461. Themis, M., et al., *Oncogenesis following delivery of a nonprimate lentiviral gene therapy vector to fetal and neonatal mice.* Mol Ther, 2005. **12**(4): p. 763-71.
462. Kingsman, S.M., K. Mitrophanous, and J.C. Olsen, *Potential oncogene activity of the woodchuck hepatitis post-transcriptional regulatory element (WPRE).* Gene Ther, 2005. **12**(1): p. 3-4.
463. Westbrook, R., et al., *Alterations in oxygen consumption, respiratory quotient, and heat production in long-lived GHRKO and Ames dwarf mice, and short-lived bGH transgenic mice.* J Gerontol A Biol Sci Med Sci, 2009. **64**(4): p. 443-51.
464. Zhang, I.W., et al., *Combined Organ Transplantation in Patients with Advanced Liver Disease.* Semin Liver Dis, 2024. **44**(3): p. 369-382.
465. Topilsky, Y., et al., *Combined heart and liver transplant attenuates cardiac allograft vasculopathy compared with isolated heart transplantation.* Transplantation, 2013. **95**(6): p. 859-65.
466. Sherman, A., M. Biswas, and R.W. Herzog, *Innovative approaches for immune tolerance to factor VIII in the treatment of hemophilia A.* Frontiers in immunology, 2017. **8**: p. 1604.
467. Kumar, S.R.P., et al., *The Balance between CD8+ T Cell-Mediated Clearance of AAV-Encoded Antigen in the Liver and Tolerance Is Dependent on the Vector Dose.* Molecular Therapy, 2017. **25**(4): p. 880-891.
468. Mingozzi, F., et al., *Induction of immune tolerance to coagulation factor IX antigen by in vivo hepatic gene transfer.* The Journal of clinical investigation, 2003. **111**(9): p. 1347-1356.
469. Pillarisetty, V.G., et al., *Liver Dendritic Cells Are Less Immunogenic Than Spleen Dendritic Cells because of Differences in Subtype Composition1.* The Journal of Immunology, 2004. **172**(2): p. 1009-1017.

470. Paul, H.S. and S.A. Adibi, *Leucine oxidation in diabetes and starvation: Effects of ketone bodies on branched-chain amino acid oxidation in vitro.* Metabolism, 1978. **27**(2): p. 185-200.